Hydrogen Production by Partial Catalytic Dehydrogenation of Kerosene

A thesis submitted to the Faculty of Energy Technology, Process Engineering and Biological Engineering of the University of Stuttgart in partial fulfilment of the requirements for the degree of Doctor of Engineering Sciences (Dr.-Ing.)

by

Karolina Pearson

born in Warsaw/Poland

Main referee:	Prof. Dr. rer. nat. André Thess
Co referee:	Prof. Dr.-Ing. Elias Klemm
Co referee:	
Date of defense:	

Institute of Engineering Thermodynamic

German Aerospace Center

Institut für Energiespeicherung

University of Stuttgart

2015

Table of Contents

Nomenclature

Abbreviations

CPOX	catalytic partial oxidation
FC	fuel cell
GCFID	gas chromatography with flame ionization detector
GCMS	gas chromatography with mass spectrometry
GCTCD	gas chromatography with thermal conductivity detector
LFC	liquid flow controller
LHV	lower heating value
MCH	methylcyclohexane
MFC	mass flow controller
MFM	Mass flow meter
PC	pressure controller
PCD	partial catalytic dehydrogenation
PS	pressure sensor
PSA	pressure swing adsorption
ppmw	parts per million weight
PEMFC	proton exchange membrane fuel cell
STP	standard temperature and pressure
TC	thermocouple
TPOX	thermal partial oxidation
ULSK	ultra- low- sulfur kerosene

Latin Symbols

A, B, C, D, E, F	substance specific coefficient for Antoine- equations of state	
Cn	carbon atom number	
CP	heat capacity flow rate	kW/K

$\dot{F}$	feed mole flow	mol/h
ΔG_R^0	standard enthalpy of reaction	
H	enthalpy	kJ/mol
ΔH_R^0	enthalpy of reaction at standard conditions	kJ/mol
K	equilibrium constant of reaction	
K_i	vapor liquid equilibrium constant	
L	catalyst bed length	mm
$\dot{L}$	mol flow of liquid	mol/h
M	molar mass	g/mol
P	performance	kW
Q	heat	kJ
$\dot{Q}$	heat stream	kW
R	molar gas constant	J/(mol K)
T	temperature	°C
V	volume	cm^3
$\dot{V}$	volume flow rate	cm^3/h
V_m	molar volume	Ncm^3/mol
$X_{f,j}$	conversion factor of component	
$X_{r,j}$	conversion rate of component	
$Y_{gas,j}$	gas component yield	Nl_j/kg_{feed}
Y_C	yield of carbon formation	g_c/kg_{feed}
a, b	substance specific coefficient for Suave-Redlich-Kwong equation of state	
c_p	specific heat capacity at constant pressure	kJ/kg K
d	diameter	mm
f_i	specific fugacity	
f_i^0	standard fugacity	
m	mass	kg
$\dot{m}$	mass flow rate	kg/h

n	amount of substance	mol
$\dot{n}$	amount of substance flow rate	mol/h
p	pressure	bar
t	time	min
t_n	at time on reaction	min
x	component share of total amount of sample	%
z	stoichiometric coefficient	
z	compressibility factor	

Greek Symbols

α	parameter considering the deviation of molecules from ideal cubic form	
Δ	difference	
δ	differential	
λ	air to fuel ration	
ν	stoichiometric factor	
ρ	density	
ψ	porosity of catalyst bed	
η	efficiency	%
φ	fugacity coefficient	

Indices

area-%	ratio of area
C	carbon / atomic carbon
c	critical
cat.	catalyst
el.	electric
el.P	electric pump

H	atomic hydrogen
i	of reaction
j	of component
j	theoretical stage of column
l	Liquid product component
loss	losses
min	minimum
max	maximum
mix	mixing
n, m, z	stoichiometric coefficient
p	product component
R	of reaction
r	reduced
s	source
therm.	thermal
wt.-%	weight content
0	beginning of reaction time

Subscripts

0	standard conditions

Abstract

Due to decreasing supplies of fossil fuels and increasing environmental pollution, the introduction of a more fuel efficient electrical power system in aircraft applications is necessary. One possibility to improve the efficiency is to run the auxiliary power unit (APU), which provides electric energy on airplanes, with an efficient proton exchange membrane fuel cell system (PEMFC). The hydrogen for this concept can be provided by partial catalytic dehydrogenation (PCD) of Jet fuel stored onboard. The difference of this alternative thermochemical catalytic process to the more common reforming process is that no water is needed as a reaction partner. Therefore, no CO is generated, which would poison the catalyst in PEMFC. Other than gaseous hydrocarbons, no gaseous side products are expected. Beyond that, a high hydrogen purity of 98 vol.-% can be achieved. The partial conversion of jet fuel of about 10 to 15 % allows further use of the converted fuel in combustion processes on board. Since the composition of kerosene is very diverse, suitable reaction conditions for a process concept of the PCD of kerosene Jet A-1 have to be defined and the efficiency of the process has to be evaluated.

In this thesis, two different process concepts for PCD of jet fuel are developed and their efficiency is evaluated by process simulation. One process concept is designed to run with regular kerosene Jet A-1, which involves a desulfurization step of the jet fuel before the PCD to reduce catalyst deactivation by sulfur poisoning. Since the sulfur containing components in Jet A-1 are found in the higher boiling range of kerosene, the desulfurization is accomplished by thermal distillation of desulfurized Jet A-1 fractions by rectification. The second concept is designed to run with desulfurized kerosene which differs in its chemical composition from regular Jet A-1.

The first part of this thesis deals with the experimental characterization of the fuels. As the hydrogen yield, conversion of the fuel and product compositions highly depend on the composition of the hydrocarbon groups in kerosene, the detailed chemical composition of kerosene Jet A-1 was investigated and model components have been defined. These model components represent the hydrocarbon groups in the Jet fuel and they can be used for the design of model mixtures to experimentally investigate hydrogen yield, product composition, conversion rates, stability of the catalytic reaction and the reaction conditions. The catalyst used for the experimental investigation is platinum with tin on an aluminum oxide carrier.

The experimental results using the model components show, that the hydrocarbon group of cycloalkanes leads to high hydrogen yield and stable reaction conditions. On the other hand, n-alkanes lead to catalyst deactivation by carbon formation on the catalyst surface and side reactions, thus causing a decline of hydrogen purity of the product gas by evolution of gaseous hydrocarbons. In a next step, the previously defined reaction conditions from the model mixture

tests are applied to real kerosene. Due to the content of long chain hydrocarbons of up to 22 carbon atoms causing catalyst deactivation by carbon formation, the stability of this reaction is strongly reduced in comparison to the model mixtures. So far, a more suitable catalyst for more stable process conditions does not yet exist.

In the second part of the thesis, the experimental results of the model components and model mixture are used for modelling the two process concepts for PCD in the process simulation. To achieve the highest possible system efficiency, a heat and material integration of the two process concepts is accomplished within the process simulation. For the definition of the system efficiency, the hydrogen yield is a key figure since it is the output of the process. The electric efficiency of both process concepts includes system losses of the fuel cell and product gas conditioning. With the experimentally investigated hydrogen yields of the model mixtures, a system efficiency for the process concept, including the desulfurization of the Jet fuel, of 17% is achieved. The process concept working with desulfurized Jet fuel has no additional energy demand for the desulfurization and achieves for system efficiency a value of 20.7%.

To compete with a regular gas turbine APU, with average efficiency of 15 to 18%, the fuel cell APU system provided with hydrogen from PCD of kerosene has to be advanced to higher hydrogen yield. This could be accomplished by the development of design fuels for aircraft applications which suit PCD conditions and catalyst development. The results in this work can provide the boundary conditions for these investigations.

1 Introduction

Today's transportation systems are challenged with an ever decreasing supply of fossil fuels as well as political and social demand for decreasing environmental pollution with combustion products. The aviation sector is a rapidly growing industry, whose release of combustion products has a high impact on the environment [1]. Next to CO_2 emissions which influence our climate, hazardous air pollutants such as CO, NO_x, SO_x and volatile organic compounds (VOCs) have a direct impact on the atmosphere and environment [2] [3]. The ambition to reduce the sources of combustion products follows several intermediate and long term developments. The release of SO_x from jet fuel combustion can be decreased by more strict Jet fuel restrictions. This is leading the efforts of fuel desulfurization and the utilization of ultra –low- sulfur kerosene (ULSK) with less than 15 ppmw sulfur, instead of the 300 ppmw average today [4], [5], [6], [7]. The complete exchange of fossil fuels in aviation could be accomplished by the utilization of Fischer-Tropsch-Kerosene, produced from biomass, waste industrial carbon sources, or even atmospheric CO_2, [8], [9], [10], [11].

Hydrogen is treated as the cleanest source for energy production by combustion in fuel cells, [12], [13]. The introduction of fuel cell systems in aviation for propulsion or on board auxiliary power units (APU) promises higher efficiencies, and therefore less emissions than state- of-the- art gas turbines [14], [15]. The gas turbine APU is providing electric power by kerosene combustion for the aircraft during ground operation. Approximately 25 % of the total emissions are produced during ground operations, including 86 % of the NO*x* emissions. In the intermediate term perspective, the introduction of a less fuel consuming technology is needed. Hydrogen powered APU systems with proton exchange membrane fuel cells (PEMFC) are part of this development, [16], [17]. The key challenge is the provision of hydrogen to the APU fuel cell system, which could be accomplished by liquid or pressure tanks. This has a massive influence on the aircraft construction, safety and weight issues, as they lead to a higher fuel consumption, which declines the efficiency of the fuel cell system [18]. A different approach is the storage of hydrogen by liquid hydrocarbons [19]. Possible reaction systems to provide hydrogen on board from liquid hydrocarbons is steam reforming, auto thermal reforming or partial oxidation, [20], [21], [22]. The kerosene stored on board can be turned over to a hydrogen rich product gas, which has to be cleansed of CO to be provided to a PEMFC. Another promising reaction system is the catalytic dehydrogenation of hydrocarbons. In particular, the high selectivity to hydrogen production from dehydrogenation of cycloalkanes to aromatic hydrocarbons shows potential to high hydrogen output and product gas purity [23], [24], [25]. The advantage of dehydrogenation of hydrocarbons over reforming reactions is that no water or oxygen is needed as reaction partner. As a result, no CO is generated, which would poison the catalyst in PEMFC. With dehydrogenation of liquid hydrocarbons, high

hydrogen purity is expected with no other gaseous side products other than gaseous hydrocarbons. The jet fuel stored on board contains cycloalkanes and other hydrocarbon groups which can be used as hydrogen storages, [26]. By partial catalytic dehydrogenation (PCD) of Jet fuel, hydrogen can be provided to the fuel cell APU system. Since the hydrocarbons are only partially dehydrogenated, the fuel can be still used for further combustion processes.

The catalyst used for dehydrogenation is usually Pt with a different carrier material, which could be γ-Al_2O_3 with precursors to reduce the acidity of the surface [27], [28], [29]. However, Pt catalysts are not resistant to the sulfur compounds in the kerosene. The sulfur would lead to catalyst deactivation by the formation of PtS in short period of time, which would not be sufficient for a robust APU fuel cell system. Therefore, the APU process concept should involve a desulfurization process or even be provided with ULSK to reduce catalyst deactivation by sulfur poisoning.

1.1 Process Concepts for Fuel Cell APU

In this work, two process concepts are developed, each working with different input specifications. The reference concept uses ultra- low- sulfur kerosene (ULSK), which is desulfurized kerosene. Fig. 1.1 shows the scheme of the reference concept.

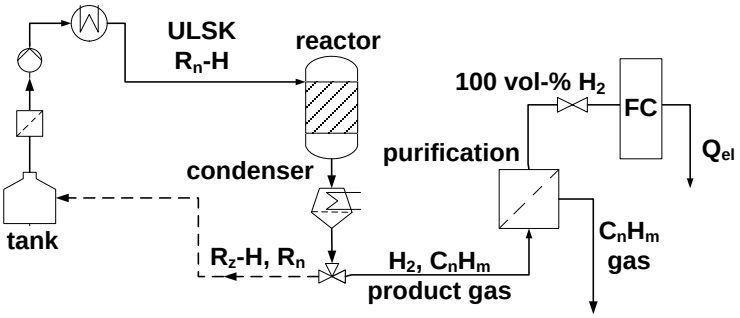

Fig. 1.1 - process scheme of the reference concept

For dehydrogenation of a desulfurized kerosene (ULSK), the reference concept includes a feed conditioning, where the kerosene has to be pressurized and heated up to process conditions. After reaching the reactor where the partial catalytic dehydrogenation takes place, the product stream is cooled down and condensed. While the condensable products can be reused in combustion for providing the enthalpy demand of the system and in the propulsion of the aircraft, the gaseous products are purified by separating hydrogen from uncondensed hydrocarbons. Due to the partial pressure of the product gas components, longer chain hydrocarbons are still present in the hydrogen rich product gas after condensation. Therefore, purification is necessary, as uncondensed hydrocarbons can reduce the efficiency of the PEMFC by occupation of the membrane [30]. The purification is accomplished by pressure

swing adsorption (PSA). The system pressure of the PSA dictates to some extent the pressure of the concept, since pressurizing the liquid input stream would demand less energy than pressurizing the product gas stream for the PSA. The pure hydrogen can be used to run the polymer membrane fuel cell (PEMFC) system.

The second process concept runs with regular sulfur containing Jet A-1 kerosene, which has to be desulfurized by fractionation before reaching the PCD reactor (Fig. 1.2).

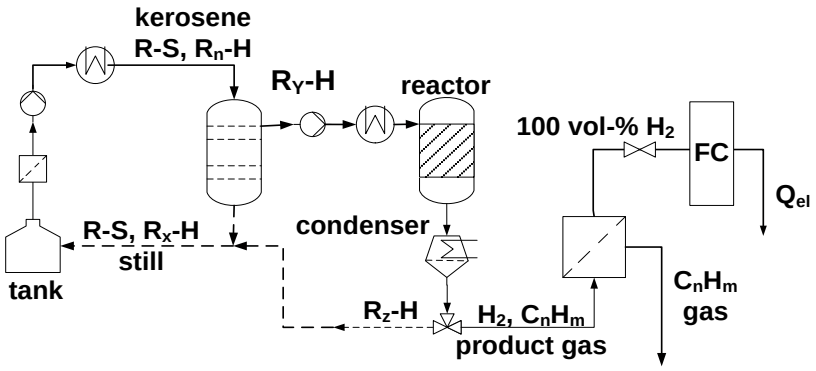

Fig. 1.2 - process scheme of process concept with fractionation

The process elements downstream of the dehydrogenation reactor are the same as with the reference concept. The difference is made by the kerosene fractionation, where a certain percentage of the feed flow is fractionated by a rectification process for desulfurization. The choice for fractionation for desulfurization results from the investigations made in preparation of this thesis [31]. The desulfurized fraction is dehydrogenated in the reactor. The still of the rectification can be reused for propulsion, together with the dehydrogenated Jet A-1 fraction. Since only a certain mass percentage of the kerosene is used for dehydrogenation, a corresponding amount of Jet A-1 has to be distillated in the rectification process. This requires that more kerosene, in comparison to ULSK with the reference concept, has to be preheated and evaporated for the rectification to achieve the required fraction for the dehydrogenation. Therefore, more heat demand is required with the process concept with rectification, leading to a reduction of the process efficiency. The integration of heat streams is therefore important to reduce the influence of the heat demand of the rectification. The total amount of Jet A-1 depends on the mass percentage of the chosen Jet A-1 fraction and the hydrogen yield of the dehydrogenation process.

Both process concepts are investigated in this work for evaluation of the system efficiency. This evolution is accomplished by process simulation, where the heat and material integration is designed for both concepts. The PCD of ULSK and Jet A-1 fractions is studied experimentally. The investigated hydrogen yields are used for modeling the PCD reactor in the process simulation. The goal is to provide a statement about the potential of PCD of jet fuel for a APU fuel cell system.

1.2 Catalytic Dehydrogenation of Hydrocarbons

The composition of kerosene is very complex and contains many different types of hydrocarbons, which differ in their chemical structure. The dehydrogenation reactions and selectivity to hydrogen is strongly dependent on the hydrocarbon group of a kerosene component. This complexity is a challenge when it comes to reaction simulations in a complex mixture. In order to identify possible product composition and hydrogen yield dependent on specific hydrocarbons composition of the kerosene, the different hydrocarbon groups have to be investigated separately.

In general the dehydrogenation of hydrocarbons is an endothermic reaction with increasing amount of substance (mol), Eq (1.1).

catalytic dehydrogenation: $$C_nH_m \rightleftarrows C_nH_{m-2x} + xH_2 \qquad \Delta H_R > 0 \qquad (1.1)$$

The thermodynamic equilibrium constant K for the component i is calculated by the van't Hoff equation (Eq. 1.3), which is derived from the Gibbs standard enthalpy of reaction ΔG_R^0 (Eq. 1.2) with T_0=298.15 K and p_0= 1 atm. For different reaction temperatures and with the heat capacity $c_{p,i}^0$, the reaction enthalpy $\Delta H_R^0(T)$ is calculated by Eq. (1.4). With the endothermic reaction, the equilibrium constant K is increasing with increasing temperature.

Gibbs standard enthalpy of reaction $$\Delta G_R^0 = -RT \cdot \sum_i \ln \left(\frac{f_i}{f_i^0} \right)^{\nu_i} = -RT \cdot \ln K \qquad (1.2)$$

van't Hoff equation $$\frac{d\ln K}{dT} = \frac{\Delta H_R^0(T)}{RT^2} \qquad (1.3)$$

standard enthalpy of reaction $$\Delta H_R^0(T) = \Delta H_R^0(T_0) + \int_{T_0}^{T} \sum \nu_i c_{p,i}^0 dT \qquad (1.4)$$

fugacity $$f_i = p_i \cdot \varphi_i \qquad (1.5)$$

For ideal gas law, the fugacity coefficient is $\varphi_i = 1$ (Eq. (1.5)), which leads to a decreasing conversion rate in the gas phase reaction of the educt with increasing partial pressure p_i and increasing number of molecules on the product side [32], .

Dependent on the component, the thermodynamic equilibrium conversion differs strongly. The process simulation tool Aspen plus provides databases of physical properties for an extensive number of hydrocarbons. Fig 1.3 presents the calculated equilibrium conversion of different

components, which represent hydrocarbon groups contained in kerosene by variation of the reaction temperatures.

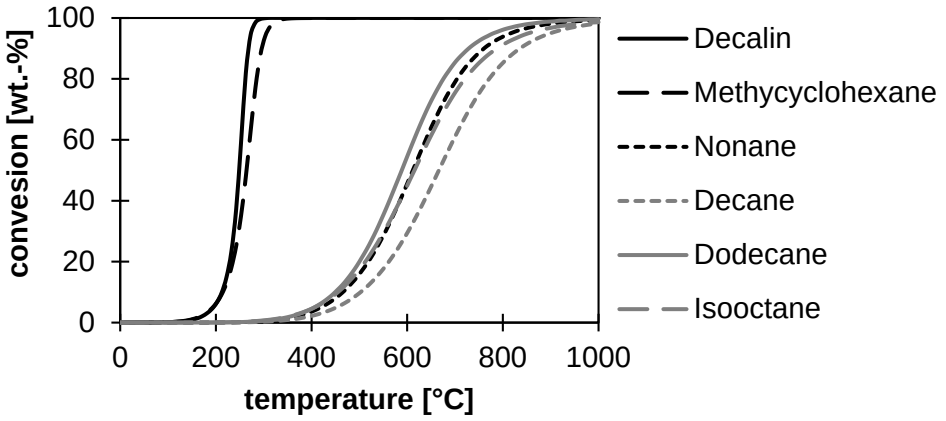

Fig. 1.3 - thermodynamic equilibrium conversion of hydrocarbons in Jet fuel over temperature variation at 1 bar pressure

As expected, with increasing reaction temperature the equilibrium conversion of any hydrocarbon is increasing. The components decalin and methylcyclohexane, which belong to the hydrocarbon group of cycloalkanes show a much higher equilibrium conversion at any given temperature than the components which belong to the hydrocarbon groups of n-alkanes and iso-alkanes. Kerosene also contains a significant amount of aromatic hydrocarbons, but since the aromatic ring cannot further dehydrogenate, these components are expected to be rather inactive. Only alkane side branches from derivatives of benzene and multi core aromatic hydrocarbons can dehydrogenate. As an example, the dehydrogenation of ethylbenzene to styrene is a common industrial process, which is operated under vacuum and temperatures between 540 to 650°C [33], [34]. Since the process concepts presented in chapter 1.1 are considered to be operated under increased pressure, the equilibrium conversion with increasing pressure is of interest. Fig. 1.4 presents the equilibrium conversion of the cycloalkane methylcyclohexane and the n-alkane decane at different reaction temperatures and variations of pressure from 1 to 30 bar.

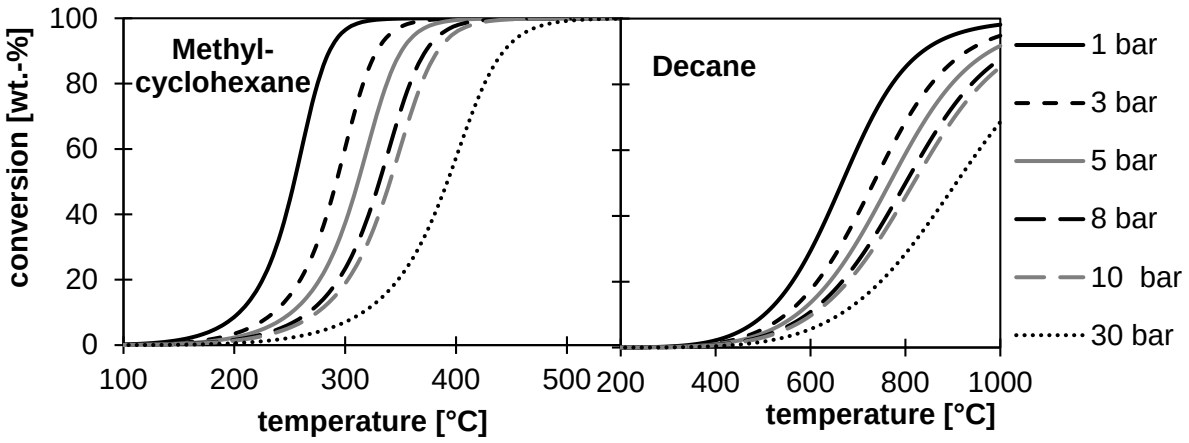

Fig. 1.4 - thermodynamic equilibrium conversion of methylcyclohexane and decane at different temperature and pressure

From the equilibrium conversion under pressure, it can be derived that with increasing pressure, the conversion to hydrogen in the PCD of kerosene will decrease. For the process concepts, it is of interest to define suitable reaction conditions which achieve a high hydrogen output by high conversion rate and also suit the pressure demand of the product gas conditioning by PSA. Though, the reaction conditions for the PCD of jet fuel cannot be chosen arbitrarily. With increasing temperature, the chemical bonds in hydrocarbons are under thermal stress and can lead to cracking and radical formation. The gaseous cracking products reduce the product gas quality. Formation of radicals enhance carbon formation, which can occupy the catalyst surface and lead to temporary deactivation [35], [36]. The investigation of suitable reaction conditions for PCD of ULSK and Jet A-1 fractions is a key issue for the evaluation of the process concepts. Furthermore, the reaction products and the influence of the hydrocarbon groups on each other in the complex mixtures are of interest to the hydrogen output, product gas quality and stability of the reaction progress.

1.3 Objectives of this work

In this thesis, the partial catalytic dehydrogenation of jet fuel is experimentally investigated and evaluated in a process simulation by its system efficiency, respectively electric efficiency and potential for the application in process concepts assigned for APU fuel cell systems. In this context, the chemical composition and physical properties of ULSK and Jet A-1 have to be analyzed in detail first. Further, the chemical composition of desulfurized Jet A-1 fractions from rectification are analyzed for the process concept with desulfurization by rectification. The hydrocarbon group composition of the fuels is used to develop simplified model mixtures which can represent the chemical composition of the analyzed fuels. The model mixtures are used both for detailed experimental investigation of the dehydrogenation of hydrocarbon groups in kerosene, and their influence on each other. Further, the experimental results of the model components and model mixture are used for modelling the two process concepts for PCD in the process simulation.

In the experimental part, the model components and model mixtures are used to identify the hydrogen yield, reaction products and possible side reactions, which cause cracking leading to a reduced product gas quality and carbon formation, ultimately causing catalyst deactivation. Further, the experimental results are used to identify suitable reaction conditions for the process concept with rectification and the reference concept. By adding sulfur containing components to the model mixtures, the experimental results can be compared with the

dehydrogenation of real fuels. This way, the method of using of simplified model mixtures for evolution of the process concept is justified.

The second part of the thesis deals with the design of the process models for both concepts. The conversion rates of the model components in the model mixtures and the liquid and gaseous product composition are used to identify simplified reactions for reactor design in the process model. The calculated heats of reaction at defined reaction conditions are used for the calculation of the heat demand of the dehydrogenation reactor. The fuel cell is not part of the simulation but the potential efficiency of PEMFC is used to calculate the system efficiency, while the thermal efficiency of the process concepts is the efficiency of the pure hydrogen production without electric transformation. To achieve the highest possible system efficiency of the process, a heat and material integration of the two process concepts is accomplished within the process simulation. For the definition of the system efficiency, the hydrogen yield is a key figure, as it is the output of the process. For both process concepts the system efficiency includes system losses of the fuel cell and product gas conditioning.

With the results of this work, the potential and conditions of the partial catalytic dehydrogenation of kerosene for APU fuel cell system can be estimated in comparison to a common gas turbine APU. Furthermore, the requirements of the jet fuel for sufficient hydrogen output from dehydrogenation is provided.

2 Hydrogen Production from Liquid Fuels

The production of hydrogen from liquid fossil or renewable fuels has the goal to provide fuel cell systems with hydrogen for stationary or mobile application. The liquid fuel is treated as a carrier and storage for hydrogen, as it is readily available and distribution systems already exist. Other possible hydrogen storage systems, especially for mobile applications, are pressure or liquid hydrogen tanks, metal hydrides, or liquid organic hydrides, which have the highest volumetric storage capacity for hydrogen [19], [37], [38], [39]. The research on hydrogen production from liquid fuels concentrates on mobile applications for propulsion, or APU systems where the fuel can be stored on board [40], [41]. Sources of renewable fuels for hydrogen production are Fischer-Tropsch- diesel or kerosene and Bioethanol for street vehicles or aviation. The production and utilization of synthetic fuels which can be designed for the specific purposes is still in progress. [42], [43], [40]. Therefore, the intermediate goal of fuel efficient systems utilizing fossil fuels is also part of the development.

The most common processes for hydrogen production from liquid fuels are steam reforming, partial oxidation or the combination of both to autothermal reforming. Reforming of long chain hydrocarbons is usually performed with different types of catalysts, but plasma induced steam reforming is also researched [44]. All three processes have in common that a hydrogen rich product gas can be produced, which has to be conditioned and cleaned of CO before use in PEMFC. The process of dehydrogenation has been common in industrial crude oil production for increasing octane rating of the fuels by increasing the content of aromatic hydrocarbons [45]. Other dehydrogenation processes are directed at the production of alkanes as preparation for polymer production. The development of dehydrogenation for the goal of hydrogen production is in the development stage and mostly directed at liquid hydrogen carriers. In chapter 2.1 to 2.3, a brief review of state of the art and state of development processes of hydrogen production from liquid fuels is presented.

2.1 Reforming of Liquid Fuels

The reforming of liquid fuels is a catalytic thermo-chemical process. The hydrocarbons of fuel are reacting with steam and/or oxygen to a hydrogen rich product gas and can be converted completely. Other gaseous products are CO_2, CO, CH_4 and H_2O. Depending on the reforming process and the defined reaction conditions, the concentration of hydrogen and other gaseous products vary. With steam reforming with water vapor, an endothermal reaction, a hydrogen concentration of 55 vol.-% up to 75 vol.-% can be expected. With exothermal partial oxidation, about 25 vol.-% of hydrogen can be expected with liquid fuels [46], [47]. The combination of both processes is the autothermal reforming, with an expected hydrogen concentration of 40 vol-%. All three processes have in common that carbon and soot formation can lead to

catalyst deactivation by occupation of the actives sites. A reaction leading to carbon formation is the Boudoard-reaction, which as a dissociation of CO. Another reaction is methane cracking, which is leading to hydrogen evolution and carbon deposit [48]. The reaction equation and standard enthalpy of reaction ΔH_R^o (T^0=298 K, p^0=1 atm) are presented in Eq. (1.6) – (1.7)

Boudoard-reaction: $$2CO \rightleftarrows C + CO_2 \qquad \Delta H_R^o = -172 kJ/mol \qquad (2.1)$$

methane cracking: $$CH_4 \rightleftarrows C + 2H_2 \qquad \Delta H_R^o = 75 kJ/mol \qquad (2.2)$$

At temperatures above 700°C, methane cracking is leading to the formation of carbon deposits. With decreasing temperature, the Boudoard-reaction is the cause of catalyst deactivation by soot formation [49]. The most common catalysts used for all three reforming processes are Ni, Pt, Ru, Pd, Rh on different types of support but mostly γ-Al_2O_3. Different type of promoters, as an example K or Na, and second metal catalyst, which could be Co or Mo are used to decrease the formation of carbon and increase sulfur resistance in case of fossil fuel feed streams [50], [51]. Hereafter, the three reforming process are described briefly.

Steam Reforming

The conversion of long chain hydrocarbons with steam to synthesis gas is usually accomplished at a reaction temperature of 700°C to 850°C and atmospheric pressure. It is an endothermic reaction and needs an external heat source [52]. The steam reforming reaction (Eq. (1.8)) is accompanied by two other reactions which occur simultaneously.

steam reforming: $$C_nH_m + nH_2O \rightleftarrows nCO + \left(n + \frac{m}{2}\right)H_2 \qquad \Delta H_R > 0 \qquad (2.3)$$

methanation: $$CO + 3H_2 \rightleftarrows CH_4 + H_2O \qquad \Delta H_R^o = -206.10 kJ/mol \qquad (2.4)$$

water-gas-shift: $$CO + H_2O \rightleftarrows H_2 + CO_2 \qquad \Delta H_R^o = -41.15 kJ/mol \qquad (2.5)$$

The methanation reaction (Eq. 2.4)) consumes hydrogen and can be suppressed to some extent by a sufficient steam to carbon ration S/C of 2.5 to 6, which depends on the optimization for the type of feed [53]. The second simultaneous reaction is the water-gas-shift reaction WGS (Eq. 2.5)). To increase the hydrogen output, the steam reforming reactor is followed by a second WGS reactor, which is operated at two stages with high temperature WGS of up to 550°C and a low temperature WGS of up to 250°C. The hydrogen concentration can be increased with this operation mode by up to 80 vol.-% [54], [55]. To remove CO completely from the product stream, further gas conditioning is needed. Pressures swing adsorption PSA, membrane process, preferential methanation and catalytic partial oxidation of CO are common processes to remove CO from hydrogen rich product gas [56], [57], [58], [59], [60].

Partial Oxidation

The understochiometric combustion or partial oxidation POX of long chain hydrocarbons can be accomplished in two different ways The thermal partial oxidation TPOX is carried out without a catalyst with sulfur containing fuels at reaction temperatures above 1200°C. The catalytic partial oxidation CPOX is used at reaction temperatures from 900°C to 1000°C [43], [48], [61]. The hydrogen concentration depends on the chosen carbon to oxygen ratio C/O<0. Eq. (2.6) presents the reaction equitation for both types of POX.

partial oxidation: $$C_nH_m + \frac{n}{2}O_2 \rightleftarrows nCO + \left(\frac{m}{2}\right)H_2 \qquad \Delta H_R < 0 \qquad (2.6)$$

For product gas conditioning, the CPOX reactor can be followed by a WGS reactor to achieve higher hydrogen concentration and reduce CO for fuel cell application [57].

Autothermal Reforming

The combination of steam reforming and POX is the autothermal reforming. The heat demand for the steam reforming reaction is provided internally by an understochiometric supply of oxygen to the feed. The overall reaction equation of autothermal reforming is shown in Eq. (2.7)

autothermal reforming: $$C_nH_m + xO_2 + (2n-2x)H_2O \rightleftarrows nCO + \left(\frac{m}{2}\right)H_2 \qquad \Delta H_R \approx 0 \qquad (2.7)$$

The reaction is obtained at a temperature of 850°C to 900°C. The methanation reaction and WGS reaction are also part of the reaction system. The same as with the other two reaction systems, CO has to be removed from the product gas with a WGS reactor stage and further gas conditioning [52].

2.2 Industrial Process of Catalytic Dehydrogenation of Hydrocarbons

Catalytic dehydrogenation of hydrocarbons in industrial processes has the goal to produce specific dehydrogenated hydrocarbons for refinement of fuels, or the preparation of hydrocarbons for further process steps, for instance, the production of polymers. The desired product components are alkanes and aromatic hydrocarbons [62]. The evolving hydrogen in these industrial processes is a side product, and is removed from the product stream. Dependent on the production process, hydrogen is recycled in the system to increase hydrogen partial pressure for suppressing carbon formation [63]. The dehydrogenation processes are highly endothermic and the heat demand of the reaction is either provided externally with burners or by internal regeneration of the catalyst. By combustion of the carbon deposit on the catalyst, the heat is provided to the reaction in a semi adiabatic process control. The catalyst used for these processes is in most cases Pt on γ-Al_2O_3 with a second metal catalyst Ir, Rh, or Re. or as precursor Sn and Ge. Some processes also work with Cr_2O_3 or Mg and Zn [57].

2.2.1 Catalytic Reforming of Naphtha

In petroleum refining, the production of high quality gasoline for automobiles requires an increased content of unsaturated hydrocarbons and branched alkanes for suitable combustion properties. The feedstock naphtha has a content of up to 70 % of n-alkanes and a maximum of 20 % of aromatic hydrocarbons. After the catalytic reforming, the content of aromatic hydrocarbons is increased up to 60 %. The dehydrogenation of n-alkanes to aromatic hydrocarbons leads over dehydrocyclization to cycloalkanes. Eq. (2.8) presents the reaction equation of dehydrogenation of n-heptane to toluene.

$$\underset{\text{n-heptane}}{C_7H_{16}} \rightleftarrows \overset{\text{dehydrocyclization}}{\underset{\text{methylcyclohexane}}{C_7H_{14} + H_2}} \rightleftarrows \overset{\text{dehydrogenation}}{\underset{\text{toluene}}{C_7H_8 + 4H_2}} \qquad (2.8)$$

The dehydrogenation can also lead to the formation of radical aromatic hydrocarbons by carbon deposit on the catalyst surface, which reduces the lifetime of the catalyst. An increased hydrogen partial pressure in the system can suppress the formation of carbon, but shifts the thermodynamic equilibrium of the reaction to the educts. Simultaneously with dehydrogenation, the evolving hydrogen is consumed in the hydrocracking reaction. Long chain alkanes are cracked to shorter chain alkanes, which increases the gasoline output. Further isomerization leads to an increased content of branched alkanes [64]. In Eq. (2.9) the reaction equation of hydrocracking with isomerization is presented.

$$\underset{\text{n-decane}}{C_{10}H_{22} + H_2} \rightleftarrows \overset{\text{hydrocarcking and isomerisation}}{\underset{\text{hexane/isohexane}}{C_6H_{14}}} + \underset{\text{n-butene}}{C_4H_{10}} \qquad (2.9)$$

The recycling of hydrogen within the process is a compromise between high selectivity towards dehydrogenation products and increased life time of the catalyst due to declined carbon deposit. The catalytic reforming of naphtha is operated at 500°C and at a system pressure between 3.5 to 25 bar. The reactions are carried out in a semiregenerative process or in a continuous catalyst regeneration reformer or, as third option, in the cycle process [63], [65].

2.2.2 Production of light Alkenes

For the production of polymers and rubber, short chain n-alkanes, between three to five carbon atoms, are dehydrogenated to n-alkenes. The feedstock is a pure alkane, which is dehydrogenated over a catalytic bed. The evolving hydrogen is either separated and recycled to reduce carbon formation on the catalyst, or in case of the oxidative dehydrogenation, the hydrogen is combusted with air to water and separated from the product stream [66]. Eq. (2.10) to (2.11) are presenting the dehydrogenation and oxidative dehydrogenation of propane to propene, respectively.

dehydrogenation: $$C_3H_8 \rightleftarrows C_3H_6 + H_2 \qquad \Delta H_R^0 = 124.4\,kJ/mol \qquad (2.10)$$

oxidative dehydrogenation: $$nC_3H_8 + \frac{n}{2}O_2 \rightleftarrows C_3H_6 + H_2O \qquad \Delta H_R^0 = -447.7\,kJ/mol \qquad (2.11)$$

The dehydrogenation is becoming more important to the chemical industry since the development of new processes allowing higher selectivity and less catalyst deactivation by carbon formation with a hydrogen partial pressure in the system. In the following, the main processes for dehydrogenation of alkanes to alkenes are described briefly. The dehydrogenation process is carried out in a temperature range between 550°C to 650°C, and a pressure range of 1 to 3.5 bar. Fig. 2.1 presents the schemes of the most common industrial processes for the dehydrogenation of light n-alkanes and the required catalyst.

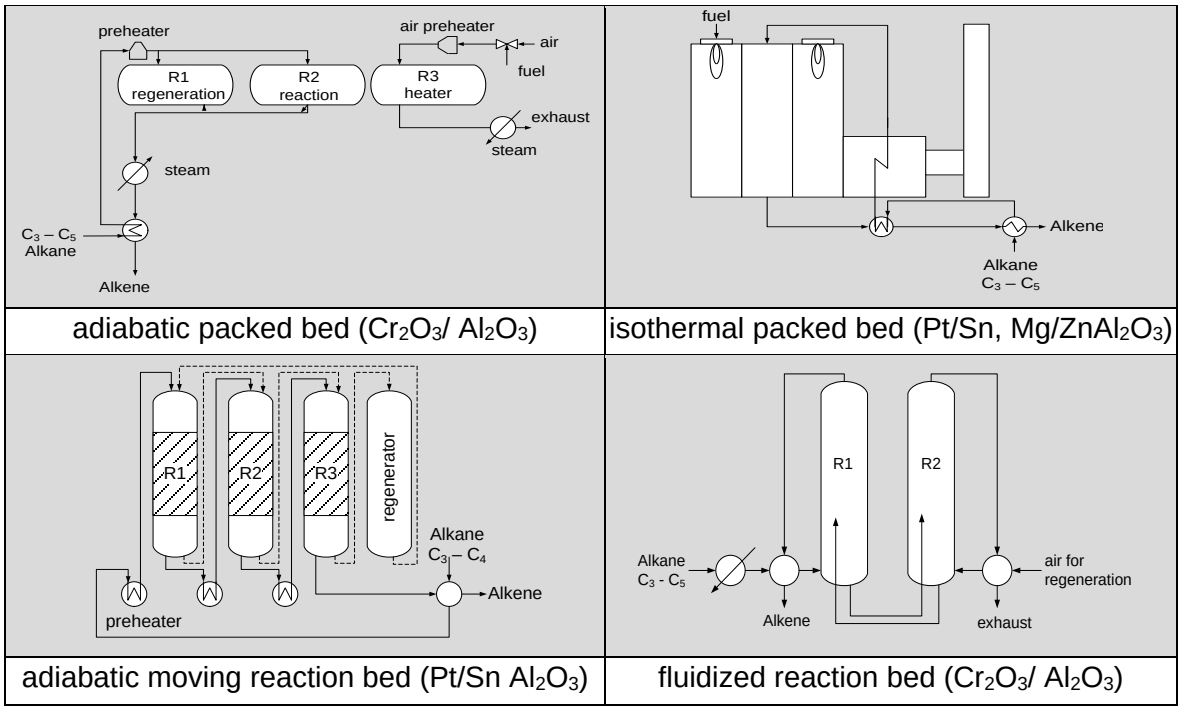

adiabatic packed bed (Cr_2O_3/ Al_2O_3) | isothermal packed bed (Pt/Sn, Mg/$ZnAl_2O_3$)

adiabatic moving reaction bed (Pt/Sn Al_2O_3) | fluidized reaction bed (Cr_2O_3/ Al_2O_3)

Fig. 2.1 schemes of main industrial processes for the dehydrogenation of light n-alkanes

The Cartofin process is operated as adiabatic packed bed reactor (top left) .The mode of the alternating reactor beds is switched from reaction to regeneration and heating. The energy demand for the endothermic reaction is provided by combustion of the carbon deposit on the catalyst during regeneration and heating with steam during the heat phase. The steam activated reforming is a tubular reactor system, which is provided with heat by burners (top right) similar to steam reforming. For regeneration, the carbon deposit is combusted with a steam/air mixture. The Oleflex process is a continuous catalyst regeneration process (bottom left). The catalytic bed is moved through several reactors were dehydrogenation is carried out. Between every reactor the catalyst bed is reheated. At last, the bed is regenerated and reheated before it reaches the first reactor. Continuous regeneration can also be accomplished in a dual fluidized bed reactor system (bottom right). The heat demand of the reaction is

provided by the heated catalyst bed in the regenerator, which is moved between dehydrogenation and regeneration reactor [57], [67], [68], [69].

2.3 Catalytic Dehydrogenation for Hydrogen Production

The research on catalytic dehydrogenation of hydrocarbons for hydrogen production focuses on detailed component studies and catalyst development. The research on dehydrogenation of specific hydrocarbon components directs on chemical hydrogen storage for mobile applications [23]. The hydrocarbon group of cycloalkanes is the most frequently chosen component group for dehydrogenation and hydrogenation for storage purposes [70]. The cyclohexane, decalin and its derivate show high conversion and selectivity to hydrogen with little carbon formation, and therefore stable reaction conditions [71], [72]. Detailed kinetic studies are available for methylcyclohexane and decalin, since the number of reactions and products is limited in comparison to other hydrocarbon groups for instant alkanes, where many side reactions occur [73], [74], [75]. In the doctoral thesis of M. Usman, a simulated process design of an on board dehydrogenation system is presented with the complete replacement of gasoline by methylcyclohexane [76].

Further fields of research for the hydrogen production by dehydrogenation of hydrocarbons concentrate specifically on the development and design of the reactor and the reaction conditions respectively. Since the dehydrogenation of hydrocarbons groups other than cycloalkanes shows complications due to cracking and carbon formation, most research concentrates on reactor development and adjustment of operation conditions for cycloalkanes. The liquid film type reactors work with low reaction temperature in the limits of the boiling range of the tested component. The reactors either work in batch mode, where the surface of the catalyst is covered with a liquid feed film or by liquid spray of the feed on the hot catalyst surface [77], [78], [79], [80], [81] . Those reactors allow mild reaction conditions with pure hydrogen evolution but with little conversion, and therefore little hydrogen output. Another reactor design which concentrates also on high hydrogen purity but in gaseous conditions and under pressure are the membrane reactors. The catalyst is impregnated on palladium composite membranes or zeolite membranes. By separating the product hydrogen from the feed stream, the reaction equilibrium is shifted to the product side. But due to thermal stressing carbon formation accrues and the permeability of the membrane is impaired [82], [83]. The membrane reactor is also tested for the production of aromatic hydrocarbons and alkanes with similar complication of catalyst deactivation and decline of porosity for hydrogen separation [84], [85].

The research on dehydrogenation of other hydrocarbon groups, which are aromatic hydrocarbons and alkanes, concentrates on the development of the process, the catalysts or

reactor design for the production of chemical components for industrial processes [86], [87]. The process development of the dehydrogenation of complex mixtures as real fuels or model mixtures representing fuels is a new research field. For experimental evaluation of the dehydrogenation of hydrocarbon mixtures, the reactors are built as catalytic fixed bed reactors under heterogeneous gas- solid conditions. In the following, resent research on the dehydrogenation of hydrocarbon mixtures is briefly summarized.

Wang et al. [26] chose a simplified six component model mixture representing Jet A, which is equivalent to European Jet A1, for experimental dehydrogenation. Although, the mixtures have no basis on real fuel hydrocarbon group composition. The chosen reaction conditions of 500°C and atmospheric pressure on Pt/ ɣ-Al_2O_3 are defined from previous experimental evaluation of decalin dehydrogenation. Deactivation of the catalyst and formation of gaseous hydrocarbons lead to a reduction in hydrogen yield and product gas quality over reaction time. No further research is accomplished for detailed product composition or optimization of the model mixture or process conditions. Lucarelli et. al. [88], [89] have tested the dehydrogenation of Jet A-1 model mixture with 5 model components which also do not refer to any average hydrocarbon composition of jet fuel. The main field of research is the development of the catalyst, which is Pt/ɣ-Al_2O_3 with several different precursors and different preparation methods. The surface area of the catalyst was examined after dehydrogenation to note any changes due to the occurring reactions. The reaction temperature is varied between 350°C and 550°C and system pressure of 5 bar and 10 bar and co feed of hydrogen to decrease catalyst deactivation by carbon deposit. The deactivation of the catalyst leads, in spite of the hydrogen co feed, to a reduction of hydrogen output and product gas quality. The conversion of feed components and the content of gaseous hydrocarbons was examined but not the product composition. Recycling of hydrogen is a method used in refining to extend catalyst life, but the method consumes hydrogen and decreases the output and system efficiency of a dehydrogenation concept providing a fuel cell systems. Resini et al. and Reyes-Carmona et al. [90], [91] have in fact tested the dehydrogenation of real Jet fuel with the objective of catalyst development. The reaction conditions are defined with 350°C and 5 bar respectively 450°C and 10 bar and co feed of hydrogen to the reactor in both cases. Sulfur poisoning and carbon deposit lead to catalyst deactivation and a reduction of hydrogen output.

In summary, the research done so far on dehydrogenation of complex mixtures concentrates on catalyst development. The development of the dehydrogenation process or the detailed research of product components and the influence of the different feed components on one another is missing, but would also be significant for catalyst development. The scope of this thesis is to provide the methods and results for the process development of partial catalytic dehydrogenation of kerosene.

3 Kerosene

With over three hundred different detectable components, the chemical composition of kerosene is very complex. The jet fuel type used in this work is Jet A-1, which is commonly used in aviation in Europe. The properties of Jet A-1 are defined in world jet fuel specifications and are mostly physical properties like density, flash point, freezing point, viscosity, etc.[92].

The chemical composition of Jet A-1 varies and depends on the origin of the crude oil which it was produced from. Still, the composition of hydrocarbon groups and carbon atom number (Cn) are very similar owing to the required physical properties. Some chemical specifications are defined, however, as the physical properties of Jet A-1 depend on them. The content of Alkenes is limited to 2 vol.-% due to their chemical reactivity and thermal instability, which reduce the chemical stability during storage [93]. The content of aromatic hydrocarbons is limited to 25 vol.-% to avoid soot formation during combustion [92]. Since jet fuel is produced from crude oil, it always has components containing sulfur. The amount of sulfur allowed in Jet A-1 is 3000 ppmw. The average content is 500 ppmw. The components containing sulfur are usually found in the higher boiling range of kerosene. They are mostly identified as aromatic or polyaromatic hydrocarbons. A representative sulfur component is dibenzothiopen, which will be used in the experimental work to investigate the influence of sulfur on the dehydrogenation catalyst [94]. Due to the negative influence of sulfur on the dehydrogenation catalyst, two different Jet fuels are used for the different variations of the process concept. The first is regular Jet A-1 with 230 ppmw sulfur content, which has to be treated in a desulfurization step before entering the dehydrogenation reactor. This desulfurization is carried out as thermal fractionation by rectification. Therefore, the sulfur content of the desulfurized fraction depends on the fraction distilled for dehydrogenation. The second Jet A-1 used in this work is named ultra-low- sulfur kerosene (ULSK), which is already desulfurized during refinery production by hydro desulfurization and contains 3 ppmw sulfur. The chemical composition differs by 25 to 30 % from the regular Jet A-1, but is still within jet fuel specification.

The jet fuel used in this work is taken from the same batch for all experimental work, as the chemical composition is important to the dehydrogenation reaction. The chemical complexity of Jet A-1 leads to diverse reactions and products that can appear in dehydrogenation. To learn about how the composition of Jet fuel influences the hydrogen yield, side reactions and product composition from partial catalytic dehydrogenation, a detailed knowledge of the Jet A-1 composition used in this work is necessary. Further, for evaluating the process concept with process simulation, dehydrogenation reactions and side reactions have to be introduced to calculate the heat demand of the reactor. Therefore, a method for analyzing complex fuel composition with gas chromatography is performed. For the detailed evaluation of the dehydrogenation reaction, model mixtures of ULSK and fractionated Jet A-1 are developed.

These model mixtures are used to experimentally investigate the influence of specific components groups in fuel on the hydrogen yield and side products, as well as to find suitable reaction conditions for the model mixtures and jet fuel.

3.1 Methodology of Kerosene Analysis

Kerosene Jet A-1 is a multi- component mixture of different hydrocarbons, with a range of carbon chains lengths of 6 to 22. Due to the diversity of the structural formulas of the hydrocarbons, the composition of the jet fuel is arranged in hydrocarbon groups, which includes cycloalkanes and n-alkanes, iso-alkanes and aromatic hydrocarbons. For partial catalytic dehydrogenation of kerosene, it is of interest to know how these hydrocarbon groups influence the hydrogen yield, product gas composition, liquid products and side products. Therefore, the hydrocarbon composition of the Jet A-1, ULSK and desulfurized kerosene fractions are analyzed and arranged into hydrocarbon groups. The molar weight, carbon atom number (Cn) and content of hydrogen groups are used to identify model components, which then are arranged in model mixtures. The analyzing method described in this chapter is also used to identify the liquid product composition of the dehydrogenated model components and model mixtures experimentally investigated in this work.

3.1.1 Identification of Kerosene Components

First, the hydrocarbons are qualitatively identified by gas chromatography with quadropol mass spectroscopy (GCMS) (Agilent *GC Ultra with Trace DSQ*). The identification of the hydrocarbons is determined by the comparison of the spectrometry of the detected components with the database of the GCMS operating software. This analysis was accomplished externally by the Institute of Combustion Technology of the German Aerospace Center. In a next step, the same sample is analyzed with gas chromatography with flame ionization detector (GCFID) (*Shimadzu GC–2010*). Both chromatography systems work with the same coating on the chromatography column (*Restek Rxi®-5ms*). The temperature program of the chromatography column and the injection temperature is adapted for both GC systems. This allows for a direct comparison of the chromatography spectrum of GCMS and GCFID, since the components reach the detector in the same order. The characteristics of the peaks, mean peak height and area are similar within the chromatography diagram of each analyzing system. Fig. 3.1 presents the signal intensity over the calculated boiling temperature of the components of Jet A-1 and ULSK of GCFID analysis. The calculated boiling point temperature is derived from the retention time and boiling points of the identified components.

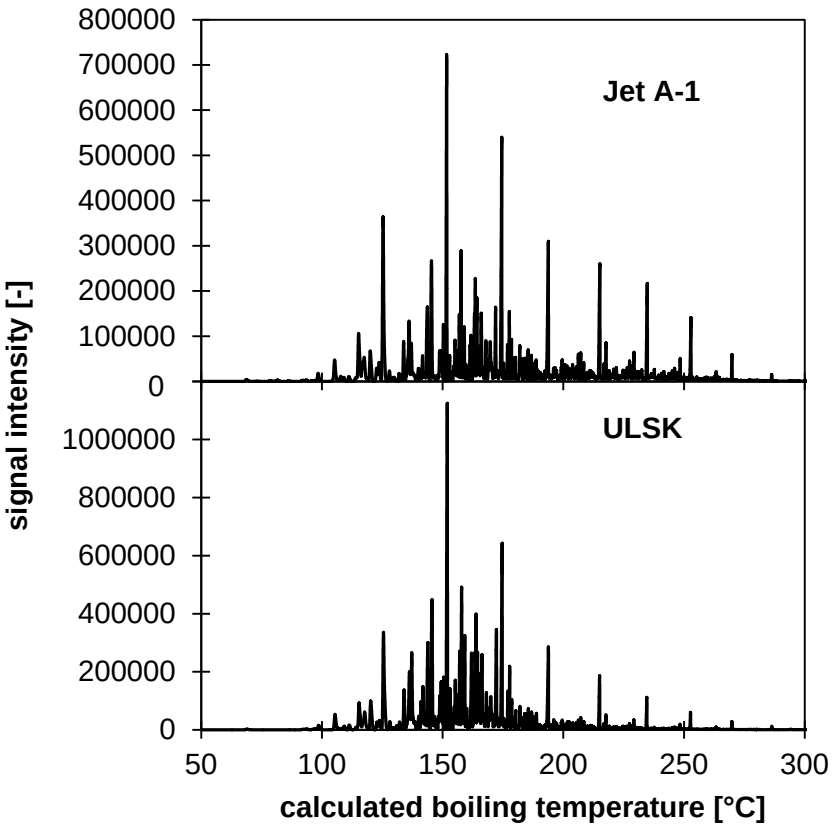

Fig. 3.1 - chromatography diagram with GCFID of Jet A-1 and ULSK

The longer the hydrocarbon chain, and thereby the higher the molar mass of a component, the higher the boiling point is. With increasing boiling point, the components reach the detector with increasing delay and higher retention time. The integral of the intensity of the single component from the FID is the peak area of the component. The signal is directly proportional to the carbon atom content of the components. The content of alkane components is very prominent in jet fuel. The alkane peaks can be used for orientation in the chromatography diagram to identify the carbon atom number (Cn) of the components. More components are detected with the GCFID which cannot be identified with the information from GCMS as the FID detector has a higher sensitivity than the MS detector. Therefore, the discrepancy between detected and identified components in GCFID has to be compensated, which is explained in chapter 3.2.

3.1.2 Calculated Boiling Point Temperature

For the identification of the boiling point distribution of the jet fuel, the retention time of the identified components in the chromatography analysis can be translated to the calculated boiling point temperature. This can also be used for better peak separation of the chromatography diagram. It is assumed that the boiling point of each component can be directly correlated with the retention time of a component. The retention time of components reaching the detector is dependent on the molar mass, true boiling point and their affinity to

the nonpolar chromatography column coating. According to the assumption, the boiling point of each identified component can be considered as the evaporation temperature of the distillated mass of all components up until that evaporation temperature respective retention time. This consideration can be used to set up a polynomial function of the true boiling point over the equivalent retention time of the identified components. Fig. 3.2 shows the distribution of the boiling point temperature of identified components from kerosene and also from the product components of dehydrogenated model mixtures.

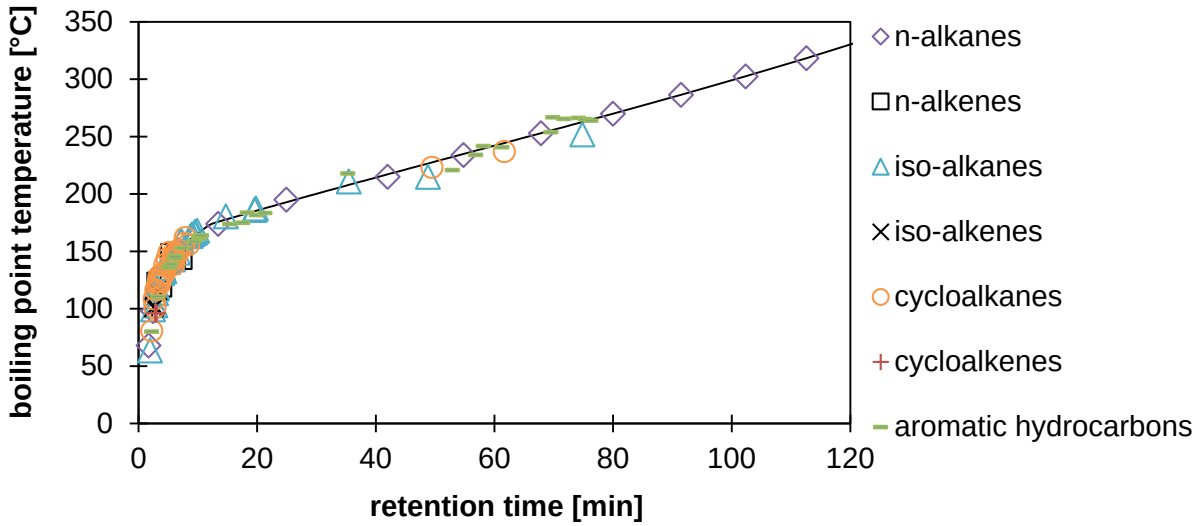

Fig. 3.2 – boiling point temperature over retention time of identified components in GCFID

The polynomial function is then used to calculate a boiling point distribution for all components in the chromatography analysis of a kerosene or kerosene fraction sample. For all identified components, the boiling point was researched in literature. Due to the complexity of the components with the carbon atom number of more than 10 carbon atoms, not all boiling points are available in the literature reviews. Though, the properties of alkanes, for which the boiling ranges are well established, contribute to the boiling range distribution. The influence of alkane boiling points is stronger above the boiling point of decane. Due to the temperature program of the GCFID, which is constant for 20 min at 80°C and then gradually increases with a rate of 1°C/min up to 250°C, the boiling point distribution leads to two different sections. Therefore, two polynomial functions were established, one for the calculation of the boiling temperature lower than the one of decane, and one for the boiling temperature higher than the one of decane, see Eq (3.1) and (3.2).

Polynomial Function for boiling range calculation up until decane

$$y = -16.814 + 69.537 \cdot x - 11.009 \cdot x^2 + 0.8048 \cdot x^3 - 0.0217 \cdot x^4 \quad (3.1)$$

Polynomial Function for boiling range calculation from decane on

$$y = 154.9 + 1.601 \cdot x - 0.0038 \cdot x^2 + 2 \cdot 10^{-5} \cdot x^3 \quad (3.2)$$

The polynomial functions are only valid for the chromatography column used in this work, since the column coating can differ in its properties from one column to another, even if the same type of coating is used.

3.2 Chemical Composition of Kerosene

After identifying the components in GCFID, the percentage of the area of each component from the overall peak area of all identified and unidentified peaks is calculated as $x_{area\text{-}\%}$. The area percentage equals the mass percentage of the carbon atoms of the components, which is calculated by the area of each identified component divided by the total area of the GCFID of all identified and non-identified components, see Eq. (3.3),

$$x_{area-\%} = \frac{x_{area}^{identified}}{\sum x_{area}} \times 100 \quad (3.3)$$

Not all detected area can be specified with Jet A-1, ULSK, and Jet A-1 fractions. To calculate the mass percentage of the identified components, area percentage $x_{area\text{-}\%}$ is corrected by the share of hydrogen atoms of the identified components. Therefore, the average molecular formula C_nH_m of the identified components is calculated by summarizing content of carbon atoms n_C and hydrogen atoms n_H. The identified area percentage is the share of the components with the identified area, see Eq (3.4) – (3.6).

$$\sum n_C = \sum (x_{area-\%}^{identified} \cdot n_C) \quad (3.4)$$

$$\sum n_H = \sum (x_{area-\%}^{identified} \cdot n_H) \quad (3.5)$$

$$x_{area-\%}^{identified} = \frac{x_{area}^{identified}}{\sum x_{area}^{identified}} \times 100 \quad (3.6)$$

Finally, the weight percentage of the identified components can be calculated by Eq. (3.7). The molecular formula from all identified components is used to calculate the mass content of the compounds $x_{wt.\text{-}\%}$,

$$x_{wt.-\%} = \frac{x_{area-\%} \cdot (n_C \cdot M_C + n_H \cdot M_H)}{n_C \cdot (M_C + \frac{\sum n_C}{\sum m_C} \cdot M_H)} \tag{3.7}$$

Were $x_{area.-\%}$ is the percentage of the area of the component in the chromatography. The number of carbon atoms is n_C and hydrogen atoms n_H. M_C and M_H is the molar mass of carbon and hydrogen atoms, respectively, and m_C is the carbon mass in the sample. The discrepancy between the average formula of the identified components and the unknown total detected components is assumed to be sufficiently small.

With dehydrogenated single components of the PCD experiments, 99% to 100% of area can be identified. Therefore, the total amount of carbon atoms “C” hydrogen atoms “H” can be specified by the chemical formula of the components. The weight percentage of condensable dehydrogenation products are identified and calculated with the same method as described for the jet fuel and Jet A-1 fractions.

3.2.1 Hydrocarbon Distribution of Kerosene

All identified components are organized by hydrocarbon groups and their carbon atom number Cn. To gain an overview of chemical composition of the jet fuel and fraction, the mass percentage of the hydrocarbon groups per Cn are added up. Since not all components detected with GCFID can be identified, the summarized mass content does not reach 100 wt.-%. To achieve a closed mass balance, two assumptions are introduced. First, it is assumed that all n-alkanes are identified, since they show a very characteristic peak shape on the chromatographic analysis. The second assumption considers the amount of aromatic hydrocarbons. The average density of aromatic hydrocarbons is considered to be 0.86 g/cm^3. ULSK shows a volumetric content of aromatic hydrocarbons of 23.9 vol.-%, while Jet A-1 has 24.3 vol.-% of aromatic hydrocarbons. Both values are close to the limit of aviation restrictions, and therefore, the amount of aromatic hydrocarbons is considered as completely identified. The unidentified mass content is then equally distributed among the summarized cycloalkanes and iso-alkanes mass composition, see table 3.1. The equal distribution of the non-identified mass content among the carbon atom number Cn of cycloalkanes and iso-alkanes is considered not to be legitimate, since the identified components decline with increasing retention time. The highest detection sensitivity is reached with kerosene among hydrocarbon components with 8 to 12 carbon chain length. With increasing retention time and molar mass, the content of the components declines and fewer components are identified.

Table 3.1 - mass content of hydro carbon groups in ULSK and Jet A-1 identified with GCFID and corrected mass content after jet fuel restrictions

		ULSK		Jet A-1	
		identified mass x_{HG}	corrected mass $x_{HG}^{corrected}$	identified mass x_{HG}	corrected mass $x_{HG}^{corrected}$
iso-alkane	[wt.-%]	18.22	28.19	15.65	27.72
cycloalkane		17.76	27.48	13.74	24.33
aromatic hydrocarbon		20.54	20.54	20.89	20.89
n-alkane		23.80	23.80	27.07	27.07
summarized mass content		80.32	100.00	77.34	100.00
Molar mass [g/mol]	[g/mol]		139.5		150

These assumptions apply to the gas chromatography analysis of jet fuel and desulfurized Jet A-1 fractions. With the gas chromatography analysis of dehydrogenated single components and model mixtures, the total mass content was identified. Fig. 3.3 shows the mass content of the identified hydrocarbons groups and the carbon atoms in Jet A-1 and ULSK distributed over the Cn. The distribution shows the difference in chemical composition of ULSK caused by the removal of sulfur containing compounds found in the higher boiling range of kerosene. This leads to a declining content of components with increasing Cn.

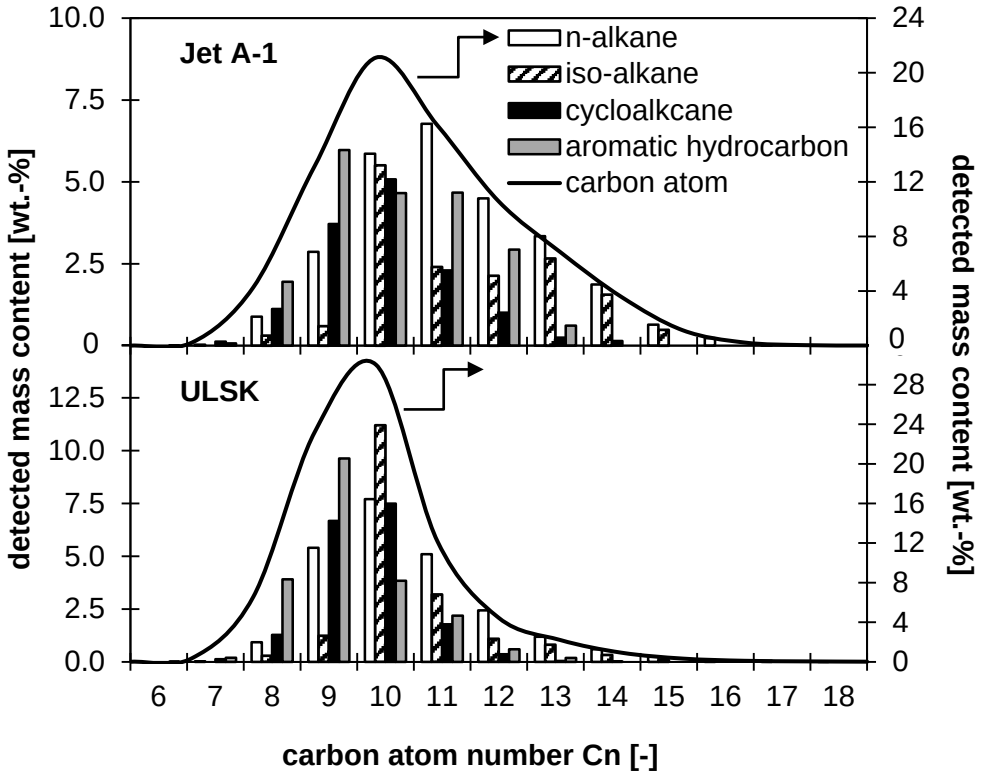

Fig. 3.3 - mass content of detected hydrocarbons groups and carbon atoms of Jet A-1 and ULSK over carbon atom number

The hydrocarbon group of cycloalkanes contains mono- and dicycloalkanes. Further aromatic hydrocarbons are also detected with one ring structure and diaromatic ring structure. The content of the mono- and di- ring structures are added together in the graphical depictions for simplification. The detailed content of hydrocarbon groups is shown in Appendix 8.1. The identified hydrocarbon group composition is also used to calculate the average molar mass of the jet fuel. It has to be taken into consideration that less components are identified at higher boiling temperature respectively with higher retention time. Therefore, the molar mass calculated from identified components is underestimated by up to 7%. Together with the hydrocarbon group composition, the specification of the average molar mass is used to identify possible model components for dehydrogenation tests. First, the molar mass of hydrocarbon groups M_{HG} is calculated by the detected mass content of the hydrocarbon groups x_{HG}, see Eq. (3.8). The carbon molar mass M_C is 12 g/mol, while the molar mass of the hydrogen atom M_H is 1 g/mol. The variable "z" contributes to the difference in molecular formula of the hydrocarbon groups, which is presented in table 3.2. The average molar mass of the jet fuel or fraction $M_{jetfuel}$ is then calculated with the cross product of the corrected, summarized hydrocarbon group content, see Eq. (3.9). The calculation of the molar mass by the molecular formula of the hydrocarbon groups are shown in table 3.2.

Table 3.2 - molecular formula of hydrocarbon groups used for calculation of the average molar mass of jet fuel and dehydrogenated components

hydrocarbon group	n-alkane/ iso-alkane	cycloalkane	dicycloalkane	aromatic hydrocarbons	diaromatic hydrocarbons
molecular formula	CnH2n+z				
z	2	0	-2	-6	-10

$$M_{HG} = \left[\frac{\sum_{n=6}^{n=18} x_{HG} \cdot n_C}{\sum_{n=6}^{n=18} x_{HG}} \right] \cdot \left[M_C + M_H \right] + z \tag{3.8}$$

$$M_{kerosene} = \sum \left[M_{HG} \cdot \sum_{n=6}^{n=22} x_{HG}^{corrected} \right] \tag{3.9}$$

3.2.2 Boiling point Distribution of Kerosene

Next to the mass content of the identified components, the identification of the kerosene components can also be used to analyze the boiling range of Jet A-1, ULSK, and Jet A-1 desulfurized fractions. The boiling point temperature is distributed over the distillated mass of the kerosene. The American Society for Testing Material has established the Standard Test Method for Boiling Range Distribution of Petroleum Fractions by Gas Chromatography ASTM D 2887 [95]. The method is used for comparison to verify the boiling point temperature distribution by the calculated boiling temperature described in chapter 3.1.2. The detected area percent of the peaks in GCFID is summarized and distributed over the calculated boiling point temperature. For simplification, the area percent is set as the weight percent of the peak. With ASTM D 2887, the temperature program slope is usually set for 14 min with the standard test method. The temperature program slope used with GCFID in this work is 220 min, which leads to a sharper peak separation for component identification. A sample of Jet A-1 was sent to an external laboratory (Petro Lab GmbH, Speyer) for analyzing the boiling range after ASTM D 2887. The comparison of the boiling range of the external laboratory and the calculated boiling point method used in this work agree closely with one another. Therefore, the calculated boiling point method is being considered as verified and used for the calculation of the boiling ranges for ULSK and Jet A-1 fractions. Fig. 3.4, presents the boiling point temperature range of Jet A-1 and ULSK over the distillated mass and the externally analyzed ASTM D 2887 boiling range distribution of Jet A-1.

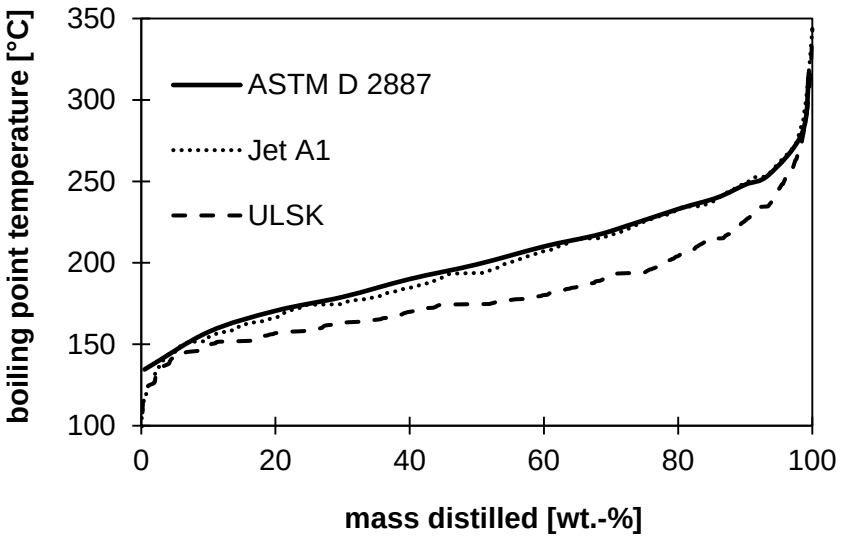

Fig. 3.4, boiling point temperature distribution over distillated mass of Jet A-1 and ULSK and ASTM D2887 standard test method for boiling range distribution of Jet A-1

The boiling point temperature distribution of Jet A-1 and the desulfurized fraction is of interest to the adaption of the model mixture for experimental investigation of dehydrogenation and

process simulation. The model mixtures are designed to adapt the chemical composition and the average molar mass, which also involves the boiling range. Owing to the simplification of the model mixture, the physical properties differ from the original kerosene.

3.3 Desulfurization of Kerosene

The desulfurization process for kerosene established at the German Aerospace Center is the fraction distillation by rectification [31]. The sulfur content in kerosene is mostly found in the higher boiling range of kerosene [96]. This allows the separation of kerosene fractions with less sulfur content than the original jet fuel. To investigate possible sulfur content and chemical compositions of jet fuel fractions, experimental investigations are performed with a batch laboratory rectification column. The method of analyzing the chemical composition, molar mass and boiling range distribution of the distillated fractions is accomplished by the method described with Jet A-1 and ULSK.

3.3.1 Rectification of Jet A-1

The experimental kerosene desulfurization by rectification is carried out in a batch rectification process. The schematic laboratory test set up is presented in Fig. 3.5.

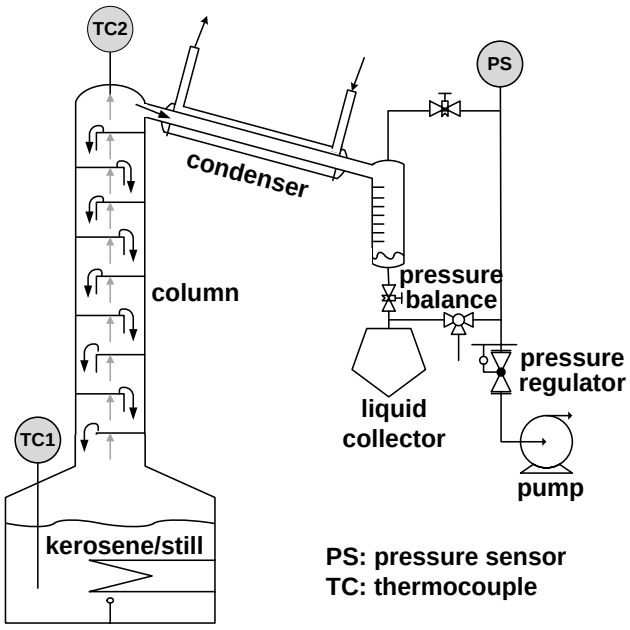

Fig.3.5 - Scheme of batch rectification test set up

The laboratory batch rectification consists of a Vigreux column, which is 1.1m tall and with an effective height of 0.9 m. The estimated stage number is 14 including condenser and still stage on top and bottom. At the bottom stage, the Jet A-1 is provided for distillation in a round bottomed flask with a capacity of 1.2 kg kerosene. With this experimental setup, the feed is

provided to the column at the bottom stage and becomes the distillation still while the experiment is performed. During distillation the composition changes due to partial evaporation of the kerosene components. The feed is heated by an electric heater with 300 Watt performance. To avoid effervescence while boiling and evaporation, an air leak tube is immersed into the still. For monitoring the still temperature, a thermocouple TC1 is immersed into the still. At the top stage of the Vigreux column, a counter current cooler (Liebig – Kühler) condensates the distillated fraction with a circulated 12°C coolant and conducts the condensed fluid over a distributor with volume scale and vacuum regulation (Thiele- Aufsatz) into a 100 ml round bottom flask. The top stage vapor temperature is monitored with a thermocouple TC2. The distillation mass flow rate depends on the vapor/ liquid -equilibrium of the still at given bottom stage temperature and pressure in the system. The pressure in the system is regulated by a vacuum pump and a pressure regulator valve. The bottom stage temperature is kept between 180 and 200°C during experimental time, while the top stage vapor temperature reaches 140°C. The boiling range of the still rises over time since lighter hydrocarbons are evaporated. The heating power cannot be raised with the test setup therefore the pressure is reduced over time from ambient pressure to evaporate the still. Fig. 3.6 presents a typical experimental run for the distillation of a 30 wt.-% fraction

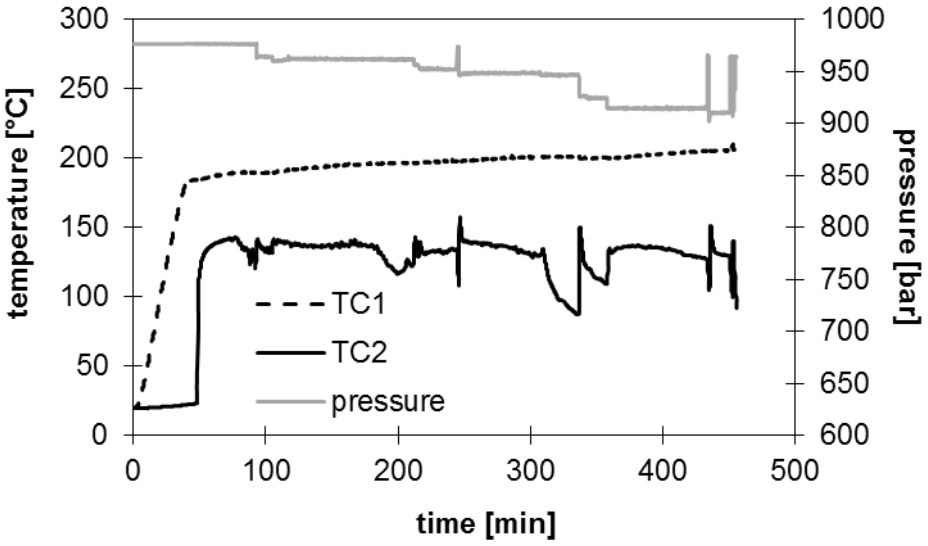

Fig. 3.6 - experimental run of Jet A-1 rectification up to the distillation of 30 wt.-%

The potential of the rectification process to remove sulfur containing components in distillated mass fractions was evaluated first. For the experimental run, one 1.2 kg batch of Jet A-1 was continuously distillated by removing 100 ml, or ca. 80 g, dependent on the fraction density, of distillated components from the jet fuel batch. The power of the electric heater and the vacuum pump performance allow removing a total of 82 wt.-% of distillated mass. The sulfur content in the distillated fractions is analyzed in an element analyzer (AnalytikJena mutli EA 5000) by burning a sample of the distilled fraction at 1000 ºC in a quartz tube and detecting the evolved

SO_2 by UV- fluorescence detector (UVFD). The mass and sulfur content in ppmw of the distillated fraction where cumulated to receive the sulfur content in the consecutive mass fractions during distillation. Fig. 3.7 presents the cumulated sulfur content of the consecutive mass fractions and the sulfur content of the six separately produced mass fractions

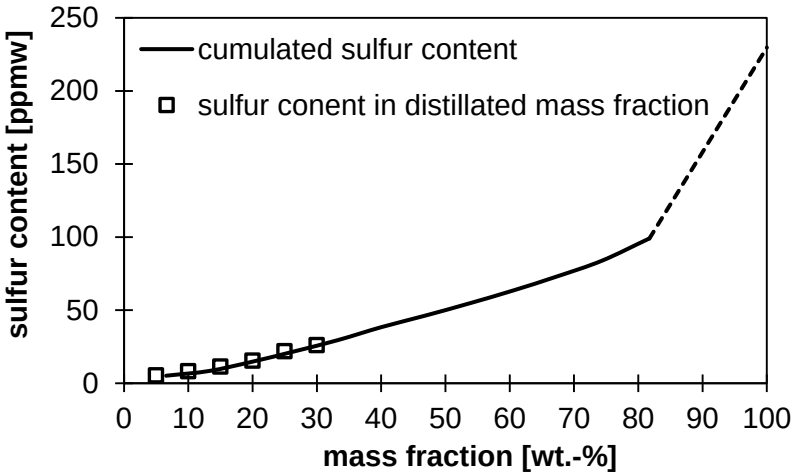

Fig. 3.7 - sulfur content [ppmw] in cumulated Jet A-1 fractions and distilled Jet A-1 mass fractions

In the next step, six mass fractions, from 5 wt.-% with 5 ppmw sulfur to 30 wt.-% with 26 ppmw sulfur, are distillated for dehydrogenation experiments and analyzed for chemical composition with GCFID. Next to the sulfur content also the distribution of the carbon atom number of the fraction changes. With lower distillated mass the average carbon chain length declines. Fig. 3.8 shows the distribution of the carbon atom number over the detected mass content of the fraction and Jet A-1.

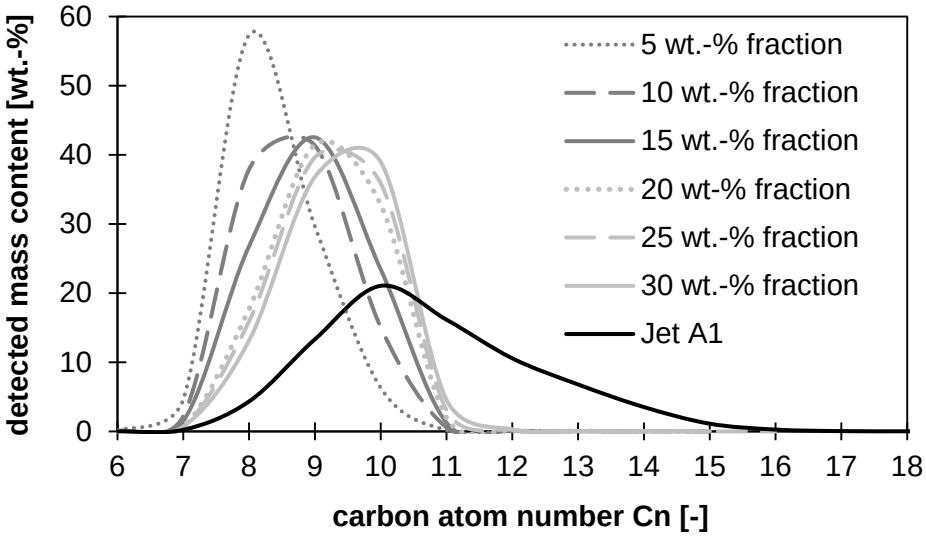

Fig. 3.8 - distribution of carbon atom number with distillited Jet A-1 mass fractions

The difference in distribution of the carbon atom number Cn also leads to the variation in boiling temperature distribution and average molar mass. Hydrocarbons with shorter chain lengths evaporate at lower boiling temperature. With increasing distilled mass fraction, this chain length of evaporated components increases. The distribution of the calculated boiling point temperature of the six different mass fractions is presented in Fig. 3.9.

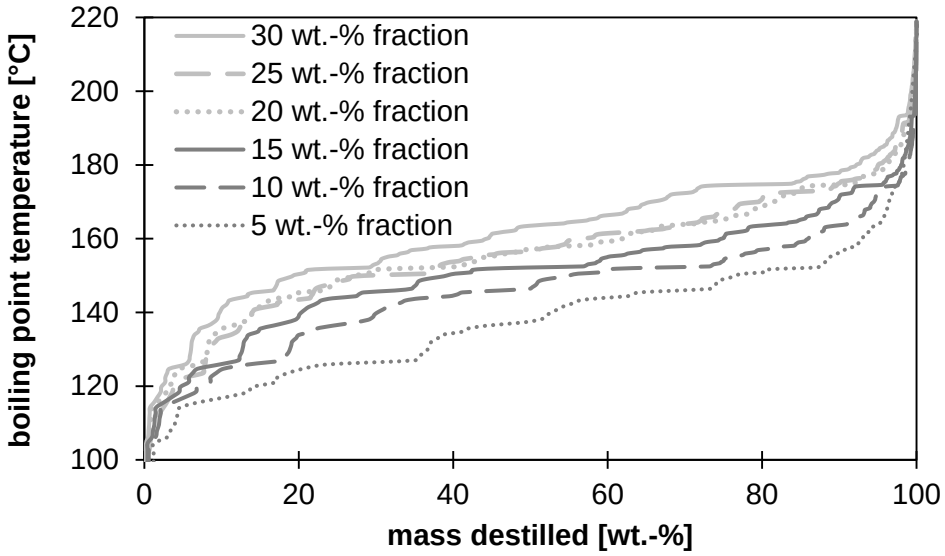

Fig. 3.9 - calculated boiling point distribution of distilled Jet A-1 mass fraction

The content of hydrocarbon groups also depends on the distillated mass fraction. The distribution of hydrocarbon groups in jet fuel varies with different carbon atom numbers. Since the distribution of the carbon atom number varies with different distillation mass fraction, the hydrocarbon content has to change as well, see Fig. 3.10.

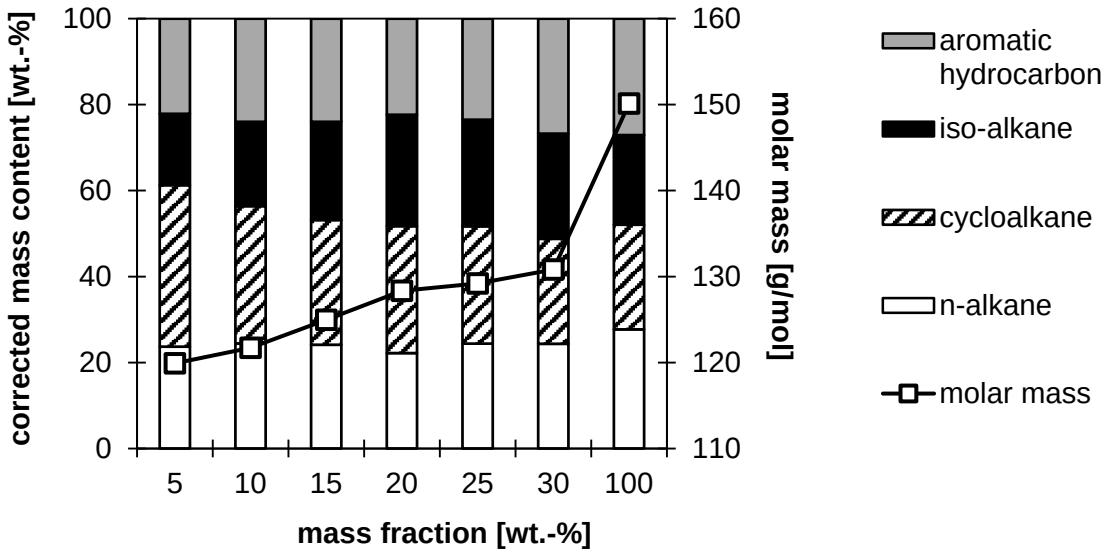

Fig. 3.10 - distribution of hydrocarbon groups and molar mass of distilled Jet A-1 mass fractions

The molar mass declines with declining mass fraction and carbon atom number Cn distribution. The compostion of the hydrocarbon groups in the Jet A-1 fractions and the molar mass are properties used to define suitable model mixtures for dehydrogenation experiments. In particular, the content of cycloalcanes is of interest to the dehydrogenation process, since most hydrogen can evolve from this hydrocarbon group. It can be observed that the content of Cycloalkanes increases with declining destillated mass fraction.

3.4 Model Mixtures

The hydrogen output of partial catalytic dehydrogenation PCD of hydrocarbons from jet fuel depends strongly on the hydrocarbon group. To investigate the influence of hydrocarbon groups on the hydrogen output and evolution of possible side products with PCD, simplified model mixtures are defined. The experimental methodology of PCD of a model mixture is explained in chapter 4. Further, model mixtures are used for the evaluation of the process concepts with rectification, and the reference process with ULSK. To introduce a PCD reactor in a process simulation, model mixtures are used to calculate the reaction enthalpy of PCD. For the process concept with rectification, “real” Jet A-1 fractions are dehydrogenated and evaluated by their hydrogen yield, side products and stability of the reaction. The results are presented in chapter 5. Owing to these experimental investigations, two model mixtures for two different fractions are defined next to a model mixture of ULSK for the reference process.

3.4.1 Method of Model Mixure Compilation

As reference for the design of the model mixture, the composition of ULSK, 10 wt.- % and 20 wt.-% Jet A-1 fractions are chosen. The aim of the model mixture design is to find model components which represent the hydrocarbon groups in the original fuel. The composition of the model components has to represent the composition of hydrocarbon groups and reach comparable molar weight to the original fuel. For the process simulation, the lower heating value is also similar to the original fuel to achieve similar enthalpy for combustion within the process, see chapter 6. The single model components chosen for the model mixture have to be obtainable in reasonable amounts to run the dehydrogenation tests. The single model components are also tested individually at the dehydrogenation test setup to gain information about how product composition influences hydrogen yield and possible reactions conditions for the model mixtures. The method of the model mixture compilation is described based on the ULSK model mixture in this chapter. The number of components in the model mixture is limited to eight commercially available hydrocarbons. This limitation is specified to suit the chemical composition and also provides a reasonable amount of test runs for the dehydrogenation test.

First, the distribution of the hydrocarbons over the carbon atom number is consulted from the GCFID analysis for ULSK. The carbon atom distribution shows that most components have a carbon chain length between 8 to 12 carbon atoms. The carbon atom number distribution is different from one hydrocarbon group to another. For cycloalkanes, a higher amount of components are found between 9 to 10 carbon chain length, while aromatic hydrocarbons are distributed among 8 to 10 carbon chain length. Alkanes and iso- alkanes are more spread in their carbon atom number Cn. The amount of components is now narrowed down by adding together the mass content of the components within one hydrocarbon group with shorter or longer carbon atom number than the assigned Cn. The mass content is added together within the selected Cn to receive a total of eight components, which are assigned for the model mixture. The only iso- alkane which is obtainable is Isooctane. Therefore, the simplification follows by which it is assumed that the influence of n-alkanes and iso- alkanes on dehydrogenation is due to their similar molecular structure. The mass content of iso- alkanes and n-alkanes is distributed between 8 to 12 carbon atom chain lengths. Isooctane is assigned as one iso- alkane and three alkanes are assigned between 9 to 12 carbon atom numbers. The obtainability of cycloalkanes is also limited. Therefore, two components are chosen for 7 and 10 carbon chain length. The total mass content is than distributed among these two components. For aromatic hydrocarbons, two components are chosen for 8 and 10 carbon atom chain length. The defined components for ULSK are considered to be also suitable for other model mixtures.

3.4.2 Composition of Model Mixtures

For the ULSK, two different model mixtures are designed. One model mixture contains the assigned eight components, and a second, more simplified model mixture only 4 components. The composition of the eight component model mixture and the boiling point of the model components is shown in table 3.3.

Table 3.3. model mixture composition of ULSK, four component model mixture, 10 wt.-% and 20 wt.-% fraction model mixture

hydrocarbon group	model compontent	boiling temperature	Cn	ULSK model mixture	4 component model mixture	10 wt.-% model mixture	20 wt.-% model mixture
		[°C]	[-]	[wt.-%]			
iso-alkane	Isooctane	99	7	3.73	28.19	3.09	1.25
cycloalkane	Methylcyclohexane	101	7	13.35	27.48	18.76	15.51
	cis/trans-Decalin	189/191	10	14.85		14.48	16.82
aromatic hydrocarbon	p-Xylene	138.4	8	4-32	20.54	17.45	8.18
	n-Butylbenzene	183	10	17.13		5.67	12.94
n-alkane	Nonane	151	9	5.29		27.55	18.01
	Decane	174	10	32.76	23.80	13.00	25.30
	Dodecane	216.2	12	9.57		-	1.98
molar mass of model mixture			[g/mol]	134.2	114.9	121.94	128.45
density at 20°C and 1 bar			[g/cm^3]	0.78	0.75	0.76	0.76

The four components of the simplified ULSK model mixture represent each of the hydrocarbon groups in fuel. With this simplified mixture a less complex product distribution is obtained with dehydrogenation tests, which allows a less complex analysis on the influence of the hydrocarbon groups on the hydrogen yield and the reaction conditions. The chemical composition of the four components is defined after the total mass content of the hydrocarbon groups of ULSK, see table 3.1.

The composition for the model mixture of the 10 and 20 wt.-% fraction is chosen also on the basis of the hydrocarbon distribution of the equivalent Jet A-1 mass fraction. The same model components are used as with the ULSK model mixture. With the 10 wt.-% fraction, the content of hydrocarbons with 12 carbon atoms is strongly reduced to less than 0.1 wt.-%. Therefore, dodecane is not used in the 10 wt.-% model mixture. The boiling range distribution of the model mixture deviates from the original ULSK or Jet A-1 in particular in the range of lower boiling temperature. This is caused by the higher content of components, with the lower boiling points in comparison to the original fuel, which are isooctane and methylcyclohexane. Still this components are chosen in order to suit the restrictions of chemical compatibility with the original fuel and obtainability for dehydrogenation test.

4 The Experimental Methodology

The partial catalytic dehydrogenation (PCD) of hydrocarbons in jet fuel contains different types of reaction paths and products dependent on the jet fuel components and their dedication to hydrocarbon groups. Hydrocarbons within a hydrocarbon group show similar reaction paths due to their molecular structure. To activate dehydrogenation reactions which lead to hydrogen evolution, the activation energy has to be reduced by a catalyst, which also can induce an undesired side reaction. The cracking of the carbon chain into shorter chain hydrocarbons decreases the hydrogen gas purity and can require hydrogenation to saturated hydrocarbons. Further, the dehydrogenation of jet fuel components can lead to formation of carbon, which is deposited on the catalyst surface and occupies the active sites, causing a decrease of catalyst activity. Dehydrogenation, cracking reactions and carbon formation are endothermic reactions. [26], [73], [97].

In jet fuel, the diversity of hydrocarbons leads to many different reaction paths and reaction products. The hydrogen yield and product distribution from PCD reactions depend on the reaction conditions, which are the reaction temperature, pressure and contact time on the catalyst surface. The investigation of suitable reactions for PCD of jet fuel to achieve high hydrogen yield, stable reaction progress with little carbon formation on the catalyst surface and few cracking products in the gas phase is accomplished in this work by experimental study.

In this chapter, the methodology of the experimental investigation of process condition, reaction products and the evaluation of the experimental results is presented. To investigate the process conditions on hydrocarbon groups in jet fuel, the simplified composition of model mixtures is used. These are derived from the hydrocarbon group composition of ULSK and Jet A-1 desulfurized fractions, see chapter 3.4. Further, the model components used in the model mixture are dehydrogenated as pure components to learn about detailed product composition and conversion rates. With the established reaction conditions, real ULSK and Jet A-1 are examined to evaluate the dehydrogenation process in hydrogen yield and reaction progress stability. The detailed knowledge of reaction products and conversion rates of model components and model mixture for specific reaction conditions can be used for input specification in process simulation to evaluate the process concept with rectification and the reference process.

4.1 Identification of Test Rig Conditions

To define the most promising reaction conditions, two different types of test rigs were built. First, an experimental set up suggested in literature for dehydrogenation under liquid/gas equilibrium conditions was tested in a batch reactor. The liquid/gas equilibrium conditions run under low temperature close to boiling temperature of the chosen model component or mixture. Cracking reactions due to thermal stressing can be limited and close contact with the catalyst by wetting the catalyst surface is achieved. [77], [79], [70], [23].

The liquid feed is injected and mixed in a suspension with a Platinum (Pt) catalyst on an activated carbon powder carrier. The feed is heated to boiling temperature at atmospheric pressure, while the evaporating hydrocarbons are condensed and led back into the batch reactor. The hydrogen evolves into the gas phase and leaves the reaction system to be collected in a gasometer for detecting the volumetric amount of gas produced. The experiment ends when no more detectable gas is evolving from gas/liquid equilibrium. The hydrogen concentration is detected with gas chromatography and thermal conductivity detector (GCTCD). The scheme of the liquid/gas equilibrium test rig is presented in Fig 4.1. Before each test, the atmosphere of the test rig is neutralized with nitrogen gas.

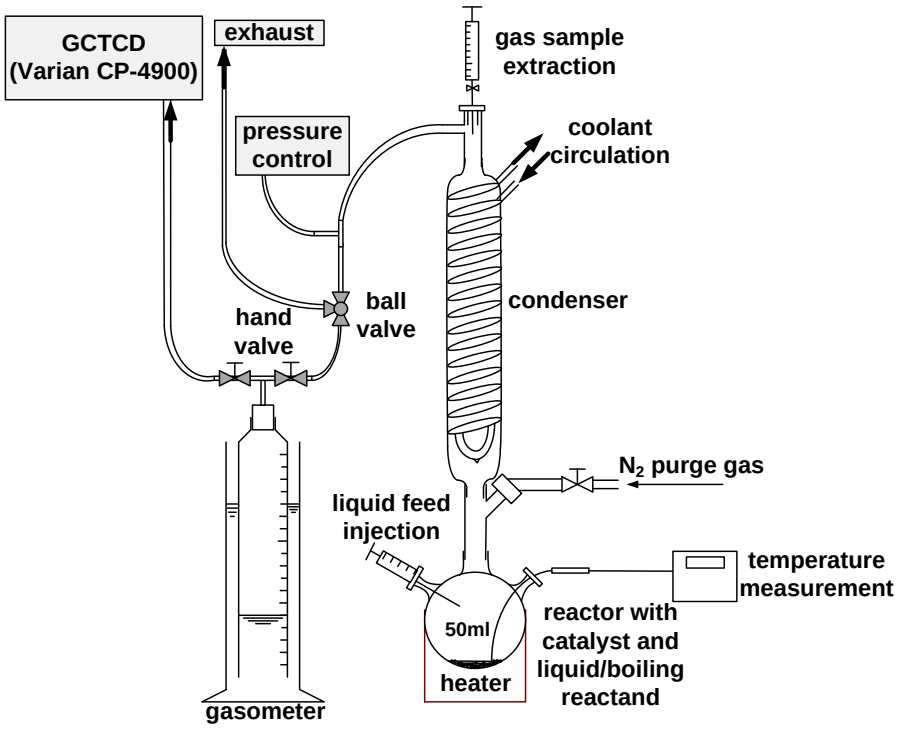

Fig. 4.1 Scheme of test rig for gas/liquid equilibrium dehydrogenation

Most publications working with gas/liquid reaction conditions use cycloalkanes as feed components, which have low activation energy and high hydrogen evolution in comparison to other hydrocarbon groups contained in jet fuel. The liquid/gas equilibrium test set up is used

to investigate the hydrogen evolution under these conditions of different model components representing different hydrocarbon groups in jet fuel. The evolving hydrogen yield is with all tested components less than 0.3 Nl_{H_2} / kg_{feed}. This hydrogen yield is considered too low for the system efficiency of both concepts for jet fuel dehydrogenation. Therefore, the reaction conditions under liquid/gas equilibrium conditions are not continued in this work.

The second experimental test rig is designed to operate the PCD under gas reaction conditions. The feed is evaporated and conditioned to reaction temperature above evaporation temperature. With increased reaction temperature, increased hydrogen yield is expected but also more cracking reaction and carbon formation. In this chapter, the experimental set up for PCD at gas reaction conditions is presented and the experimental methodology is described upon gas phase reaction conditions.

4.2 Dehydrogenation Reactions of Long Chain Hydrocarbons

The four hydrocarbon groups in jet fuel, presented in chapter 3, are expected to have characteristic dehydrogenation reactions due to their molecular structure. Still, the reaction paths of long chain hydrocarbons can interfere with each other and lead to different side reactions and multiple reaction products, including cracking products and carbon formation. The scheme in Fig. 4.2 suggests different reaction paths of hydrocarbon groups starting from long chain alkanes [66], [88], [98].

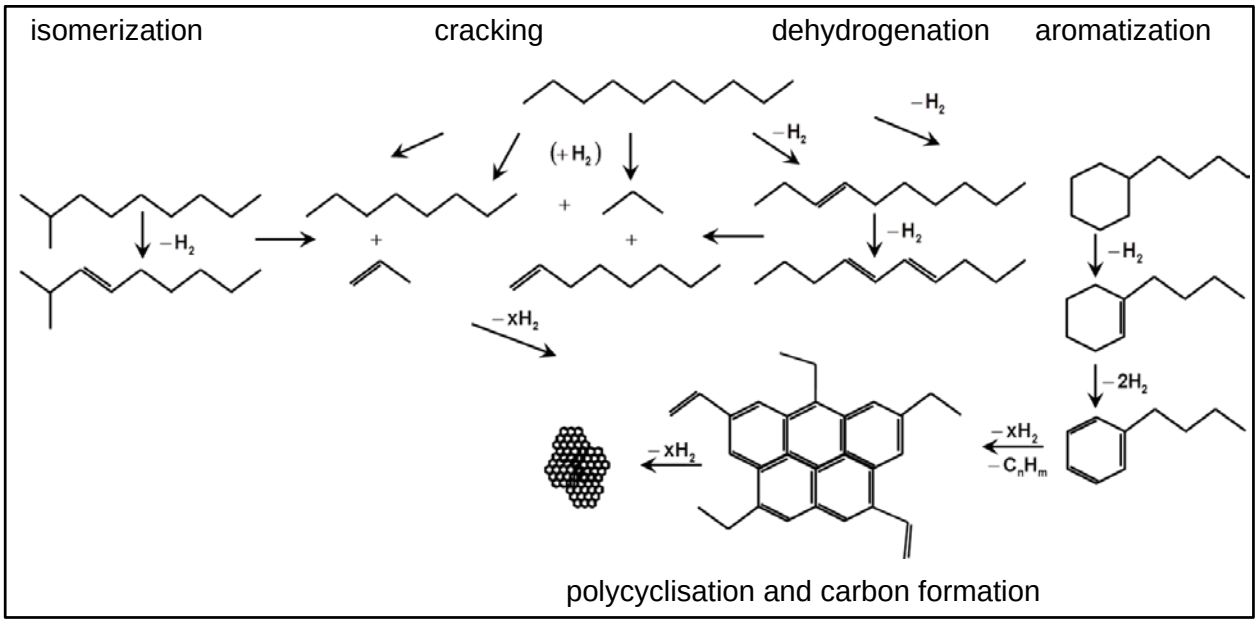

Fig. 4.2 - Scheme of suggested reaction paths of dehydrogenation of different hydrocarbon groups

The hydrogen yield of a component depends on the reaction path a molecule takes and the total conversion rate of the component. Both, conversion rate and path are influenced by reaction conditions and catalyst properties.

The dehydrogenation of alkanes to alkenes leads to the stoichiometric evolution of one hydrogen molecule H_2, or in case of dialkenes, a maximum of two hydrogen molecules. Further alkanes can also follow the aromatization path, which follows cyclisation to cycloalkanes and then aromatic hydrocarbons which evolve up to 4 hydrogen molecules. The aromatization path of n-alkanes often follows radical formation and can cause formation of polyaromatic hydrocarbons, which are the preliminary stage to carbon formation.

The aromatization of the hydrocarbon group cycloalkanes to aromatic hydrocarbons follows the preliminary step of dehydrogenation to cycloalkanes. The formation of aromatic hydrocarbons from cycloalkanes has a high potential of hydrogen evolution, and causes only minimal carbon formation, since no intermediate radicals are formed. Aromatic hydrocarbons have a very stable molecular structure and rather do not convert or interfere with other components and products. Further reactions only appear with alkane side branches of the aromatic ring, which can involve dehydrogenation, cracking to shorter chain hydrocarbons and radical formation leading to carbon formation.

Cracking reactions of alkanes leading to shorter chain alkanes and alkenes can consume hydrogen, known as hydrocracking. This reaction is caused by thermal strain on the carbon chain and is also catalyzed. Short chain hydrocarbons, up to five carbon atoms, are in gas phase of the product gas after condensation of partially dehydrogenated fuel. They decrease the hydrogen gas purity and should be avoided with suitable reaction conditions. Another side reaction of alkanes is the isomerization, leading to isoalkanes where no hydrogen is evolving. Isoalkanes can dehydrogenate to isoalkenes, or can form shorter chain hydrocarbons by cracking.

These reaction paths can be observed with PCD model components experimentally investigated in this work.

4.3 The Dehydrogenation Catalyst

The catalyst most often used for dehydrogenation of long chain hydrocarbons is Platinum, due to its high activity. Platinum is not resistant to sulfur however, and therefore, sulfur containing fuels cause catalyst deactivation due to the formation of platinum sulfide PtS_2. The noble metal catalyst is applied on different carrier materials, which is most often ɣ-Al_2O_3 or activated carbon due to its high surface area. [99], [29], [81], [28], [25] In case of ɣ-Al_2O_3, support precursors like Sn, Ca, or Cl, Ni are applied with the Pt on the surface to reduce the acidity of the carrier material which causes cracking and carbon formation [90], [78], [100]. Another potential carrier material is Zeolith, which is used in membrane reactors to separate the hydrogen product gas

from other products. Membrane reactors for dehydrogenation have the disadvantage of carbon formation in the membrane pores, which highly decreases the permeability [101], [102], [67], [103].

The catalyst used for the experimental work in this thesis is bimetallic 1 wt.-% Pt – 1 wt.-%Sn on ɣ-Al_2O_3 spherical pellets with a diameter of 1.8 mm and is developed especially for dehydrogenating of Jet fuel by JohnsonMatthey. The pore volume of the catalyst pellets is 0.55 ml/g. The average pore diameter is 6.9 nm with BET surface area of 202 m^2/g. The dispersion of Pt is ~16 % which is measured by pulsed carbon monoxide chemisorption. The catalyst preparation and characterization was performed by JohnsonMatthey. First, ɣ-Al_2O_3 support was impregnated by a solution of H_2PtCl_6 and dried under vacuum in a rotary evaporator. Then, it was further heated at 110°C for 2 h and calcined at 500 ºC (10ºC/min) for 8 h. A second impregnation was performed using a solution of $SnCl_2$- H_2O (Alfa Aesar). To achieve desired Pt/Sn ratio the product was dried in a rotary evaporator. The platinum catalyst was activated before each dehydrogenation test over 2 h at 350°C using a 1.2 l/h hydrogen flow at 1.3 bar. The experimental examination, was performed under the assumption that the catalyst represents the state of knowledge for dehydrogenation of long chain hydrocarbons and complex mixtures. Still, the catalyst does not show sulfur resistance, which leads to the necessity of desulfurization of jet fuel in the process concepts.

4.4 The Experimental Setup

The experimental setup for partial catalytic dehydrogenation of kerosene, model mixtures and model components is shown in Fig. 4.3. The reaction is performed in gas phase over the solid catalyst surface. The system can be pressurized to investigate reaction conditions under pressure for the process concepts due to the pressure required for product gas conditioning by PSA.

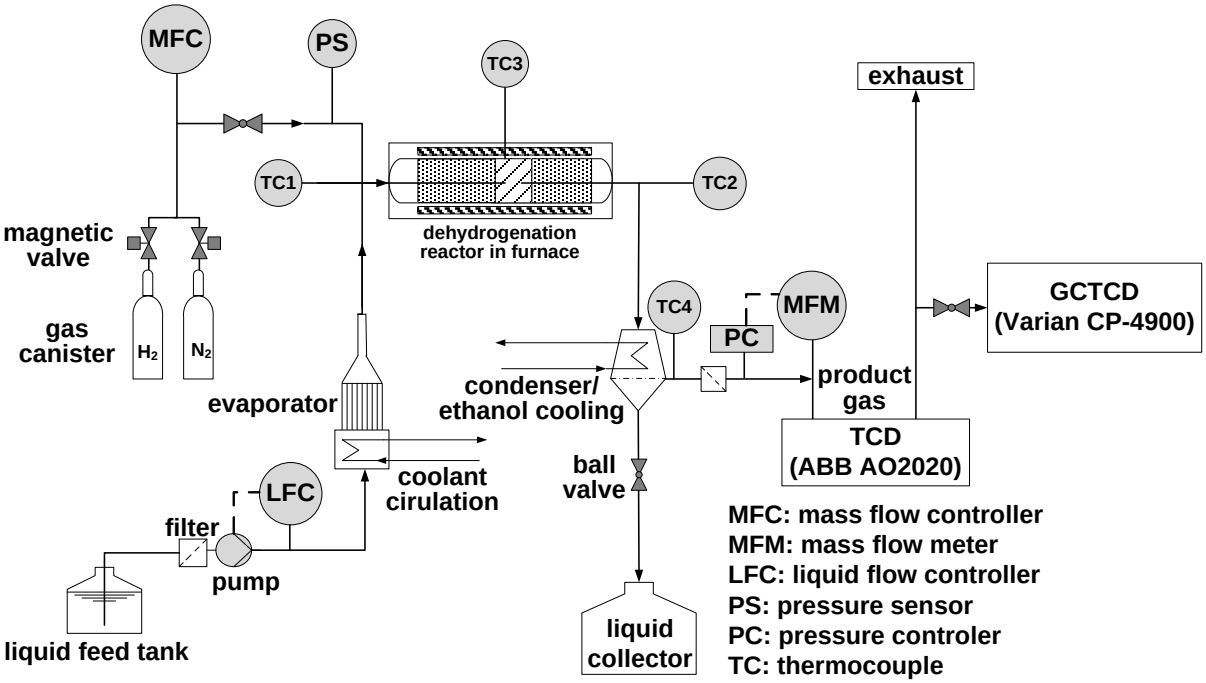

Fig. 4.3 - experimental setup for partial catalytic dehydrogenation

The dehydrogenation tests are performed in a fixed bed tubular reactor (inner diameter d=15 mm and tube length L=375mm), which is placed in a programmable electric furnace. The catalyst bed starts 5 mm upstream of the center of the furnace. To regulate the reactor and catalytic bed temperature, a thermocouple TC1 is placed 5 mm in the catalyst bed. The reactor is operated between 350°C and 500°C. A second thermocouple, TC2, is placed 10 mm upstream from the end of the catalytic bed to measure the axial temperature gradient in the bed material. A third thermocouple, TC3, is placed vertical to TC1 on the surface of the steel reactor tube to measure the temperature decrease induced by the endothermic reaction. The temperature, TC4, is measured at the outlet of the condenser and is used to correct the volume flow of the product gas stream. The feed mass flow is provided to the reactor by a micro gear pump, which is controlled by a liquid flow controller LFC (8 g/h to 45 g/h kerosene). The feed is evaporated in a capillary evaporator (max 350°C) and superheated to operation temperature before it reaches the reactor bed. The feed flow is cooled with a 12°C coolant circulation within the evaporator casing before being heated up to evaporation temperature. The constant temperature gradient of the feed stream at the inlet of the electrical heated capillaries reduces pressure fluctuation due to evaporation. Hydrogen is provided over a mass flow controller MFC and heated up until operation temperature of the reactor. The hydrogen flow is used for catalyst activation before the experimental run. Also, the reaction is started under a pure hydrogen atmosphere. Downstream of the reactor tube, the product gas and dehydrogenated hydrocarbon components run through a counter current condenser, which is cooled by ethanol at -10°C. The condensable products are collected in the condenser and are weighed after the

test and analyzed with the GCMS and GCFID to detect the mass content of product components and the conversion rate of the feed components, see chapter 3. The product gas is measured by a mass flow meter MFM. The pressure of the system is regulated from 1 bar to 8 bar by a pressure controller PC, which is located downstream of the condenser. A pressure sensor PS upstream of the reactor tube is used to monitor an accidental pressure drop of the system by clogging.

The hydrogen concentration is measured online by a thermal conductivity detector (ABB AO2020), while the gaseous hydrocarbons (CH_4, C_2H_6, C_2H_4, C_3H_8, C_3H_6, C_4H_{10}) are analyzed in a gas chromatography every five minutes of reaction time (Varian CP-4900 Micro-GC). The carbon deposition on the catalyst is analyzed after the dehydrogenation test with an element analyzer (AnalytikJena mutli EA 5000) by burning the carbon on the catalyst surface at 1050°C in a quartz tube and detecting the evolved CO_2 by non-dispersive infrared CO_2 spectrometry (NDIR).

4.5 Design of Experiment

The experimental tests are performed to define suitable process conditions for both PCD concepts by variation of the reaction temperature, pressure and contact time of the feed stream on the catalyst. The reaction conditions are evaluated by the hydrogen yield, product compositions and stability of the reactions of defined single model components, which are expected to have most influence on the PCD of the model mixtures, ULSK and Jet A-1 fractions. The defined reaction conditions are then used for PCD of model mixtures to investigate the hydrogen yield and product composition for the process model of both process concepts. The hydrogen yield and product composition of the product gas stream and the liquid condensate product are extracted from the experimental data and evaluated for the process concepts.

4.5.1 Preparation of Experiment

For the preparation of each experimental run, the mass of catalyst $m_{catalyst}$ with the catalyst bed density of $\rho_{catalystbed}$=0.574 g/ml is defined for a specific contact time on the catalyst surface. The contact time is the time in seconds that a feed stream spends passing through the cavity volume of the catalyst $V_{Catalystcavity}$ at reaction conditions. The feed flow rate for the chosen component, model mixture or fuel is adjusted to the reaction conditions. The mass of the catalyst bed is calculated by the chosen contact time of the feed stream on the catalyst. The contact time depends on the catalyst bed volume $V_{catalystbed}$, temperature TC1, pressure p,

the mass flow of feed $\dot{m}_{Feed}$, the molar mass of feed M_{feed} and the porosity of the catalyst bed $\psi = 38.2\%$, see Eq. (4.1), (4.2),(4.3).

$$t = \frac{V_{Catalystcavity}}{\dot{V}_{feed}} = \frac{V_{catalystbed} \cdot \psi \cdot p \cdot M_{feed}}{\dot{m}_{feed} \cdot R \cdot TC1} \tag{4.1}$$

$$V_{cataystbed} = L_{catalystbed} \cdot \frac{\pi}{4} \cdot d^2 \tag{4.2}$$

$$m_{cat.} = V_{catalystbed} \cdot \rho_{catalystbed} \tag{4.3}$$

The length of the reaction bed $L_{catalystbed.}$ is limited from 15 mm to 45 mm, which is 1 to 3 times the inner diameter of the tubular reactor. This prevents macroscopic leak current which would be the case if the bed would be shorter than 15 mm. A bed length exceeding 45 mm would lead to a horizontal temperature gradient over 5 K through the catalyst bed with most endothermic reactions. The reaction temperature is regulated at the beginning of the catalyst bed, where the endothermic PCD reaction is starting. The concentration of the dehydrogenated components increases through the catalyst bed with progressing reaction front. The steady heat transfer from the electric furnace to the catalyst bed causes an increase of the catalyst temperature at the exit of the catalyst, where less reaction enthalpy is needed due to the reduced concentration of feed components and increasing reaction products. A longer reaction bed would cause an even stronger concentration and temperature gradient. With increasing catalyst bed temperature, more thermal cracking of the hydrocarbon components is likely. Since the dimensions of the reaction bed are limited, the feed mass stream has to be adjusted to the defined contact time, depending on the reaction temperature and system pressure. Further, the temperature of the evaporator is also adjusted to the experimental reaction conditions and the evaporation temperature of the chosen feed. Thermal stress during evaporation can lead to carbon deposits in the capillaries of the evaporator. The maximum evaporation temperature is 320°C at 8 bar pressure of the system.

All experiments where run for 5.5 h. At the startup, a hydrogen flow of 1.2 Nl/h flows over the heated and pressurized catalyst bed, while the feed flow is slowly raised within 10 min until reaching test conditions and the hydrogen flow is reduced to zero. This practice reduces the immediate carbon formation on the catalyst surface by gradually increasing the partial pressure of the reactant on the catalyst surface. After the experimental time has finished, the feed flow is shut off and the system is purged with nitrogen to lead condensable products remaining in

the reactor into the liquid condenser. After the system is cooled down and depressurized, the catalyst and the condensate is removed for analyzing.

4.5.2 Evaluation of Experimental Data

To calculate the net product gas flow, $\dot{V}_{productgas}$, the measured product gas flow $\dot{V}_{MFM}$ is corrected in four steps, Eq. (4.4).

$$\dot{V}_{productgas} = \dot{V}_{MFM} - \dot{V}_1^{correction} - \dot{V}_2^{correction} - \dot{V}_3^{correction} \tag{4.4}$$

The first correction is to subtract the hydrogen flow $\dot{V}_{H_2}^{startup}$ in the startup phase of each experiment $\dot{V}_1^{correction}$ from the product gas $\dot{V}_{MFM}$, Eq. (4.5).

$$\dot{V}_1^{correction} = \dot{V}_{H_2}^{startup} \tag{4.5}$$

Second, the expansion of the evaporated hydrocarbons pressing gas out of the test facility is considered until the pressure equilibrium of incoming and outgoing gas is balanced in the test rig. This increased gas flow of the products (Eq. (4.6)) which is not evolving from produced gas but from pressed out hydrogen in the system and has to be subtracted.

$$\dot{V}_2^{correction} = \dot{V}_{feed}^{vapor} \cdot \exp\left(\frac{t_n - t_0}{V_{reactor}} \cdot \dot{V}_{feed}^{vapor} \frac{p \cdot T_{STP}}{p_{STP} \cdot TC1} \right) \tag{4.6}$$

$$\dot{V}_{feed}^{vapor} = \frac{\dot{m}_{feed}}{M_{feed}} \cdot V_m \tag{4.7}$$

The volume flow rate $\dot{V}_{feed}^{vapor}$ of the feed is calculated for standard conditions in the gas phase with the molar volume V_m=22.414 l/mol at standard pressure of p_{STP}=1.01325 bar and standard temperature of T_{STP}=273.15K, Eq. (4.7). The volume of the reactor tube is $V_{reactor}$=141.4 ml.

The third correction takes into account that the volume of the condensable products is part of the system volume. The condensable product components are condensed and collected in the condenser, which is part of the test rig volume. The received liquid reduces the condenser volume over time. This liquid volume manipulates the volume flow equilibrium by additionally pressing out the volume of the hydrocarbons that are collected as liquid, and has to be subtracted from the product gas $\dot{V}_{MFM}$, (Eq. (4.8)). The difference of density of the feed and the condensate is assumed to be negligible.

$$\dot{V}_3^{corrected} = \frac{p \cdot T_{STP}}{TC4} \cdot \dot{m}_{feed} \cdot \rho_{feed} \quad (4.8)$$

TC4 is the outlet temperature of the product gas stream, which is in average 293.15 K. It is assumed that the condensable products have the same temperature. The pressure p is the system pressure of the experimental run.

To calculate the actual volume flow of the produced gas component hydrogen or a specific gaseous hydrocarbon, the change of product gas concentration in the test rig has to be taken into account. The concentration of the product gas c_{gas} reaches the detector with a time delay, during which more product gas is building up and mixing in the volume of the test rig, Eq. (4.9). The effective volume of the test rig $V_{testrig}^{effective}$ considers the volume change described of the test rig Volume $V_{testrig}$=0.5Nl due to the collection of liquid condensate in the condenser, Eq. (4.10).

$$\dot{V}_{gas}^{component} = ((\dot{V}_{produktgas} \cdot c_{gas}^{tn}) + (c_{gas}^{tn} - c_{gas}^{tn-1})) \cdot V_{testrig}^{effective} \cdot p \quad (4.9)$$

$$V_{testrig}^{effective} = V_{testrig} - V_{catalystbed} - \int_{t_o}^{t_n} m_{feed} \cdot \rho_{feed} dt_n \quad (4.10)$$

The product gas yield of hydrogen or gaseous hydrocarbons over time Y_{H_2/C_nH_m} $[Nl_{H_2/C_nH_m}/kg_{feed}]$ is calculated by Eq. (4.11):

$$Y_{H_2/C_nH_m} = \frac{\dot{V}_{gas}^{component}}{\dot{m}_{feed}} \quad (4.11)$$

The total mass of hydrogen produced during the experimental time over the total feed mass $[g_{H_2}/kg_{feed}]$ is used to compare the hydrogen gas yield directly at different reaction conditions, (Eq. (4.12)).

$$Y_{H_2} = \int_{t_o}^{t_n} \frac{m_{H_2}}{m_{feed}} dt_n \quad (4.12)$$

The formed carbon on the catalyst is calculated as the carbon yield $Y_{C/cat.}$ [$g_c/kg_{cat.}$], which is the carbon mass detected on the catalyst m_C divided by the mass of the fresh catalyst $m_{cat.}$. It is used for the assessment of the stability of the reaction progress, which is effected by the catalyst activity. Further, the carbon yield is also calculated by the total mass of the feed $Y_{C/feed}$,

which is used as a specification of dehydrogenation reactions for the process concept, see Eq. (4.13) – (3.14).

$$Y_{C/cat.} = \frac{m_C}{m_{cat.}} \tag{4.13}$$

$$Y_{C/feed} = \frac{m_C}{m_{feed}} \tag{4.14}$$

The GCFID analysis of the feed components in model mixtures or pure model components, and the dehydrogenated condensed products collected from the condenser are used to calculate the conversion rate of the feed stream. The same methods are used as described in chapter 3 to detect the mass content of the feed components and the product components before and after the dehydrogenation experiment.

The conversion rate of pure model components and the components in the model mixture is calculated by the mass content $x_{wt.-\%}$ of the feed component and the $x_{wt.-\%}$ non-converted feed component of partially dehydrogenated condensate, subtracted and divided by the original component content in the feed, see Eq. (4.15).

$$x_{wt.-\%}^{converted} = 1 - \frac{x_{wt.-\%}^{non-converted}}{x_{wt.-\%}^{feed}} \tag{4.15}$$

The liquid product compositions and conversion rate of the single components can be identified in detail with GCFID. The product composition of the dehydrogenated model mixtures exceeds 100 different product components, which causes peak overlapping and reduces the unambiguous identification. Therefore, it is assumed that the products appearing from the dehydrogenation of pure model components are similar to the product components of the model mixture tests. To check the mass balance, the mass of the dehydrogenated single component, the liquid products, the mass content of the gaseous products and the carbon formation are aggregated and compared to the feed mass.

4.5.3 Test Matrix

The process conditions of the partial catalytic dehydrogenation of ULSK and Jet A-1 fractions are investigated with experimental dehydrogenation of the pure model components and the model mixtures. To evaluate the process concept with rectification and the reference concept with ULSK the hydrogen yield, the gaseous and liquid products, the conversion rate of the model components in the mixtures and the formation of carbon are of interest. Further the stability of the reaction progress which can degrade due to deactivation of the catalyst surface by carbon deposit and sulfur poisoning is observed. Strong degradation would lead to

insufficient hydrogen evolution over time for both concepts. Therefore reaction conditions have to be defined which show high hydrogen output and stable reaction progress with model mixtures. The pure model components and model mixtures are used for process simulation to identify possible dehydrogenation reactions and to integrate conversion rates to calculate the heats of reaction, and by this, the heat demand of the dehydrogenation reactor within both concepts. The calculated heat demand and dehydrogenation fuel properties are then used to identify suitable heat and material integration of the system as well as present possible system efficiencies.

For the experimental investigation of reaction conditions, two components are identified which are expected to have the greatest effect on hydrogen output and the stability of the reaction. Alkanes are likely to cause deactivation of the catalyst by carbon deposition. Cycloalkanes, on the other hand, are likely to dehydrogenate to aromatic hydrocarbons. The dehydrogenation reaction is more stable toward cracking and radical formation. From this information, the model component methylcyclohexane (MCH) appears to have high potential for hydrogen evolution. Decane is chosen to represent alkanes.

The influence of reaction temperature is tested on the first two chosen model components by varying the catalyst bed temperature TC1 between 350°C and 500°C. The system pressure is kept at 1 bar, while the contact time on the catalyst is 2 sec.

The dehydrogenation reactor in both concepts would primarily run as a pressurized system to avoid pressurizing the product gas for gas cleaning. The influence of pressure is tested with 1, 3, 5 and 8 bar. Pressure is expected to have a negative influence on the hydrogen yield, especially on the conversion of MCH. The thermodynamic equilibrium indicates that pressure would shift the dehydrogenation reaction towards MCH [76]. To influence the conversion towards hydrogen production, the contact time can be increased. Therefore, tests with an increased contact time of 4 sec in the pressurized systems are performed. In order to meet the conditions of the minimum and maximum length of catalytic bed of chapter 4.5.1, the feed mass flow was increased with 3 bar to 20 g/h and with 5 and 8 bar to 40 g/h. The experimental results on temperature, pressure and contact time variation are used to define suitable reaction conditions for a pressurized and non-pressurized PCD reactor. In the case where the hydrogen yield of model mixtures in a non-pressurized reactor is sufficient to overcome the expenditure of energy to pressurize the product gas for the PSA, the reaction conditions are defined at 1 bar.

Next, all model components used in the model mixtures are tested as pure components with two different reaction conditions. The information of product composition etc. is used for evaluation of the hydrocarbon groups. In the next step, two component model mixtures are dehydrogenated, with the cycloalkane MCH as one component and a second hydrocarbon representing another hydrocarbon group. The experimental results give information about how

alkanes, iso-alkanes and aromatic hydrocarbons influence the hydrogen output from cycloalkanes.

Finally, the chosen reaction conditions are tested on the model mixtures for ULSK and the model mixtures of Jet A-1 fractions to find the most suitable reaction condition and to decide on a pressurized or non-pressurized system. Lastly, the final tests with sulfur containing model mixtures and real ULSK and kerosene fractions are performed to assess the stability of PCD with sulfur and real fuels. The tabulated test matrix is presented in Appendix 8.2 table 8.3.

5 Experimental Results of PCD

The experimental evaluation of partial catalytic dehydrogenation of ULSK and Jet A-1 desulfurized fractions demonstrate the possibilities, but also vulnerabilities of hydrogen production for the process concept with rectification and the reference concept. The information gained from the experimental study presented in this chapter is important for the understanding of dehydrogenation of complex hydrocarbon mixtures, and can be used for evaluation of the process. Due to the chemical complexity of jet fuel, the model components and model mixtures are used for investigation of suitable reaction conditions, which is shown in chapters 5.1 to 5.3. With this method of simplification of real jet fuel, detailed product compositions are available, which allow deduction of dehydrogenation reactions, side reactions and influences of components on each other. These results can also provide the boundary conditions of further catalyst development or design of jet fuel for fuel cell APU systems provided with hydrogen from PCD.

5.1 Experimental Evaluation of Reaction Conditions

The hydrogen output and product composition from PCD of complex hydrocarbon mixtures, model mixtures and model components is strongly dependent on the chosen reaction conditions. The reaction temperature in the heterogeneous gas phase reaction provides the reaction enthalpy for dehydrogenation reactions on the catalyst surface, but also can cause undesired cracking reactions to short chain or gaseous hydrocarbons. An increased pressure in the reaction system is desired due to the design of both concepts, which require product gas cleaning by pressure swing adsorption. A pressurized system has a negative influence on the reaction equilibrium dependent on the hydrocarbon group and might decrease hydrogen yield. By varying the contact time on the catalyst surface, the limitation of dehydrogenation reactions by pressure and temperature can be influenced to some extent. The formation of carbon on the catalyst surface and by this the deactivation of the catalyst over time is unavoidable, since this reaction path is part of the dehydrogenation reactions but can be limited by the choice of reaction conditions.

5.1.1 Evaluation of Reaction Temperature

First, the two components decane and methylcyclohexane (MCH) are chosen for detailed evaluation of process conditions. The cycloalkane MCH is expected to show a hydrogen yield with few side reactions, while the n-alkane decane is expected to show cracking carbon formation. The influence of reaction conditions on the PCD of these model components can be used for evolution. The influence of reaction temperature on decane was tested at a pressure of 1 bar with a 2 sec contact time by varying temperature TC1 between 350°C and

500°C. With this chosen contact time, the restrictions for the catalyst bed length defined in chapter 4.5.1 are maintained. For MCH, the temperature variation was narrowed between 375°C and 450°C. With both components, the feed flow was 10 g/h, while the mass of the catalyst bed for decane was varied from 3.0 g to 3.7 g and for MCH from 4.5 g to 5.0 g. The difference in catalyst bed mass is caused by the different gas densities of the components at reaction conditions. The evaporation temperature for decane is determined to be 200°C and for MCH at 120°C due to the respective boiling point of each component. In order to prevent carbon formation on the metal surface, which would obstruct the capillaries of the evaporator, it is important to keep the amount of heat provided to the capillary evaporator as low as possible.

Fig. 5.1 shows the conversion rate of decane, MCH and the carbon formation on the catalyst bed [$g_C/kg_{Cat.}$] of both components over different operation temperatures TC1. The conversion rate of the model components indicates the potential for hydrogen output of the component MCH. With decane, an increasing conversion rate can also indicate an increase of gaseous side products and carbon formation next to higher hydrogen yield. The formation of carbon is an indicator for the deactivation of the catalyst bed by occupation of the active sites of the Pt catalyst. With a reaction temperature of 400°C, the conversion rate of MCH is 14 times higher than that of decane. For decane, the conversion rate increases with reaction temperature except from 375 to 400°C. With MCH, the conversion rate decreases by 0.5 % at 450°C in comparison to 425°C. At 425°C, the highest conversion of MCH is achieved with 69 %.

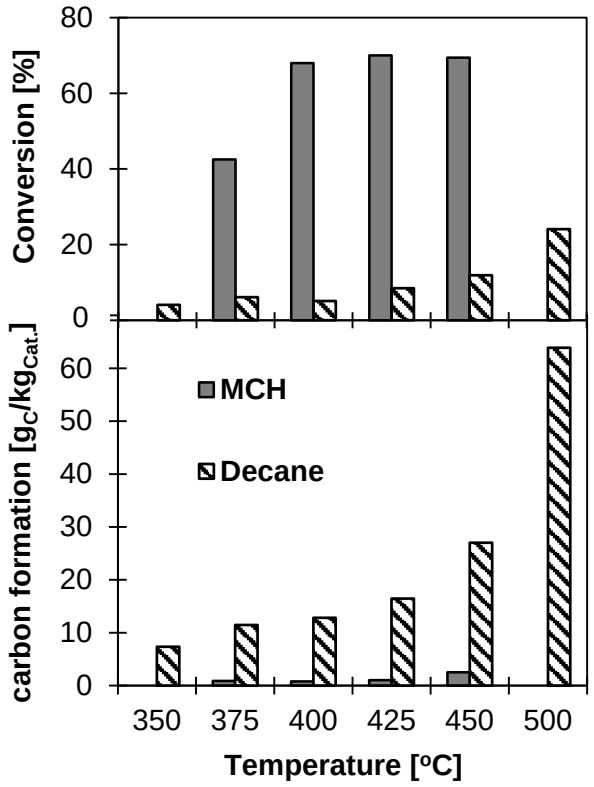

Fig. 5.1 - Conversion rate [%] and carbon formation on the catalyst [$g_C/kg_{cat.}$] of decane and MCH over temperature variation at 1 bar and 2 sec. contact time.

The comparison between the two components shows that carbon formation is, in average, 200 times larger for decane compared to MCH. From 450°C, the increase of carbon from decane is most apparent. From 400°C to 425°C, when the conversion of MCH is highest, the carbon formation from decane remains beneath 20 $g_C/kg_{Cat.}$. Therefore, having both the optimum conversion as well as the minimum in carbon formation, this temperature range is taken into consideration to choose suitable reaction conditions for further tests.

In Fig. 5.2, the influence of the hydrogen yield of decane and MCH [nl_{H2}/kg_{feed}] at different reaction temperatures, TC1, on conversion rate and carbon formation is presented. Further, the yield of saturated and non- saturated gaseous hydrocarbons as a sum from C1 to C4 (C_nH_m) carbon atoms is shown. The progress of the product gas yield and product gas concentration over reaction time gives information about how side reactions influence the desired dehydrogenation reactions for hydrogen output. It is obvious that the deposit of carbon on the catalyst surface causes deactivation and a decrease in hydrogen yield from decane with time. With higher reaction temperature, the increased conversion rate of decane leads to more hydrogen evolution in the beginning of the reaction time. However, with increasing amount of carbon deposit on the catalyst, the deactivation is more prominent. In contrast to decane, the hydrogen yield from MCH is more constant and up to 5 times higher.

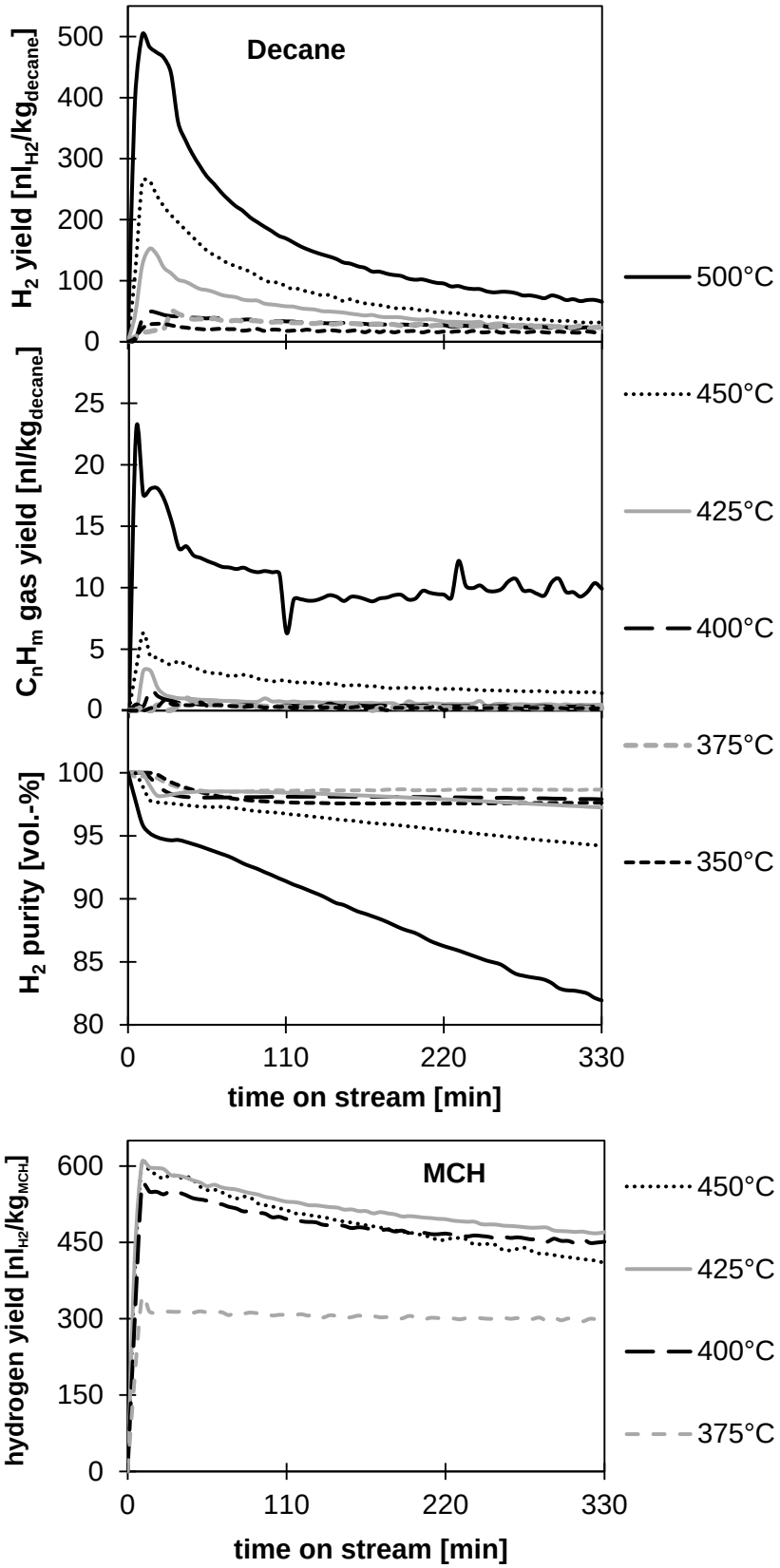

Fig. 5.2 - hydrogen yield [nl_{H2}/kg_{feed}] of decane and MCH, yield of gasous hydrocarbons C_nH_m from decane [nl_{H2}/kg_{decane}] and hydrogen purity in product gas of decane [vol.-%] dehydrogenation over reaction time at different operation temperature

Further, gaseous hydrocarbons derived from the cracking reactions of decane increase with reaction temperature, and reduce the hydrogen purity of the product gas. The decline of hydrogen purity is caused by the constant evolution of gaseous hydrocarbons, while the hydrogen yield is decreasing due to catalyst deactivation. The reason for the constant evolution of gaseous hydrocarbons can be found by the cracking reaction, which can derive from catalytic cracking and from thermal cracking, while dehydrogenation has to be catalyzed. Thermal cracking occurs on the hot surface of the steel reactor or other hot parts of the test rig, such as the evaporator and hot inactive catalyst sites [104], [35], [105]. The presence of hydrogen can even encourage cracking reactions by hydrocracking [9]. Therefore, with increasing temperature, more reaction products appear and the evolution is almost independent from catalyst activity.

The dehydrogenation of the component MCH shows almost only hydrogen in the product gas. Less than 0.01 vol.-% of methane in the product gas composition was detected throughout the reaction time at any tested operation temperature. The temperature range between 400°C to 450°C is similar. The detected carbon deposit on the catalyst leads to a slide degradation of the hydrogen yield over time. The difference in hydrogen evolution between the three reaction conditions is made by the conversion rate of the MCH, which increases the hydrogen yield, but also carbon formation which leads to degradation. At 375°C, the conversion of MCH is 26.5 % less, this is represented by the decreased hydrogen yield. Even so, no carbon formation was detected with this reaction condition, and therefore a stable reaction progress is achieved. At 425°C, the hydrogen yield over time is the highest in the balance between conversion rate and catalyst deactivation.

Condensable product composition:

Up to 72 different components are detected in the condensate of dehydrogenated decane. The reactions involve dehydrogenation to alkenes (Eq. (5.1)), cycloalkanes (Eq. (5.2)) and aromatic hydrocarbons (Eq. (5.3)), [106], [87]. Other reactions are isomerization to iso-alkanes, cracking to shorter chain hydrocarbons and even carbon chain growth to longer chain hydrocarbons than decane. Thus, the formation of aromatic hydrocarbons increases the hydrogen yield, since the stoichiometry of the reaction allows up to 4 hydrogen molecules to dehydrogenate.

dehydrogenation: $$C_{10}H_{22} \rightleftarrows C_{10}H_{20} + H_2 \qquad \Delta H_R^0 = 125.6\,kJ/mol \qquad (5.1)$$

dehydrocyclisation: $$C_{10}H_{22} \rightleftarrows C_{10}H_{18} + 2H_2 \qquad \Delta H_R^0 = 36.5\,kJ/mol \qquad (5.2)$$

aromatization: $$C_{10}H_{22} \rightleftarrows C_{10}H_{14} + 4H_2 \qquad \Delta H_R^0 = 235.9\,kJ/mol \qquad (5.3)$$

The reaction temperature has a stronger influence on the composition of the condensable products and carbon formation, since with rising temperature, formation of aromatic

hydrocarbons increases. Fig. 5.3 presents the hydrocarbon group composition of the condensable product components from decane dehydrogenation at different reaction temperatures, 1 bar system pressure and 2 sec of contact time on the catalyst.

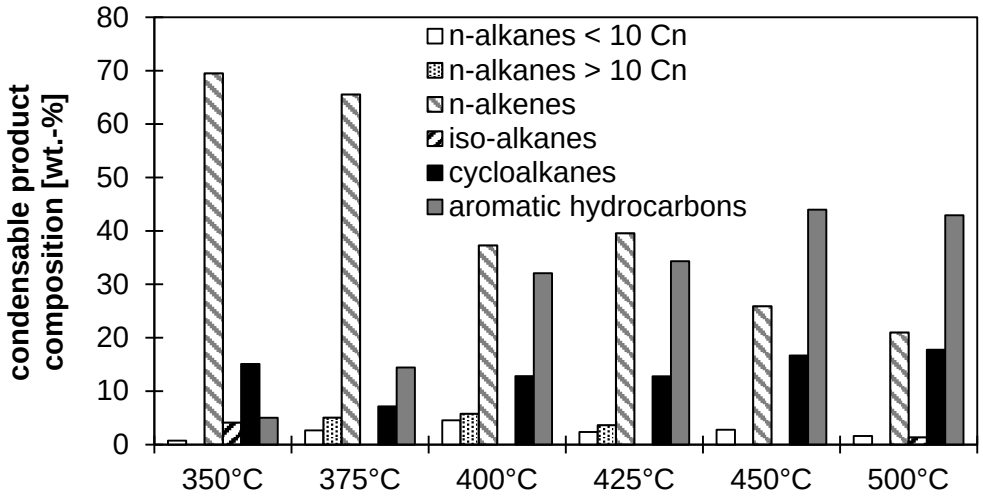

Fig. 5.3 - condensable product composition of dehydrogenated decane dependent on the reaction temperature at 1 bar system pressure and 2 sec of contact time

The product components accompanying a specific hydrocarbon group are added up to alkanes, alkenes, isoalkanes cycloalkanes and aromatic hydrocarbons. The alkane products are presented in two separate groups of alkanes with a carbon atom number Cn shorter than 10 carbon atoms and longer than 10 Cn. The variation of the hydrocarbon group composition with different reaction temperature indicates the influence of reaction conditions on the reaction paths. The hydrogen yield is also influenced, since with progressive dehydrogenation of decane to aromatic hydrocarbons, more hydrogen is evolving. The product hydrocarbon group of alkenes is declining with temperature, while the conversion of aromatic hydrocarbons and cycloalkanes increases. This indicates that aromatic hydrocarbons are formed by dehydrocyclization of decane. With the formation of aromatic hydrocarbons, the stoichiometric amount of hydrogen molecules is higher than with the dehydrogenation of alkanes. On the other hand, formation of carbon, as presented in other work [107], [66] is caused by aromatic ring condensation, which is formed by radical aromatic hydrocarbons. Next to the increased conversion rate of the decane with higher reaction temperature, the conversion to more aromatic hydrocarbons leads to higher hydrogen yield with decane while the catalyst is still active. The identified product alkanes are shorter chain alkanes than decane; meaning hexane, heptane and nonane, but also longer chain alkanes of undecane, dodecane and even tridecane. This indicates that not only cracking to shorter chain alkanes is possible, but also chain growth from radicals. With rising temperature, the distribution of product alkanes shifts to more short chain alkanes, which are a product of cracking reactions. In summary, with increasing reaction temperature, conversion of decane to aromatic hydrocarbons and the

formation of shorter chain alkanes increases, while the formation of alkenes decreases. As a conclusion, the formation of aromatic hydrocarbons leads to more hydrogen evolution, but with further reactions due to more carbon deposits, the activity of the catalyst is limited.

The condensable product composition of dehydrogenated MCH shows, in comparison to decane, only few product components. The main product is the aromatic hydrocarbon toluene. The reaction equation of MCH to toluene shows that up to 3 moles of H_2 can evolve, Eq. (5.4). The high hydrogen yield of the experiment is derived not only from the conversion rate, but also from the amount of hydrogen molecules in the aromatization reaction. The maximum possible hydrogen output from MCH as a pure component without kinetic limitations can be calculated to 684.83 $nl_{H2}/kg_{MCH.}$

aromatization: $$C_7H_{14} \rightleftarrows C_7H_8 + 3H_2 \qquad \Delta H_R^0 = 204.8 kJ/mol \qquad (5.4)$$

Several reaction steps take place over cycloalkenes to complete aromatization to toluene. For the dehydrogenation of MCH, 4 intermediate components are identified in this work in GCMS and GCFID: 4-methylcyclohexene, 3-methylcyclohexene and 1-methylcyclohexene. Ethylcyclopentane is also detected, which is formed by restructuring the molecule structure without dehydrogenation. Usman et al. [108] suggests a reaction kinetics of dehydrogenation of MCH on a Pt catalyst, but it does not involve intermediate reaction products. The variation of temperature has little influence on the reaction path of MCH to toluene. With temperature variation at 1 bar and 2 sec of contact time, the turnover of MCH to toluene is at each temperature 93.1 wt.-% with a maximum variation of 0.3 %. The rest of the product mass is 6.39 wt.-% of hydrogen with a variation of 0.2%. With increasing temperature, the amount of intermediate products methylcycloalkenes changes from 0.26 wt.-% to 0.87 wt.-% and in average, 0.03 wt.-% is carbon and gaseous hydrocarbons. Within the tested temperature range, the reaction progress is influenced by less than 0.5 %.

Finally, the total hydrogen yield as [g_{H2}/kg_{feed}] and the carbon deposition on the catalyst from decane and MCH are used to define an optimized reaction temperature, TC1, for further investigations. The target temperature should allow high hydrogen yield with the lowest possible carbon deposit. The ratio of both parameters show a maximum at TC1=400°C, see Table 5.1.

Table 5.1 – hydrogen yield of MCH dehydrogenation and correlation with decane carbon formation at different operation temperature in the catalytic bed.

operation temperature TC1	[°C]	375	400	425	450
H_2 yield	$[g_{H2}/kg_{feed}]$	28.93	43.40	50.13	49.10
carbon deposit	$[g_C/kg_{Cat.}]$	11.60	14.63	18.46	23.29
ratio	$[(g_{H2}/kg_{feed}) / (g_C/kg_{Cat.})]$	2.49	2.97	2.71	2.11

5.1.2 Evaluation of Pressure and Contact Time

Since both process concepts described in chapter 1 would primarily run as a pressurized system, the influence of pressure is investigated on the model components decane and MCH. The goal is to identify reaction conditions under pressure which suit the desire of high hydrogen yield and stable reaction progress, while having few side reactions. In general, pressure is expected to have a negative influence on dehydrogenation reactions, since the thermodynamic equilibrium indicates that pressure would shift the reaction towards the educts (Le Chatelier's principle). It is of interest to investigate the influence of pressure on the hydrogen yield and the production of side products to see if a specific pressure level shows more promising results according to requirements of the process concepts.

The pressure is varied by 1, 3, 5, and 8 bar, initially at 400°C and 2 sec of contact time. Further, to influence the conversion rate of the model components toward more hydrogen production despite the influence of pressure, the tests are also performed at increased contact time of 4 sec on the catalyst. In order to meet the conditions of the minimum and maximum length of catalytic bed, the feed flow of decane was increased at 3 bar to 20 g/h, and to 40 g/h at 5 and 8 bar. For MCH, a feed flow of 20 g/h and 40 g/h was used for 5 bar and 8 bar, respectively. Fig. 5.4 shows the conversion rate and carbon formation of decane and MCH at different pressures and contact times of 2 and 4 sec.

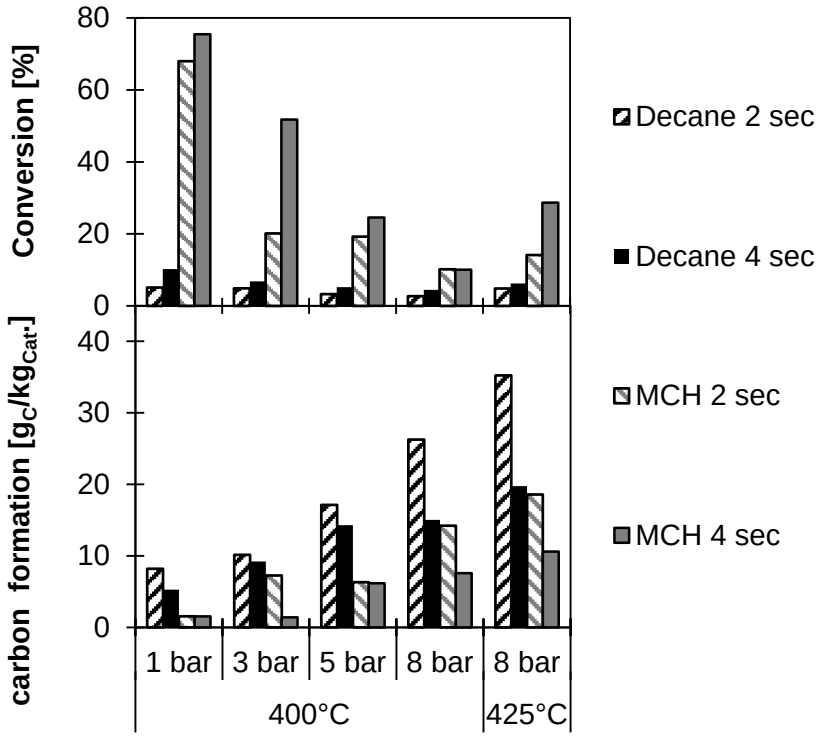

Fig. 5.4 - conversion rate and carbon formation on the catalyst of decane and MCH with 2 sec and 4 sec of contact time over pressure variation at 400°C and 425°C

Influence of pressure on the conversion rate:

The conversion rate of MCH declines from 69 % at 1 bar to 10 % at 8 bar at 2 sec. The conversion of decane also drops by almost 50 % at 8 bar pressure. In average, an increase in contact time raises conversion of decane by 1.5 times. With MCH, an increase in contact time leads to higher conversion in the pressure range up to 5 bar. At 3 bar, the conversion rate can be influenced by 61 %, and at 8 bar, no additional conversion was detected. Between 1 and 8 bar, the conversion rate is gradually declining with both components. As a result, no tested pressure level above 1 bar shows convenient conversion rates for a pressurized system.

Nonetheless, a high system pressure for the process concept is desired. A higher conversion rate of MCH has to be achieved to raise the amount of hydrogen evolution. Therefore, the reaction temperature was raised at 8 bar to 425°C. As a result, the conversion rate of MCH is raised by 50 % with 4 sec of contact time, while the conversion of decane increases by 22 %. As a conclusion, the increase of temperatures together with higher contact time at 8 bar leads to higher conversion rates for both components and potentially more hydrogen evolution.

Influence of pressure on the carbon formation:

Pressure clearly has an increasing influence on carbon formation with both components. The contact time of 4 sec shows less carbon formation per catalyst mass. However, the carbon deposit is strongest at the entrance of the catalyst bed. Therefore, the formation of carbon is not equally spread on the catalyst surface. As a result, a longer catalyst bed has less carbon deposit downstream and the relative amount of carbon to the catalyst becomes smaller. This also leads to a more active catalyst bed over time which influences the conversion rate.

The influence of pressure on both components leads to a decrease of conversion and an increase in carbon formation, meaning that a higher percentage of the conversion rate runs towards carbon formation. The dependency of carbon formation at higher pressure is especially strong with the n-alkane. It follows that with a decreasing conversion rate, the hydrogen yield with both components is declining, see Fig. 5.5.

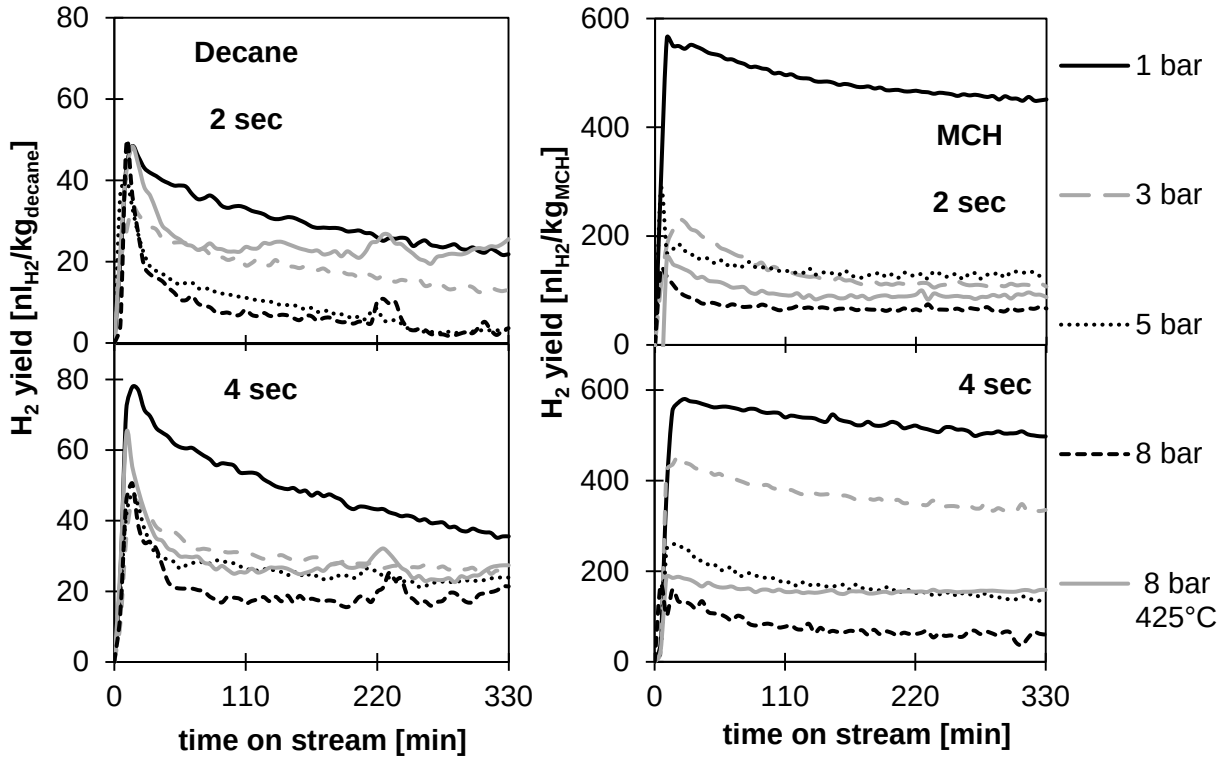

Fig. 5.5 - hydrogen yield of decane and MCH with 2 sec and 4 sec of contact time over pressure variation at 400°C and 425°C at 8 bar

Influence of pressure on the hydrogen yield:

Following the declining conversion rate from 1 to bar 8 bar system pressure, the hydrogen yield decreases gradually with both components. With MCH, the reaction progress is mostly stable despite increasing carbon formation with higher pressure. The increase of contact time allows higher hydrogen evolution, which is most prominent at 3 bar, since the conversion rate

increase was the strongest. The increase of reaction temperature at 8 bar from 400°C to 425°C also follows the conversion rate by increasing the hydrogen yield, especially with a contact time of 4 sec. As a conclusion, the hydrogen yield from PCD of MCH can be directly influenced by the conversion rate, since little of the conversion rate is contributing to side reactions. Further, the reactivity of MCH on the catalyst allows stable reaction conditions, despite carbon deposited on the catalyst surface.

The hydrogen evolution of decane also follows the conversion rate and decreases with increasing pressure. The increase of contact time leads to more hydrogen evolution. Though, the decline of hydrogen yield over time is noticeable, with 2 sec of contact time and different pressure, as well as with 1 bar and 4 sec of contact time. At 2 sec of contact time, the occupation of the catalyst surface with carbon is stronger than with a longer reaction bed, causing the decline of hydrogen yield over time. However, at higher pressure and increase of contact time, the reaction progress is more stable. At 8 bar pressure, an increase of reaction temperature to 425°C shows more hydrogen yield and with stable reaction progress. The increase of reaction temperature with decane leads to higher carbon formation. This indicates that hydrogen is evolving from carbon formation of decane, since the hydrogen yield rises with 4 sec from 400°C to 425°C by 27.8 %.

The results of hydrogen yield show that between 1 bar and 8 bar, the hydrogen yield decreases gradually with both components. This indicates that for the choice of a suitable reaction condition for the process concepts, no tested pressure above 1 bar shows advancement over the other. For running a gas cleaning system with pressure swing adsorption, the highest tested pressures would be favorable.

Influence of pressure on cracking products:

Fig. 5.6 shows the hydrogen purity as the average volume content in the product gas and the average gaseous hydrocarbon yield over the total reaction time. In comparison to temperature variation, the pressure has only a small influence on the evolution of gaseous hydrocarbons with decane. With declining hydrogen yield, cracking products are also decreasing with rising pressure, which leads to a similar hydrogen purity. Cracking reactions appear from catalytic cracking and thermal cracking. With increasing pressure, the partial pressure of hydrogen in the reaction system increases, and cracking reactions are suppressed. Also, catalyst activity is declining due to carbon deposit. An increase of contact time leads to more hydrogen evolution and more gaseous hydrocarbons. The catalytic dehydrogenation has a higher contribution to the gas products. Therefore, hydrogen purity increases with higher contact time. The increase of the reaction temperature to 425°C at 8 bar leads to 70 % more gaseous hydrocarbons, which indicates that cracking reactions are determined from thermal cracking

as well. Due to increasing carbon formation, less active catalyst surface is available, and the hot inactive surface induces a cracking reaction. This negative influence can be corrected by increasing contact time, which leads to more hydrogen yield. Since more active catalyst is available, more dehydrogenation and fewer cracking reactions are evolving. In contrast, with MCH, by increasing pressure, the content of gaseous hydrocarbons does not increase. Only with the reactions conditions of 8 bar, 400°C and 2 sec of contact time was 0.2% of methane detected in the product gas.

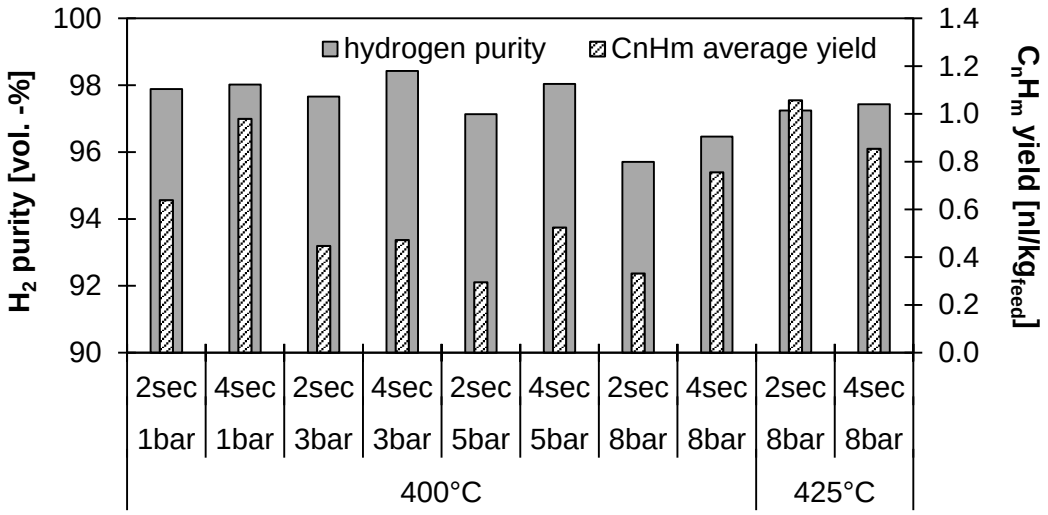

Fig. 5.6 – average hydrogen purity and C_nH_m gas yield over reaction time of dehydrogenated decane dependent on pressure and contact time at 400°C and at 425°C with 8 bar

Influence of pressure on condensable product composition:

The variation in pressure influences the conversion of MCH to toluene to some extent, Fig. 5.7 presents the condensable product distribution of Decane and MCH summarized in hydrocarbon groups. The pressure increase shows an increase in intermediate cycloalkene products, while the conversion towards toluene is suppressed. An increase of contact time can influence the conversion of MCH towards more hydrogen yield, which indicates a higher conversion rate toward aromatic hydrocarbons.

With decane, pressure reduces the conversion towards aromatic hydrocarbons, while at the same time, the content of cycloalkanes is decreasing. This indicates that formation of aromatics occurs over cyclisation of the carbon chain [109]. An increase in contact time leads to higher content of aromatic hydrocarbons and cycloalkenes in the condensate, while n-alkenes are declining, which contributes to more hydrogen output. The increase of temperature to 425°C at 8 bar at 4 sec of contact time shows an increase in aromatic hydrocarbons with both components. With increased pressure of 5 and 8 bar, the content of n-alkanes products increases, while a higher contact time decreases the content. By increasing the reaction

temperature, the distribution of longer chain and shorter chain alkanes shifts towards shorter chains alkanes, which are cracking products.

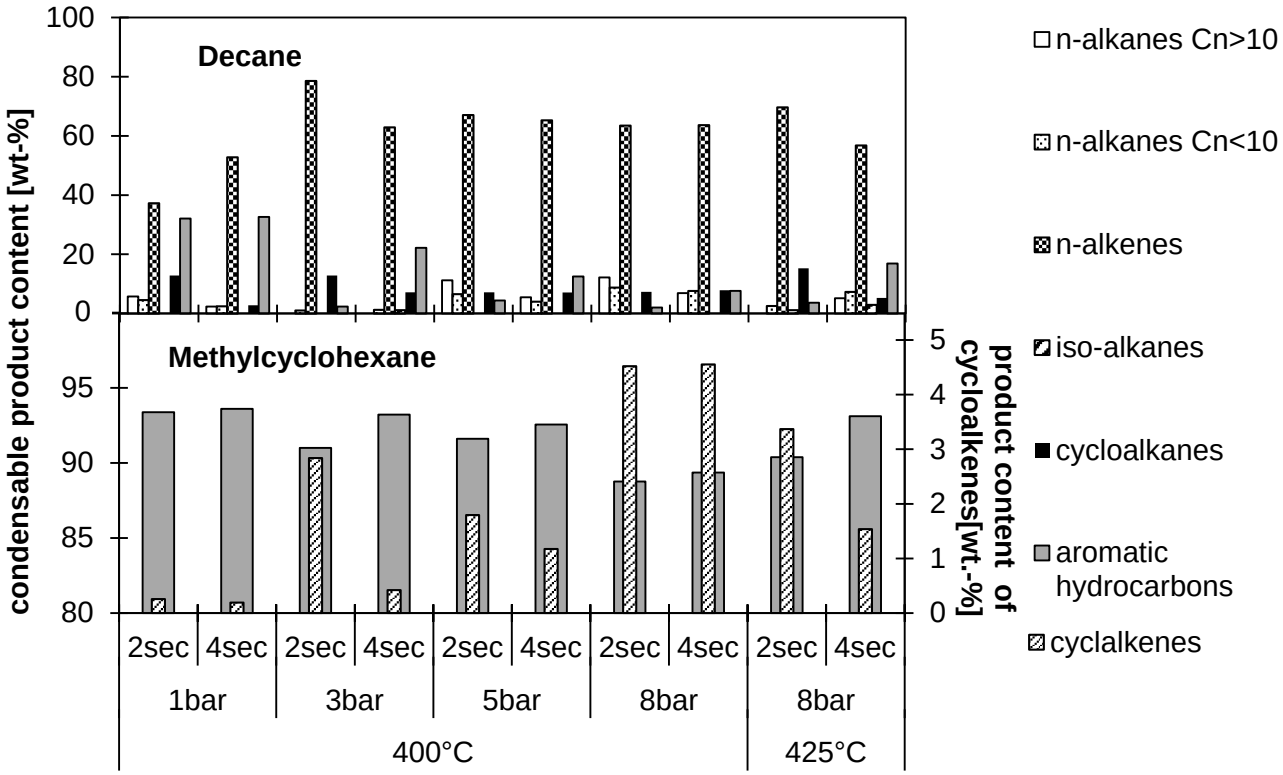

Fig. 5.7 - condensable product composition of dehydrogenated decane and MCH dependent on pressure and contact time at 400°C and at 425°C with 8 bar

Selection of reaction conditions for further tests:

In consideration for suitable reaction conditions on model mixtures and kerosene, the hydrogen yield, product composition and carbon formation have to be taken into account. When testing model mixtures, the carbon deposit of decane can decrease the dehydrogenation of MCH and influence the overall hydrogen output. Two operation conditions are selected for the model components and model mixtures. The highest hydrogen yield and lowest carbon deposit were achieved with 1 bar and reaction temperature at 400°C. The influence of contact time at 1 bar is much smaller than with increased pressure. The catalyst bed length with 4 sec of contact time would be 6.5 cm for decane and 9.3 cm for MCH, which exceeds the defined experimental method restrictions. With 2 sec of contact time and with all model components, the bed length can be kept under 4.5 cm at 1 bar and 400°C reaction conditions. Between 1 and 8 bar at 400°C, the hydrogen yield is decreasing, while carbon formation is increasing with both tested model components. An increase of contact time influences hydrogen yield, hydrogen purity and carbon formation in a positive way, in particular with decane. Since no optimum pressure for dehydrogenation above 1 bar is experimentally obtained, maximum pressure of 8 bar is chosen as the pressure swing adsorption for the process concept is more efficient at higher

pressure. An increase in reaction temperature leads to higher hydrogen yield, which is needed for a sufficient process system. The chosen reaction conditions for further testes with model components mixtures and kerosene are:

- Low pressure operation conditions: 1 bar, 400°C and 2 sec contact time and 10 g/h feed mass stream
- High pressure operation conditions: 8 bar, 425°C and 4 sec contact time and 40 g/h feed mass stream.

5.2 PCD of Model Components

The two chosen reaction conditions presented above are tested for all eight model components representing hydrocarbon groups in ULSK and Jet A-1 fractions. The detailed experimental conditions are shown in appendix 8.2 table 8.3. The aim is to receive information about hydrogen yield and hydrogen purity, as well as product compositions of gaseous and condensable products for evaluation of possible reaction path to integrate into process simulation. By these experimental results, both reaction conditions can be further evaluated as to their suitability for the process concepts.

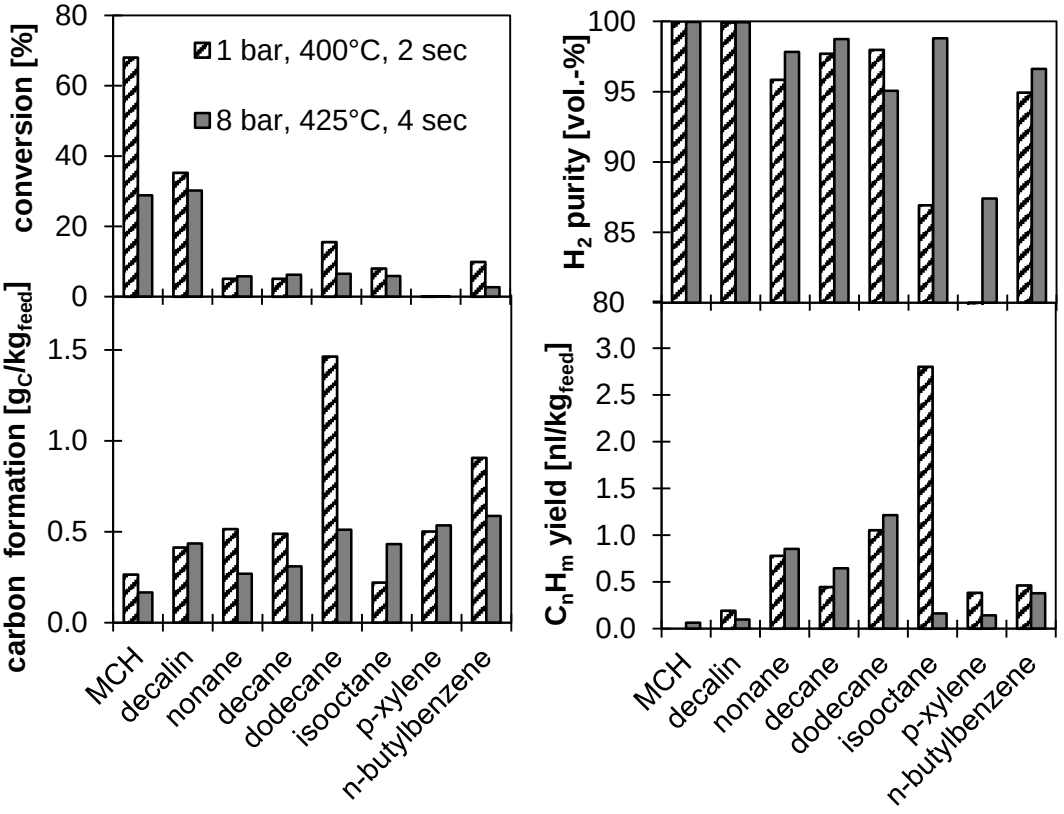

Fig. 5.8 - conversion rate, carbon formation by mass of feed, hydrogen purity and gaseous hydrocarbon yield of model components at two defined reaction conditions of PCD

Fig. 5.8, presents the conversion rate, the carbon formation by the mass of feed, hydrogen purity and average gaseous hydrocarbon yield over the reaction time. The cycloalkane decalin shows similar results to MCH, but at higher pressure the formation of carbon is increasing with decalin and more gaseous side products are evolving. Another noticeable difference between MCH and decalin is that the conversion rate of decalin is not influenced by the reaction conditions as much as MCH.

All alkanes show a decrease with carbon formation and an increase of gaseous hydrocarbons at higher pressure. Nonane has very similar results to decane, but dodecane shows a higher conversion rate at a lower pressure of 1 bar. The increase of gaseous hydrocarbons at higher pressure leads to a decline of hydrogen purity with nonane and dodecan. But with dodecane, the hydrogen purity decreases with higher pressure reaction conditions, which can be derived from the decreased conversion rate, which contributes more towards cracking than with the other two alkanes. With nonane and decane, the increased hydrogen pressure suppresses carbon formation, but leads to cracking products. The model component isooctane has a high evolution of gaseous hydrocarbons at low pressure, which also decreases hydrogen purity. However with 8 bar, the cracking to gaseous side products is suppressed but carbon formation increases. The aromatic hydrocarbons p-xylene and n-butylbenzene show little conversion rate, which contributes strongly to carbon formation and evolution to gaseous hydrocarbons, which is reducing hydrogen purity from the hydrogen in the test rig.

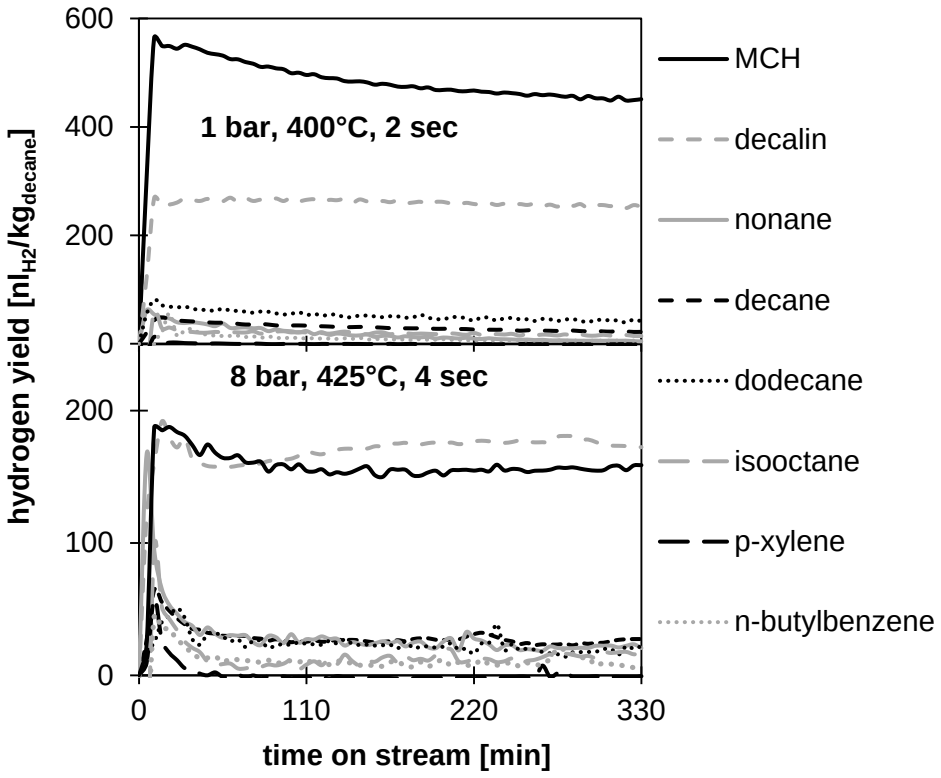

Fig.5.9 – hydrogen yield of PCD of model components at two defined reaction conditions

The conversion rate of the model components is followed by the hydrogen yield, which is presented in Fig. 5.9. The hydrogen yield of decalin at higher pressure reaction condition is reduced by 34 % of the hydrogen yield at 1 bar reaction condition. The n-alkanes nonane and decane show similar hydrogen output at high pressure reaction condition. At 1 bar reaction conditions, dodecane has the highest hydrogen yield. With 8 bar reaction conditions, the hydrogen yield increases with nonane, remains the same with decane and decrease with dodecane. Isooctane shows a rapid decrease in hydrogen yield over reaction time at higher pressure reaction conditions, which is caused by catalyst deactivation. The aromatic hydrocarbon p-xylene shows no hydrogen evolution, while with the component n-buytlbenzene, hydrogen yield is an average of 8 nl_{H2}/kg_{feed}, which does not differ between the two reaction conditions.

Gaseous product composition of model components:

The detailed gaseous product distribution of all model components is presented in table 5.2.

Table 5.2– gaseous product distribution of model components with two reaction conditions

model component		H_2	CH_4	C_2H_4	C_2H_6	C_3H_6	C_3H_8	C_4H_{10}
		[vol.-%]						
MCH	1 bar 400°C 2 sec	100.0						
decalin		99.92	0.08					
nonane		95.85	2.71	0.40	0.69	0.20	0.15	
decane		97.70	0.99	0.10	0.53	0.11	0.42	0.15
dodecane		99.11	0.73	0.02	0.08	0.01	0.04	0.01
isooctane		86.93	13.07					
p-xylene		76.91	23.09					
n-butylbenzene		94.94	4.23		0.76	0.07		
MCH	8 bar 425°C 4 sec	99.96	0.04					
decalin		99.94	0.06					
nonane		97.83	0.88	0.19	0.67	0.12	0.31	
decane		98.49	0.51	0.44	0.08	0.21	0.01	0.26
dodecane		90.60	1.49	0.49	1.62	0.39	0.81	4.61
isooctane		98.80	1.14				0.06	
p-xylene		71.73	28.27					
n-butylbenzene		96.62	0.94		1.96	0.15	0.32	

Since the n-alkane nonane shows less hydrogen yield with 1 bar reaction conditions, more of the conversion rate contributes toward cracking reactions, mostly methane. At higher pressure in the system, more longer saturated hydrocarbons with longer carbon chain are detected. With dodecane, less hydrogen is produced at high pressure and the conversion contributes more towards the gaseous cracking product butane (C_4H_{10}).

With isooctane, the only cracking product detected was methane at low pressure reaction condition, while at higher pressure, propane was also produced. The gaseous product distribution of the aromatic hydrocarbons depends strongly on the amount of product gas evolving, which is almost zero by the end of the test run. Therefore, the distribution contains hydrogen from the startup phase of the experiment. With p-xylene, only methane was detected, but the component n-butylbenzene also shows longer chain hydrocarbons cracked from the butane side branch of the aromatic hydrocarbons. With increased pressure, less methane and especially longer chain gaseous hydrocarbons appear.

The increase of longer chain saturated hydrocarbons in the gas phase leads to the assumption that different types of cracking reactions occur with higher hydrogen pressure than at lower pressure. With lower pressure, thermal cracking on the hot surfaces dominates, while at higher pressure, the partial pressure of hydrogen is much higher and hydrocracking, a catalyzed reaction, is more common. This can be derived from the increasing amount of saturated gaseous hydrocarbons that appear from an increased amount of C2 to C4 carbon chain length cracking. At temperatures above 300°C and pressurized hydrogen, long chain alkanes are cracked to shorter chain alkanes [9], [110].

Condensable products composition of model components:

The mass distribution of the condensable products from PCD of pure model components is presented in table 5.3. The detected products in the condensate are summarized according to their affiliation to hydrocarbon groups.

The conversion product of cis/trans- decalin by aromatization is naphthalene, with the intermediate product tetralin [24], see Eq. (5.5) and (5.6).

reaction to tetralin: $\rightleftarrows C_{10}H_{18} \rightarrow C_{10}H_{12} + 3H_2 \qquad \Delta H_R^0 = 209.9\,kJ/mol$ (5.5)

reaction to naphthalene: $\rightleftarrows C_{10}H_{18} \rightarrow C_{10}H_8 + 5H_2 \qquad \Delta H_R^0 = 333.2\,kJ/mol$ (5.6)

With 1 bar reaction conditions, almost 70 % of all converted decalin is fully dehydrogenated to naphthalene. With increased pressure at 8 bar, the aromatization is slightly decreased.

The liquid product distribution of dehydrogenated alkanes shows less aromatic hydrocarbon and more n-alkene products with higher pressure. The dehydrocyclization reactions would lead to more hydrogen evolution than dehydrogenation. Isomerization reactions are also common with alkanes, where no hydrogen is evolved, but the chemical structure of the molecule changes. With higher pressure, more isomers are produced. This demands more energy for the reaction enthalpy towards reactions without hydrogen evolution.

Table 5.3 – condensable product mass distribution of model components at two different reactions conditions

model component		n-alkanes	iso-alkanes	n-alkenes	iso-alkenes	cyclo-alkanes	cyclo-akenes	aromatic hydro-carbons
		[wt.-%]						
MCH	1 bar 400°C 2 sec						0.28	99.72
decalin							30.13	69.87
nonane		0.52	4.21	43.43		3.62		48.22
decane		11.32	0	40.96		14.09		33.63
dodecane		4.92	2.98	68.17		0.14		23.80
isooctane					100			
p-xylene								100
butylbenzene								100
MCH	8 bar 425°C 4 sec					0.03	1.62	98.35
decalin							33.14	66.86
nonane		4.59	5.72	54.70		2.89		32.11
decane		13.21	3.05	60.24		5.60		17.90
dodecane		7.60	4.63	72.90		2.47		12.40
isooctane					99.45	0.55		
p-xylene								100
butylbenzene							0.28	99.72

The conversion of isooctane contributes with both reaction conditions towards a few iso-alkenes, meaning: 2,4,4-Trimethyl-1-pentene, 2,4,4-Trimethyl-2-pentene, 2,3,4-Trimethyl-pentene and 3,5-Dimethyl-1-hexene. With aromatic hydrocarbons, the conversion of p-xylene and n-butylbenzene mostly contributes toward carbon formation. Since carbon is not detected in GCFID, the conversion of aromatic hydrocarbons cannot be calculated by the turnover of the feed to the condensate. Therefore, the conversion is calculated from the products content, not from the change of mass content of the feed. The detailed liquid products detected in GCMS and GCFID of all model components are presented in the appendix 8.4 together with the components identified in Jet A-1 and ULSK. The distribution of the liquid products in the single component tests are used to define model reactions for the modeling of the dehydrogenation reactor in the process simulation for both process concepts.

The results show that most hydrogen evolution can be expected from cycloalkanes. For the dehydrogenation of model mixtures, it is of interest for the process concepts to achieve high conversion rate of the model components representing cyclolalkanes. Other components can influence the conversion of cycloalkanes by catalyst deactivation through carbon formation and decrease hydrogen purity by cracking reactions. The experimental results of single

components PCD tests show that the highest hydrogen potential would be available with the lower pressure reaction conditions. The influence of the components on each other in model mixtures has to be obtained in order to decide about the most suitable reaction condition for the process concepts.

5.3 PCD of Model Mixtures, ULSK and Jet A-1 Fractions

In the next step, the model components are tested in the two ULSK model mixtures, and the two model fractions designed for the evaluation of the process. The model mixtures are tested at the two chosen reaction conditions. The highest hydrogen output can be expected from MCH at 1 bar. The influence of other hydrocarbon groups can decrease these conversions and hydrogen output of this cycloalkane. To identify which hydrocarbon group has the most influence on the conversion rate of MCH due to catalyst deactivation and side reactions, three tests with two- component- mixtures are performed at 1 bar reaction condition. One of which is MCH, and the second is another component representing a different hydrocarbon group.

5.3.1 PCD of Two Component Mixtures

For the two- component- mixtures, the same four model components are used as with the four-component ULSK model mixtures, which are presented in chapter 3.4.2. The compositions are defined after the relative content of the hydrocarbon group cycloalkanes to the other three hydrocarbon groups. The three mixtures are prepared and tested with 55.7 wt.-% MCH with 44.3 wt.-% p-xylene (dotted line), 49.7 wt.-% MCH with 50.3 wt.-% isooctane (solid line) and 53.9 wt.-% MCH with 46.1 wt.-% decane (broken line). The difference in hydrogen yield indicates the influence on MCH, since this component would have the highest contribution to the hydrogen evolution, see Fig. 5.10.

Although the aromatic hydrocarbon p-xylene causes a lot of carbon formation with pure component tests, the mixture with MCH shows the most stable reaction progress, high hydrogen yield and moderate carbon formation, see table 5.4. The hydrogen output from MCH as a pure component with 1 bar reaction conditions is 476.7 nl_{H2}/kg_{MCH}. The stream of MCH is half of the pure component test, while the hydrogen yield is a third of the hydrogen yield of MCH as a pure component. The component p-xylene influences the conversion of MCH. The decreased partial pressure of the more reactive component MCH leads to less conversion on the catalyst. On the other hand, the influence of p-xylene on the catalyst is also decreased. Overall, the evolution of gaseous hydrocarbons is very small and hardly affects the hydrogen purity of the product gas.

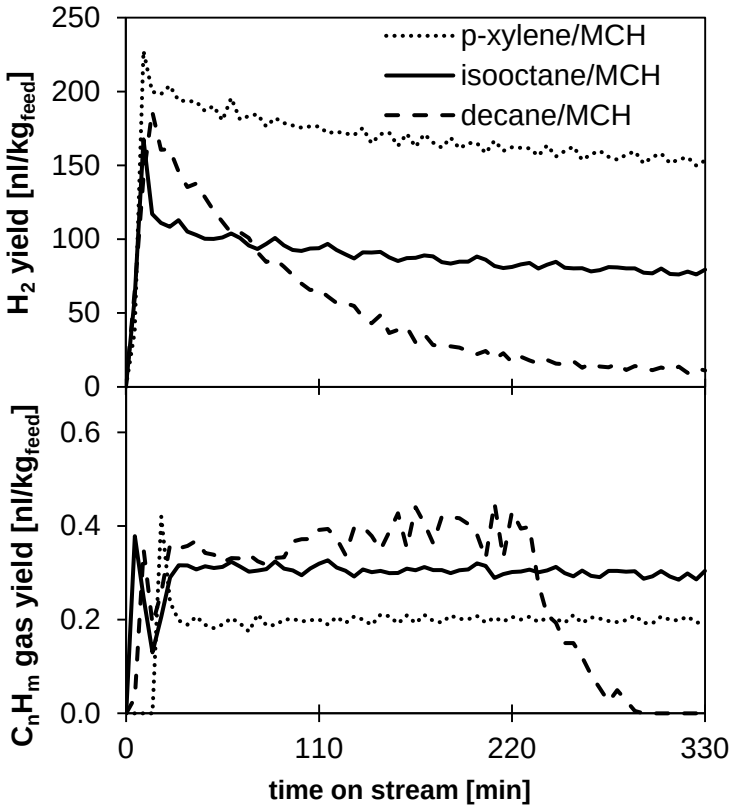

Fig. 5.10 - hydrogen yield and yield of gaseous hydrocarbons over reaction time of 2-components mixtures at 1 bar reaction conditions

With isooctane, and especially with decane, the results are different. The hydrogen yield, mostly produced from MCH, strongly decreases, as well as the conversion rate of MCH. With decane as second component, the amount of product gas decreases rapidly. The drop of the gaseous hydrocarbons at 230 min is caused by too little gas formation, which leads to leakage at the GCTCD. The only gaseous hydrocarbon detected in the product gas was methane for p-xylene and isooctane mixtures. In addition to this, with the decane mixture, 0.1 vol-% of ethane also was registered. Most cracking products appear with decane, while with p-xylene, the highest hydrogen purity is achieved. The results of pure isooctane would lead to the conclusion that most cracking should appear with this 2-component mixture, though decane and isooctane show similar gaseous hydrocarbon yield.

The conversion rates of the components within the mixtures, carbon formation and average hydrogen purity over reaction time is presented in table 5.4.

Table 5.4 - Conversion rate and carbon formation of MCH in 2- component mixtures

two- component mixtures		pure MCH	p-xylene/ MCH	isooctane/ MCH	decane/ MCH
conversion rate of MCH	[%]	68.0	44.9	21.34	12.16
conversion rate of second component	[%]	-	0.07	13.05	3.89
carbon formation	[g_C/kg_{feed}]	0.26	0.33	0.27	0.58
H_2 purity	[vol.-%]	100.0	99.99	99.7	99.37

Carbon formation with decane is doubled when compared to the other two mixtures, causing stronger deactivation over time. The conversion of decane must lead to carbon formation. Further the reactivity of Isooctane and decane occupy the catalyst surface. Therefore, not only carbon occupies the catalyst surface, but a declined partial pressure of MCH on the catalyst surface leads to less conversion of the cycloalkane. On the other hand, the component p-xylene shows very little conversion, which leads to the conclusion that the aromatic hydrocarbon has only a small influence on conversion of the cycloalkane. Iso-alkanes and especially n-alkanes occupy the catalyst by carbon formation and occupation of the active sites on the catalyst.

5.3.2 PCD of Four Component Model Mixture

The four- component model mixture described in chapter 3.4.2 is tested with the two defined reaction conditions. The content of each component in the mixture is MCH 27.5 wt.-%, decane 23.8 wt.-%, isooctane 28.2 wt.-% and p-xylene 20.5 wt.-%.

Fig. 5.11, illustrates the hydrogen yield, gaseous hydrocarbon yield and hydrogen purity of the four- component model mixture over reaction time. Considering that pure MCH has an almost three times higher hydrogen yield with low pressure reaction conditions than at 8 bar, it was expected that with 1 bar reaction conditions, the hydrogen yield would be higher. However, the partial pressure of each component has to be taken into consideration. The concentration of the component MCH is about a quarter of what it would be as a pure component, therefore, contact with the catalyst surface is less likely. With 8 bar pressure, the partial pressure of MCH is 2 bar and therefore the contact with active sites is more likely. Further, the gaseous hydrocarbons caused by thermal cracking evolve stronger with lower pressure. Considering the single component results, most gaseous cracking products at 1 bar reaction conditions can be derived from isooctane and decane conversion.

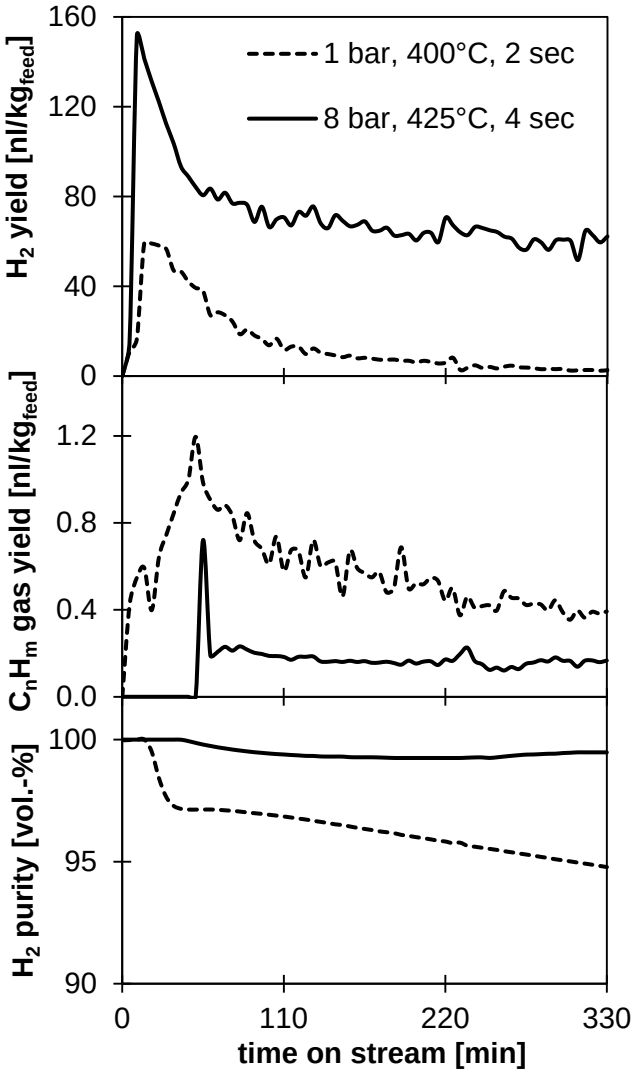

Fig. 5.11 -hydrogen yield, yield of gaseous hydrocarbons and hydrogen purity over reaction time of the 4- component model mixture's two different reaction conditions

At higher pressure, the partial pressure of hydrogen, especially in the beginning of the experiment, is much higher, thus cracking reactions are suppressed. This influences the product gas purity of hydrogen. At 1 bar reaction condition, the hydrogen purity declines in the end of the experimental time to 95 vol.-%. With 8 bar reaction condition, a purity of 99 vol.-% is preserved. Table 5.5 presents the detailed gaseous product distribution of the average time on stream. At higher pressure, less methane but more saturated hydrocarbons are detected, which can be derived from the increased hydrogen partial pressure in the system. With pure component tests also different type of cracking products were detected. At lower pressure more products from thermal cracking to methane can be seen while at higher pressure more longer chain hydrocarbons from hydrocracking are detected. Both types of cracking have been observed with hydrocarbons at similar conditions by different authors.[111], [112].

Table 5.5- average gaseous product concentration over the total time on stream of 4-component model mixture at two different reaction conditions

four componente model mixture	H_2	CH_4	C_2H_4	C_2H_6	C_3H_6	C_3H_8	C_4H_{10}
	[vol.-%]						
1 bar, 400°C, 2 sec	96.47	0.49		0.05			
8 bar, 425°C, 4 sec	99.48	0.18		0.11		0.04	

The results of hydrogen yield are also confirmed by the conversion rate of the components in the model mixture, see Fig 5.12. The conversion of all components, especially MCH, is much higher with 8 bar reaction condition.

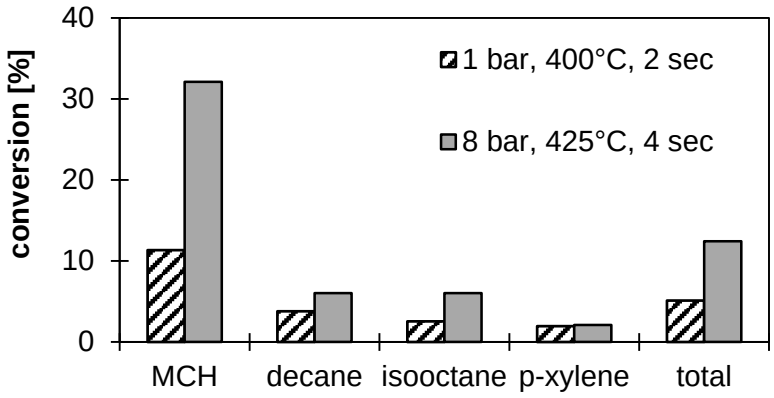

Fig. 5.12 - conversion rate of components and total conversion in 4- component model mixture at two different reaction conditions

With MCH, the conversion has almost tripled, while with decane it is 1.6 times higher. With isooctane it is 2.4 times higher and p-xylene conversion does not change. The increased conversion of the components also contributes to carbon formation on the catalyst. With 8 bar reaction condition, the carbon formation is much higher with 18.53 g_C/kg_{cat}. than at 1 bar with 9.9 $g_C/kg_{Cat.}$.However, since the amount of catalyst with both reaction conditions is very similar (4.2 g with 8 bar and 4.1 g with 1 bar), the carbon formation per feed mass is with 8 bar only half of the carbon formation with 1 bar (0.35 g_C/kg_{feed} at 8bar and 0.72 g_C/kg_{feed} at 1 bar). Due to the single components results, it is assumed that most carbon formation is produced from decane and p-xylene conversion. At 8 bar reaction conditions, the partial pressure of the components is increased and the contact time on the catalyst surface extended. Both factors lead to a higher conversion rate and more hydrogen output, but also to more carbon deposit on the catalyst surface. The formation of carbon and cracking products show a correlation with model mixtures and pure component tests. With increased evolution of cracking products also more carbon per feed mass is produced. The mechanism to carbon formation leads over radical formation which are produced from cracking reactions [36]. Next to the hydrogen yield

and stability of the reaction, the composition of the dehydrogenated fuel is of interest for evaluation. Table 5.6 shows the composition of the dehydrogenated four component model mixture. With 8 bar reaction condition, where the hydrogen yield is the highest, the formation of aromatic hydrocarbons changes the composition to a greater extent than with the low pressure reaction conditions.

Table 5.6 - composition of liquid hydrocarbons of dehydrogenated 4- component model mixture at two different reaction conditions

four componente model mixture	n-alkanes	n-alkenes	iso-alkanes	iso-alkenes	cyclo-alkanes	cyclo-alkenes	aromatic hydrocarbons
	[wt.-%]						
1 bar, 400°C, 2 sec	22.14	0.76	28.20	0.13	24.98	0.18	23.60
8 bar, 425°C, 4 sec	21.62	0.54	26.46	0.23	19.40	0.02	31.74

The formation of cycloalkanes, which are the primary stage to formation of aromatic hydrocarbons, is higher with 1 bar reaction condition, while more aromatic hydrocarbons evolve from cycloalkanes with 8 bar reaction condition. The promotion of formation of aromatic hydrocarbons is most likely also leading towards higher carbon deposit. The aromatic hydrocarbon content in the condensate of the 8 bar reaction condition would exceed the aviation restrictions of Jet A-1 specification [113]. Thus, the dehydrogenated fuel requires mixing with the original fuel to comply with specifications for jet engine combustion. The experimental evaluation of the four component model mixture leads to the conclusion that the high pressure reaction conditions are more suitable for the dehydrogenation process concept. The hydrogen yield and the hydrogen purity can be expected to be higher than with lower pressure reaction conditions.

5.3.3 PCD of ULSK Model Mixture

In this step, the ULSK model mixture with 8 components, designed for the evaluation of the process concept, is experimentally investigated. The results of the four component model mixture shows that a higher hydrogen yield can be expected with 8 bar reaction conditions (black solid line). To confirm the previous experimental investigation, the ULSK model mixture is tested with both reaction conditions. Further, the influence of sulfur components on the hydrogen yield and stability of conversion is investigated by adding 3 ppmw sulfur (S) with the component benzothiophen to the ULSK model mixture (grey solid line). The sulfur component is chosen from the average boiling range of sulfur components in Jet A -1 [96]. Fig. 13 shows the experimental results of the product gas yield and hydrogen purity over reaction time.

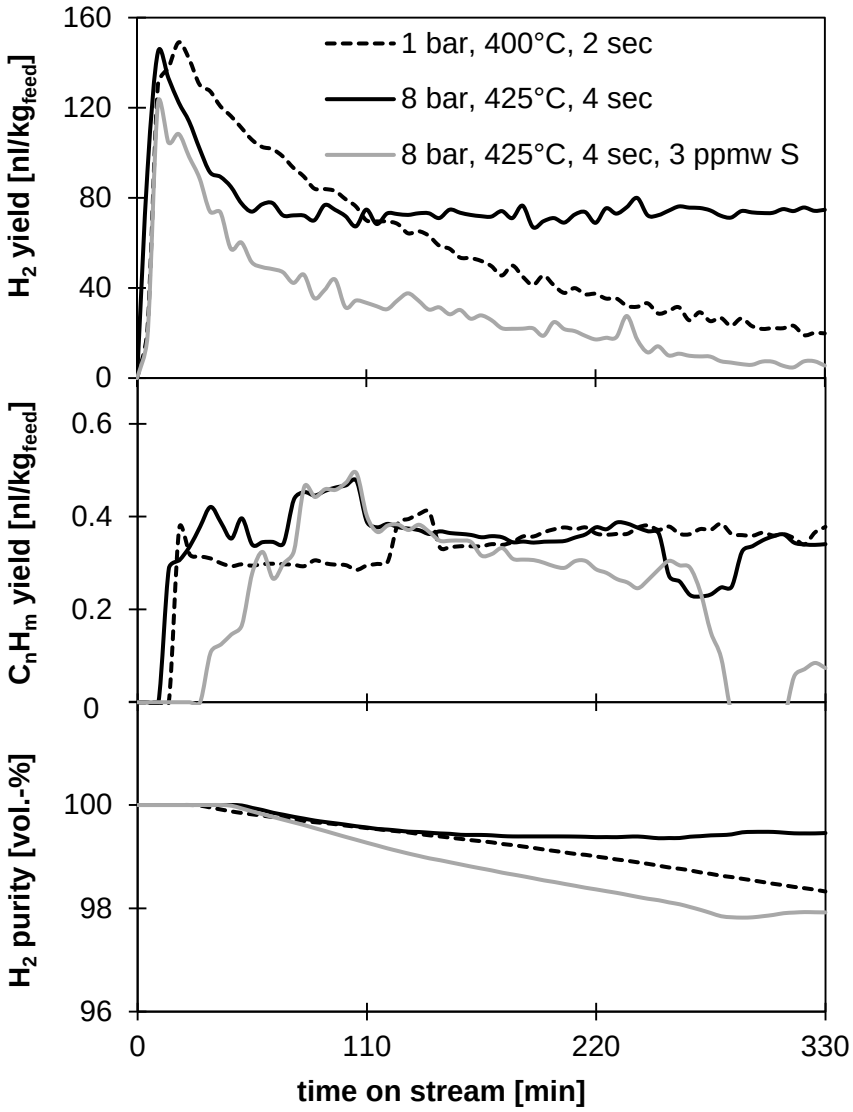

Fig. 5.13 - hydrogen yield, yield of gaseous hydrocarbons and hydrogen purity over reaction time of the ULSK model mixtures at two different reaction conditions and ULSK model mixture with 3 ppmw of sulfur at 8 bar reaction conditions

The hydrogen yield of the ULSK model mixture shows a higher stability in hydrogen evolution over time at 8 bar reaction conditions than at lower pressure. Therefore, the test with the sulfur containing ULSK model mixture was performed at 8 bar reaction condition. It is expected that sulfur has a deactivating impact on the catalyst. With only 3 ppmw S, the reactivity of the catalyst is already declining rapidly over time. It even shows less hydrogen yield than the sulfur-free model mixture at 1 bar reaction condition (black broken line). In comparison to the less complex four- component model mixture, the hydrogen yield at 8 bar reaction conditions without sulfur shows better stability and slightly higher hydrogen yield. Also at 1 bar reaction condition, the average hydrogen yield of the four component mixture is only 24 % of the ULSK model mixture. The content of cycloalkanes is the same with both model mixtures, but with ULSK model mixture, decalin is part of the composition, which showed in single model component tests less influence by the different reaction conditions than MCH.

Furthermore, the evolution of gaseous side products shows similar results for both reaction conditions without sulfur content. With 8 bar reaction conditions, the yield of gaseous hydrocarbons is 4 % higher. Due to the higher hydrogen yield of 8 bar reaction condition, the hydrogen purity remains at a higher level than with 1 bar reaction condition. Other than with the four component model mixture, the content of Isooctane is much smaller, since the model mixture is designed to fit the molar mass of the real ULSK. The influence of cracking products at lower pressure from isooctane is therefore decreased. Most cracking products appear from n-alkanes, which show more cracking product at higher pressure in the single component test.

With sulfur content, not only the average time on stream hydrogen yield, but also cracking products from alkanes and iso- alkanes are decreased by 19 % in comparison to the 8 bar reaction condition without sulfur. This leads to the conclusion that cracking reactions are not only caused by thermal cracking, but are also catalyzed. Any type of catalyzed reaction is decreased due to the deactivation of the actives sites of the catalyst by sulfur poisoning. The hydrogen purity of the product gas follows the hydrogen yield. Although less gaseous hydrocarbons are produced, the decline of hydrogen yield leads to less hydrogen purity than with the other two experiments.

Table 5.7, shows the distribution of the gaseous products of the total evolved product gas. The main outcome of cracking products is methane with 1 bar reaction condition, and the 8 bar reaction condition with sulfur. With the sulfur containing model mixture, more ethane is produced. When the hydrogen yield is high at 8 bar reaction condition, less methane but longer chain saturated hydrocarbons are detected in the product gas.

Table 5.7 – average gaseous product concentration over the total time on stream of ULSK model mixture at two reaction conditions and 3 ppmw sulfur containing ULSK model mixtures at 8 bar reaction condition

ULSK Model Mixture	H_2	CH_4	C_2H_4	C_2H_6	C_3H_6	C_3H_8	C_4H_{10}
	[vol.-%]						
1 bar, 400°C, 2 sec	99.25	0.68		0.07			
8 bar, 425°C, 4 sec	99.57	0.23		0.14		0.06	
8 bar, 425°C 4 sec with 3 ppmw S	98.85	0.61		0.42		0.12	

Gaseous hydrocarbons are caused by both, hydro cracking and thermal cracking. With declining activity of the catalyst, the contribution of cracking products to product gas composition increases, since less hydrogen is produced.

Fig. 5.14, presents the conversion rate of the model components of the model mixture. The conversion is indicating which components are responsible for the evolution of hydrogen and side products

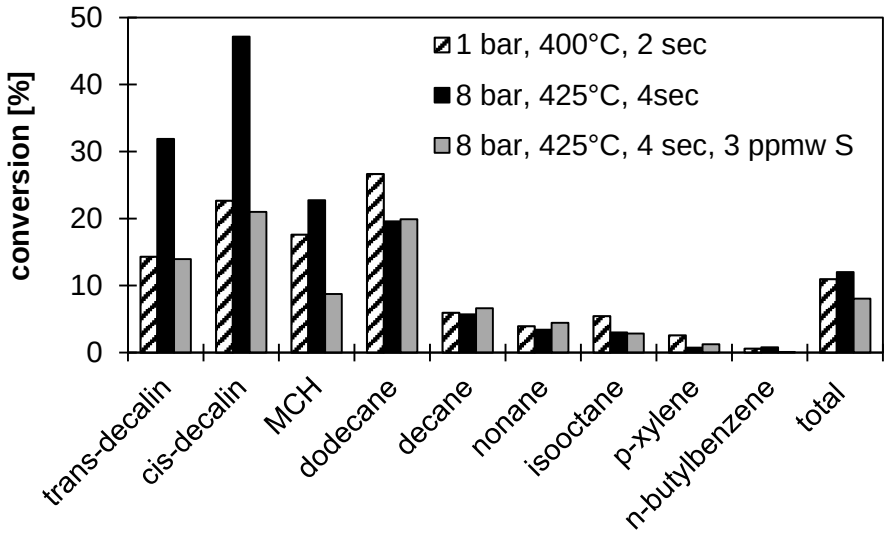

Fig. 5.14 - conversion rate of model components and total conversion in ULSK model mixture at two different reaction conditions and 3 ppmw sulfur containing ULSK model mixtures at 8 bar reaction condition

The conversion of the cycloalkanes is highest with 8 bar reaction conditions without sulfur. The cycloalkane MCH converts to toluol. The model component decalin is available as an isomeric mixture of trans- and cis- decalin, with a ratio of 60 wt.-% to 40 wt.-%. The conversion rate of the isomers differs by which cis-decalin shows higher conversion. Decalin is converting to naphthalene with the intermediate product of tetralin. The amount of hydrogen evolution also depends on the stage of aromatization of the cycloalkanes. In the ULSK model mixture with 1 bar reaction condition, 83 % of total converted decalin is fully dehydrogenated to naphthalene. At higher pressure, 86.8 % of the converted decalin dehydrogenates to naphthalene. With the sulfur containing ULSK model mixture, the stage of aromatization of decalin decreases strongly. Only 71.7 % of converted decalin has dehydrogenated to naphthalene.

The conversion of n-alkanes is higher at 1 bar than at 8 bar. With sulfur, the conversion rate increases slightly, which causes more cracking reactions. The contribution of the conversion rate to cracking products must be higher, since more gaseous side products are detected. With the sulfur containing model mixture, the conversion of alkanes is increased in comparison to the experiment without sulfur. Isooctane is also a source of gaseous hydrocarbons and has the highest conversion at 1 bar. Aromatic hydrocarbons show in general little conversion, which mostly leads to cracking products and carbon formation. The total conversion of the ULSK model mixture is between 8 to 12 %.

Table 5.8, shows the carbon formation on the catalyst surface and the contribution of the feed stream to the carbon formation. Comparable to the previous experiments, the carbon formation per feed stream is decreasing with higher pressure, since the feed stream is four times higher with higher pressure. The total amount of carbon detected is higher with increased pressure. The amount of catalyst is similar with both reaction conditions, therefore more carbon is found on the catalyst surface at high pressure reaction conditions.

Table 5.8 – carbon formation on the catalyst and by feed mass of ULSK model mixture and two different reaction conditions and ULSK model mixture with 3 ppmw sulfur at 8 bar reaction condition

carbon formation	1 bar, 400°C, 2 sec	8 bar, 425°C, 4 sec	8 bar 425°C, 4 sec, 3 ppmw S
$g_C/kg_{cat.}$	16.40	22.23	35.7
g_C/kg_{feed}	1.04	0.36	0.53

With the sulfur containing model mixtures, the carbon formation is increased once more at 8 bar reaction condition. The formation of carbon on inactive catalyst can be derived from literature [114], [115], [116], [117]. Since the catalyst is deactivating due to formation of platinum sulfide (PtS_2), carbon formation is not catalyzed, but caused by thermal stressing of the hydrocarbons of the feed. Instead of catalyzing the dehydrogenation reaction, the deactivated hot surface of the catalyst shows localized corrosion, where the hydrocarbons are decomposed to carbon and hydrogen over formation of large aromatic hydrocarbons. The formation of carbon can also be observed on other metal surfaces of the test rig, especially at the evaporator, which is built of stainless steel. A temperature above 350°C and active centers on metal surface are enough to cause carbon formation by thermal stressing of hydrocarbons in fuels.

The composition of aromatic hydrocarbons of the dehydrogenated model mixtures confirms the conversion rate of the model components, see table 5.9. With increasing conversion rate, the content of cycloalkanes is decreasing, while the content of aromatic hydrocarbons is increasing in the same manner. The conversion of n-alkanes also contributes to the formation of aromatic hydrocarbons, since components can be found in the condensates of the experiment, which are found in the single model component experiments with n-alkanes. At lower pressure, the dehydrogenation to alkenes is higher than at increased pressure.

Table 5.9 - composition of liquid hydrocarbons of dehydrogenated ULSK model mixture at two different reaction conditions

ULSK model mixture	n-alkanes	n-alkenes	iso-alkanes	iso-alkenes	cyclo-alkanes	cyclo-alkenes	aromatic hydrocarbons
	[wt.-%]						
1 bar, 400°C, 2 sec	44.47	2.03	3.48	0.02	20.59	0.97	28.44
8 bar, 425°C, 4 sec	46.37	0.67	3.72	0.04	18.09	1.00	30.11
8 bar, 425°C, 4sec, 3 ppmw S	44.36	0.95	3.71	0.02	23.77	0.70	26.49

The results of the experimental dehydrogenation of the ULSK model mixture confirm the results of the evolution of the four component model mixture. The most promising reaction condition for the process concept with ULSK is at higher pressure of 8 bar, due to the hydrogen yield and hydrogen purity. Though, the content of sulfur containing components is also of great concern to the stability of the process, since even 3 ppmw S lead to rapid catalyst deactivation. Sulfur deactivation cannot be avoided with regular jet fuel unless a catalyst is developed that shows sulfur resistance. Furthermore, the content of long chain alkanes is a factor leading to carbon formation, which also occupies the active sites on the catalyst. This formation of carbon on the catalyst can be reduced by choosing a catalyst support and an additional precursor metal decreasing acid sites. Furthermore, the carbon formation on the surface of the reactor and other operational parts with shigh temperature can be reduced by choosing a coating on the alloy or other construction material that suits the conditions, but does not offer metal active sites for thermal stressing of the fuel.

Concluding, although a high content of cycloalkanes is of interest for the hydrogen evolution, the composition of the dehydrogenated model mixtures shows a high content of aromatic hydrocarbons due to conversion of cycloalkanes, which is exceeding aviation restrictions. Also, the content of n-alkenes is specifically limited by 2 vol.-% for Jet A-1. This has to be taken into consideration when using the dehydrogenated fuel for aircraft propulsion.

5.3.4 PCD of Ultra- Low- Sulfur Kerosene (ULSK)

In the next step, real ULSK and Jet A-1 fractions are dehydrogenated in the test rig. First, two different reaction conditions are tested with ULSK to observe if these show similar tendencies of gaseous product results in comparison to the ULSK model mixture. Furthermore, the actual ULSK fuel is evaluated by its potential of hydrogen yield, hydrogen purity and reaction stability of PCD for the process concept. With the results from the ULSK model mixtures and the actual ULSK, one reaction condition is chosen for further tests with Jet A-1 desulfurized fractions and

Jet A-1 fraction model mixtures. The gaseous product results of the ULSK model mixture with 3 ppmw S (grey solid line) are compared directly with the real ULSK at 8 bar reactions condition (black solid line) in Fig. 5.15, in order to demonstrate the comparability of the PCD of the ULSK model mixtures with real ULSK. The product results from the ULSK model mixtures are used for evaluation of the reference process.

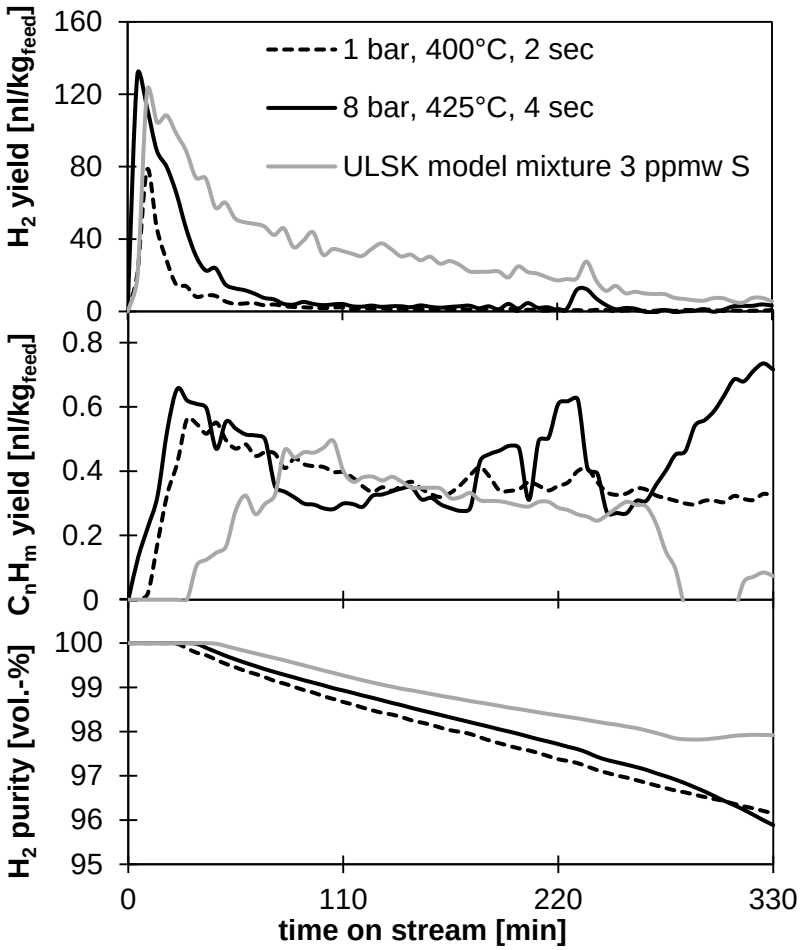

Fig. 5.15 - hydrogen yield, yield of gaseous hydrocarbons and hydrogen purity over reaction time of ULSK at 1 bar and 8 bar reaction conditions and ULSK model mixture with 3 ppmw S at 8 bar reaction conditions

Comparing the hydrogen yield of ULSK at 1 bar (black broken line) and 8 bar shows the similar pattern as with the previous model mixtures. The hydrogen yield can be increased with higher pressure. The average yield of gaseous side products is comparable with both reaction conditions. Cracking reactions are not influenced by increased hydrogen pressure. Due to the higher hydrogen yield, the hydrogen purity is also slightly increased at 8 bar. However, after 120 minutes, almost no hydrogen is produced due to catalyst deactivation. This leads to a steep decline of hydrogen purity with both reaction conditions over time, since only gaseous hydrocarbons are still produced. The average concentration in the first 120 minutes of reaction

time show similarities to the ULSK model mixture, see table 5.10. With low pressure reaction conditions, only methane is detected as a cracking product, while with higher pressure, further saturated cracking products are detected.

Table 5.10 – average gaseous product concentration of ULSK at two reaction conditions in the first 120 min of reaction time

ULSK	H_2	CH_4	C_2H_4	C_2H_6	C_3H_6	C_3H_8	C_4H_{10}
	[vol.-%]						
1 bar, 400°C, 2 sec	99.37	0.63					
8 bar 425°C, 4 sec	99.75	0.16		0.06		0.03	

The PCD of the ULSK model mixture with 3 ppmw sulfur starts out with a comparable level of hydrogen yield, but cracking products appear later, 30 minutes into the reaction time. The degradation slope is 50% less steep than with the real ULSK. This allows the conclusion that not only the content of sulfur in the fuel causes degradation, but also the content of hydrocarbons, which are not considered in the model mixture. An indication of which components cause the strong degradation is shown in table 5.11, where the carbon formation of the real ULSK is enhanced in comparison to the model mixture.

Table 5.11 - carbon formation on the catalyst and by feed mass of ULSK

carbon deposit	1 bar, 400°C, 2 sec	8 bar 425°C, 4 sec
$g_C/kg_{cat.}$	19.36	42.03
g_C/kg_{feed}	1.23	0.67

The longest carbon chain in the ULSK model mixtures is dodecane with 12 carbon atoms. The composition of hydrocarbons in the real ULSK shows that 4.57 wt.-% of all identified components have more than 12 carbon atoms, of which 2.75 wt.-% are n-alkanes and 1.51 wt.-% iso-alkanes. With regular Jet A-1, the content of hydrocarbons with more than 12 carbon atoms is much higher at 15.33 wt.-%. Since long chain hydrocarbons are more likely to cause carbon formation due to thermal stressing, the content of longer chain hydrocarbons in the real fuel causes the deactivation by carbon deposit on the catalyst. Additional long chain n-alkanes are more likely to produce gaseous hydrocarbons by cracking reactions. This can be observed with the single component tests by comparing the cracking products from nonane, decane and dodecane.

Avoiding carbon formation should be a priority to advance PCD of fuels next to sulfur resistance of the catalyst. Due to the complexity of the ULSK, with a hydrocarbon composition of 200 detected peaks, a detailed conversion rate is not available, since products and feed

components are frequently overlapping in the chromatography analysis. The conversion rate is estimated by the turnover of the peaks from ULSK to dehydrogenated ULSK. For the 1 bar reaction conditions, a total conversion rate of 9 % is estimated, while for the 8 bar reaction condition, a conversion rate of 11 % is estimated for the total reaction time of 330 minutes. Most of the conversion likely contributes toward cracking products and carbon formation rather than towards hydrogen production.

5.3.5 PCD of Jet A-1 Fractions

The reaction condition chosen for experimental evaluation of the Jet A-1 fraction is 8 bar, since tests of model mixtures and ULSK show a higher hydrogen yield at increased pressure. The six fractions between 5 wt.-% and 30 wt.-% are produced by thermal distillation in the lab scale batch rectification, with a sulfur content of 5.3 to 26 ppmw S. The distribution of hydrocarbon groups in the fractions is moved towards a higher content of cycloalkanes and less aromatic hydrocarbons. Furthermore, the content of long chain hydrocarbons with more than 12 carbon atoms is strongly reduced in comparison to Jet A-1. With increasing distillated mass fraction, the distribution of hydrocarbon groups, carbon atom number and sulfur content become more similar to regular Jet A-1. As seen in the experimental test of ULSK and ULSK model mixture in chapter 5.3.4, sulfur has a significant influence on the catalyst activity and reaction stability. Therefore, it is of use to choose Jet A-1 fractions with little sulfur content. For the process concept with rectification, the energy demand for the desulfurization is important to the system efficiency. Since the total kerosene mass stream has to be evaporated for the rectification, but only a certain percentage can be used for dehydrogenation, the ratio of heat demand to distillated mass is advancing with higher distillated mass ratio. Though, with suitable heat integration of the rectification process, the influence on the system efficiency can be limited. The PCD tests of Jet A-1 fractions are performed to choose suitable fractions for the process concept with rectification. The hydrocarbon composition of the fraction is then used to design model mixtures. The evaluation criteria are hydrogen yield and hydrogen purity. Furthermore, it is of interest to choose a fraction of high distilled mass for the process concept, which contradicts with the sulfur content. Therefore, the distribution of hydrocarbons in the mass fraction is also important to the hydrogen yield, which is the key figure for choosing a suitable fraction. Fig 5.16, presents the gaseous product yields and hydrogen purity over reaction time of six different Jet A-1 fractions at 8 bar reaction condition.

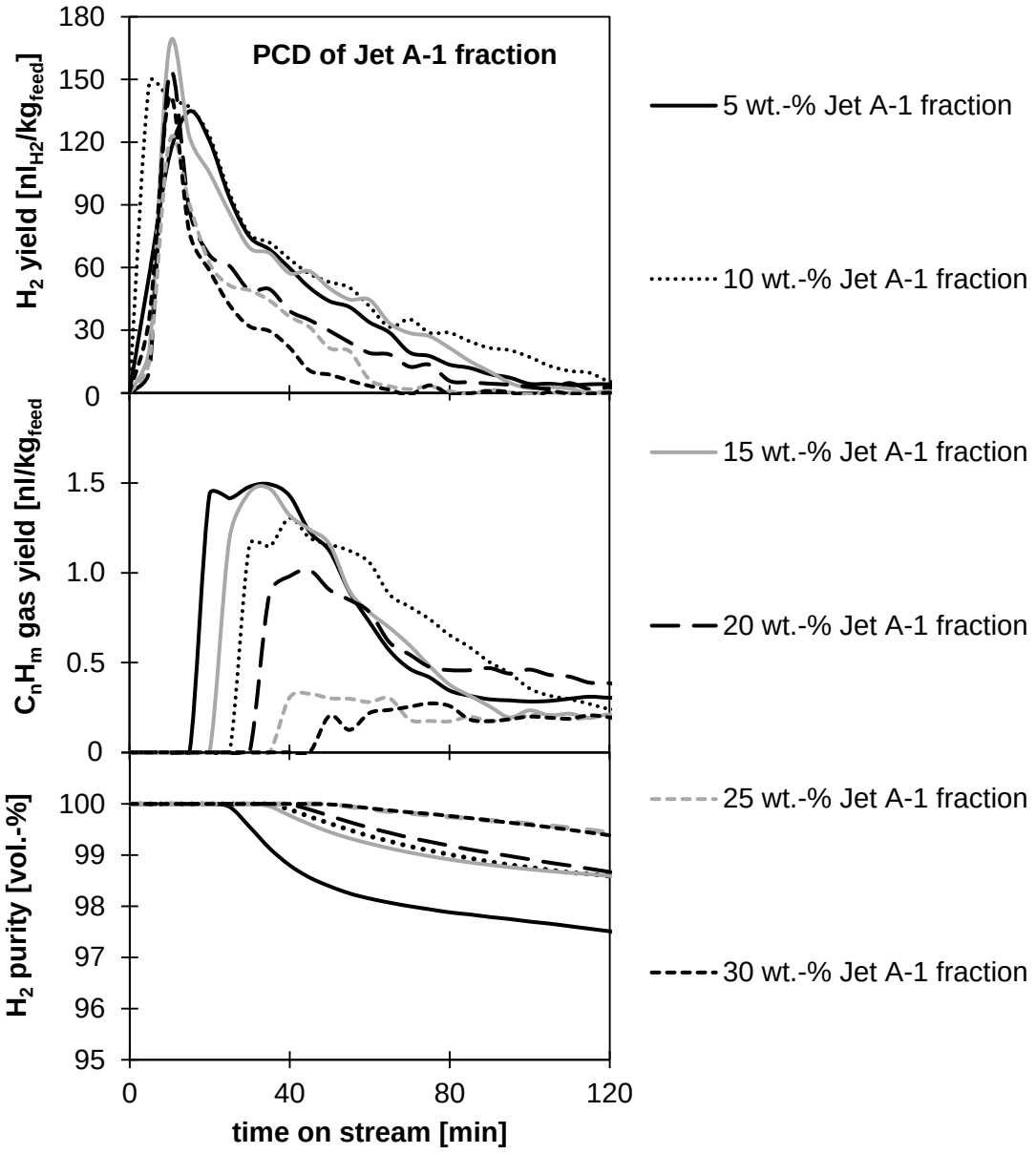

Fig. 5.16 - hydrogen yield, yield of gaseous hydrocarbons and hydrogen purity over reaction time of Jet A-1 fraction at 8 bar reaction condition

The experiments were performed for 330 minutes, identical to the previous experiments. Since the hydrogen and gaseous hydrocarbon yield is decreasing strongly over time, the first 120 minutes of the reaction time are presented to emphasize the difference of the fractions when the catalyst is still active and gaseous products are produced. The deactivation of the catalytic reaction follows the same pattern as with ULSK, where sulfur poisoning and carbon formation are responsible.

With increasing sulfur content and distillated mass of the fraction, the hydrogen yield is declining more rapidly over time. The 5 wt.-% fraction has the highest potential for hydrogen yield, since the content of cycloalkanes is the highest. The 10 wt.-% fraction, with the second highest amount of cycloalkanes shows, in average, slightly higher hydrogen yield, while less cracking products are detected. These results were confirmed in a repetition of the

experiments. The main reason for this behavior is found in the detailed composition of the fractions. The second main difference in compositions next to the difference in hydrocarbon distribution is that more hydrocarbons are found with less than nine carbon atoms in the 5 wt.-% fractions. In the comparison of single component tests with nonane and decane, more cracking products appeared with the shorter chain alkane, while with dodecane, cracking also increased in comparison to decane. The increase of cracking to saturated shorter chain alkanes and gaseous hydrocarbons consumes hydrogen, as well as carbon chain growing to longer chain alkanes. The break point is ten carbon atoms. The hydrogen purity of 5 wt.-% fraction shows the strongest reduction due to the highest cracking product yield.

The average hydrogen yield for the first 120 minutes between 15 to 30 wt.-% is decreasing with increasing mass content of sulfur and distillate mass fraction. The deactivation of the catalyst shows also effects on the cracking products. After 120 min, the yield of detected gaseous hydrocarbons has declined strongly with all fractions and reaches a common average value of 0.3 Nl/kg_{feed}. With the 25 to 30 wt.-% fraction, the gaseous product yields are the lowest. Therefore, these fractions are not taken into consideration for model mixtures. Between 15 and 20 wt.-% fractions, more cracking products appear with 15 wt.-%, which leads to slightly lower hydrogen purity than 20 wt.-% fraction, while the hydrogen yield is still higher with 15 wt.-% fraction. All experiments start out at 100 vol.-% hydrogen with little cracking reaction taking place. When gaseous hydrocarbons are evolving, the hydrogen purity decreases over time. Since more gaseous reaction products are evolved with less sulfur poisoning the hydrogen purity declines with less sulfur. The most common detected cracking products are methane and ethane, see table 5.12.

Table 5.12 - average gaseous product concentration of Jet A-1 fractions at 8 bar reaction condition in the first 120 min of reaction time

Jet A-1 fractions		H_2	CH_4	C_2H_4	C_2H_6	C_3H_6	C_3H_8	C_4H_{10}
		[vol.-%]						
5	wt.-%	98.56	0.92		0.32			
10		99.38	0.44		0.11		0.06	
15		99.32	0.46		0.14		0.08	
20		99.49	0.33		0.12			
25		99.83	0.13		0.04			
30		99.83	0.13		0.04			

The gradient of catalyst activity can also be followed by the carbon formation on the catalyst surface, or per feed mass stream presented in table 5.13.

Table 5.13 - carbon formation on the catalyst and by feed mass of Jet A-1 fractions 8 bar reaction condition after 330 min of reaction time

carbon deposit	5 wt.-%	10 wt.-%	15 wt.-%	20 wt.-%	25 wt.-%	30 wt.-%
ppmw S	5.33	8.15	11.33	15.36	21.80	26.0
$g_C/kg_{cat.}$	25.03	26.25	31.14	31.72	46.03	52.27
g_C/kg_{feed}	0.44	0.50	0.52	0.55	0.82	0.91

With increasing mass fraction, the amount of carbon deposit increases and deactivates the catalyst. The content of long chain hydrocarbons increases with the distillated mass, which causes more carbon formation on an inactive catalyst by sulfur poisoning.

The 10 wt.-% fraction is chosen for the experimental evolution as the model mixture, since it shows the highest potential for the process concept with rectification. Furthermore, a model mixture for the 20 wt.-% fraction is defined, since it is of interest for the efficiency of the process to choose a fraction with the mass percentage being as high as possible. The influences on the system efficiency of the hydrogen yield and distillated fraction are presented in chapter 6.

5.3.6 PCD of Jet A-1 Fraction Model Mixtures

The two chosen Jet A-1 fractions, 10 wt.-% and 20 wt.-%, are prepared as model mixtures for experimental evaluation. The composition of the fraction model mixtures is presented in chapter 3. Both model mixtures are also tested with the equivalent content of sulfur to the real Jet A-1 fractions of 8 and 15 ppmw by adding benzothiophen to the feed. The main differences in the composition of the model mixtures are the content of MCH and decalin, and the content of the n-alkanes, where much more nonane is added to 10 wt.-% fraction model mixture. Dodecane was only added to the 20 wt.-% fraction model mixture. The results of the gaseous products of the four model mixtures are presented in Fig. 5.17.

As expected, the 10 wt.-% fraction model mixture shows the highest hydrogen yield with stable reaction course over time (black solid line). The average hydrogen yield 126.4 nl/kg_{feed} is used as a target value for the process concept with rectification. With high reactivity as well, the yield of cracking products is the highest, since nonane is the main hydrocarbon in the mixture. With additional sulfur, the effect of catalyst poisoning is immediately noticeable (grey solid line). Not only does the reaction begin with a lower level of hydrogen yield, but also a clear slope caused by catalyst deactivation is detected. With less catalyst activity, less cracking products are detected in the gas phase. Further, hydrogen purity is decreasing much stronger due to less hydrogen production.

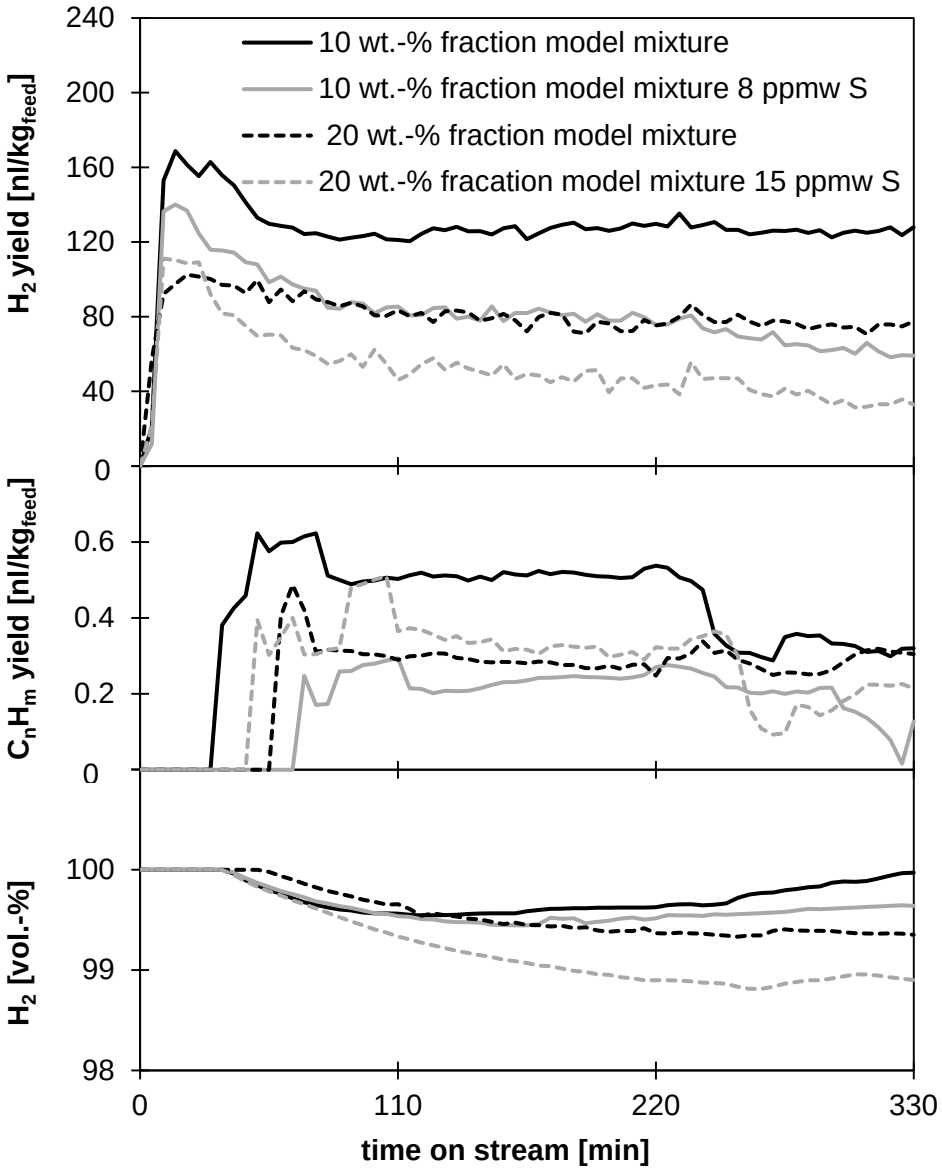

Fig. 5.17 - hydrogen yield, yield of gaseous hydrocarbons and hydrogen purity over reaction time of 10 wt.-% model fraction with and without 8 ppmw sulfur (S) and 20 wt.-% model fraction with and without 15 ppmw sulfur (S)

The 20 wt.-% fraction also shows a stable reaction course over time (black broken line), but at a lower level of hydrogen and cracking products yield, which follows the tendency of the real Jet A-1 fractions. The content of cycloalkanes in both fractions only differ by 0.91%, but 4.75 % more of n-alkanes are with the 20 wt.-% fraction model mixture. The content of alkanes influences both carbon formation and the evolution of hydrogen by dehydrogenation. These components decrease the conversion of cycloalkanes which is shown with PCD of two component mixtures in chapter 5.3.1. With the addition of 15 ppmw sulfur, the activity of the catalyst decreases over time. Unlike the 10 wt.-% fraction model mixtures, the yield of gaseous hydrocarbons remain the same with additional sulfur, which it most likely caused by the content of dodecane showing a similar conversion rate. The influence of sulfur is with both fraction model mixtures weaker on the hydrogen yield as with ULSK model mixture, which is derived

from the differences in composition. With higher cycloalkane content, hydrogen is more likely to be produced, even with a gradually deactivating catalyst. The composition of product gas in table 5.14 shows that hydrogen purity is decreasing due to higher content of methane and ethane with the sulfur containing model mixtures.

Table 5.14 - average gaseous product concentration of 10 wt- % and 20 wt.-% fraction model with and without sulfur content at 8 bar reaction condition

fraction model mixture	H_2	CH_4	C_2H_4	C_2H_6	C_3H_6	C_3H_8	C_4H_{10}
	[vol.-%]						
10 wt.-%	99.73	0.12		0.11		0.04	
10 wt.-% 8 ppmw S	99.63	0.29		0.08			
20 wt.-%	99.57	0.25		0.14		0.04	
20 wt.-% 15 ppmw S	99.24	0.61		0.15			

Further, the cracking product of propane disappears with additional sulfur, which might be caused by deactivation of the catalyst. With sulfur, the catalyst surface is deactivated and catalyzed cracking is declining. However, due to the hot but inactive catalyst, surface thermal cracking is more likely. The results of the gaseous products are confirmed by the conversion rate of the model components, presented in Fig 5.18.

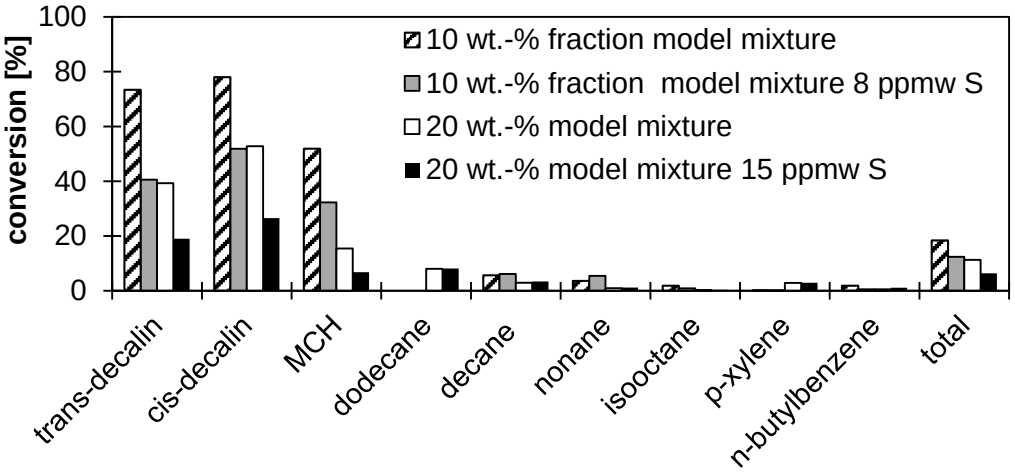

Fig 5.18 - conversion rate of model components and total conversion in fraction model mixture with and without sulfur at 8 bar reaction condition

The cycloalkanes, which contribute most to the hydrogen yield, are converted strongest with the 10 wt.-% fraction model mixture. Little carbon formation and no sulfur lead to a highly active catalyst. Therefore, not only the content of cycloalkanes is important, but also the deactivation of the catalyst by undesired side reactions and catalyst poisoning, respectively. The content of

sulfur and higher content of n-alkanes with the 20 wt.-% fraction model mixtures decrease the activity and the conversion rate of cycloalkanes.

The content of decalin makes a difference in the aromatization toward naphthalene, which evolves most hydrogen. With the 10 wt.-% fraction model mixture, 70.44 % of the conversion of decalin contributes towards naphthalene. The rest is tetralin. With 8 ppmw sulfur, the rate does not differ by much with 69.17 %. The sulfur deactivation does not influence the rate towards aromatization. But with the 20 wt.-% fraction model mixtures, the rate towards naphthalene is even 86.89 %. Sulfur deactivation decreases the rate to 79.60 %. The factor of partial pressure on the catalyst, and competition of other hydrocarbon groups have a great influence on the conversion, as well as carbon formation and sulfur poisoning

The distribution of condensable products of the four experiments is presented in table 5.15, which follows the conversion rate of the model components in the feed. With high conversion of cycloalkanes, more aromatic hydrocarbons and intermediate products of cyclalkenes are detected. With sulfur content, the conversion of n-alkanes has increased, which also contributes to more n-alkenes and towards aromatic hydrocarbons and iso-alkenes. From n-alkanes conversion of the 10 wt.-% fraction model mixture, 1.66 wt.-% aromatic hydrocarbons are produced. With sulfur, the conversion towards aromatic hydrocarbons even increases by 3.38 wt.-%. With 20 wt.-% fraction model mixtures, 0.1 wt.-% of n-alkanes conversion can be found as aromatic hydrocarbons, and with sulfur, 0.39 wt.-% of aromatic hydrocarbons from n-alkanes are identified. The content of iso-alkanes is even higher in the condensable products, although isooctane has been converted. Most iso - alkanes can be derived from nonane and decane, since the iso - alkanes can also be found in the single components test.

Table 5.15 - composition of liquid hydrocarbons of dehydrogenated fraction model mixture with and without sulfur at 8 bar reaction condition

Fraction	n-alkanes	n-alkenes	iso-alkanes	iso-alkenes	cyclo-alkanes	cyclo-alkenes	aromatic hydrocarbons
Model Mixture	[wt.-%]						
10 wt.- %	38.32	0.53	3.14	0.05	15.19	3.56	39.22
10wt.-%, 8 ppmw S	35.87	0.63	3.24	0.01	24.90	2.17	33.17
20 wt.-%	44.23	0.83	1.25		22.42	0.99	30.28
20 wt.-%, 15 ppmw S	44.06	0.83	1.25		27.58	0.76	25.51

With the content of sulfur, more carbon formation is detected. Since it is assumed that carbon formation on the catalyst surface is derived from aromatization and poly-aromatization of n-alkanes, the higher conversion and contribution towards aromatics of alkanes are most likely

a cause of the carbon formation [118]. The deposition of carbon on the catalyst surface and the formation per feed mass is presented in table 5.16.

Table 5.16 - carbon formation on the catalyst by feed mass of 10 and 20 wt.-% fraction model mixture with and without sulfur at 8 bar reaction condition

	10 wt.-% model mixture		20 wt.-% model mixture	
carbon formation	-	8 ppmw S	-	15 ppmw S
$g_C/kg_{cat.}$	17.58	22.42	20.27	27.89
g_C/kg_{feed}	0.33	0.42	0.35	0.48

The conversion of aromatics p-xylene and n-butylbenzene contribute towards other aromatic hydrocarbons, cracking products and, mostly likely, also towards carbon formation.

For the process concept with rectification, the results of the 10 wt.-% faction model mixture are most promising. But with higher mass content on the 20 wt.-% fraction model mixture, the system efficiency has to be evaluated first in the process simulation.

5.4 Summary and Conclusion of the Experimental Evaluation of PCD

The objective of the experimental evolution of partial catalytic dehydrogenation of jet fuel, model mixture and model components was first to find suitable reaction conditions which fit the boundary conditions of the process concepts for an APU fuel cell system. This requires high hydrogen yield, hydrogen purity and stability of the reaction course in a pressurized system in order to integrate a pressure swing adsorption for product gas conditioning.

The second aim was to learn about product composition, dehydrogenation reactions and side reactions leading to cracking products of the different hydrocarbon groups in the jet fuel. It is also of interest how hydrocarbon groups influence each other in perspective of hydrogen evolution, carbon formation and cracking products. This information is used to develop simplified reaction schemes for the defined model components in jet fuel model mixtures for the specified reaction conditions to integrate into the process simulation in the following chapter. With the design of the simplified dehydrogenation reactor for the process concepts, the heat demand of the reactor is calculated by the heat of reactions, which is then used for heat and material integration and, finally, for efficiency evaluation.

The complexity of the Jet A-1 fractions and ultra- low- sulfur kerosene required the use of model components and model mixtures in order to investigate the product composition and influence of hydrocarbon groups on hydrogen yield and undesired side reactions. The results of the single component tests showed that the n-alkanes can cause carbon formation over dehydrocyclization to aromatic and poly aromatic hydrocarbons. Further, they are a source of

gaseous cracking products. Increased system pressure and temperature can enhance these side reactions depending on the hydrocarbon chain length. The model component isooctane also causes cracking products, but this reaction can be suppressed under high hydrogen pressure. The content of cycloalkanes is important to hydrogen evolution, since they are the main source of hydrogen through aromatization. A pressurized system reduces conversion as single components, but with a model mixture and complex jet fuel, higher conversion can be expected due to the increased partial pressure on the catalyst surface. Aromatic hydrocarbons do not show high reactivity. Cracking products and carbon formation is mostly detectable for these components. The model mixtures show promising hydrogen yield and stable reaction course with the reaction condition of 8 bar pressure, 425°C reaction temperature and contact time on the catalyst of 4 seconds. The content of sulfur deactivates the catalyst surfaces and leads to a reduction of hydrogen yield over reaction time, which is followed by increasing carbon formation on the deactivated catalyst surface, enhancing the catalyst deactivation.

The PCD tests of real ULSK and Jet A-1 fractions showed a strong decline of reactivity, which leads to almost complete catalyst deactivation after 120 minutes of reaction time. This is caused not only by sulfur poisoning, but also by the carbon formation of the long chain hydrocarbons found in the real fuel, which are not part of the model mixtures. Since no stable reaction course can be achieved with real ULSK and Jet A-1 fractions, the stable results of the model mixture have to be used for evolution of the process concepts. Therefore, the calculated efficiencies are a result of advanced catalyst performance, where deactivation by sulfur poisoning and carbon formation is avoided.

The detailed product composition of the single component tests, and the results of conversion rates, hydrogen yield and cracking products of the model mixtures are used to define simplified reactions for the simulation of the process concepts. These lead to the hydrogen output and product gas quality detected in experimental work. Further, the liquid product composition allows the evolution of the dehydrogenated fuel. Since the dehydrogenation of cycloalkanes and alkanes lead to formation of aromatic hydrocarbons, the composition of the dehydrogenated jet fuel would exceed aviation restrictions. This is of interest to further use of fuel for combustion and propulsion on board an aircraft.

6 Process Simulation

The partial catalytic dehydrogenation of ULSK and Jet A-1 fractions is used for process concepts, which are developed for APU applications. A process simulation can be used to design a heat and material integrated APU system which can be evaluated by its efficiency. The process simulation is introduced in the flow sheet simulation tool Aspen Plus, which is a powerful tool for chemical process design. Single model elements like reactors, heat exchangers, distillation columns, etc. can be individually configured and connected with material, heat and work streams. The database allows the choice of a large number of thermodynamic property methods to calculate the conditions of the model elements. The Method for heat integration of the process concepts is the Pinch- Analysis, where the increase of system efficiency is obtained by setting thermodynamic targets of heat recovery. For the synthesis of a heat exchanger network, the enthalpy streams of each system are extracted from the flow sheet simulation and used to generate preliminary thermodynamic targets for maximum heat recovery. In a second step, a most satisfactory final heat exchanger grid is designed individually for each concept [119], [120].

The chemical complexity of kerosene shows the need for simplification to use experimental data in a process simulation. Therefore, data from the experimentally investigated model mixtures are introduced and simplified dehydrogenation reactions are defined in the process simulation tool. The method of defining the dehydrogenation reactions is described in this chapter. The flow sheet simulation is used to evaluate the process concepts for APU applications, which is the scope of the dehydrogenation process developed.

The two process concepts develop in this work are the process concept with rectification and the reference concept which is provided with ULSK. Both concepts are described in detail in the introduction in chapter 1.1. The main difference with both concepts is the rectification which leads to different input specifications for the model mixture and especially the amount of fuel that needs to be preheated and recycled in the system.

The experimental study of the Jet A-1 fractions shows that hydrogen yield is different with different mass fraction and regular ULSK due to diverse chemical composition. Next to suitable heat integration, the system efficiency depends strongly on the hydrogen yield, since it is the main output of the process. The heat demand of the reboiler with the rectification has to be considered with the heat integration. For the reference concept, only the feed input stream has to be prepared for the reactor. The heat demand for both systems will be explained in detail in chapter 6.4.

6.1 Modelling of Kerosene in Aspen Plus

Within the process simulation, three different models of the kerosene are used. To calculate the reactions and the heat demand of the dehydrogenation reactor, “real” components are selected from the Aspen Plus database, PURE10, to describe the composition of the model mixtures. These components are defined by chemical and thermodynamic properties, such as the molecular structure and the Gibbs free energy. For the reference concept, a model mixture of ULSK is entered in the flow sheet simulation, while for the process concept with rectification, fraction model mixtures for 10 wt.- % and 20 wt.-% were used. This real component model mixture differs in physical properties to ULSK and Jet A1 fractions, especially with evaporation. Therefore, the heat demand for vaporization in the reference process and rectification with the process concept is calculated with pseudo components. The pseudo components are defined by physical properties of kerosene, such as boiling behavior and density of the fuel, but do not describe chemical properties or the distilled weight fraction at a specific boiling point. The properties of the pseudo components for Jet A-1 are generated in Aspen Plus by implementing the boiling range measured according to ASTM D2887, the mass density of 0.7987 kg/dm^3 and the molar weight of 150 g/mol. This input is used by Aspen Plus to generate by default 10 pseudo components by breaking the boiling range according to ASTM D 2887 into 11 cuts, which are the same as the input boiling range data, see Fig. 6.1.

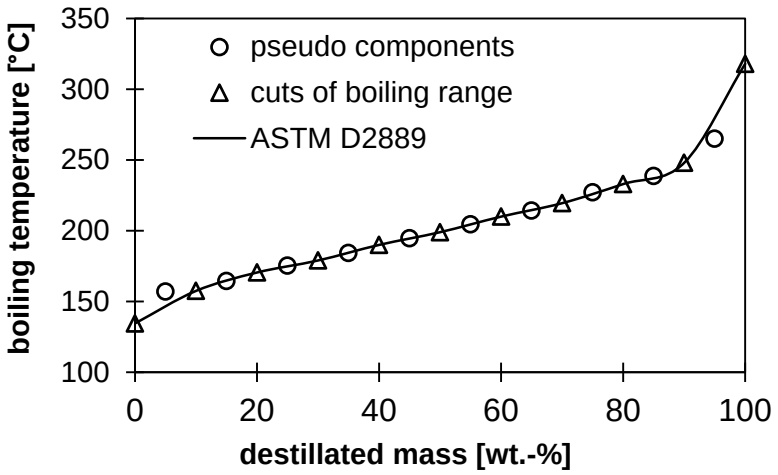

Fig. 6.1 - boiling range implemented in flow sheet simulation with generated boiling point cuts and boiling point temperatures of pseudo components

The middle point of each cut is used as the “true” boiling point of the pseudo component. The boiling points and physical properties of the 10 pseudo components are presented in table 6.1. For generating the pseudo components of ULSK for the reference process, the calculated boiling point curve which is presented in chapter 4.1 was integrated in Aspen Plus with 11 boiling points between 0 and 100 wt.-% of distillated mass. The sulfur content is neglected

since no desulfurization process is needed. Further, no sulfur is introduced into any model mixture used in Aspen Plus, since no stable reaction conditions were achieved with sulfur containing mixtures in the experimental study. The properties of the ULSK pseudo components are presented in appendix 8.4 table 8.5.

Next to the modelling of Jet A-1 in the flow sheet simulation, the modelling of the rectification in the flow sheet simulation is important to the heat demand calculation of rectification. The input specifications for the process concept are obtained from the properties of the laboratory rectification column. These specifications have to be adapted from a non-ideal batch rectification, to continuous model rectification in Aspen Plus. The sulfur contents in the distillated mass fractions of the experiment are used for these adjustments. In addition, the sulfur content in the kerosene fractions can be estimated for any mass fraction in the flow sheet simulation. Aspen Plus allows the adjustment of the property curves to the pseudo components. This allows tying the content of sulfur to the single pseudo components. However, the sulfur content measured in the consecutive fractions during distillation is attached to the fractionated mass in the experimental work, and does not match the mass and the true boiling points of the pseudo components. To achieve a sulfur distillation curve similar to the experimental study, the sulfur content has to be adjusted to the properties of the pseudo components. For the experimental distillation, 13 distilled fractions are extracted with the laboratory batch rectification. The sulfur contents of the 13 experimental fractions are not compatible with the 10 pseudo components. In order to adjust the amount of experimental fractions to the simulation, the 13 mass fractions with their total sulfur contents are reduced to 10 fractions by polynomial curve fitting in MatLab®. In the next step, a 10 by 10 Matrix of pseudo components with 10 mass fractions between 10 wt.-% and 100 wt.-% is generated in Aspen Plus by sensitivity analysis with the rectification model Radfrac. The design rectification model Radfrac is described in chapter 6.3. The matrix and fitted sulfur distillation curve as a vector is used to solve a linear equation system. Since the solution would also involve negative values, the linear system is solved with nonlinear curve- fitting function (lsqcurvefit) where only positive values are allowed. The vector solution is then the fitted sulfur content of each pseudo component, see table 6.1. The sulfur content of the pseudo component mixture is used to develop the rectification model and adjust the properties of the model to the experimental results of the rectification.

Table.6.1 - physical properties and fitted sulfur content of pseudo components for Jet A-1

pseudo components	boiling point	mass density	molecular weight	mass content	fitted sulfur content
	[°C]	[kg/dm³]	[g/mol]	[wt-%]	[ppmw]
PC157C	156.97	0.77	122.19	0.36	0.0
PC164C	164.42	0.78	126.31	5.09	0.0
PC175C	175.28	0.78	132.57	9.42	0.0
PC184C	184.21	0.79	137.87	20.36	0.0
PC195C	194.65	0.79	144.27	14.02	58.50
PC205C	204.53	0.80	150.54	12.71	224.17
PC214C	214.20	0.80	156.86	10.12	141.30
PC227C	227.08	0.81	165.59	11.57	203.84
PC239C	238.62	0.82	173.71	7.15	702.93
PC265C	265.06	0.83	193.42	9.21	1146.74

6.2 Modeling of the Rectification Process

The column operation model chosen to obtain the rectification is the Aspen Plus RadFrac model. It is relevant for all types of multistage vapor- liquid fractionation operations and suitable for narrow boiling systems. By defining the minimum input specification of flow rate, stage number, reflux ratio, distillation to feed ratio and column pressure, the reboiler heat duty and condenser duty are calculated. The mathematical description of a distillation process in a rectification column is the theoretical stage method. For each theoretical stage j and component i, the mass balance (6.1), enthalpy balance (6.2), and vapor liquid equilibrium coefficient (6.3) equation of the individual pseudo components is described under steady state conditions.

$$\dot{L}_{j+1} l_{i,j+1} + \dot{V}_{j-1} v_{i,j-1} + \dot{F}_j f_{i,j} - \dot{L}_j l_{j,i} - \dot{V}_j v_{i,j} = 0 \tag{6.1}$$

$$\dot{L}_{j+1} H_{j+1,l} + \dot{V}_{j-1} H_{j-1,v} + \dot{F}_j H_{f,j} - \dot{L}_j h_{j,l} - \dot{V}_j H_{i,v} - Q_{mix} - Q_s - Q_{loss} = 0 \tag{6.2}$$

$$K_i = \frac{l_i}{v_i} \tag{6.3}$$

where $\dot{V}$ is the mole flow of the vapor, $\dot{L}$ is mole flow of the liquid and $\dot{F}$ is the feed mole flow, while l, v, f are the mole fraction in liquid, vapor and feed. The molar enthalpy of the corresponding streams is represented by H. Q_{mix} is the heat of mixing, Q_s the external heat source and Q_{loss} represents the heat losses. Fig. 6.2 presents a general scheme of a column stage [121], [32].

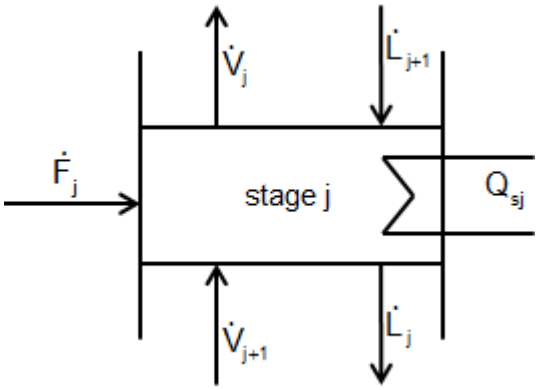

Fig.6.2 - Scheme of a column stage

The selection of a thermodynamic method for the calculation of the equilibrium coefficient is an important step for simulation accuracy. Aspen Plus provides a number of thermodynamic models. The equation of state property method chosen for this rectification model is developed especially for hydrocarbon mixtures, and mainly suitable for pseudo components. The Braun K10 property method, an activity coefficient model, is suitable for heavier hydrocarbons at pressures under 10 bar and temperatures from 170°C to 430°C and is described in the Aspen Physical Property System 2009 [121], [122]. To calculate the partial vapor pressure, a modified Antoine equitation is used. Here, A, B, C, D, E and F are fitted substance specific coefficients for real components and pseudo components, Eq. (6.4).

$$\ln p_i = A + \frac{B}{T + C} + D \ln T + E T^F \tag{6.4}$$

The Radfrac model is designed as a regular one distillation column with one feed stream, a partial condenser at the top stage, and a reboiler at the bottom stage. Typically, the inlet of the column is chosen at the middle stage. The input data available to design the RadFrac model is from the experimental batch rectification. Although, heat losses of the laboratory rectification are not considered in the simulation model.

Further, with the batch rectification, the composition of feed respective the still changes over time, while the feed stream of the simulation model being performed with steady feed composition. This leads to an increasing enthalpy demand with the batch rectification, decreasing pressure over time. Both factors lead to a worse sulfur separation with the experimental test set up. Physical properties, boiling temperature distribution and molar mass (10 wt.-% pseudo fraction 132.2 g/mol and 20 wt.-% pseudo fraction 134.4 g/mol) of the fraction of the simulated pseudo component fraction will differ from the experimental values. To calculate the heat demand of the simulated rectification, the distillated mass fraction and the reflux reaction of the column is integrated in the flow sheet simulation at specific pressure,

defined at 1 bar. The variable input data is the reflux ratio, which is determined for the Radfrac model by fitting the sulfur distillation curve of the experimental data to the simulated sulfur distillation curve.

The experimental Vigreux column does not have a regulated reflux ratio. First, a RadFrac column is laid out to fit the features of the experimental set up. The initial value for the reboiler duty is given at 300 W and the feed flow is set at 1.2 kg. Further, the distillation mass flow rate is estimated for the experiment and defined at 0.475 kg/h. The number of stages of the experimental Vigreux column is estimated to be 14, including the bottom and the top stage. These 14 stages are used as input to the simulation. Increasing the number of stages beyond 14 does not show a meaningful improvement in distillation selectivity of the sulfur content in the distillated fraction. The feed flow enters at stage seven. With a sensitivity analysis, the reboiler heat duty is varied at different reflux ratios, while the mass flow rate is calculated by the Radfrac model. With the RadFrac model running at 1 bar and the phase equilibrium calculated with a reflux ratio of 2.7, the sulfur content of the distillated mass fraction [wt.-%] meets the experiment sulfur distillation curve, see Fig. 6.3.

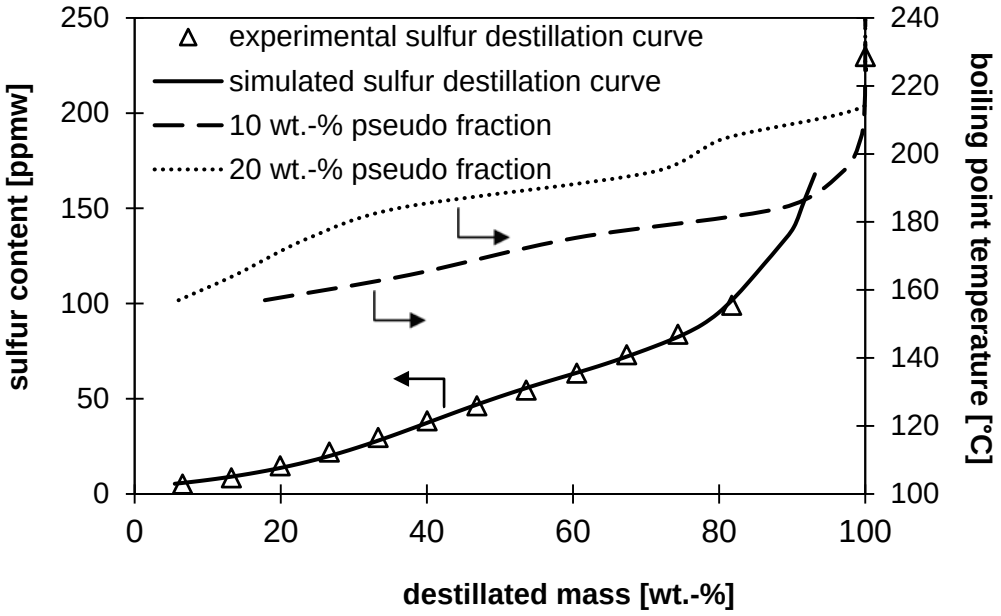

Fig. 6.3 – comparison of experiments and simulated sulfur distillation curve of rectification and the boiling temperature distribution of 10 and 20 wt.-% pseudo component fraction

With the input data of the reflux ratio available, the rectification model is used to adjust flow rates and distillation to feed ratio to calculate the energy demand within the process concept.

6.3 Modelling of Dehydrogenation Process

The partial catalytic dehydrogenation of a multi component mixture has many various reaction paths which influence each other. The reactions and products appearing depend on the feed

mixture and reaction conditions. All reactions are endothermic. The experimental results show that dehydrogenation of a hydrocarbon mixture is strongly dependent on kinetics, and is far from thermodynamic equilibrium. The reaction kinetics of a PCD of multi- components mixtures is unknown. Although, the conversion rate and stoichiometry of the feed components towards defined products is available from experimental data. Therefore, the reactor model RStoic in Aspen Plus is chosen to be suitable for calculating the heat demand of dehydrogenation within the process concept. RStoic calculates the heat of reaction from the heats of formation in the database by the enthalpy difference based on the conversion of the reference reactant selected for each reaction at reference conditions (temperature 25°C, pressure 1 atm, fluid phase is vapor phase). The method of calculating the heat of reaction and the heat content in the gas streams, as well as the separation of condensable product components and gaseous products are chosen from the Aspen Plus property methods system. The heat demand of the dehydrogenation reactor is calculated from the turnover of the input component and defined products, no kinetic data is involved. This limits the calculation to specified reaction conditions, which is the same as defined in the experimental work: 425°C and 8 bar pressure. This condition is chosen to be suitable for the process concept by making a compromise between hydrogen yield, stable product gas flow and a pressurized system for gas cleaning. The dehydrogenation of model mixture in the experiment leads to a product distribution of up to 110 different products. Not all of these product components are available in the Aspen Plus database. Therefore, simplified reaction schemes are introduced into RStoic to calculate the heat demand of the dehydrogenation reactor.

6.3.1 Property Methods for Vapor-Liquid Equilibrium

The choice of the property method depends on the problem specification. The vapor liquid equilibrium calculated in this flow sheet simulation has to express the condition of a complex mixture consisting of hydrogen, light hydrocarbons and heavier hydrocarbons. The property method describes the condition state functions of pressure, temperature and volume in gas and liquid phase of a thermodynamic system.

To calculate the heat of reaction, the reaction enthalpy is corrected by a cubic equation of state to take into account the pressure deviation from the ideal gas law. The reaction enthalpy has to be completed with a real gas term.

Standard enthalpy of reaction of component j:

$$\Delta H_R^0(T) = \Delta H_R^0(T_0) + \int_{T_0}^{T} \sum \nu_j c_{p,j}^0 dT \tag{6.5}$$

Reaction enthalpy at isothermal conditions with real gas supplement

$$\Delta H_R(T,p) = \Delta H_R^0(T,p_0) + \sum \nu_j (H - H_{id})_{T,p,j} \tag{6.6}$$

$$(H - H_{id})_{T,p,j} = -\int_{\infty}^{V} \left[p - T\left(\frac{\partial p}{\partial T}\right)_V \right] dV + p * V - R \tag{6.7}$$

Next to the reaction enthalpy, the vapor liquid equilibrium of the non-ideal mixture of hydrocarbons and hydrogen has to be calculated with real gas equation of state, which is derived from Van-der-Waals equation of state. All reactors, heat exchangers and condensers with “real” components are calculated with the Soave-Redlich-Kwong equation of state (SRK). With an additional temperature dependent term, the Van-der-Waals equation is exceeded with accuracy above the critical temperature T_c for any pressure [123].

$$p = \frac{RT}{V_m - b} - \frac{a\alpha}{V_m(V_m + b)} \tag{6.8}$$

The molar Volume V_m is derived from the compressibility factor z.

$$z = \frac{pV_m}{RT} \tag{6.9}$$

The parameter “a” is the measure of attraction between molecules and “b” the volume excluded by a mole of molecules. Both parameters are derived from enthalpy of mixing rules by Huron and Vidal. The quadratic mixing terms for SRK are retrieved from the thermodynamic property method script in Aspen Plus. The parameter “ α “ considers the deviation of molecules from ideal cubic form by including the acentric factor ω.

$$\alpha = [1 + (0.48 + 1.57\omega - 0.176\omega^2)(1 - T_r^{0.5})]^2 \tag{6.10}$$

$$\omega_i = -\log_{10}\left(\frac{p_i^{sat.}}{p_{c,i}}\right)_{T_r} \text{ for } T_r = \frac{T}{T_c} \tag{6.11}$$

Comparable results with vapor liquid equilibrium can be achieved with Peng- Robinson equation of state, which is also derived from the Van- der- Waals equation of state [124].

While all process elements involving real component mixtures are calculated with SRK equation of state, the heat demand for evaporation and rectification of pseudo components is calculated with Braun K10 property method.

6.3.2 Integration of Model Mixtures in Process Simulation

The complex reaction system of kerosene dehydrogenation enforces strong simplification to embed a PCD reactor in flow sheet simulation. The complex mixture of kerosene is introduced as a simplified model mixture. Different model mixtures are used to represent the chemical composition of ULSK in the reference concept, and the 10 wt.-% and 20 wt.-% Jet A-1 fractions for the process concept with rectification. The composition of the model mixtures and their properties are described in chapter 4.3. The model mixture fractions 10 wt.-% and 20 wt.-% for the process simulation differ in their hydrogen yield due to the differences in composition. The hydrogen output of the model fractions is not only dependent on the cycloalkane content, but also on the content of longer chain hydrocarbons. By introducing the experimental results in the model reactor the difference in hydrogen output leads to different thermal efficiency of process concepts.

In the flow sheets of both process concepts, kerosene is first introduced as pseudo components to ensure calculation of the heat demand and compressor performance in order to obtain kerosene at process conditions. Before the feed stream enters the PCD reactor, the composition of the stream is switched to the respective real component model mixtures, while the stream conditions of temperature, pressure and mass flow are copied from the pseudo component stream. To implement dehydrogenation reactions of model mixture, experimental information is needed about liquid and gaseous product composition, carbon formation and component conversion rate. Since the alkane components nonane, decane and dodecane used in the model mixtures can result in to 72 different liquid product species, a strong simplification of chosen reaction paths is necessary. For defining the reaction products and reactions for the process simulation, the product information from the single components experimental tests is used.

First, the composition of the hydrocarbon groups of the liquid product components are analyzed and arranged by their carbon atom number, see chapter 4. In this way, an overview is gained of product distribution. Then, the mass content of different hydrocarbon groups is summarized by adding the components by their carbon atom number. The carbon atom number with the biggest share in the hydrocarbon group is chosen to be the one with the summarized mass content. In this way, a maximum of one or two liquid products per hydrocarbon group have to be picked from the list of detected products if available in the Aspen database. Alkanes and Alkenes are usually available in the database, unlike detected aromatic hydrocarbons, cylcoalkanes or iso- alkanes which have a very complex molecule structure. Therefore, simplified representatives with the same carbon atom number have to be chosen from the Aspen Plus database. For nonane, decane and dodecane, with the most complex product distribution, the liquid products are systematically defined by one alkene, two different aromatic hydrocarbons or cycloalkane as intermediate product, one isoalkane and one

cracking product, which is a shorter chain hydrocarbon than the feed component. With decane, a significant amount of undecane was detected in the single component experiments. Therefore, this product is also taken into account. For each component, a reaction leading to carbon formation is introduced. In this way, a maximum of 6 different reactions is introduced into RStoic reactor for the alkane feed components.

The components MCH, cis- and trans- Decalin in model mixtures have less complex product distributions. This allows a selection of liquid reaction products directly from the product distribution. In this case, one aromatic hydrocarbon and one cylcloalkane are chosen. For MCH, the cracking product benzene is also introduced, since it was detected with the single component tests. The model mixture component isooctane dehydrogenates to different isomers of isooctane, of which one is chosen as a representative. The aromatic hydrocarbons show no hydrogen evolution, however, they do show gaseous hydrocarbons and carbon deposition. The liquid product analysis shows only a distribution of different aromatic hydrocarbons formed by restructuring to different derivatives or cracking. Therefore, reactions to carbon formation and cracking products are chosen from the Aspen database. With all model mixture components, the formation of carbon is considered as well. In table 6.2, all integrated reactions in PCD reactor are tabulated with their stoichiometric factors " ν ".Due to the low boiling range of the10 wt.-% model fraction, the component dodecane is not part of the model mixture of the fraction. For the other two model mixtures, all reactions of table 6.2 are used.

Table 6.2 stoichiometric reactions for model mixtures components integrated in RStoic reactor model in process simulation

No	ν	Model component	ν	1. Product (l)	ν	2. Product	ν	3. Product
1	1	Nonane C_9H_{20}	1	Hexane C_6H_{14}	1	Propene C_3H_6		
2			1	2-Methyloctane C_9H_{20}				
3			1	Butylcyclopentan C_9H_{18}	1	Hydrogen H_2		
4			1	Methyl 3-ethylbenzene C_9H_{12}	4	Hydrogen H_2		
5			1	Nonene C_9H_{18}	1	Hydrogen H_2		
6			9	Carbon C	10	Hydrogen H_2		
7	1	Decane $C_{10}H_{22}$	1	Decene $C_{10}H_{20}$	1	Hydrogen H_2		
5			1	1.3-Diethylbenzene $C_{10}H_{14}$	4	Hydrogen H_2		
9			1	Propylcyclohexane C_9H_{18}	1	Methane CH_4		
10			0.5	Nonane C_9H_{20}	0.5	Undecane $C_{11}H_{24}$		
11			1	2- Methylnonane $C_{10}H_{22}$				
12			10	Carbon C	11	Hydrogen H_2		
13	1	Dodecane $C_{12}H_{26}$	1	Octane C_8H_{18}	2	Ethene C_2H_4		
14			1	3-Methylundecane $C_{12}H_{26}$				
15			1	Ethylcyclohexan C_8H_{16}	1	Methan CH_4	1	Propen C_3H_6
16			1	Hexylbenzene $C_{12}H_{18}$	4	Hydrogen H_2		
17			1	Dodecene $C_{12}H_{24}$	1	Hydrogen H_2		
18			12	Carbon C	13	Hydrogen H_2		

No	ν	Model component	ν	1. Product (l)	ν	2. Product	ν	3. Product
19	1	Isooctane C_8H_{18}	1	2,4,4-Trimethylpentene C_8H_{16}	1	Hydrogen H_2		
20			8	Carbon C	9	Hydrogen H_2		
21	1	n-Butylbenzene $C_{10}H_{14}$	1	Styrene C_8H_8	1	Ethan C_2H_6		
22			10	Carbon C	7	Hydrogen H_2		
23	1	p-Xylene C_8H_{10}	1	Benzene C_6H_6	1	Methane CH_4	1	Carbon C
24			1	Toluene C_7H_8	1	Hydrogen H_2	1	Carbon C
25			8	Carbon C	10	Hydrogen H_2		
26	1	Cis-/trans-Decahydronaphthlene $C_{10}H_{18}$	1	Tetrahydro-naphthalene $C_{10}H_{12}$	3	Hydrogen H_2		
27			1	Naphthalene $C_{10}H_8$	5	Hydrogen H_2		
28			10	Carbon C	9	Hydrogen H_2		
29	1	Methylcyclohexane C_7H_{14}	1	Toluene C_7H_8	3	Hydrogen H_2		
30			1	Benzene C_6H_6	2	Hydrogen H_2	1	Methane CH_4
31			7	Carbon C	7	Hydrogen H_2		

The conversion rate of every defined reaction is integrated in Aspen Plus Stoic reactor. It is needed to define the product yields especially of hydrogen and gaseous hydrocarbons for the system efficiency calculation. To calculate the conversion rate of each single reaction the conversion rates "X_j "of the feed components j in the model mixture are integrated in the PCD reactor, Eq. (6.12). The values of X_j are taken over from the detected conversion rates of model components in the model mixtures of the experimental results. Where $m_{j,0}$ is the feed mass before the reaction and m_j after the experiment has ended. In the next step the mass content of a specific liquid product component "x_l"among all product components "p" is calculated by the mass m_l of a specific liquid product over the summarized mass of all product components "m_p", see Eq (6.13). Furthermore, each reaction among a converted component is evaluated

by a conversion factor "$X_{f,i}$" This factor defines how much of the conversion rate is contributing to that specific reaction. It is calculated by the mass content of each liquid product component over the summarized mass content of all product components, Eq. (6.14). Finally the conversion rates for each single reaction is calculated as the result of multiplication the conversion factor of each reaction with the conversion rate of the feed component "j", Eq. (6.15). The conversion rates and conversion factors are calculated in EXCEL and integrated in Aspen Plus RStoic reactor. A detailed list of the integrated values is found in Appendix 8.4 table 8.6.

Total conversion rate of feed component j:

$$X_j = \frac{m_{j,0} - m_j}{m_{j,0}} \cdot 100[\%] \tag{6.12}$$

Mass content of liquid product component l:

$$x_l = \frac{m_l}{\sum_{j=1}^{j=n} m_p} \cdot 100[\%] \tag{6.13}$$

Conversion factor of single reaction i:

$$X_{f,i} = \frac{x_l}{\sum_{i=1}^{i=n} x_l} \tag{6.14}$$

Conversion rate of single reaction i

$$X_{r,i} = X_{f,i} \cdot X_j[\%] \tag{6.15}$$

Establishing a conversion factor for each single reaction is important to the product gas composition and carbon formation. Each reaction has its defined contribution to the gaseous products which, in total, expresses the gaseous hydrocarbon yield Y_{CxHy}, hydrogen yield Y_{H2} and carbon output Y_C. These values are needed for the calculation of the efficiency of the process concepts in the simulation. The gaseous hydrocarbons are separated from the product gas and reused in a dual fuel burner, with dehydrogenated ULSK or Jet A-1 fraction to power the dehydrogenation process. The carbon formed as a side product is part of the total mass balance. It is treated as heating power loss of the kerosene since the missing carbon content in the dehydrogenated ULSK and Jet A-1 fractions reduces the lower heating value of the fuel. Though, the carbon has a maximum of 2.8 % of the total heating power loss of the kerosene

in the system. The biggest influence on the efficiency of the process concept is the hydrogen yield, since electric performance of the fuel cell depends on it.

The conversion factor for single component reactions can be derived from the experimental product distribution. In this case, the hydrogen yield, the content of gaseous hydrocarbons and carbon formation is calculated from the stoichiometric conversion of the feed component. However, the conversion factors do not represent the distribution of the products in the model mixture, only the conversion rate of the feed components in the model mixture is derived directly from the experimental results. The conversion rate of the feed component not only differs from the single component tests, but also the product distribution itself. For all feed components, the chosen reaction products are simplified from the components having been actually measured in the experiment. Therefore, a direct correlation to the product distribution from the actual measured chromatography analysis is not possible. Only the conversion factor is similar to the measured product distribution in the model mixture for prominent products of the MCH and Decalin, since those feed components show not more than three different dehydrogenation products. On that account, a conversion factor for most reactions is derived from the single component tests, but has to be adjusted to achieve comparable results for hydrogen gas yield, gaseous hydrocarbons and carbon formation with the simulated reactor and the experimental results.

The calculated yield of hydrogen or (/) gaseous hydrocarbon from the summarized reactions “i” of one feed component “j” is shown in Eq. (6.16).

$$Y_{H_2/C_xH_y} = \frac{\sum X_{r,i} \cdot n_{j,0} \cdot \nu_{H_2/C_xH_y} \cdot V_m}{m_{j,0}} [nl/kg_{feed}] \qquad (6.16)$$

Table 6.3 presents the comparison of the gaseous yield results and carbon formation of the experimental data and the calculated data of the simulation. The data show strong similarity and therefore the output of the simulation is used for efficiency calculations of the system based apon experimental data.

Table 6.3 - hydrogen, hydrocarbon gas, and carbon yield of experimental results and output of the model dehydrogenation reactor in the flow simulation

		Experiment Model Mixtures			RStoic Model Mixtures		
	Units	ULSK	10 wt-% Fraction	20 wt-% Fraction	ULSK	10 wt-% Fraction	20 wt-% Fraction
Y_{H2}	nl/kg_{feed}	75.30	126.39	80.39	75.20	128.20	80.30
Y_{CxHy}	nl/kg_{feed}	0.33	0.42	0.25	0.34	0.42	0.26
carbon formation	g_C/kg_{feed}	0.36	0.33	0.35	0.37	0.34	0.34
enthalpy demand	kJ/mol_{H2}				73.54	74.00	73.15

Further, the liquid product distribution of the hydrocarbon groups is also considered in the choice of conversion factors to fit as closely as possible to the liquid product distribution of the experimental results. Table 6.4 presents the hydrocarbon group distribution in the condensate of the simulated dehydrogenation.

Table 6.4 –distribution of hydrocarbon groups of the simulated condensate of model mixtures

Model Mixture	n-alkanes	n-alkenes	iso-alkanes	iso-alkenes	cyclo-alkanes	cyclo-alkenes	aromatic hydrocarbons
	[wt.-%]						
ULSK	45.33	1.74	4.06	0.12	17.44	0.98	30.33
10 wt.- %	39.52	0.93	3.18	0.06	13.46	2.83	40.04
20 wt.-%	44.90	0.42	1.34	0.00	21.92	1.58	29.85

The simplification of adjusting the conversion factors to satisfy the gaseous product distribution was chosen to be legitimate due to the overall objective of the simulation. The aim of the process simulation is to calculate the process efficiency of the heat integrated process concept and reference concept. A more detailed reaction distribution would not improve the accuracy of the process efficiency, since other factors like heat integration have a stronger influence. The average enthalpy demand of the dehydrogenation reactor is 73.6 kJ/mol_{H2}. The heat demand depends not only on the conversion rate and hydrogen yield, but also on the feed flow into the reactor. With increasing hydrogen yield, less kerosene has to be converted to achieve the same system performance. Therefore, the molar conversion stays similar, same as the heat demand of the endothermic reaction.

6.4 Heat and Material Integration

The goal of this chapter is to describe the heat integration network designed for both the process concept with rectification, and reference concept. To design a working heat exchanger network for heat integration, it is not necessary to choose a network of maximum heat recovery. The aim is to build flow sheets for both processes with realistic heat integration. This means that the heat exchanger network should have an economic number of heat exchangers, so the whole system will not exceed practical size and complexity. The first step of interest is to know the possible energy recovery for both systems. From the basis of the optimum heat recovery, a heat exchanger network can be designed that suits both low complexity and the target of close to maximum heat recovery. The feed flow rate in the process system and reference system are both set up for an electric performance $P_{el.}$ of 90 kW, Eq. (6.17). This target performance is chosen to fit a regular APU of an Airbus A320, which is a common medium haul aircraft.

$$P_{therm.} = m_{H_2} \cdot LHV_{H_2} \tag{6.17}$$

$$P_{el.} = \eta_{PSA} \cdot \eta_{FC} \cdot \dot{m}_{H_2} \cdot LHV_{H_2} \tag{6.18}$$

The thermal performance $P_{therm.}$ of the system is derived from the hydrogen output of the dehydrogenation reactor, Eq. (6.17). The efficiency of the gas cleaning with PSA η_{PSA} is defined by 80 %, which is a common target efficiency for PSA for hydrogen purification from hydrocarbons [125], [126]. The electric fuel cell efficiency is set at 50 % and refers to the hydrogen heating power [127], [128], while the lower heating value LHV_{H2} of hydrogen is known as 120 MJ/kg. Considering the hydrogen output after the PSA and the electric efficiency of the PEMFC the electric performance $P_{el.}$ the process is calculated by Eq. (6.18)

For both process concepts, the hydrogen flow rate has to be set at 6.75 kg/h hydrogen product to achieve a 90 kW system performance including PSA and PEMFC. For the thermal efficiency $P_{therm.}$ 2.7 kg/h hydrogen product is needed. This condition is satisfied by an adjustment of the kerosene feed flow, which depends on the hydrogen yield of the dehydrogenation reactor, see Eq. (6.16).

The heat integration design is built on the target values of the base case process performance. The base case means the simulated hydrogen yield is calculated on the hydrogen yield of the experimental work. In the chapter 6.6.3, the efficiency of a theoretical maximum hydrogen yield will be presented on the basis of the heat integration described here.

For the process concept with rectification, two different fractions, 10 wt.-% and 20 wt.-%, are used in the experimental work and in process design. The difference in heat demand on rectification and dehydrogenation reactor does not change the possibilities in heat recovery within the process. Therefore, the heat integration is described here with one process concept using the 10 wt.-% fraction.

6.4.1 Internal heat source

Both process concepts with and without rectification require an internal heat source to provide the heat demand for the dehydrogenation, preheating, and evaporation of the feed streams. This internal heating demand can be satisfied by introducing an adiabatic fuel burner in the system. Fig. 6.4 presents a schematic PCD reactor with integrated heating by flue gas of a burner.

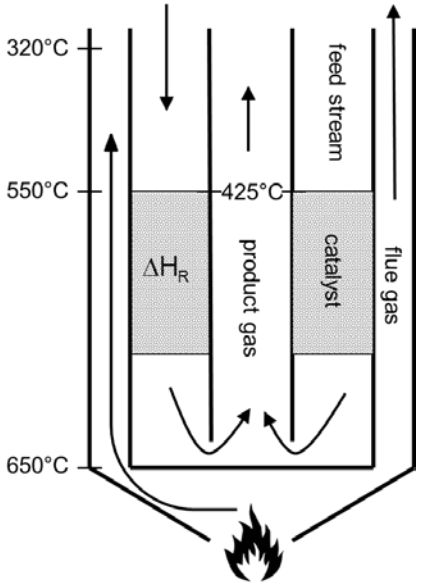

Fig.6.4 - Scheme of a PCD reactor with integrated heating by flue gas

The temperature gradient from the burner flue gas to the dehydrogenation should be moderate, since high temperature gradients in a real dehydrogenation reactor might cause cracking and coke formation. To take this into consideration, the temperature outlet of the burner is defined by 650°C, which is achieved by a high air-to-fuel ratio. The temperature gradient of the flue stream for heating the dehydrogenation reactor is 100 K. This way, the heat transfer into the reactor for the endothermic reactions is guaranteed. The air mass stream for the burner is defined on the temperature outlet of the flue gas before heating the dehydrogenation which is 650°C. The fuel mass stream is calculated by design specification in Aspen Plus to meet the temperature outlet of the burner of 550°C after providing the head demand to the PCD reactor at a reaction temperature of 425°C. The feed stream is preheated first by the product gas

stream and second heat up to reaction temperature by the flue gas stream. The flue gas leaves the heating of the reactor and the preheating of the fuel at 320°C.

After satisfaction of this specification, the heat stream of the flue gas is used to preheat the air stream. This heat transfer is defined by the heat exchanger restrictions explained later in this chapter. Therefore, the air stream temperature depends on the amount of feed for the dehydrogenation reaction and the fuel stream for the burner. The burner could be operated as a dual fuel burner with dehydrogenated kerosene and additionally, with the off gas of the PSA containing hydrocarbons and hydrogen. The LHV of the dehydrogenated kerosene is calculated by remaining liquid components after condensation. To limit the temperature of the burner flue gas to 650°C, the combustion has to be operated with a high air to fuel equivalence ratio (λ), see Eq. (6.19)- (6.21).

$$C_xH_y + \left(x + \frac{y}{4}\right)O_2 \rightarrow xCO_2 + \frac{y}{2}H_2O \tag{6.19}$$

$$\lambda = \frac{\dot{m}_{air}}{\dot{m}_{air}^{stochiometric}} \tag{6.20}$$

$$\dot{m}_{air}^{stochiometric} = \left(\dot{n}(C) + \frac{\dot{n}(H)}{4} \cdot M(O_2)\right) \cdot \left(\frac{0.79 \cdot M(N_2)}{0.21 \cdot M(O_2)} + 1\right) \tag{6.21}$$

The number of hydrogen and carbon atoms in the input fuel stream to the burner is extracted from the flow sheet simulation. The amount of air used for the combustion influences the overall efficiency of the system, since the air has to be preheated to decrease the amount of fuel used for combustion.

6.4.2 System boundary

For both systems, the boundary conditions of the heat and material balance are set to define the heat integration, and to calculate the efficiency of systems. For the reference concept, the scheme of the system boundary is shown in Fig. 6.5.

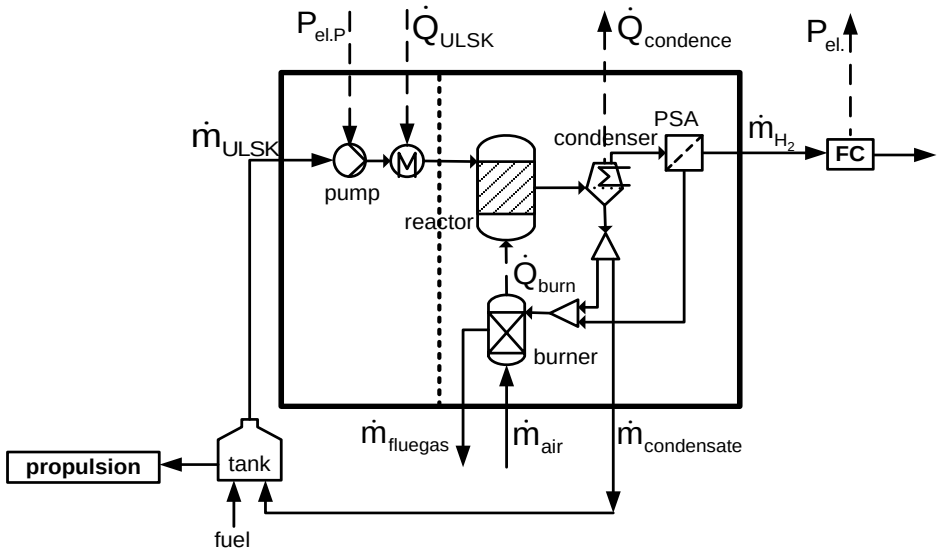

Fig.6.5 - scheme of system boundary for reference concept

The incoming streams for the mass balances are the ULSK feed flow $\dot{m}_{ULSK}$ for dehydrogenation, and the air for combustion $\dot{m}_{air}$. The tank size is considered to be sufficient to fulfill the mass balance. The outgoing streams are the hydrogen product gas $\dot{m}_{H_2}$, the exhaust from the burner $\dot{m}_{fluegas}$ and the part of condensable products of the dehydrogenated ULSK $\dot{m}_{condendate}$, which are not used in the burner for providing the heating within the system boundary. Eq. (6.22) and (6.23) present the mass balance of the reference process .The carbon deposit, which is caused by side reactions, has to be subtracted from the material balance and energy balance, since it is part of the loses. The PSA offgas contains separated hydrocarbons of the product gas stream after condensation and 20 % of the hydrogen product. The material efficiency of the PSA defined to be 80 %.

Mass balance:

$$0 = \dot{m}_{fluegas} + \dot{m}_{condensate} + \dot{m}_{H_2}(+\dot{m}_C) - \dot{m}_{feed} - \dot{m}_{air} \tag{6.22}$$

$$\dot{m}_{condensate} = \dot{m}_{product}^{condensed} - \dot{m}_{condensate}^{burner} \tag{6.23}$$

For the energy balance of the reference system is defined in Eq. (6.24). Where the heat load has to be provided to the feed stream and dissipated from the condenser for product condensation $\Delta\dot{Q}$. Further external electric power is needed for the pressurizing the liquid feed for reaction $P_{el.P}$.

Energy balance:

$$0 = \dot{H}_{Feed} - \dot{H}_{H_2} - \dot{H}_{condensate} - \dot{H}_{fluegas} - \dot{H}_C - \dot{H}_{air} + \Delta\dot{Q} + P_{el.P} \quad (6.24)$$

$$\dot{H}_{air} \approx 0 \quad (6.25)$$

$$\Delta\dot{Q} = \dot{Q}_{ULSK} - \dot{Q}_{condence} \quad (6.26)$$

Respectively, in case of the process concept with rectification, the still from the rectification and the dehydrogenated Jet A-1 fraction not used in the burner are leaving the system. The partly dehydrogenated Jet A-1 fraction and the kerosene still are reused in the kerosene tank for propulsion see Fig. 6.6.

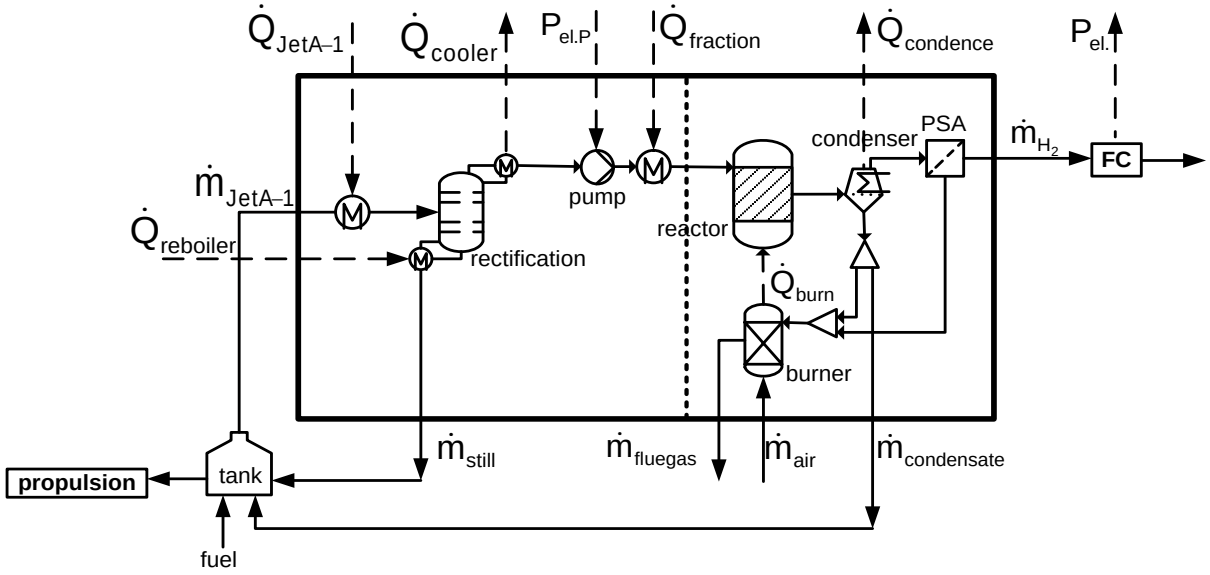

Fig. 6.6 - scheme of system boundary for process concept with rectification

The rectification still has to be added up for the mass balance of the system.

$$0 = \dot{m}_{fluegas} + \dot{m}_{still} + \dot{m}_{condensate} + m_{H_2}(+\dot{m}_C) - \dot{m}_{feed} - \dot{m}_{air} \quad (6.27)$$

For the energy balance, the heat demand of the rectification has to be considered, which is provided to the reboiler.

$$0 = \dot{H}_{Feed} - \dot{H}_{H_2} - \dot{H}_{still} - \dot{H}_{condensate} - \dot{H}_{fluegas} - \dot{H}_C - \dot{H}_{air} + \Delta\dot{Q} + P_{el.P} \quad (6.28)$$

$$\dot{H}_{air} \approx 0 \quad (6.29)$$

$$\Delta\dot{Q} = \dot{Q}_{JetA-1} + \dot{Q}_{reboiler} + \dot{Q}_{fraction} - \dot{Q}_{cooler} - \dot{Q}_{condence} \quad (6.30)$$

For internal heat and material integration, several streams can be reused in both systems to preheat: the Jet A-1 feed, the Jet A-1 fraction and the combustion air for the burner. Preheated

air for combustion reduces the amount of fuel needed in the burner to heat up the air to combustion temperature.

For the flow sheet simulation, both systems are provided with two different types of model components, pseudo components and real component model mixtures. The dotted line within the system boundary marks the switch from pseudo components which are used with preheating, rectification and conditioning to reaction temperature and pressure. To the right of the dotted mark, real components are used to define dehydrogenation reactions in the model reactor. Not only the model components are switched, but also the property methods are changed. To the left, the property method of Braun K10 is used, while to the right, the vapor liquid equilibrium is calculated with SRK property method.

6.4.3 Methodology of heat integration

To design a working heat exchanger network, all streams, which can function as heat loads or heat sinks, have to be identified and arranged to find the maximum energy recovery possible. A common tool to identify maximum heat recovery is the graphical “Pinch - Analysis”. Aspen energy analyzer offers the possibility to extract the heat loads and heat sinks from a flow sheet and arrange them in so called hot and cold composite curves. Here, the heat integration with the Pinch - Analysis for both process concepts, and the design of the heat exchanger grids are described briefly.

First, all streams which need to be heated up are extracted from the flow sheet as cold streams in a temperature “T” over enthalpy “H” diagram. The same occurs with the streams which need to be cooled down in the system, called the hot streams. The enthalpy change of a stream is defined by the temperature change from supplied temperature, T_S, to target temperature, T_T, and the heat capacity flow rate CP. This is the specific heat capacity of the stream multiplied by the stream mass flow, see Eq. (6.31) – (6.33).

$$\dot{Q} = \int_{T_S}^{T_T} \dot{m} \cdot c_p \cdot dT = CP \cdot (T_T - T_s) = \Delta H \tag{6.31}$$

$$CP = c_p \cdot \dot{m} \tag{6.32}$$

For phase changes of the stream, the specific heat capacity has to be adjusted. The slope of a hot or cold stream in the T/H- Diagram is represented by:

$$\frac{dT}{dQ} = \frac{1}{CP} \tag{6.33}$$

Since only the enthalpy changes of the stream are represented in the T/H- Diagram, a given stream can be plotted anywhere on the enthalpy axis with the provision that the same slope runs between the same supply and target temperature. In the next step, all hot streams can

be shifted to one hot composite curve. Similarly, all cold streams are shifted to a cold composite curve. This is accomplished by moving the streams on the enthalpy axis within the same temperature range. Streams which overlap in temperature range can be added up by summarizing the heat capacity flow rate within the shared temperature range (e.g. see T/H-Diagram in Fig. 6.7) [129]. The hot composite curve has to have a higher temperature at any given enthalpy than the cold composite curve to ensure a temperature gradient between streams. Both composite curves can be shifted on the enthalpy axis until they reach a predefined minimum temperature approach ΔT_{min}. This closest approach is called the “pinch”. For a given value of ΔT_{min}, the utility quantities predicted are the minimum required to solve the heat recovery problem [119]. The overlap between the composite curves represents the maximum amount of heat recovery possible within the process. The difference in enthalpy at the lower end of the hot composite curve to the cold composite curve represents the minimum amount of external cooling required. On the other end, the enthalpy difference represents the minimum amount of external heating required. For maximum heat recovery within the process, no external heat should be provided to hot streams beneath the pinch, or cooling to streams above the pinch. Otherwise, this would raise the requirement of external cooling and heating and reduce the internal heat recovery. On the other hand, restrictions for a working heat exchanger grid might request a less than ideal heat recovery.

In a next step, the heat exchanger network is set up with a grid table, where the heat exchanger performance and the temperature gradient of hot and cold stream outlet temperatures are defined. The target temperature difference between hot stream inlet and cold stream outlet temperature in a gas to gas heat exchanger is set at 50 K. This ensures practical surface size of heat exchanger construction. The heat exchangers for preheating and evaporating kerosene have to have a minimum temperature approach of 20 K which is the temperature difference of cold stream outlet and hot stream inlet temperature. Within heat exchangers, evaporation or condensation is allowed, but temperature crossover with the temperature and enthalpy profile of the heat exchanger must be avoided. The aim of the grid table is to design a heat exchanger network performing at maximum heat integration. Still, the heat exchanger restrictions described here have to be followed to ensure a practical and working process system. Therefore, deviations from ideal heat recovery are allowed. When the grid is designed, the heat exchanger network is integrated into Aspen Plus flow sheet simulation. In the following chapters, the heat integration of the reference concept and process concept with rectification are described by the method explained here.

6.4.4 Heat Integration of the Reference Concept

The heat sinks and loads of the reference concept are extracted and arranged to hot and cold composite curves in a T/H-Diagram, see Fig. 6.7. The input data of the streams, temperature

range, mass flow, heat capacity and resulting enthalpy are available in table 6.5. The available hot streams, or heat loads, are the flue gas stream of the burner and the product gas and condenser for the product gas. The streams that perform as heat sinks are the kerosene feed stream, the air stream for the burner, the dehydrogenation reactor and the hydrogen product stream leaving the PSA, which can be heated up to the operating temperature of the fuel cell.

Table 6.5. hot and cold stream data of reference process for heat integration

stream	total flow rate [kg/h]	temperature range [°C]	specific Cp [kJ/kg K]	enthalpy [kW]	stream type
flue gas	2195.9	650.5 – 126.7	1.0936	348.1	hot
hot product stream	1010	425.0 – 325.5 325.5 – 250.9 250.9 – 238.2 238.2 – 216.4	2.8708 2.6315 8.7985 6.3077	205.1	hot
ULSK	1010	20 -115.5 115.5 – 210.7 210.7 – 305.9 305.9 – 333.2 333.2 – 425	2.1953 2.5615 2.9254 10.184 2.91	358.7	cold
air	2174.3	20 – 222	1.0216	124.5	cold
hydrogen	5.341	30 - 80	14.373	1.08	cold
$Q_{reactor}$	-	425.0 – 425.5	-	68.18	cold
$Q_{condesation}$	-	216.4 - 30	-	152.4	hot

The hot product stream is partly condensed in the first heat exchanger after leaving the PCD reactor. After preheating the ULSK feed stream, the hot product gas stream enters the total condenser with vapor fraction of 56 %. The closest temperature approach with the temperature and enthalpy profile within the heat exchanger is 12°C. The evaporation of the ULSK feed stream is accomplished with the flue gas stream, where the temperature approach within the heat exchanger is 18°C

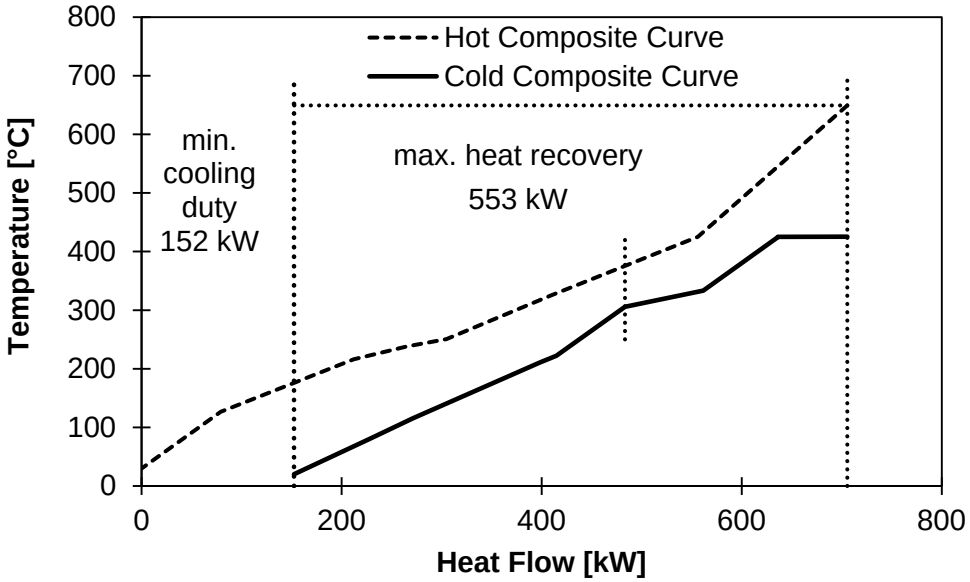

Fig. 6.7 - hot and cold composite curve of reference process

The overlapping of the hot and cold composite curve shows a threshold situation of heat streams. It is possible to provide the heat demand to all cold streams entirely by internal heat recovery. The heat demand can be covered by heat exchange of hot streams and the heat load of the internal burner. Only an external source of cooling is necessary. Further, the closest temperature approach, or pinch point, is the closest temperature difference of the hot and cold streams. In the case of the reference concept, this is 95°C. The pinch point indicates that heat exchanger restrictions can be fulfilled with maximum heat recovery. The segment with the closest temperature approach of the hot composite curve contains the hot product gas and flue gas stream, and the cold composite curve contains the kerosene streams, see Table 6.4. With the information of Fig. 6.7, a heat exchanger grid (Fig. 6.8) is designed, which is then introduced in the flow sheet, Fig. 6.9.

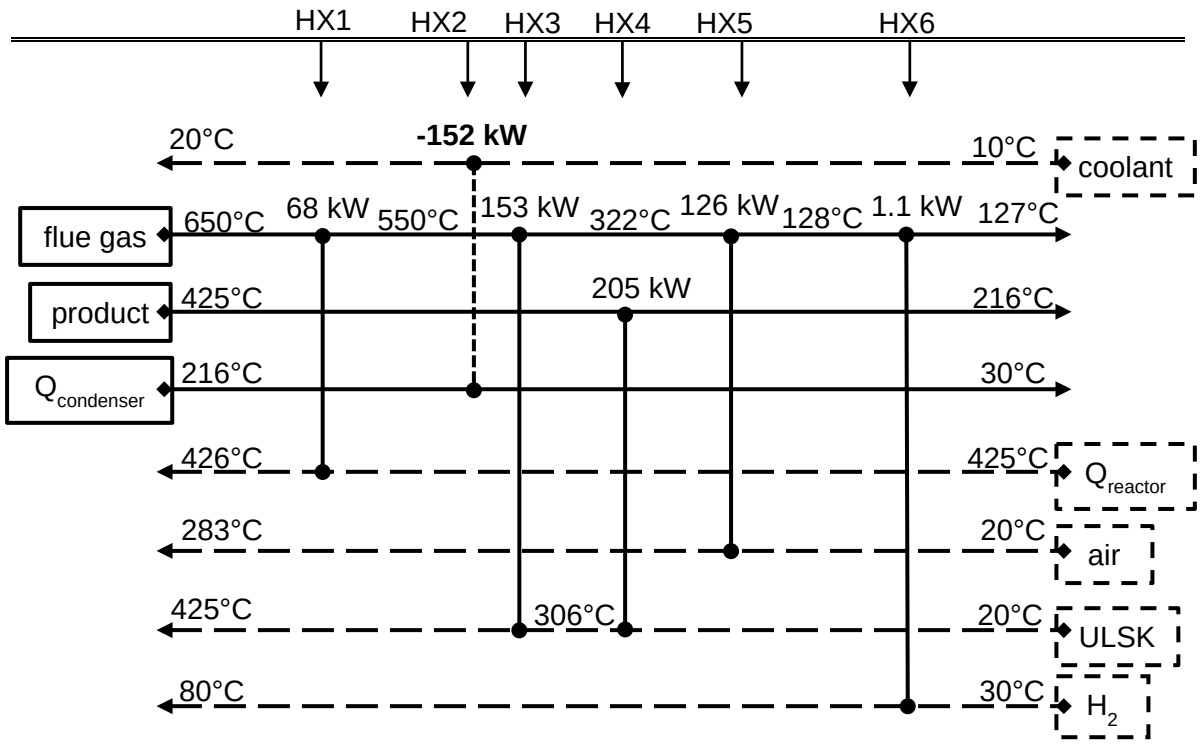

Fig. 6.8 - grid table of heat exchanger network designed for the reference process

The coolant for the condenser is the only external source of cold stream, and is emphasized with a dotted line. A source of 10°C cold coolant stream is assumed. Since the heat exchanger restrictions described in the previous chapter can be followed, maximum heat recovery is reachable.

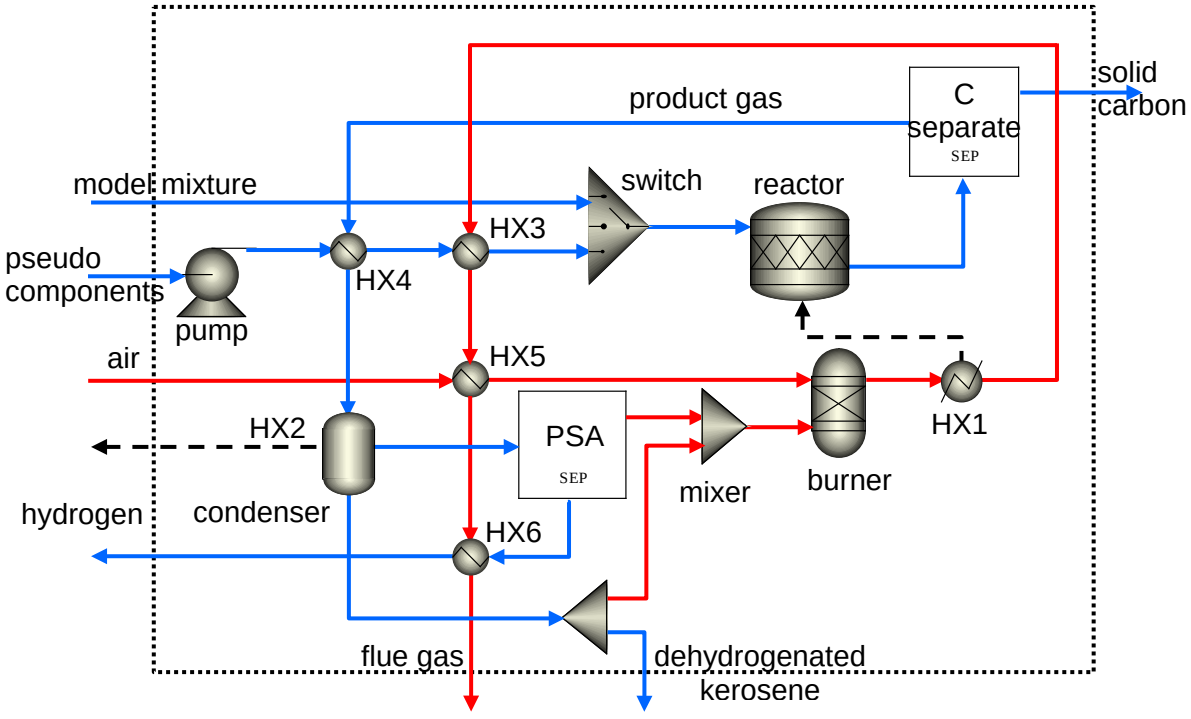

Fig. 6.9 - flow sheet with heat exchanger network of reference concept

The flow sheet presents two different material cycles within the system. The ULSK evaporation and dehydrogenation, the product stream and hydrogen purification is presented with the blue streams. The second cycle is the burner and fuel gas, which is providing the required heat to the dehydrogenation system. This part of the process is marked with the red streams.

First, the pseudo component feed flow is pressurized in a compressor. Then, the feed flow is heated up by the hot product gas stream in the heat exchanger HX4. In the next step, the kerosene feed stream is vaporized and heated to reaction conditions with the fuel gas from the burner (HX3). In the switch block, the mass flow, temperature, and pressure of the pseudo component stream is copied to the model mixture, which continues into the reactor. In the reactor, the reactions described in chapter 6.2.3 are performed. Then, the product gas stream enters the separator block, where the solid carbon from the previous dehydrogenation reaction is separated. This separator block is needed to achieve flow sheet convergence. The property methods, which are described in chapter 6.4 do not handle solid streams. Therefore, the solids have to be removed from the stream in order to calculate energy and mass balance in the blocks further downstream. The separated carbon is considered in the total mass balance and the efficiency of the reference concept. Next, the product gas stream is cooled down. The gaseous products and condensable products are separated in the condenser block (HX2).

The condition is set to 8 bar and 30°C outlet stream temperature. With the partial pressure of the long chain hydrocarbons in the gas phase at condenser conditions, a certain content remains in the product gas phase. To protect the PEMFC from performance reduction by occupying catalyst membrane surface, hydrogen purification by PSA is needed. In table 6.6, the content of gaseous hydrocarbons with carbon atom number of C1 to C5, long chain hydrocarbons with carbon atom number above C5 and hydrogen is shown before and after purification.

Table 6.6 - stream composition on input and output stream to condensation and PSA, calculated with SRK property method

streams	input stream in condenser	Outlet stream not condensed products	PSA offgas stream	Pure Hydrogen stream
	kg/h			
gaseous hydrocarbons	0.31	0.23	0.23	0
longer chain hydrocarbons	1002.2	0.84	0.84	0
hydrogen	6.83	6.75	1.35	5.4

After condensation, the product gas stream still contains 10.7 wt.-% long chain hydrocarbons. In the condensed dehydrogenated ULSK, 1.2 wt.-% of the produced hydrogen and 25.4 wt.-% of gaseous hydrocarbon components are dissolved. The condensate stream is split and partly used as fuel for combustion, the rest leaves the system in to the tank. The uncondensed gas stream enters the PSA block. The block model is executed as a calculator block, which separates the hydrogen from other components in the stream. The PSA off gas stream does not only contain the separated hydrocarbons, but also 20 wt.-% of produced hydrogen after condensation, respectively 19.8 wt.-% of the total produced hydrogen.

The system pressure of 8 bar is relatively low for PSA, since common PSA systems run mostly at 10 to 15 bar. On the other hand, the purity of product stream after condensation is with 99 vol.-% hydrogen relatively high in comparison to refinery fuel gas with 60 to 70 vol.-% used as input stream for PSA [126]. Therefore, an efficiency of the PSA of 80 % is assumed to fit common standard. The PSA offgas is then reused in the burner, which is co-fed with condensed dehydrogenated kerosene.

The adiabatic burner provides the heat demand to the dehydrogenation reactor (HX1). The hydrogen atom to carbon atom ratio of the mixed feed stream to the burner has a molar ratio of 2.75. The mass flow of the air to the burner is also extracted from the flow sheet, see table 6.4. The calculated air to fuel equivalence ratio λ is 5.7 to reach an adiabatic temperature of 650°C of the flue gas, which leaves 17 vol.-% of oxygen in the flue gas for the reference process.

With the last two heat exchangers, the fuel gas preheats the air flow into the burner (HX5) to increase the burner efficiency, and the hydrogen product gas is preheated to 80°C, which is the operation temperature of PEMFC (HX6). The flue gas leaves the system with a temperature of 127°C, see Fig. 6.8.

6.4.6 Heat Integration of Process Concept with Rectification

The heat integration for the process concept including the rectification is carried out with the same methodology as described with the reference concept. First, the enthalpy streams are extracted from the process flow sheet with Aspen Energy Analyzer, see table 6.7.

Table 6.7: hot and cold stream data for heat integration of process concept with rectification and 10 wt.-% Jet A-1 fraction

Stream	total flow rate [kg/h]	temperature range [°C]	specific Cp [kJ/kg K]	enthalpy [kW]	stream type
flue gas	2182	650.6 - 78	1.0930	377	hot
product	589.6	425.0 - 304.9 304.9 - 208.8	2.8284 2.5218	95.3	hot
Jet A-1	5896	20 -74.7 74.7 -133.1 133.1 – 196.6 196.6 – 197.0	2.1421 2.3796 2.6009 26.991	711.4	cold
fraction	589.6	176.3 - 235.4 235.4 – 292.7 292.7 – 320.9 320.9 – 372.9 372.9 – 423.8	2.7858 3.0392 10.527 2.8633 2.9752	153.1	cold
still	5306.4	199.8 – 85.4 85.4 - 30	2.5375 2.1147	600.5	hot
air	2163	20 - 271	1.0261	155	cold
$Q_{rectfi.\ cooler}$	2181.5	180 – 178.8 178.8 – 176.8	92.445 102.83	192.3	hot
$Q_{reboiler}$	7218.6	196.7 -197.8 197.8 – 199.8	29.585 27.55	174.27	cold
$Q_{reactor}$	-	425.0 - 425.5	-	69.1	cold
$Q_{condesation}$	-	208.8 - 30	-	115.2	hot

All cold streams and hot streams are identified and arranged to a hot and cold composite curve, which describes the maximum possible heat integration of the system, see Fig. 6.10. The overlapping of both curves shows that the total heat demand cannot be covered with internal heat recovery. The same applies with the cooling demand. The pinch point, ΔT_{min}, is defined by 20 K and is chosen from the heat integration recommendation [130]. The streams at the pinch have to be operated with a minimum temperature approach of 20 K in order to achieve the given heat recovery.

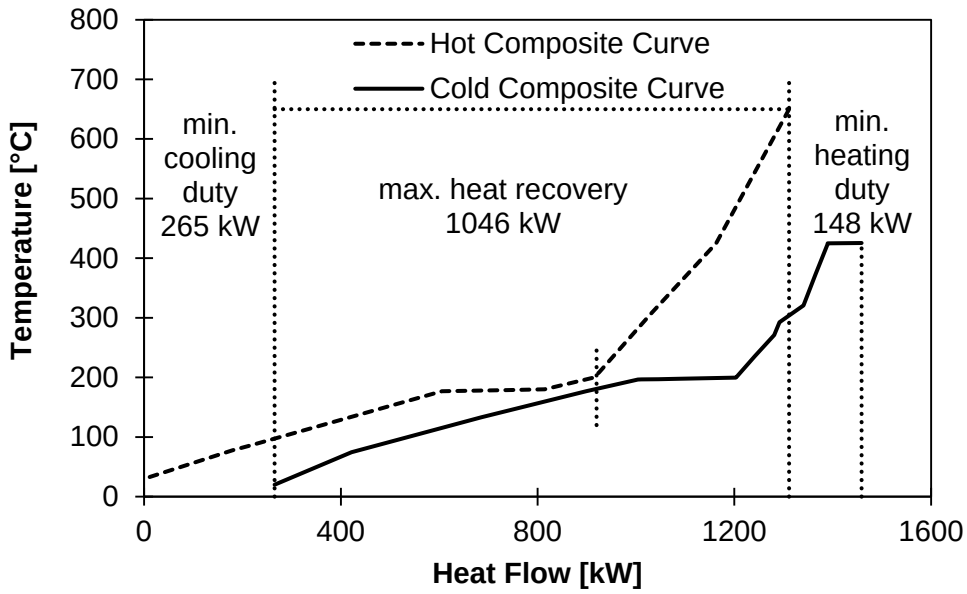

Fig. 6.10 - hot and cold composite curve of reference process

The pinch temperature for the hot composite curve is 216.6°C and 196.6°C for the cold composite curve. The hot composite curve to the right of the pinch consists of the flue gas stream and the product gas stream, while the cold composite curve consists of the air for the burner, the kerosene fraction, and the enthalpy for the dehydrogenation reactor, as well as the heat demand of the reboiler. To the left of the pinch, the hot composite curve consists of the flue gas, the still, the cooler of the rectification and the condenser of the product stream, while the cold composite curve consists of the kerosene feed stream, the air, and the condenser again. The results of the pinch analysis show the maximum possible heat recovery. However, it does not consider the technical feasibility of a heat exchanger network. The design of the heat exchanger grid for the process system follows the same objectives as for the reference concept. Further restrictions are introduced, since the rectification requires suitable operation conditions.

The reboiler of a rectification demands a small temperature gradient of the heat stream to avoid thermal cracking of the long chain hydrocarbons, leading to the deposit of carbon in fuel and changing the chemical composition of the still, which is reused for propulsion. Therefore a heat stream with a temperature difference of cold stream outlet and hot stream inlet of 20 K is needed to provide the heat demand to the reboiler. This is the only external heating duty needed in the process concept and can be carried out by a hot oil stream. External cooling is required to run the condensation of the dehydrogenated fraction. Further cooling is needed to cool down the hot still stream before it is reused in the kerosene tank for propulsion. The heat exchanger grid table for the process concept with rectification is presented in Fig. 6.11.

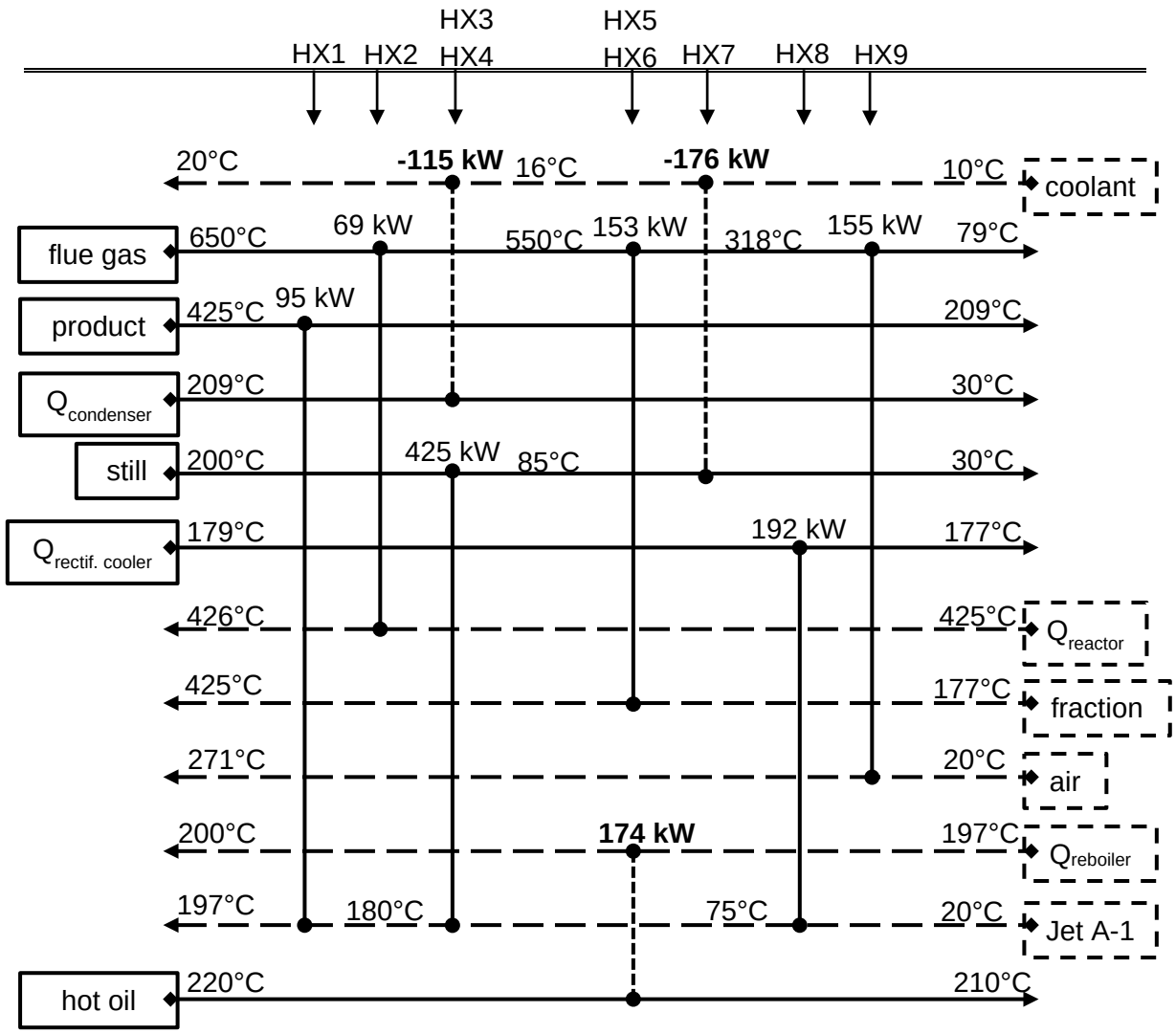

Fig. 6.11: grid table of heat exchanger network designed for process concept with rectification and 10 wt.-% Jet A-1 fraction

In the next step, this grid table is used to integrate the heat exchangers in the process flow sheet. The external utility stream for providing external heating is shown as a dotted line in the flow sheet as heat streams (HX6). The heat load of this external heating demand is then introduced as energy expenditure in the efficiency calculation of the system. The difference in total heat recovery of the grid table and the T/H-diagram derives from heat exchanger restrictions defined for the process. No internal stream would provide enough heat load with the temperature restriction of 20 K for the heat exchanger of the reboiler. Since more external heating than the minimum heating demand is required, more external cooling is required as well. Similar to the reference concept, the process concept consists of the main process part, which contains the rectification and the dehydrogenation reactor. The heat providing part contains the burner, where the input and output streams are colored red, see Fig. 6.12.

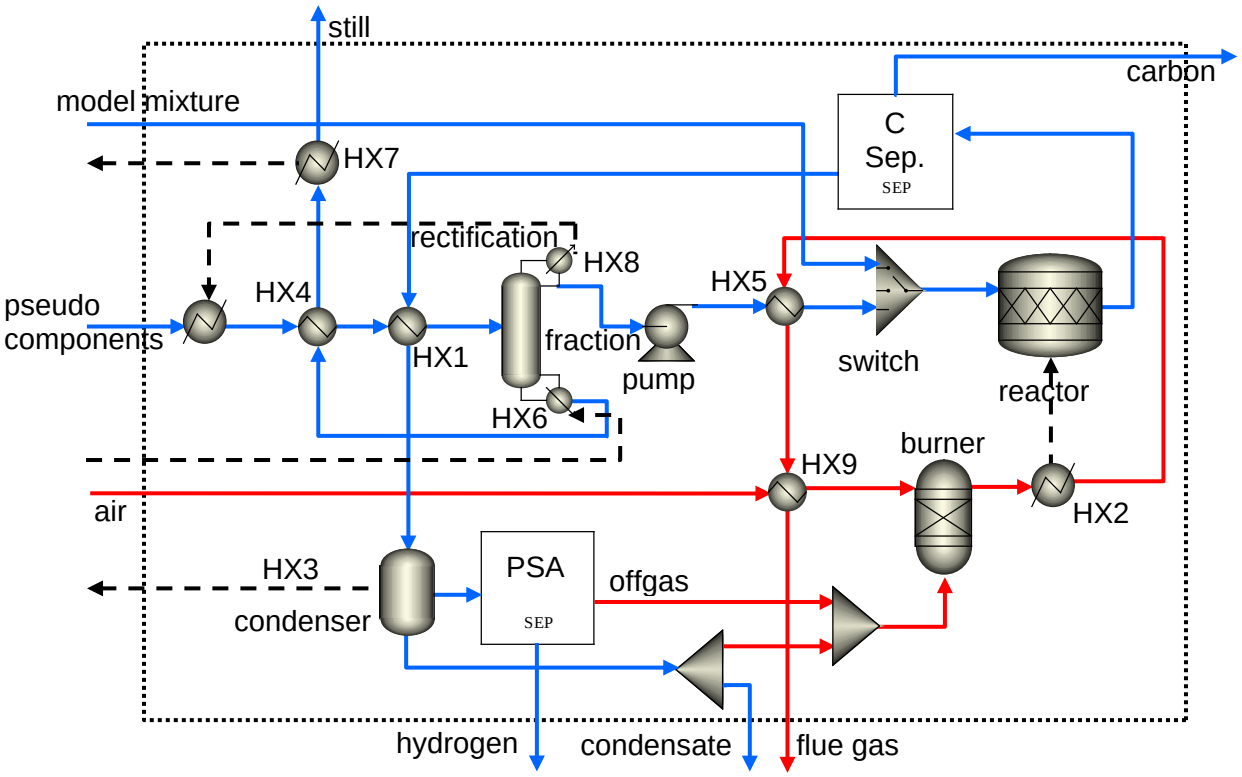

Fig. 6.12 - flow sheet with heat exchanger network of process concept with rectification and 10 wt.-% Jet A-1 fraction

In the dehydrogenation cycle, Jet A-1 enters the system as pseudo components, and is preheated by the heat stream recovered from the condensation of fraction on the top stage of the rectification (HX8). Then, the pseudo component stream is heated by the hot still stream from the bottom stage of the rectification (HX4). The still stream has to be cooled down a second time by external cooling (HX7). Before the kerosene enters the rectification, it is heated up by the hot product gas stream from the dehydrogenation reaction (HX1). An external heat stream is provided to the heat demand for the reboiler stage of the rectification (HX6). In the heat exchanger grid table, this heat demand is provided by a hot oil stream. The recovering of the hot streams of the rectification for preheating the kerosene feed streams leads to a significant advancement for the efficiency of the system. The reboiler heat duty per feed mass stream is reduced by 446 kJ/kg_{feed}.

After the condensed Jet A-1 fraction leaves the top stage of the rectification, the liquid stream is pressurized to 8 bar. The switch block copies the heat load and mass flow of the pseudo components fraction to the real component model mixture fraction, which then enters the dehydrogenation reactor. The product gas stream is treated the same way as described with the reference process. First, the solid carbon is separated from the product gas stream. Then, the product gas stream is cooled down and condenses at 8 bar and 30°C (HX3). The liquid product stream splits and is partly used as fuel for combustion, while the non-condensed gas stream is conditioned in the PSA. The composition of the liquid and gas products before and

after condensation are shown in table 6.8. The hydrogen atom to carbon atom ratio in the mixed input stream to burner is 2.8. The calculated air to fuel equivalence ratio λ, is 6.5 to achieve an adiabatic burner temperature of 650°C, leaving 18 vol.-% of oxygen in the fuel gas.

The composition of the product gas stream before and after gas cleaning is presented in table 6.7. After condensation, the gaseous product gas stream contains 16.6 wt.-% of long chain hydrocarbons, which is higher than with the reference process. This contributes to the composition of the 10 wt.-% fraction model mixtures, which contain lighter hydrocarbons than ULSK model fraction.

Table 6.8. - stream composition on input and output stream to condensation and PSA of process concept

streams	input stream in condenser	Outlet stream not condensed products	PSA offgas stream	Pure Hydrogen stream
	kg/h			
gaseous hydrocarbons	0.31	0.21	0.21	0
longer chain hydrocarbons	582.3	1.39	1.39	0
hydrogen	6.8	6.75	1.35	5.4

The burner proceeds with PSA offgas and the partial dehydrogenated Jet A-1 fraction. The flue stream from the burner is used to provide the heat demand of the dehydrogenation reactor (HX2), and then to evaporate and superheat the pseudo component fraction to reaction temperature (HX5). In the last step, the fuel gas preheats the air flow for the burner (HX9). Preheating of the hydrogen stream for the PEMFC is not carried out, since after heat integration, no hot stream is available at a suitable temperature. The heating of the stream has to be carried out by the reaction enthalpy of the fuel cell.

The same process flow sheet is used for efficiency calculation of a system with a 20 wt.-% fraction. Due to the heat recovery of the process, the system efficiency mostly depends on the hydrogen yield of the fraction in dehydrogenation reactor. The heat stream of the rectification, the still and the condensation of the fraction are used to preheat the feed stream. The external utility stream for the reboiler only depends on the mass flow needed for the dehydrogenation reactor to achieve 90 kW power. This means that in case of the same hydrogen yield of the 10 wt.-% and 20 wt.-% fraction, the reboiler duty between the two fractions only differs in the amount of enthalpy needed for the evaporation of the fraction. Since this boiling point distribution range between 10 wt.-% and 20 wt.-% is similar (see chapter 4.2), the difference in utility heat loads has a very small influence on the overall efficiency. The internal heat

demand provided by the burner is adjusted to the heat demand of the dehydrogenation reactor. The external utility cooling is treated with the efficiency calculation as freely available.

As an alternative to this heat exchanger grid, it would be possible to use the product gas instead of the flue gas for the preheating of the air stream with 20 wt.-% fraction concept. The heat load of the product stream is higher, since the mass stream is bigger. This is caused due to the need of a higher fraction mass stream because of the lower hydrogen yield of the 20 wt.-% fraction. With higher temperature of the air stream into the burner, less fuel would be used for combustion and the efficiency is increased by 1.7 %. This alternative heat exchanger network would only function for an increased hydrogen yield of up to 120 $nl_{H2}/kg_{fraction}$. The fraction mass stream, and therefore the product stream, is reduced by 20 % for 90 kW, and the heat load of the product stream would be too small to heat up the air mass stream, which also rises due to the slightly higher heat demand of the reactor. The heat exchanger grid table of the base case 20 wt.-% fraction process concept and the alternative process flow sheet and grid table are available in Appendix 8.4.

6.5 System Efficiency

The system efficiency or electric efficiency for the reference concept and process concept with rectification is presented in this chapter. Both concepts are evaluated with the heat integration shown in the previous chapter. The system efficiency is defined as the ratio of generated electric energy minus internal electric consumption to consumed thermal energy.

The following assumptions are made for calculating the efficiency of both concepts. First, it is assumed that with a facility performance of 90 kW, the isolation allows that no heat losses are taken into consideration. The second assumption considers the cooling streams for the systems to be available freely, since coolant is available on board for turbine cooling systems and air conditioning [131]. This means that external heat sinks are not part of the consumed thermal energy. Further, the electric power for the air fan providing air for combustion in the internal burner is neglected. The pump performance to pressurize the liquid feed in both systems to 8 bar is introduced as electric energy consumption with a pump efficiency of 70 %.

6.5.1 System Efficiency of Reference Concept

The reference concept does not need any external heat streams. The thermal energy demand for the reaction enthalpy of dehydrogenation and the preheating of the ULSK stream and air stream to the burner is provided by the adiabatic combustion of dehydrogenated ULSK and PSA offgas. The combustion enthalpy from these internal fuel streams are the energy demand of the system, and therefore, are treated as energy expenditure, which reduces the efficiency of the system. The loss of heat performance of the fuel is caused by the separation of the mass stream of the condensate and the PSA offgas. This mass stream is than not part of the fuel

and can be reused for propulsion. Further, the lower heating value (LHV) of the ULSK is decreased after partial catalytic dehydrogenation, since evolved hydrogen, gaseous cracking products and carbon are not part of the condensate. The loss of enthalpy content of the dehydrogenated ULSLK has to be considered when it is reused for propulsion. Next, the loss of LHV due to the dehydrogenation has to be taken into consideration, since the actual LHV of kerosene of 43.4 MJ/kg is the LHV of model mixture of 43.2 MJ/kg, which is used in the reactor. The efficiency of the system is calculated for both, real ULSK and also for Jet A-1 fractions. The difference of LHV of the model mixture compared to ULSK would lead to an over estimation of the efficiency. The difference of LHV has to be subtracted from the heat losses in the efficiency calculation.

The PSA offgas consists of gaseous hydrocarbons and hydrogen. The PSA hydrogen separation is defined by 80 %, this leaves 20 % of the hydrogen in the PSA offgas to the burner. The LHV of the PSA offgas can be extracted from the flow sheet or calculated by Eq. 6.34

$$LHV_{PSAoffgas} = \frac{0.2 \cdot (\dot{m}_{H} - m_{H_2}^{cond.}) \cdot LHV_{H_2} + (\dot{m}_{C_nH_mgas} - m_{C_nH_mgas}^{cond.}) \cdot LHV_{C_nH_mgas}}{\dot{m}_{cond.}} \tag{6.34}$$

The gaseous products which are dissolved in the condensated dehydrogenated ULSK are not part of the PSA offgas, and have to be subtracted. The mass stream composition of the PSA offgas is presented in the previous chapter.

To calculate the loss of heating power of the ULSK, the LHV of the condensated products is of interest, since it can be reused in propulsion, see Eq. 6.34.

$$LHV_{cond.} = \frac{\dot{m}_{ULSK} \cdot LHV_{ULSK} - \left(\dot{m}_{H_2} - m_{H_2}^{cond.}\right) \cdot LHV_{H_2} - \left(\dot{m}_{C_nH_mgas} - \dot{m}_{C_nH_mgas}^{cond.}\right) \cdot LHV_{C_nH_mgas} - \dot{m}_{C} LHV_{C}}{\dot{m}_{cond.}}$$

The gaseous hydrocarbon products which are removed from the fuel are part of PSA offgas, therefore, the loss of enthalpy from gaseous hydrocarbons is already considered with the condensate. In the simulation flow sheet, the condensate consists of model components and model products of the dehydrogenation reactions. The efficiency calculation considers the LHV of condensate of dehydrogenated kerosene. For the loss of heat performance of the ULSK, it has to be taken into consideration that not the total amount of condensate is returned to the tank, but some is used for the burner, see Eq. 6.36 and 6.37

$$\dot{Q}_{fuel}^{loss} = \dot{m}_{ULSK} \cdot LHV_{ULSK} - (\dot{m}_{cond.} - \dot{m}_{cond.}^{burner}) \cdot LHV_{cond.} - (\Delta H_{model}^{ULSK}) \tag{6.36}$$

$$\Delta H_{model}^{ULSK} = \dot{m}_{ULSK} \cdot (LHV_{Pseud.} - LHV_{model}) \tag{6.37}$$

Further, carbon mass stream from carbon formation is leaving the system unused and has to be considered as a loss. The difference in enthalpy content of condensate and the ULSK feed stream is 3.5 %, which is caused by the decline of mass flow and LHV. The decline of LHV of the dehydrogenated ULSK in comparison to the feed stream is 1%. The system efficiency is then calculated by the net electric output of the hydrogen provided to the PEMFC, which is affected by the efficiency of the PSA of 80 % and the PEMFC efficiency of 50 % as well as the efficiency of the pump to pressurize the fuel, which is defined by 70 %. The losses are added up by the electric performance of the compressor, and the loss of heating power of the kerosene, see Eq. 6.38.

$$\eta_{\text{system}}^{\text{reference}} = \frac{\dot{m}_{H_2}^{\text{cond.}} \cdot LHV_{H_2} \cdot \eta_{PSA} \cdot \eta_{PEMFC} - P_{el.P} \cdot 1.3}{\dot{Q}_{\text{fuel}}^{\text{loss}}} \tag{6.38}$$

The thermal efficiency of the reference process does not consider the efficiency of the PEMFC and therefore represents the output pure hydrogen from process, see Eq. 6.39.

$$\eta_{\text{thermal}}^{\text{reference}} = \frac{\dot{m}_{H_2}^{\text{cond.}} \cdot LHV_{H_2} \cdot \eta_{PSA} - P_{el.P} \cdot 1.3}{\dot{Q}_{\text{fuel}}^{\text{loss}}} \tag{6.39}$$

Table 6.9, shows the system efficiency and thermal efficiency of the base case performance defined with the experimental input specification for a 90 kW electric system. The input specifications are the conversion rates and conversion factors of the dehydrogenation reactions leading to a hydrogen gas yield and product compositions, which fits the experimental results of dehydrogenation the ULSK model mixture.

Table 6.9. – efficiency, fuel and system performance of the base case reference concept

reference concept	$\eta_{\text{system}}^{\text{reference}}$	$\eta_{\text{thermal}}^{\text{reference}}$	$P_{el.P}$	$\dot{Q}_{\text{fuel}}^{\text{loss}}$	$LHV_{PSAOffgas}$	$LHV_{cond.}$	Y_{H_2}
	[%]		kW		MJ/kg		nl_{H2}/kg_{feed}
	20.7	41.8	0.7	430.8	86.5	42.9	75.2

The efficiency of the system is mainly dependent on the hydrogen output of the dehydrogenation reactor. The input specifications of the experimental data with model mixtures in the simulation indicates the possible efficiency of the reference concept if investigated hydrogen yield can be achieved under stable conditions with desulfurized or regular kerosene. To predict theoretical maximum system efficiency, the conversion rate of the model components can be increased to achieve theoretically higher hydrogen yields.

6.5.2 System Efficiency of Process Concept with Rectification

The LHV of the condensate is calculated the same as with the reference concept, except the feed mass flow is exchanged with the mass flow of the Jet A-1 fraction. The LHV of the pseudo

component fraction and the 10 wt.-% model fraction differs from 43.5 to 43.2 MJ/kg. The loss of the heating performance of the Jet A-1 differs due to the reuse of the still, see. Eq. 6.41

$$\dot{m}_{JetA-1} = \dot{m}_{fraction} + \dot{m}_{still} \tag{6.40}$$

$$\dot{Q}_{fuel}^{loss} = \dot{m}_{fraction} \cdot LHV_{,fraction} - (\dot{m}_{cond.} - \dot{m}_{cond.}^{burner}) \cdot LHV_{cond.} - (\Delta H_{model}^{fraction}) + \dot{m}_{still} \cdot LHV_{still} \tag{6.41}$$

$$\Delta H_{model}^{fraction} = \dot{m}_{fraction} \cdot (LHV_{Pseud.} - LHV_{model}) \tag{6.42}$$

The PSA offgas used for the burner is calculated the same as with the reference process. The difference in product composition of the two Jet A-1 fractions leads to a deviation in LHV of the PSA offgas and the condensate. Two different fraction model mixtures 10 wt.-% and 20 wt.-% Jet A-1 fraction are integrated with the process concept. The LHV of the fraction, the condensate, the PSA offgas and the still of the 10 wt.-% and 20 wt.-% model fractions are presented in table 6.10

Table – 6.10 lower heating values of fuel streams within the process concept with 10 and 20 wt.-% Jet A-1 fraction

LHV of fuel streams	pseudo c. fraction	model fraction	pseudo c. still	PSA offgas	condensate
	MJ/kg				
10 wt.-%	43.5	43.2	43.4	78.3	42.7
20 wt.-%	43.6	43.2	43.3	86.4	42.9

The composition of the PSA offgas of the 10 wt.-% fraction has a higher content of gaseous hydrocarbons which decreases the LHV. The loss of heating performance of the kerosene depends on the fraction distilled and on the hydrogen yield. For the system efficiency calculation, the heat demand of the reboiler of the rectification has to be added up with the energy losses of Jet A-1, see Eq. 6.43

$$\eta_{system}^{process} = \frac{\dot{m}_{H_2}^{cond.} \cdot LHV_{H_2} \cdot \eta_{PSA} \cdot \eta_{PEMFC} - P_{el.P} \cdot 1.3}{\dot{Q}_{fuel}^{loss} + \dot{Q}_{reboiler}} \tag{6.43}$$

The thermal efficiency of the process concept is calculated equivalent to the reference process which is without the efficiency loses from the fuel cell, see Eq. (6.44).

$$\eta_{thermal}^{process} = \frac{\dot{m}_{H_2}^{cond.} \cdot LHV_{H_2} \cdot \eta_{PSA} - P_{el.P} \cdot 1.3}{\dot{Q}_{fuel}^{loss} + \dot{Q}_{reboiler}} \tag{6.44}$$

Since more external heat demand has to be integrated with the process concept than with the reference concept, the efficiency of the system will be smaller unless the hydrogen yield would be much higher with Jet A-1 fraction model mixture than with the ULSK model mixture. The efficiency of the concept mainly depends on the hydrogen yield, see Table 6.11.

Table 6.11 - efficiency, fuel and system performance of the base case process concept with rectification

process concept	$\eta_{system}^{process}$	$\eta_{thermal}^{process}$	$P_{el,P}$	$\dot{Q}_{PSAoffgas}$	$\dot{Q}_{fuel}^{loss}$	$\dot{Q}_{reboiler}$	Y_{H_2}
	[%]		[kW]				$[nl_{H2}/kg_{feed}]$
10 wt.-%	16.1	32.3	0.6	64.2	381.1	174.3	128.2
20 wt.-%	11.7	23.6	0.96	58.1	443.2	315.2	80.3

The mass stream of the fraction needed for the 90 kW systems depends on the hydrogen yield. With the hydrogen yield of the 20 wt.-% model mixture being lower than with the 10 wt.-%, the reboiler heat duty has to rise due to the higher amount of feed mass stream needed for dehydrogenation. Furthermore, the amount of fuel for combustion is increasing with the higher feed stream, which needs to be evaporated and preheated to reaction temperature. This also causes a higher air mass stream for combustion, which has to be heated. After heating the Jet A-1 feed stream, the flue stream is used for preheating the combustion air. With increasing Jet A-1 feed stream, the enthalpy of the flue stream for the heat transfer to the air is declining. The air mass stream is than heated up, but with less temperature increase, causing more fuel consumption in the burner. The burner heating performance is adjusted to the reactor heat demand and the feed stream. The air stream temperature can only be preheated after heat exchanger restrictions defined in the previous chapter.

6.5.3 Variation of the Hydrogen Yield

The conditions in the dehydrogenation reactor are defined by the model components, the model reaction, the conversion rates and the conversion factors of the reaction. These are defined to suit the experimental conditions and to calculate a fitted hydrogen yield and product composition, which leads to a calculated heat of reaction for the reactor. The system efficiency mainly depends on the hydrogen yield calculated from the conversion rate of the model components. To achieve a higher efficiency of the system, a higher hydrogen yield would be necessary. The experimental results show a specific hydrogen yield which depends on the model mixture composition, the reaction conditions and the catalyst. In the flow sheet simulation, the conversion rates of model components can be raised to achieve an increased hydrogen yield, thereby increasing the efficiency of the system. This sensitivity analysis has to be run under defined conditions in order to calculate a theoretical maximum hydrogen yield. Cycloalkane components lead to the most hydrogen yield and do not cause side products like

carbon and gaseous hydrocarbons. The conversion of other components comes with negative side products. Therefore, only the conversion rate of cycloalkanes is increased up to 100 % to calculate a theoretical maximum efficiency of the system. Fig. 6.13 shows the system efficiency dependent on the hydrogen yield, which is gradually increased from the experimental database case.

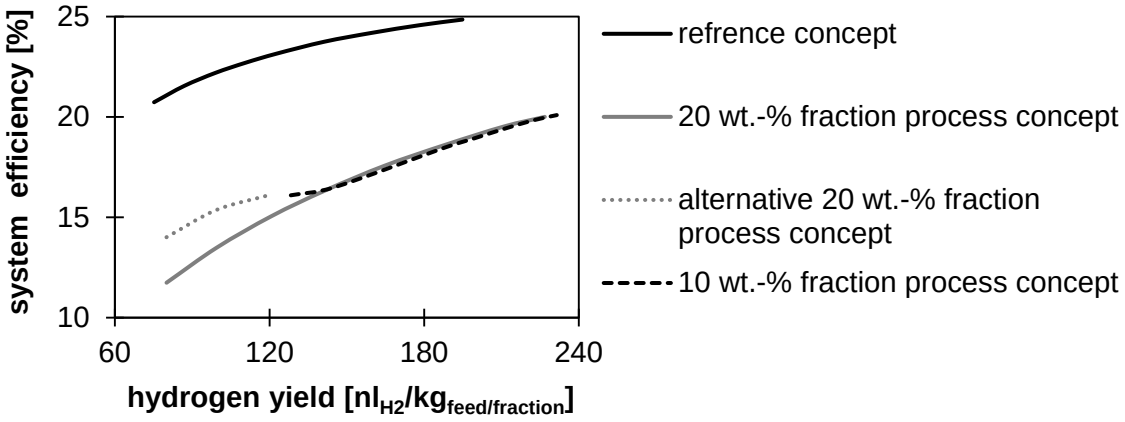

Fig.6.13 - system efficiency dependent on the variation of the hydrogen yield by increasing the conversion rate of cycloalkanes

For the reference concept, the total conversion of the cycloalkanes would lead to an system efficiency of 24.9 %. The maximum thermal efficiency of the reference concept would be 49.7 %. The process concept shows that the maximum achieved efficiency with 20 wt.-% fraction is 20 % while the maximum thermal efficiency would be 40.1 %. The maximum efficiency of the process concept with the 10 wt.-% fraction only differs by 0.1 %. By increasing the conversion of cycloalkanes, the hydrogen yield of both fractions can be set to the same amount. The difference in cycloalkane content makes the difference in the theoretical maximum hydrogen yield. For all concepts, it has to be taken into consideration that an increased conversion of cycloalkanes leads to more aromatic hydrocarbons in the condensate, which will exceed aviation restrictions.

In case the same amount of hydrogen is produced with both mass fractions, the mass flow of the fraction has to be the same to achieve the system performance of 90 kW. The reboiler heat demand only differs in the amount of enthalpy that is needed to distillate the fraction with higher boiling range, since the distillated mass stream stays the same. The feed stream into the rectification has to be adjusted to the required fraction mass stream. The equivalent amount of still is then leaving the rectification system, and therefore an equivalent enthalpy stream of the still can be used for preheating the feed stream. The heat stream, which is recovered from the condensation enthalpy of the fraction only differs in the enthalpy needed for condensation of a higher boiling range. The heat recovery of the dehydrogenation product stream is, in case of the same hydrogen yield, similar with both fractions, since the mass stream and temperature

are the same. The composition is also very similar, leading to similar heat capacity. The higher efficiency of the alternative heat exchanger grid for the 20 wt.-% fraction is caused by the higher air preheating. The external heat demand for the reboiler stays the same.

6.6 Conclusion of Process Simulation

The objectives of the process simulation of the process concept with rectification and the reference process is to identify possible heat integration of the system, and on the basis of the energy targets, to calculate the efficiency of both systems. The results can be used for comparing a fuel cell APU system provided with hydrogen from PCD of Jet fuel with a regular gas turbine APU used to generate electric energy on board an airplane while on land operation. The heat and material integration is accomplished with pinch analyses for both concepts. For the reference concept using ULSK as input stream, the energy demand can be covered by an integrated burner and the recovering of enthalpy streams within the system. The process concept with rectification demands an external heat source to provide the enthalpy demand to the reboiler of the rectification. Both systems require a significant amount of energy for evaporation of the fuel streams, since the hydrogen output from PCD has to generate 90 kW of electric energy from a PEMFC with a thermal efficiency of η_{PEMFC} = 50 %. This leads to a massive circulation of fuel within the system. Fig. 6.14 presents the energy balance of the fuel streams of both processes without the fuel cell concerning the system efficiency but considering the thermal efficiency of the PSA of η_{PSA} = 80 %. Comparing the two concepts, the circulation of the fuel stream is almost 6 times higher for the process concept with rectification than for the reference concept. Considering a regular Airbus A320 with a maximum tank capacity of 19220 l or 24028 kg jet fuel [132], to run the reference concept for one hour, 4.2 % of the tank filling is used for the PEMFC APU system, of which 99.2 % is recovered and can be reused for propulsion. For the process concept with rectification with 10 wt-% fractionation, 24.5 % of the tank filling would have to be evaporated to run a PEMFC APU system for one hour, of which 99.8 % can be reused in the tank

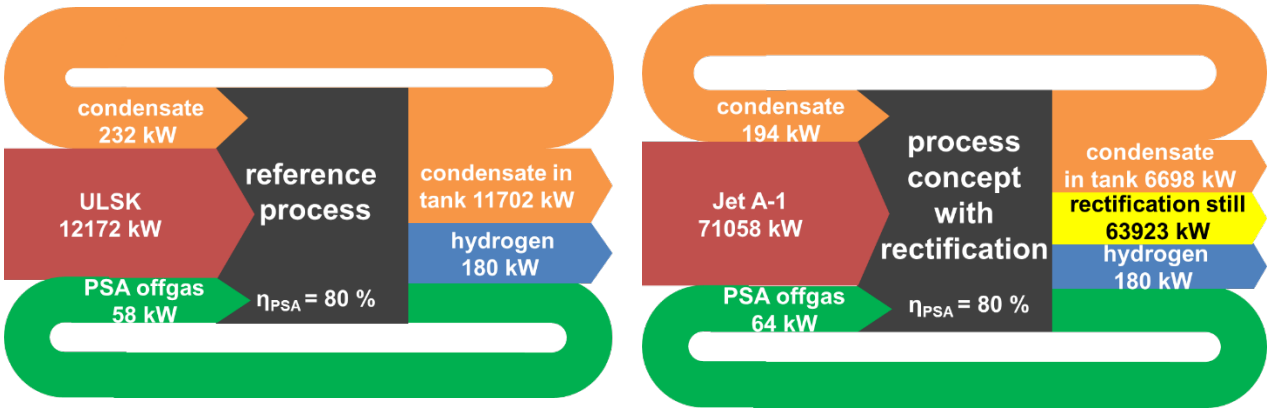

Fig. 6.14 – energy balance of fuel streams for the reference process (left) and the process concept with rectification with 10 wt-% fractionation (right)

Within the reference concept, 2 % of the fuel mass stream is recycled for combustions to provide heat for the system. The hydrogen mass stream leaving after the PSA is 0.5 % of the input mass stream of ULSK. For the process concept, only 0.3 % of input mass stream is reused in combustion, while the hydrogen product stream is 0.09 % of the total feed mass stream of Jet A-1.

Considering the amount of fuel that has to be conditioned and recycled in the system, the process concept with rectification requires, in comparison to the reference concept, more utilization of periphery systems, in particular an external heat source for the rectification. Further, the rectification process itself is on one hand an effective desulfurization process, but requires adjustment in sizes, process performance and execution to fit transportation and aviation requirements.

The reference system running with desulfurized kerosene requires less expenditure for implementation into an aviation environment. The desulfurization of jet fuel is a widely researched field, due to environmental issues of releasing SO_2 from combustion. The provision of desulfurized jet fuel can become more frequent with more strict environmental restrictions [1]. Due its higher potential for system efficiency and it being the less demanding concept when it comes to process elements, heat and material integration, the reference process is the most promising process concept for the PCD of jet fuel presented in this work.

7 Summary and Conclusion

The partial catalytic dehydrogenation (PCD) of kerosene has the potential to provide a hydrogen rich product gas of over 95 vol.-% of hydrogen purity. This product gas contains only hydrocarbons as impurities, which can be removed by a (pressure swing adsorption) PSA for high purity hydrogen suitable for a polymer membrane fuel cell (PEMFC). The process is therefore suitable for fuel cell auxiliary power unit (FC APU) systems despite the fact that catalytic dehydrogenation requires desulfurized kerosene or a desulfurization system before the reactor to reduce or even avoid catalyst deactivation by sulfur poisoning. The objective of this work is to develop and evaluate two process concepts which can provide hydrogen to a PEMFC, one working with regular kerosene Jet A-1 including a desulfurization system by thermal fractionation and a reference concept provided with ultra- low- sulfur kerosene (ULSK). In this context, the PCD of kerosene is investigated experimentally to define suitable reaction conditions and learn about the reaction products and boundary conditions leading to reaction stability and high hydrogen yield and purity of the product gas. For this scope, methods are developed which allow the evaluation of the complex dehydrogenation reactions and the introduction of experimental results into a process simulation to evaluate the efficiency of both process concepts. Detailed chemical composition of Jet A-1 and ULSK are investigated, and the complex hydrocarbon mixture of the evaluated samples is distributed among hydrocarbon groups contained in kerosene. This allows the definition of model components and model mixtures representing the chemical composition of kerosene.

For the desulfurization process, the concept of rectification is chosen. The sulfur containing components are removed due to their high boiling range within the kerosene hydrocarbon composition. With the rectification process, kerosene fractions between 5 wt.-% and 30 wt.-% of the original Jet A1 are produced, whose sulfur content and physical and chemical properties are dependent on the distillated mass fraction. Those fractions are analyzed in detail and experimentally evaluated to identify fractions for the further investigation of the reference concept and process simulation.

The defined model components are used to design model mixtures for ULSK and the chosen Jet A-1 fractions. The simplification of the complex kerosene enables the examination of PCD dependent on the chemical structure of the chosen components and the influence of hydrocarbon groups upon one another regarding hydrogen yield, product composition and stability of the reaction. Further, the simplified model mixtures can be introduced in the process simulation, and the heat demand for the reactor is calculated from the chosen reaction products of the experimental results.

First single component tests are performed at different reaction conditions of temperature, pressure and contact time on the catalyst. The results are used to prepare the selection of

reaction conditions. By experimental evaluation of the model mixtures, the reactions conditions are defined at 425°C, 8 bar system pressure and 4 sec of contact time. By adding the sulfur component dibenzothiophen to the model mixtures, the influence of the actual sulfur content in the real ULSK and Jet A-1 fraction is tested on the catalyst and compared to the dehydrogenation of the real fuel and fraction.

The hydrocarbon group of cycloalkanes shows high potential for hydrogen output, but their conversion can be decreased due to catalyst deactivation from carbon deposit on the catalyst surface. In particular, n-Alkanes show a tendency towards carbon formation. An increased hydrogen partial pressure reduces carbon formation and increases catalyst life time. Though, increased gaseous cracking products can appear from n-alkanes while cracking from the tested iso-alkanes is suppressed with increased hydrogen partial pressure. The hydrocarbon group of aromatic hydrocarbons shows little conversion. Though the components contribute to carbon formation, which also can be reduced by increased hydrogen pressure of the system. The addition of sulfur causes strong deactivation of the catalyst, but the hydrogen yield is mostly dependent on the hydrocarbon composition of the tested mixture. With high content of cycloalkanes and hydrocarbons with shorter carbon atom chains of up to ten carbon atoms, relatively stable reaction progress is achieved despite the sulfur. With the real ULSK and Jet A-1 fractions, the content of long chain hydrocarbons, cannot be completely removed with rectification. The formation of carbon increases strongly, which leads to quick catalyst deactivation in addition to the sulfur poisoning.

For the modelling of the PDC reactor in the process simulation, simplified reactions are chosen from the product composition of the dehydrogenation tests of the model components and the conversion rates are taken from model mixtures. For the process concept with desulfurization by thermal fractionation, a low pressure rectification system is combined with an 8 bar dehydrogenation reactor by pressurizing the liquid Jet A-1 fraction. From the experimental evaluation, the 10 wt.-% and 20 wt.-% Jet A-1 fractions were chosen. For the reference process, the ULSK is pressurized and then evaporated before entering the reactor. In both cases, the product gas conditioning is accomplished by PSA, which also depends on increased pressure for high efficiency purification of hydrogen. To achieve a as high as possible system efficiency, the internal heat and material streams are integrated. In this way, the heat for evaporation of the feed stream is provided. The heat demand to the reactor is provided by combustion of the dehydrogenated condensate and the off gas from the PSA.

The system efficiency of both concepts are calculated to provide 90 kW of electrical power to an operating aircraft. For the process concept with rectification and 10 wt.-% Jet A-1, an efficiency of 16.5 % including PEMFC is achieved, resulting in an experimental hydrogen yield of 128.2 Nl_{H2}/kg_{feed}. The reference concept shows an system efficiency of 20.7 % with a hydrogen yield of 75.2 Nl_{H2}/kg_{feed}. For the evaluation of the concepts, the amount of fuel that

has to be conditioned and recycled in the system is also important. The desulfurization of kerosene by rectification reduces the sulfur in the fraction efficiently. However, the feed demand when operating the fractionation at low mass stream output is not suitable for a APU concept, which needs to be compact. For the consideration of a APU concept, the PCD should be provided with a desulfurized fuel. Therefore, the reference concept shows more potential including higher efficiency.

As a conclusion to the experimental investigations, the dehydrogenation of hydrocarbons in fuel mixtures provides a high quality product gas which can be used for fuel cell application. The hydrocarbon composition of kerosene is not ideal to the process, however, since formation of carbon cannot be avoided under suitable conditions for an APU system. The product output and catalyst life is highly dependent on the feed composition. Therefore, the provision of a fuel with a defined composition which suits the dehydrogenation process as well as propulsion on an aircraft is needed to develop a robust system. The experimental results in this work provides detailed information to design fuels for dehydrogenation. As the development of renewable Fischer- Tropsch fuels are sulfur free, they can be refined for the defined application.

8 Appendix

8.1 Hydrocarbon Group Composition of Kerosene

In the following the detailed hydrocarbon groups composition over the carbon atom number Cn of Jet A-1 and ULSK are presented. The detailed composition is used in the graphical depiction in chapter Fig. 3.3.

Table 8.1 - detailed composition of hydrocarbon groups in Jet A-1

Jet A-1	n-alkane	iso-alkane	cyclo-alkane	dicyclo-alkane	aromatic hyro-carbons	diaromatic hydro-carbons	summarized content
Cn	C_nH_{2n+2}	C_nH_{2n+2}	C_nH_{2n}	C_nH_{2n-2}	C_nH_{2n-6}	C_nH_{2n-10}	
6	0.00	0.00	0.00	0.00	0.01	0.00	0.01
7	0.04	0.00	0.14	0.00	0.08	0.00	0.26
8	1.03	0.36	1.30	0.00	2.09	0.00	4.78
9	3.32	0.69	4.31	0.00	6.41	0.00	14.73
10	6.80	6.39	5.04	0.85	4.51	0.53	24.12
11	7.86	2.79	1.69	0.98	4.48	0.58	18.37
12	5.21	2.48	1.17	0.00	2.17	1.06	12.09
13	3.88	3.09	0.28	0.00	0.66	0.00	7.91
14	2.17	1.81	0.16	0.00	0.00	0.00	4.14
15	0.75	0.56	0.00	0.00	0.00	0.00	1.31
16	0.27	0.00	0.00	0.00	0.00	0.00	0.27
17	0.05	0.00	0.00	0.00	0.00	0.00	0.05
18	0.02	0.00	0.00	0.00	0.00	0.00	0.02
summary	31.39	18.15	14.10	1.83	20.40	2.17	88.04
corrected	31.39	24.52	19.05	2.47	20.40	2.17	100.00

Table 8.2 - detailed composition of hydrocarbon groups in ULSK

ULSK	n-alkane	iso-alkane	cyclo-alkane	dicyclo-alkane	aromatic hyro-carbons	diaromatic hydro-carbons	summarized content
Cn	C_nH_{2n+2}	C_nH_{2n+2}	C_nH_{2n}	C_nH_{2n-2}	C_nH_{2n-6}	C_nH_{2n-10}	
6	0.00	0.00	0.00	0.00	0.01	0.00	0.01
7	0.03	0.00	0.15	0.00	0.21	0.00	0.39
8	1.08	0.33	1.48	0.00	4.19	0.00	7.08
9	6.27	1.44	7.75	0.00	10.34	0.00	25.79
10	8.94	13.00	7.82	0.88	3.98	0.15	34.78
11	5.92	3.71	1.49	0.57	2.24	0.11	14.04
12	2.83	1.26	0.42	0.00	0.42	0.23	5.16
13	1.38	0.94	0.05	0.00	0.20	0.00	2.58
14	0.69	0.38	0.02	0.00	0.00	0.00	1.09
15	0.30	0.09	0.00	0.00	0.00	0.00	0.38
16	0.13	0.00	0.00	0.00	0.00	0.00	0.13
17	0.05	0.00	0.00	0.00	0.00	0.00	0.05
18	0.02	0.00	0.00	0.00	0.00	0.00	0.02
summary	27.62	21.15	19.17	1.45	21.60	0.50	91.48
corrected	27.62	25.46	23.07	1.75	21.60	0.50	100.00

8.2 Experimental Test Matrix

The experimental test matrix presented in table 8.3, follows the methodology described in chapter 4.5.3.

Table 8.3 –test matrix of dehydrogenation experiments of model components, model mixtures, Jet A-1 fractions and ULSK

Feed	mass stream	reaction temperature TC1	system pressure	contact time	catalyst bed length	evaporation temperature
[-]	kg/h	[°C]	[bar]	[sec]	[cm]	[°C]
decane	10	350	1	2	3.00	200
		375			3.12	
		400			3.24	
		425			3.36	
		450			3.48	
		500			3.72	
MCH	10	375	1	2	4.52	120
		400			4.75	
		425			4.87	
		450			5.04	
decane	20	400	3	2	2.16	250
			5		2.6	275
	40	425	8		1.62	300
					1.68	
	10	400	1	4	6.47	200
	20		3		4.32	250
			5		5.18	275
	40	425	8		3.24	300
					3.67	
MCH	10	400	3	2	1.56	165
	20		5		1.88	190
	40	425	8		2.38	220
					2.43	
	10	400	1	4	9.38	120
	10		3		3.13	165
	20		5		3.75	190
	40	425	8		4.75	220
					4.87	

Feed	mass stream	reaction temperature TC1	system pressure	contact time	catalyst bed length	evaporation temperature
[-]	kg/h	[°C]	[bar]	[sec]	[cm]	[°C]
decalin	10	400	1	2	3.33	205
	40	425	8	4	3.46	320
nonane	10	400	1	2	3.59	160
	40	425	8	4	3.72	260
dodecane	10	400	1	2	2.70	230
	40	425	8	4	2.80	330
isooctane	10	400	1	2	4.03	120
	40	425	8	4	4.18	220
p-xylene	10	400	1	2	3.33	170
	40	425	8	4	3.45	270
n-butylbenznene	10	400	1	2	3.43	190
	40	425	8	4	3.56	330
p-xylene/MCH	10	400	1	2	4.53	130
isooctne/MCH					4.34	110
decane/MCH					3.89	160
4 component model mixture	10	400	1	2	4.02	140
	40	425	8	4	4.17	240
ULSK model mixture	10	400	1	2	3.43	220
	40	425	8	4	3.56	320
with 3 ppmw sulfur	40	425	8	4	3.56	320
ULSK	10	400	1	2	3.31	240
	40	425	8	4	3.43	320
5 wt.-% Jet A-1 fraction	40	425	8	4	4.08	320
10 wt.-% Jet A-1 fraction					3.92	
15 wt.-% Jet A-1 fraction					3.82	
20 wt.-% Jet A-1 fraction					3.72	
25 wt.-% Jet A-1 fraction					3.69	
30 wt.-% Jet A-1 fraction					3.66	
10 wt.-% Jet A-1 fraction	40	425	8	4	3.86	320
with 8 ppmw sulfur						
20 wt.-% Jet A-1 fraction					3.72	
with 15 ppmw sulfur						

8.3 Identified Component Composition

The following table presents all identified components analyzed be GCMS and GCFID from the condensates of the single compnents dehydrogenation tests and the composition of ULSK and Jet A-1.

8.4 – identified components with GCMS and GCFID analyzing method of product components from single components tests and the detected content in ULSK and Jet A-1

No.	name	formula	hydrocarbon group	detected product components								components	
				MCH	decalin	nonane	decane	dodecane	iso-octane	n-butyl-benzene	p-xylene	ULSK	Jet A-1
1	Hexane	C6H14	n-alkanes			x	x	x				x	x
2	Heptane	C7H16	n-alkanes			x	x	x				x	x
3	Octane	C8H18	n-alkanes			x	x	x				x	x
4	Nonane	C9H20	n-alkanes			x	x	x				x	x
5	Decane	C10H22	n-alkanes				x	x				x	x
6	Undecane	C11H24	n-alkanes				x	x				x	x
7	Dodecane	C12H26	n-alkanes				x	x				x	x
8	Tridecane	C13H28	n-alkanes									x	x
9	Tetradecane	C14H30	n-alkanes									x	x
10	Pentadecane	C15H32	n-alkanes									x	x
11	Hexadecane	C16H34	n-alkanes									x	x
12	Heptadecane	C17H36	n-alkanes									x	x
13	Octadecane	C18H38	n-alkanes									x	x
14	Nonadecane	C19H40	n-alkanes									x	x
15	Eicosan	C20H42	n-alkanes									x	x
16	Henikosan	C21H44	n-alkanes										x
17	Dokosan	C22H46	n-alkanes										x

No.	name	formula	hydrocarbon group	detected product components								components	
				MCH	decalin	nonane	decane	dodecane	iso-octane	n-butyl-benzene	p-xylene	ULSK	Jet A-1
18	1-Heptane	C7H14	n-alkenes					x					
19	1-Octene	C8H16	n-alkenes				x						
20	Nonene-1	C9H18	n-alkenes			x							
21	Nonene-3 cis	C9H18	n-alkenes			x							
22	Nonene-3 trans	C9H18	n-alkenes			x	x						
23	Nonene-2	C9H18	n-alkenes			x	x						
24	Nonene-1	C9H18	n-alkenes			x							
25	1-Decene	C10H20	n-alkenes				x	x					
26	5-Decene	C10H20	n-alkenes				x						
27	3-Decene	C10H20	n-alkenes				x						
28	4-Decene	C10H20	n-alkenes				x						
29	2-Decene	C10H20	n-alkenes				x						
30	4,6-Decadiene	C10H18	n-alkenes				x						
31	6-Dodecene	C12H24	n-alkenes					x					
32	3-Dodecene trans	C12H24	n-alkenes					x					
33	3-Dodecene cis	C12H24	n-alkenes					x					
34	2-Dodecene	C12H24	n-alkenes					x					
35	5-Dodecene	C12H24	n-alkenes					x					
36	Pentane, 2,2,4-trimethyl-	C8H18	iso-alkanes						x				
36	Hexane, 2,4-dimethyl-	C8H18	iso-alkanes						x				
37	Pentane, 2,3,4-trimethyl	C8H18	iso-alkanes						x				

No.	name	formula	hydrocarbon group	detected product components								components	
				MCH	decalin	nonane	decane	dodecane	iso-octane	n-butyl-benzene	p-xylene	ULSK	Jet A-1
38	Heptane, 2-methyl-	C8H18	iso-alkanes									x	x
39	Heptane, 3-methyl-	C8H18	iso-alkanes									x	x
40	Hexane, 2,3,5-trimethyl-	C9H20	iso-alkanes									x	x
41	Heptane, 2,6-dimethyl-	C9H20	iso-alkanes									x	x
42	Heptane, 2,5-dimethyl-	C9H20	iso-alkanes									x	x
43	Heptane, 2,4-dimethyl-	C9H20	iso-alkanes				x					x	x
44	Heptane, 2,3-dimethyl-	C9H20	iso-alkanes									x	x
45	Heptane, 4-ethyl-	C9H20	iso-alkanes									x	x
46	Octane, 4-methyl-	C9H20	iso-alkanes			x							
47	Octane, 2-methyl-	C9H20	iso-alkanes			x						x	x
48	Octane, 3-methyl-	C9H20	iso-alkanes			x						x	x
49	Heptane, 3-ethyl-	C9H20	iso-alkanes									x	x
50	Heptane, 2,4,6-trimethyl-	C10H22	iso-alkanes										
51	Octane, 3,5-dimethyl-	C10H22	iso-alkanes										
52	Octane, 2,6-dimethyl-	C10H22	iso-alkanes				x						
53	Octane, 4-ethyl-	C10H22	iso-alkanes				x						

No.	name	formula	hydrocarbon group	detected product components								components	
				MCH	decalin	nonane	decane	dodecane	iso-octane	n-butyl-benzene	p-xylene	ULSK	Jet A-1
54	0 - unbekanntes Iso-Alcane	C10H22	iso-alkanes										
55	Nonane, 5-methyl-	C10H22	iso-alkanes				x						
56	Nonane, 4-methyl-	C10H22	iso-alkanes				x						
57	Nonane, 2-methyl-	C10H22	iso-alkanes				x						
58	Octane, 3-ethyl-	C10H22	iso-alkanes				x						
68	Nonane, 2,6-dimethyl-	C11H24	iso-alkanes									x	x
69	Octane, 5-ethyl-2-methyl-	C11H24	iso-alkanes									x	x
70	Decane, 5-methyl-	C11H24	iso-alkanes									x	x
71	Decane, 4-methyl-	C11H24	iso-alkanes									x	x
72	Decane, 3,7-dimethyl-	C12H26	iso-alkanes									x	x
73	Undecane, 6-methyl-	C12H26	iso-alkanes					x					
74	Undecane, 5-methyl-	C12H26	iso-alkanes					x					
75	Undecane, 4-methyl-	C12H26	iso-alkanes					x					
76	Undecane, 2-methyl-	C12H26	iso-alkanes					x				x	x
77	Undecane, 3-methyl-	C12H26	iso-alkanes					x				x	x
78	Undecane, 2,6-dimethyl-	C13H28	iso-alkanes									x	x

No.	name	formula	hydrocarbon group	detected product components								components	
				MCH	decalin	nonane	decane	dodecane	iso-octane	n-butyl-benzene	p-xylene	ULSK	Jet A-1
79	Undecane, 2,5-dimethyl-	C13H28	iso-alkanes									x	x
80	Dodecane, 4-methyl-	C13H28	iso-alkanes									x	x
81	Dodecane, 2-methyl-	C13H28	iso-alkanes									x	x
82	Undecane, 6-ethyl-	C13H28	iso-alkanes									x	x
83	Tridecane, 6-methyl-	C14H30	iso-alkanes									x	x
84	Dodecane, 2,5-dimethyl-	C14H30	iso-alkanes									x	x
85	Tridecane, 2-methyl-	C14H30	iso-alkanes									x	x
86	Tridecane, 3-methyl-	C14H30	iso-alkanes									x	x
87	Dodecane, 4,6-dimethyl-	C14H30	iso-alkanes					x					
88	Tetradecane, 4-methyl-	C15H32	iso-alkanes									x	x
89	Tetradecane, 2-methyl-	C15H32	iso-alkanes									x	x
90	Dodecane, 2,6,10-trimethyl-	C15H32	iso-alkanes									x	x
91	1-Pentene, 2-methyl-	C6H12	iso-alkenes			x		x					
92	Petane, 3-methyl-	C6H14	iso-alkenes			x							

No.	name	formula	hydrocarbon group	detected product components								components	
				MCH	decalin	nonane	decane	dodecane	iso-octane	n-butyl-benzene	p-xylene	ULSK	Jet A-1
93	1-Pentene, 2,4,4-trimethyl	C8H16	iso-alkenes						x				
94	2-Pentene, 2,4,4-trimethyl	C8H16	iso-alkenes						x				
95	1-Hexene, 3,5-dimethyl-	C8H16	iso-alkenes						x				
96	Pentene, 2,3,4-trimethyl-	C8H16	iso-alkenes						x				
97	Cyclohexane	C6H12	cycloalkanes				x		x				
98	Cyclohexane, methyl-	C7H14	cycloalkanes	x					x			x	x
99	Cyclopentane, ethyl-	C7H14	cycloalkanes	x								x	x
100	Cyclopentane, 1,2,4-trimethyl-	C8H16	cycloalkanes									x	x
101	Cyclohexane, 1,3-dimethyl- Cis	C8H16	cycloalkanes									x	x
102	Cyclohexane, 1,2-dimethyl- Trans	C8H16	cycloalkanes									x	x
103	Cyclopropane, pentyl-	C8H16	cycloalkanes					x					
104	Cyclohexane, 1,3-dimethyl- Trans	C8H16	cycloalkanes									x	x
105	Cyclopentane, 1-ethyl-3-methyl-	C8H16	cycloalkanes									x	x

No.	name	formula	hydrocarbon group	detected product components								components	
				MCH	decalin	nonane	decane	dodecane	iso-octane	n-butyl-benzene	p-xylene	ULSK	Jet A-1
106	Cyclohexane, 1,4-dimethyl-	C8H16	cycloalkanes									x	x
107	Cyclohexane, 1,2-dimethyl- Cis	C8H16	cycloalkanes									x	x
108	Cyclopentane, propyl-	C8H16	cycloalkanes									x	x
109	Cyclohexane, ethyl-	C8H16	cycloalkanes									x	x
110	Cyclohexane, 1,1,3-trimethyl-	C9H18	cycloalkanes									x	x
111	0 - unbekanntes Cycloalkan	C9H18	cycloalkanes						x				
112	Cyclohexane, 1,2,3-trimethyl	C9H18	cycloalkanes									x	x
113	Cyclopentane, 1-methyl-2-propyl- (Configuration 1)	C9H18	cycloalkanes										x
114	Cyclohexane, 1,2,3-trimethyl-	C9H18	cycloalkanes				x					x	x
115	Cyclohexane, 1,2,4-trimethyl-	C9H19	cycloalkanes				x					x	x
116	Cyclopentane, 1-methyl-2-propyl- (Configuration 2)	C9H18	cycloalkanes				x						
117	Cyclohexane, 1,3,5-trimethyl-	C9H19	cycloalkanes				x						

No.	name	formula	hydrocarbon group	detected product components								components	
				MCH	decalin	nonane	decane	dodecane	iso-octane	n-butyl-benzene	p-xylene	ULSK	Jet A-1
118	Cyclohexane, 1,1,2-trimethyl-	C9H18	cycloalkanes				x						
119	Cyclopropane, 1-methyl-2-pentyl-	C9H18	cycloalkanes					x					
120	Cyclohexane, 1-ethyl-3-methyl- (Configuration 1)	C9H18	cycloalkanes				x						
121	Cyclohexane, 1,1,2,3-tetramethyl-	C10H20	cycloalkanes				x						
122	Cyclohexane, 1-ethyl-4-methyl-	C9H18	cycloalkanes				x						
123	Cyclopentane, 2-ethyl-1,1-dimethyl-	C9H18	cycloalkanes				x						
124	Cyclohexane, 1-ethyl-3-methyl- (Configuration 2)	C9H18	cycloalkanes										
125	0 - unbekanntes Cyclohexane	C10H22	cycloalkanes										
126	Cyclopentan, butyl-	C9H18	cycloalkanes			x							
127	Cyclooctane, methyl-	C9H18	cycloalkanes									x	x
128	Cyclopentane, 1,2-dimethyl-3-(1-methylethyl)-	C10H20	cycloalkanes									x	x
129	Cyclohexane, propyl-	C9H18	cycloalkanes			x	x						

No.	name	formula	hydrocarbon group	detected product components								components	
				MCH	decalin	nonane	decane	dodecane	iso-octane	n-butyl-benzene	p-xylene	ULSK	Jet A-1
130	Cyclooctane, 1,2-dimethyl-	C10H20	cycloalkanes				x						
131	Cyclohexane, 1,2,3,5-tetramethyl-	C10H20	cycloalkanes				x					x	x
132	Cyclodecane	C10H20	cycloalkanes				x						
133	Cyclohexane, 1-ethyl-2,3-dimethyl-	C10H21	cycloalkanes				x						
134	Cyclohexane, 1-ethyl-2,4-dimethyl-	C10H20	cycloalkanes				x						
135	Cyclohexane, 1-Isopropenyl-2-methyl-	C10H18	cycloalkanes									x	x
136	Cyclohexane, 1-methyl-2-propyl- (Configuration 1)	C10H20	cycloalkanes				x						
137	Cyclohexane, 1,2-diethyl-	C10H20	cycloalkanes				x						
138	Cyclohexane, 2-ethyl-1,3-dimethyl- (Configuration 1)	C10H20	cycloalkanes				x						
139	Cyclohexane, 1-methyl-4-(1-methylethyl)-	C10H20	cycloalkanes									x	x
140	Cyclopentane, pentyl-	C10H20	cycloalkanes				x						

No.	name	formula	hydrocarbon group	detected product components								components	
				MCH	decalin	nonane	decane	dodecane	iso-octane	n-butyl-benzene	p-xylene	ULSK	Jet A-1
141	Cyclopentane, (2-methyl-butyl)-	C10H20	cycloalkanes									x	x
142	Cyclohexane, 1-methyl-2-propyl- (Configuration 2)	C10H20	cycloalkanes				x						
143	Cyclohexane, 1-isopropyl-3-methyl-	C10H20	cycloalkanes				x						
144	Cyclohexane, 1-(ethylmethyl)-3-methyl-	C10H20	cycloalkanes									x	x
145	Cyclohexane, 2-ethyl-1,3-dimethyl- (Configuration 2)	C10H20	cycloalkanes									x	x
146	Naphthalene, decahydro- Trans	C10H18	cycloalkanes		x		x						
147	Cyclohexane, butyl-	C10H20	cycloalkanes				x						
148	Cyclohexane, 1-ethyl-2,2,6-methyl-	C11H22	cycloalkanes									x	x
149	Naphthalene, decahydro- Cis	C10H18	cycloalkanes		x		x						
150	Cyclopentane, hexyl-	C11H22	cycloalkanes									x	x
151	Cyclohexane, 1,2-diethyl-3-methyl-	C11H22	cycloalkanes										
152	Naphthalene, 2-methyl-decahydro-	C11H20	cycloalkanes									x	x

No.	name	formula	hydrocarbon group	detected product components								components	
				MCH	decalin	nonane	decane	dodecane	iso-octane	n-butyl-benzene	p-xylene	ULSK	Jet A-1
153	Cyclohexane, pentyl-	C11H22	cycloalkanes										
154	Naphthalene, 4-methyl-decahydro-	C11H20	cycloalkanes									x	x
155	Cyclododecane	C12H24	cycloalkanes									x	x
156	Cyclohexane, hexyl-	C12H24	cycloalkanes									x	x
157	Cyclohexane, heptyl-	C13H26	cycloalkanes									x	x
158	Cyclotetradecane	C14H28	cycloalkanes									x	x
159	Cyclohexene, 4-methyl-	C7H12	cycloalkenes	x									
160	Cyclohexene, 3-methyl-	C7H12	cycloalkenes	x									
161	Cyclohexene, 1-methyl-	C7H12	cycloalkenes	x									
162	1,2,3,4,4a,5,6,8a-Octahydro-naphthalene	C10H16	cycloalkenes		x								
163	Isoadamantane	C10H16	cycloalkenes		x								
164	2-methyl-trans-3a,4,7,8a-tetrahydroindane	C10H16	cycloalkenes		x								
165	Bicyclopentylidene	C10H17	cycloalkenes		x								
166	naphthalene, 1,4-dihydro	C10H10	cycloalkenes		x							x	x
167	Tetralin	C10H12	cycloalkenes		x								

No.	name	formula	hydrocarbon group	detected product components								components	
				MCH	decalin	nonane	decane	dodecane	iso-octane	n-butyl-benzene	p-xylene	ULSK	Jet A-1
168	Benzene	C6H6	aromatics				x			x		x	x
169	Benzene, methyl-	C7H8	aromatics	x			x			x	x	x	x
170	Benzene, ethyl-	C8H10	aromatics				x			x	x	x	x
171	Benzene, 1,4-dimethyl-	C8H10	aromatics				x			x	x	x	x
172	Benzene, 1,3-dimethyl-	C8H10	aromatics				x			x	x	x	x
173	Benzene, 1,2-dimethyl-	C8H10	aromatics				x			x	x	x	x
174	Styrol	C8H8	aromatics							x		x	x
175	Benzene, 1-methylethyl-	C9H12	aromatics		x	x		x			x	x	x
176	Benzene, propyl-	C9H12	aromatics			x	x					x	x
177	Benzene, 1-ethyl-3-methyl-	C9H12	aromatics							x		x	x
178	Benzene, 1-ethyl-4-methyl-	C9H12	aromatics									x	x
179	Benzene, 1-ethyl-2-methyl-	C9H12	aromatics			x						x	x
180	Benzene, 1,3,5-trimethyl-	C9H12	aromatics									x	x
181	Benzene, 1-ethyl-2-methyl-	C9H12	aromatics									x	x
182	Benzene, 1,2,4-trimethyl-	C9H12	aromatics				x						
183	Benzene, (1-methylpropyl)-	C10H14	aromatics				x			x			

No.	name	formula	hydrocarbon group	detected product components								components	
				MCH	decalin	nonane	decane	dodecane	iso-octane	n-butyl-benzene	p-xylene	ULSK	Jet A-1
184	Benzene, 1-methyl-3-(1-methylethyl)-	C10H14	aromatics				x			x		x	x
185	Benzene, 1-methyl-4-(1-methylethyl)-	C10H14	aromatics									x	x
186	Benzene, 1-butenyl-	C10H12	aromatics				x						
187	Benzene, 1,2,3-trimethyl-	C9H12	aromatics					x				x	x
188	Benzene, 1-methyl-3-propyl-	C10H14	aromatics				x			x		x	x
189	n-Butylbenzene	C10H14	aromatics		x		x	x		x			
190	Benzene, 1-methyl-4-propyl-	C10H14	aromatics							x		x	x
191	Benzene, 1,3-diethyl-	C10H14	aromatics				x						
192	Benzene, (2-methyl-1-propenyl)-	C10H12	aromatics									x	x
193	Benzene, 4-ethyl-1,2-dimethyl-	C10H13	aromatics				x						
194	1-methyl-4-(1-methylethenyl) benzene	C10H12	aromatics		x								
195	Benzene, 1,2,3,4-tetramethyl-	C10H14	aromatics				x						

No.	name	formula	hydrocarbon group	detected product components								components	
				MCH	decalin	nonane	decane	dodecane	iso-octane	n-butyl-benzene	p-xylene	ULSK	Jet A-1
196	Benzene1-ethenyl-3-ethyl-	C10H12	aromatics							x			
197	Benzene, 1,2-diethyl-	C10H14	aromatics				x						
198	Benzene, 2-butenyl-	C10H12	aromatics							x			
199	Benzene, (2-methyl-2-propenyl)-	C10H12	aromatics							x			
200	Benzene, 1-ethyl-2,4-dimethyl-	C10H14	aromatics							x			
201	Benzene, 2-ethyl-2,4-dimethyl-	C10H14	aromatics					x					
202	Benzene, 1-ethenyl-4-ethyl-	C10H12	aromatics							x			
203	Benzene, 1-ethenyl-3-ethyl-	C10H12	aromatics				x						
204	1H-Indene, 2,3-dihydro-4-methyl-	C10H12	aromatics									x	x
205	Benzene, 2-ethyl-1,4-dimethyl-	C10H12	aromatics				x						
206	Benzene, 1-butenyl-	C10H12	aromatics							x			
207	Benzene, 2-ethyl-1,3-dimethyl-	C10H14	aromatics				x						
208	Benzene, 1-ethenyl-2,4-dimethyl-	C10H14	aromatics				x						

No.	name	formula	hydrocarbon group	detected product components								components	
				MCH	decalin	nonane	decane	dodecane	iso-octane	n-butyl-benzene	p-xylene	ULSK	Jet A-1
209	Benzene, 1-ethenyl-2,4-dimethyl-	C10H14	aromatics				x						
210	Benzene, 1-methyl-4-(1-methylpropyl)-	C11H16	aromatics									x	x
211	Benzene, (1,1-dimethylpropyl)-	C11H16	aromatics									x	x
212	Benzene, (1,2-dimethylpropyl)-	C11H16	aromatics									x	x
213	Naphthalene	C10H8	aromatics		x		x						
214	Benzene, 2,4-diethyl-1-methyl-	C11H16	aromatics										
215	Benzene, (1-methylbutyl)-	C11H16	aromatics										
216	Naphthalene, tetrahydro-	C10H12	aromatics			x						x	x
217	Benzene, (3-methyl-2-butenyl)-	C11H14	aromatics									x	x
218	Benzene, (2,2-dimethyl-1-methylenepropyl)-	C12H16	aromatics					x					
219	Benzene, 1-methyl-2-(1-ethylpropyl)	C12H18	aromatics					x					
220	Benzene, 1,3,5-triethyl-	C12H18	aromatics					x					

No.	name	formula	hydrocarbon group	detected product components								components	
				MCH	decalin	nonane	decane	dodecane	iso-octane	n-butyl-benzene	p-xylene	ULSK	Jet A-1
221	Benzene, hexyl	C12H18	aromatics					x					
222	Benzene, 1,4-dimethyl-2-(2-methylpropyl)	C12H18	aromatics					x					
223	Benzene, (1-methylpentyl)-	C12H18	aromatics					x					
224	Naphthalene, 2-methyl-tetrahydro-	C11H14	aromatics					x					
225	Benzene, (1-methylpentyl)-	C12H18	aromatics				x	x					
226	Benzene, (1,3-dimethylbutyl)	C12H18	aromatics					x					
227	Benzene, hexyl-	C12H18	aromatics									x	x
228	Benzene, (1,3-dimethylbutyl)-	C12H18	aromatics									x	x
229	Naphthalene, 5-methyl-tetrahydro-	C11H14	aromatics									x	x
230	Naphthalene, 1-methyl-	C11H10	aromatics									x	x
231	Naphthalene, 2,6-dimethyl-tetrahydro-	C12H16	aromatics									x	x
232	Naphthalene, 2-methyl-	C11H10	aromatics									x	x
233	Naphthalene, 1,1,6-trimethyl-tetrahydro-	C13H18	aromatics									x	x

No.	name	formula	hydrocarbon group	detected product components								components	
				MCH	decalin	nonane	decane	dodecane	iso-octane	n-butyl-benzene	p-xylene	ULSK	Jet A-1
234	Naphthalene, 5,7-dimethyl-tetrahydro-	C12H16	aromatics									x	x
235	Benzene, 1-(2-butenyl)-2,3-dimethyl-	C12H16	aromatics									x	x
236	Naphthalene, 2-ethyl-	C12H12	aromatics									x	x
237	Naphthalene, 1-ethyl-	C12H12	aromatics									x	x
238	Naphthalene, 1,6-dimethyl-	C12H12	aromatics									x	x
239	Naphthalene, 1,5-dimethyl-	C12H12	aromatics									x	x
240	Naphthalene, 1,4-dimethyl-	C12H12	aromatics									x	x
241	Naphthalene, 1,3-dimethyl-	C12H12	aromatics									x	x
242	unknown substance	C11H24	others				x						
243	unknown substance	C9H18	others				x						

8.4 Additional Data to Process Simulation

In the following additional information to the process simulation presented in chapter 6 are provide. Table 8.5 presents the physical properties of the pseudo components of ULSK used for the feed conditions before the dehydrogenation reactor of reference concept.

Table 8.5 - physical properties pseudo components for ULSK

pseudo components	boiling point	specific gravity	molecular weight	mass content
	[°C]	[kg/l]	[g/mol]	[wt-%]
PC162C	161.59	0.77	126.20	6.55
PC170C	170.255	0.77	131.17	50.76
PC183C	182.66	0.78	138.57	14.29
PC197C	196.90	0.79	147.45	9.55
PC211C	210.83	0.79	156.545	6.55
PC226C	225.64	0.80	166.67	5.36
PC237C	237.31	0.81	174.99	4.98
PC253C	252.58	0.82	186.32	1.02
PC267C	266.69	0.82	197.274	0.77
PC276C	275.62	0.83	204.42	0.17

Table 8.6 presents the detailed conversion rates and conversion factors integrated in the model of the dehydrogenation reactor of the process concept with rectification and the reference concept.

Table 8.6 -: conversion rate and conversion factors of reactions integrated in Aspen plus process simulation

Model Component	Conversion rate			React. No.	Conversion factor		
	Reference process	10 wt.-% Model	20 wt.-% Model		Reference process	10 wt.-% Model	20 wt.-% Model
Nonane	3.39	3.59	0.91	1	0.038	0.068	0.068
				2	0.078	0.077	0.077
				3	0.08	0.054	0.054
				4	0.309	0.292	0.292
				5	0.485	0.475	0.475
				6	0.010	0.034	0.034
Decane	5.96	5.62	1.91	7	0.625	0.625	0.625
				8	0.256	0.165	0.165
				9	0.028	0.083	0.083
				10	0.054	0.094	0.094
				11	0.032	0.032	0.032
				12	0.005	0.001	0.001

Model Component	Conversion rate			React. No.	Conversion factor		
	Reference process	10 wt.-% Model	20 wt.-% Model		Reference process	10 wt.-% Model	20 wt.-% Model
Dodecan	15.69		7.98	13	0.026		0.026
				14	0.046		0.046
				15	0.010		0.024
				16	0.643		0.619
				17	0.276		0.276
				18	0.009		0.009
Issoctane	3.02	1.81	0.2	19	0.992	0.992	0.992
				20	0.008	0.008	0.008
n-Butylben-zene	0.0	1.818	0.0	21	0.86	0.95	0.98
				22	0.14	0.05	0.02
p-Xylene	0.71	0.0	0.74	23	0.00	0.00	0.003
				24	0.58	0.42	0.418
				25	0.42	0.58	0.578
trans -Decalin	36.28	77.992	39.28	t-26	0.848	0.667	0.80
				t- 27	0.152	0.333	0.20
				t- 28	0.002	0.000	0.00
cis - Decalin	54,119		52.78	c- 26	0.848	0.667	0.80
				c- 27	0.152	0.333	0.20
				c- 28	0.002	0.000	0.00
Methylcyclo-hexane	17.2	51.86	15.45	29	0.999	0.999	0.999
				30	0.000	0.001	0.001
				31	0.001	0.000	0.000

8.4.1 Process Concept with Rectification and 20 wt-% Jet A- fraction

The efficiency process concept with rectification is also calculated for a 20 wt.-% Jet A-1 fraction. The stream data of the process and the heat exchanger grit table are presented in table 8.7 and Fig .8.1.

Table 8.7 hot and cold stream data for heat integration of process concept with rectification and 20 wt.-% Jet A-1 fraction

Stream	Total flow rate [kg/h]	Temperature range [°C]	specific Cp [kJ/kg K]	Enthalpy [kW]	Stream type
flue gas	2447	650. – 384.7 384.7 -75.55	1.0930 1.0571	207.1 218	hot
product	948	425 – 367.15	2.9169	44.43	hot
kerosene	4741	20 – 100.9 100.9 – 196.6	2.2 2.54	554.7	cold
fraction	984.2	177.3 – 235.8 235.8 – 293.1 293.1 – 321.2 321.2 – 373.1 373.1 – 425	2.7869 3.0402 10.578 2.8638 2.9750	245,8	cold
still	3793	204 – 119 119 - 30	2.6354 2.1818	236.2 204.5	hot
air	2420	20 – 182.1	1.0190	111	cold
$Q_{rectfi.\ cooler}$	3508	180.3 – 179.4 179.4 – 177.3	98.225 108.57	84.48 224.1	hot
$Q_{reboiler}$	7305	198.9 - 201.5 201.5 – 198.9	32.789 28.477	170.7 145.1	cold
$Q_{reactor}$	-	425 – 425.5	-	68.3	cold
$Q_{condesation}$		367.1-30	-	291.1	hot

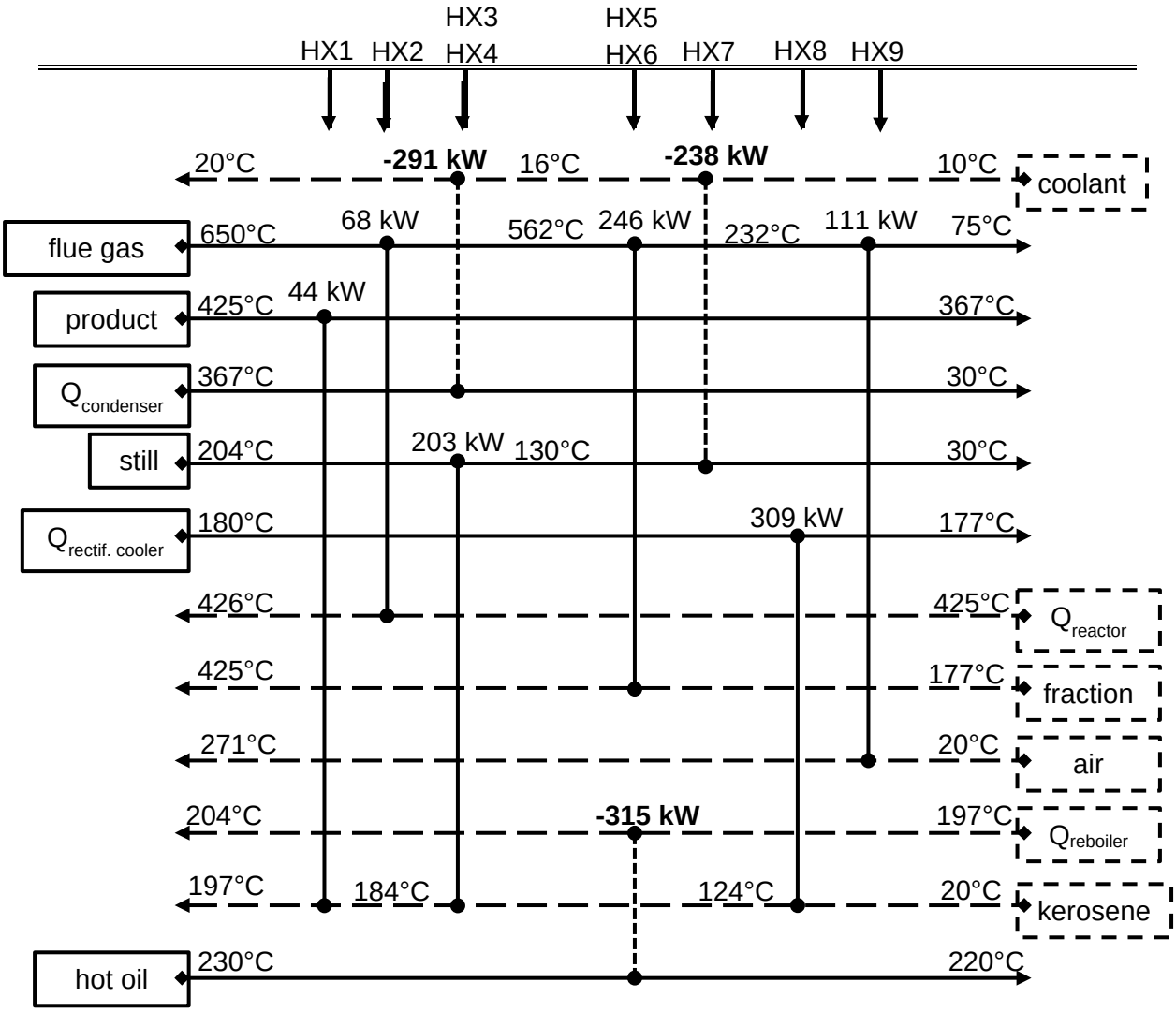

Fig. 8.1 - grid table of heat exchanger network designed for process concept with rectification and 20 wt.-% Jet A-1 fraction

8.4.2 Alternative Process Concept with Rectification

The heat exchanger system for process concept with rectification and 20 wt.-% is also designed for an alternative process concept which allows better exploitation of heat streams and therefore higher efficiency. But this heat exchanger system is limited to a hydrogen yield of up to 120 $Nl_{H2}/kg_{fraction}$. Table 8.8 presents the enthalpy streams of the system while Fig. 8.2 shows the alternative grid table and Fig. alternative flow sheet for this variation of the process.

Table 8.8 - hot and cold stream data for heat integration of alternative process concept with rectification and 20 wt.-% Jet A-1 fraction

Stream	Total flow rate [kg/h]	Temperature range [°C]	specific Cp [kJ/kg K]	Enthalpy [kW]	Stream type
flue gas	2208	650 – 428.5 428.5 - 180.3	1.126 1.069	152.5 162.7	hot
product	947.9	425 – 342.1 342.1 – 266.9 266.9 – 180.5	2.8841 2.6679 5.0452	62.96 52.80 114.8	hot
kerosene	4741	20 – 100.9 100.9 – 196.6	2.1992 25432	234.2 320.5	cold
fraction	948.2	177.3 – 235.8 235.8 – 293.1 293.1 – 321.2 321.2 – 373.1 373.1 – 423.8	2.7869 3.0402 10.578 2.8638 2.975	42.96 45.9 78.04 39.17 39.72	cold
still	3793	204 – 119 119 - 30	2.6354 2.1818	236.2 204.5	hot
air	2191	20 – 317.1	1,0293	186.1	cold
$Q_{rectfi.\ cooler}$	3508	180.3 – 179.4 179.4 – 177.3	98.225 108.57	84.48 224.1	hot
$Q_{reboiler}$	7305	198.9 – 201.5 201.5 – 204	32.789 28.477	170.1 145.1	cold
$Q_{reactor}$	-	425 – 425.5	-	68.33	cold
$Q_{condesation}$		180.5 - 30	-	104.9	hot
hydrogen	5.402	30 - 80	14.373	1.078	cold

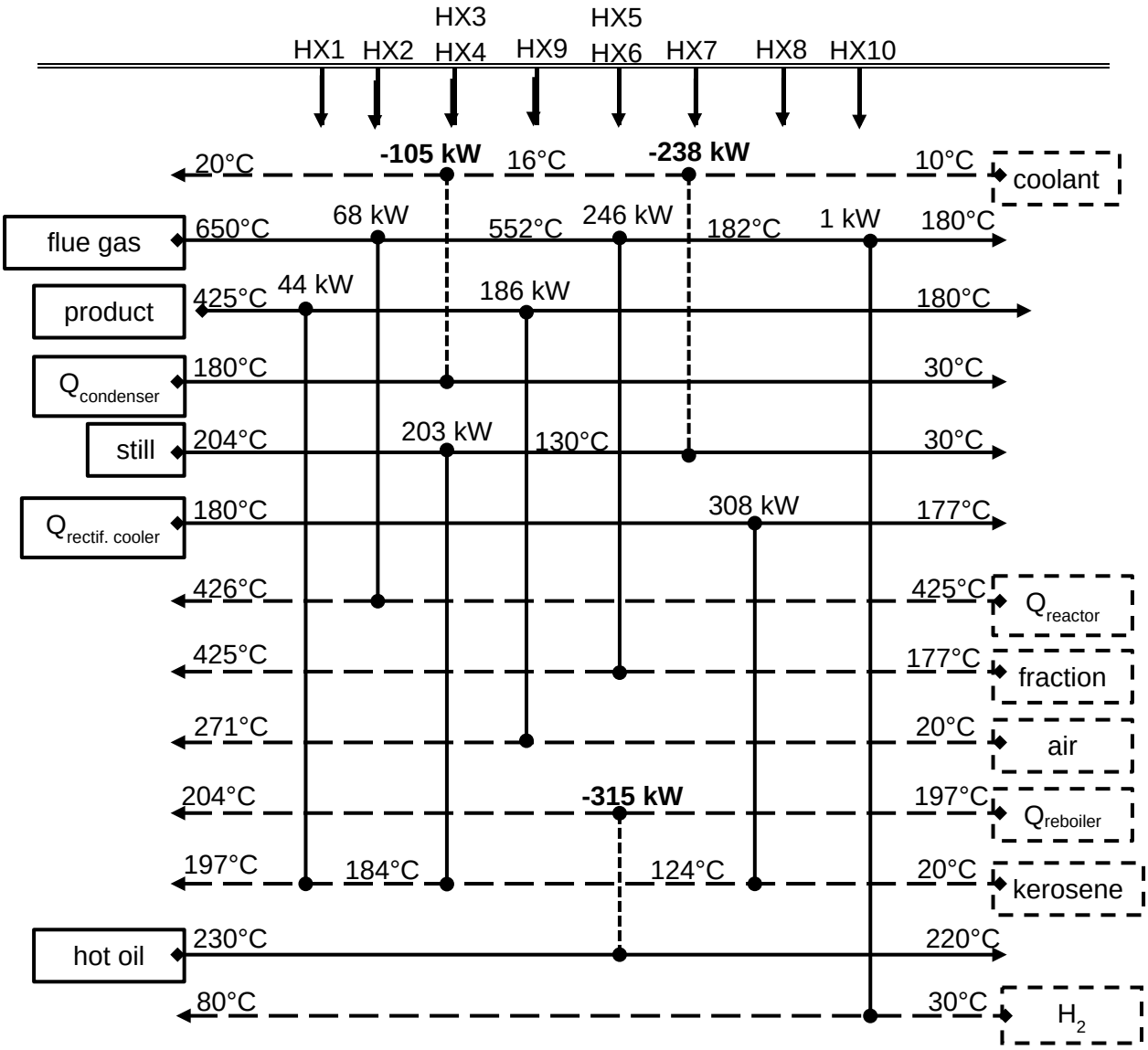

Fig. 8.2 - alternative flow sheet with heat exchanger network of process concept with rectification and 20 wt.-% Jet A-1 fraction

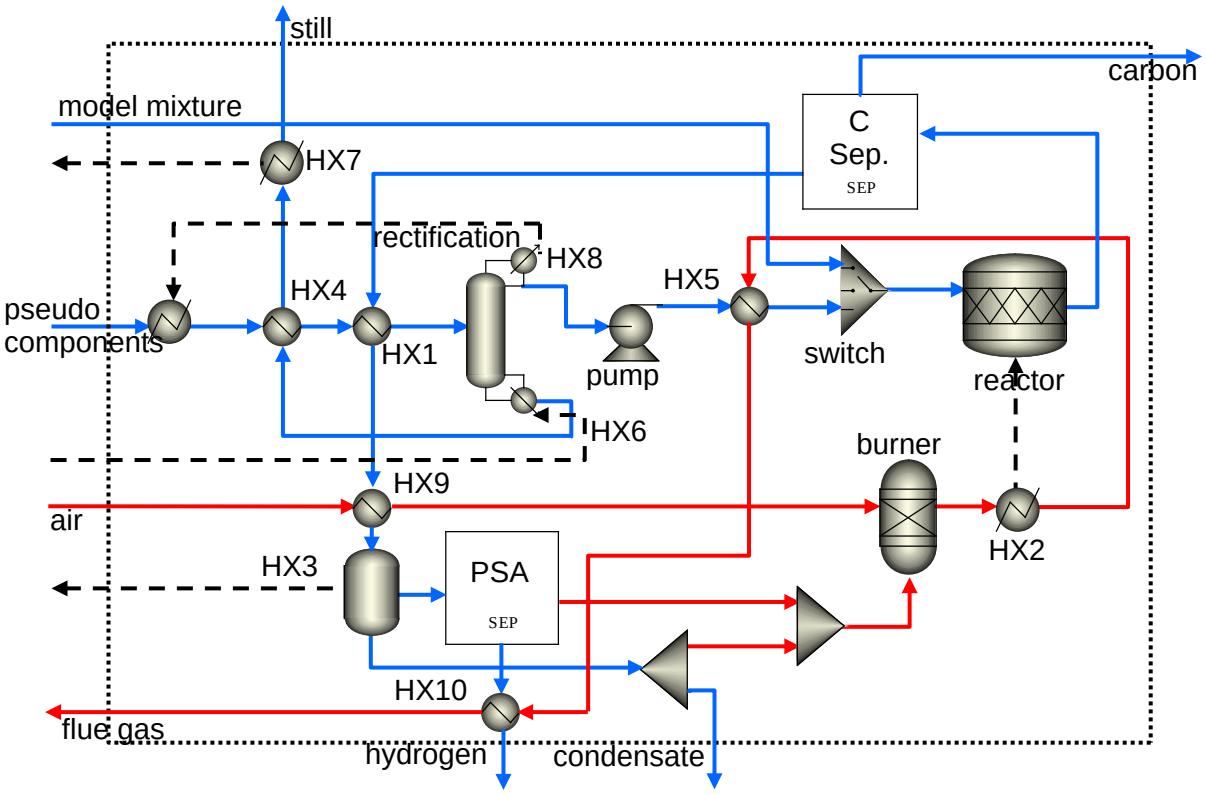

Fig. 8.2 - alternative flow sheet with heat exchanger network of process concept with rectification and 20 wt.-% Jet A-1 fraction

9 Literature

[1] Macintosh A, Wallace L. International aviation emissions to 2025: Can emissions be stabilised without restricting demand? Energy Policy 2009;37(1):264–73.

[2] Grossman AS, Haywood JM, Rind D, Subbaraya BH. Aviation and the Global Atmosphere. Geneva, Switzerland: 1999.

[3] Lee DS, Pitari G, Grewe V, Gierens K, Penner JE, Petzold a., et al. Transport impacts on atmosphere and climate: Aviation. Atmos. Environ. 2010;44(37):4678–4734.

[4] Brown RC, Anderson MR, Miake RC, Kolb CE, Sorokin AA, Buriko YY. Aircraft exhaust sulfur emissions. Geophys. Res. Lett. 1996;23(24):3603–6.

[5] Kjellstro E, Feichter J, Sausen R, Hein R. The contribution of aircraft emissions to the atmospheric sulfur budget 1999;33.

[6] Shooter D. Sources and sinks of oceanic hydrogen sulfiede - an overview. Atmos. Environ. 1999;33(January 1998):3467–72.

[7] Brown RC, Anderson MR, Kolb CE. Aircraft sulfur emissions and the formation of visible contrails. Geophys. Res. Lett. 1997;24(4):385–88.

[8] Takeshita T, Yamaji K. Important roles of Fischer–Tropsch synfuels in the global energy future. Energy Policy 2008;36(8):2773–84.

[9] Klerk A de. Fischer-Tropsch-Refining. Wiley-VCH, 2011.

[10] Dagaut P, Karsenty F, Dayma G, Diévart P, Hadj-Ali K, Mzé-Ahmed A, et al. Experimental and detailed kinetic model for the oxidation of a Gas to Liquid (GtL) jet fuel. Combust. Flame n.d.;161(3):835–47.

[11] Bauldreay JM, Bogers PF, Al-Sharshani A. Use of Surrogate Blends to Explore Combustion-Composition Links for Synthetic Paraffinic Kerosines. In:. Iash 2011, 12th int. conf. stability, handl. use liq. fuels. Sarasota, Florida USA: 2011.

[12] Muradov N, Veziroglu T. “Green” path from fossil-based to hydrogen economy: An overview of carbon-neutral technologies. Int. J. Hydrogen Energy 2008;33(23):6804–39.

[13] Dunn S. Hydrogen futures: toward a sustainable energy system. Int. J. Hydrogen Energy 2002;27(3):235–64.

[14] Renouard-Vallet G, Saballus M, Schmithals G, Schirmer J, Kallo J, Friedrich KA. Improving the environmental impact of civil aircraft by fuel cell technology: concepts and technological progress. Energy Environ. Sci. 2010;3(10):1458.

[15] Renouard-Vallet G, Saballus M, Schumann P, Kallo J, Friedrich KA, Müller-Steinhagen H. Fuel cells for civil aircraft application: On-board production of power, water and inert gas. Chem. Eng. Res. Des. 2012;90(1):3–10.

[16] Schuhmann P, Graf C, Friedrich KA. Modeling and Simulation of a PEM Fuel Cell System for Aircraft Applications P.Schumann. ECS Trans. 2008;12(1):651–61.

[17] Steffen CJ, Freeh JE, Larosiliere LM. Solid Oxide Fuel Cell / Gas Turbine Hybrid Cycle Technology for Auxiliary Aerospace Power. 2005.

[18] Khandelwal B, Karakurt A, Sekaran PR, Sethi V, Singh R. Hydrogen powered aircraft : The future of air transport. Prog. Aerosp. Sci. 2013;60:45–59.

[19] Aardahl CL, Rassat SD. Overview of systems considerations for on-board chemical hydrogen storage. Int. J. Hydrogen Energy 2009;34(16):6676–83.

[20] Xinhai X, Peiwen L, Yuesong S. Small-scale reforming of diesel and jet fuels to make hydrogen and syngas for fuel cells: A review. Appl. Energy 2013;108:202–17.

[21] Pasel J, Meisner J, Pors Z, Samsun R, Tschauder a, Peters R. Autothermal reforming of commercial Jet A-1 on a 5kWe scale. Int. J. Hydrogen Energy 2007;32(18):4847–58.

[22] Sarioglan a, Olgun H, Baranak M, Ersoz a, Atakul H, Ozdogan S. Diesel evaporation as the first step of hydrogen production. Int. J. Hydrogen Energy 2007;32(14):2895–2901.

[23] Lázaro MP, García-Bordejé E, Sebastián D, Lázaro MJ, Moliner R. In situ hydrogen generation from cycloalkanes using a Pt/CNF catalyst. Catal. Today 2008;138(3-4):203–9.

[24] Wang Y, Shah N, Huggins FE, Huffman GP. Hydrogen Production by Catalytic Dehydrogenation of Tetralin and Decalin Over Stacked Cone Carbon Nanotube-Supported Pt Catalysts. Energy & Fuels 2006;(9):2612–15.

[25] Usman MR. The Catalytic Dehydrogenation of Methylcyclohexane over Monometallic Catalysts for On-board Hydrogen Storage, Production, and Utilization. Energy Sources, Part A Recover. Util. Environ. Eff. 2011;33(24):2231–38.

[26] Wang B, Froment G, Goodman D. CO-free hydrogen production via dehydrogenation of a Jet A hydrocarbon mixture. J. Catal. 2008;253(2):239–43.

[27] Ballarini AD, Zgolicz P, Vilella IMJ, de Miguel SR, Castro A a., Scelza O a. N-Butane dehydrogenation on Pt, PtSn and PtGe supported on γ-Al2O3 deposited on spheres of α-Al2O3 by washcoating. Appl. Catal. A Gen. 2010;381(1-2):83–91.

[28] Ballarini AD, Ricci CG, de Miguel SR, Scelza O a. Use of Al2O3–SnO2 as a support of Pt for selective dehydrogenation of light paraffins. Catal. Today 2008;133-135:28–34.

[29] Kariya N, Fukuoka A, Ichikawa M. Efficient evolution of hydrogen from liquid cycloalkanes over Pt-containing catalysts supported on active carbons under “wet–dry multiphase conditions.” Appl. Catal. A Gen. 2002;233(1-2):91–102.

[30] Kortsdottir K, Lindström RW, Lindbergh G. The influence of ethene impurities in the gas feed of a PEM fuel cell. Int. J. Hydrogen Energy 2013;38(1):497–509.

[31] Frick V. Verfahrenskonzept zur Wasserstofferzeugung durch katalytische Umwandlung definierter Kerosinfraktionen. Universtität Stuttgart, 2011.

[32] Baerns M, Behr A, Brehm A, Gmeling J, Hinrichsen K-O, Hofmann H, et al. Technische Chemie. Wiley-VCH, 2013.

[33] Höllein V. Palladiumbasierte Kompositmembranen zur Ethylbenzol- und Propan-Dehydrierung. Universität Erlangen-Nürnberg, 2004.

[34] Lee WJ, Froment GF, Eb EBF. Ethylbenzene Dehydrogenation into Styrene : Kinetic Modeling and Reactor Simulation 2008;3:9183–94.

[35] Good GM, Voge HH, Greensfelder BS. Catalytic Cracking of Pure Hydrocarbons. Ind. Eng. Chem. 1945;39(8):1032–36.

[36] Shah YT, Stuart EB, Sheth KD. Coke Formation during Thermal Cracking of n-Octane. Ind. Eng. Chemestry Process Des. Dev. 1976;15(4):518–24.

[37] Jiang H, Yang H, Hawkins R, Ring Z. Effect of palladium on sulfur resistance in Pt–Pd bimetallic catalysts. Catal. Today 2007;125(3-4):282–90.

[38] Ross DK. Hydrogen storage: The major technological barrier to the development of hydrogen fuel cell cars. Vacuum 2006;80(10):1084–89.

[39] Sotoodeh F, Huber BJM, Smith KJ. Dehydrogenation kinetics and catalysis of organic heteroaromatics for hydrogen storage. Int. J. Hydrogen Energy 2012;37(3):2715–22.

[40] Martin S, Lucka K, Wörner A, Vetter A. Reformierung von Biokraftstoffen als Beitrag für eine zukünftige nachhaltige Wasserstoffwirtschaft. Chemie Ing. Tech. 2011;83(11):1965–73.

[41] Engelhardt P, Maximini M, Beckmann F, Brenner M. Integrated fuel cell APU based on a compact steam reformer for diesel and a PEMFC. Int. J. Hydrogen Energy 2012;37(18):13470–77.

[42] Kumabe K, Sato T, Matsumoto K, Ishida Y, Hasegawa T. Production of hydrocarbons in Fischer–Tropsch synthesis with Fe-based catalyst: Investigations of primary kerosene yield and carbon mass balance. Fuel 2010;89(8):2088–95.

[43] Martin S, Wörner A. On-board reforming of biodiesel and bioethanol for high temperature PEM fuel cells: Comparison of autothermal reforming and steam reforming. J. Power Sources 2011;196(6):3163–71.

[44] Slovetskii DI. Plasma-chemical processes in petroleum chemistry (review). Pet. Chem. 2006;46(5):295–304.

[45] Rahimpour MR, Jafari M, Iranshahi D. Progress in catalytic naphtha reforming process: A review. Appl. Energy 2013;109:79–93.

[46] Hartmann M, Deutschmann O, Lichtenberg S, Hebben N, Zhang D. Experimentelle Untersuchung der katalytischen Partialoxidation von Modellkraftstoffen unter definierten Randbedingungen. Chemie Ing. Tech. 2009;81(7):909–19.

[47] Önsan IZ. Catalytic Processes for Clean Hydrogen Production. TURKISH J. Chem. 2007;31:531–50.

[48] Barthmann U. Reaktionstechnische Untersuchung zur katalytischen partiellen Oxidation von Methan mit Sauerstoff zu Synthesegas in Festbettreaktoren. Ruhr-Universitaet Bochum, 1999.

[49] Barbier J. Deactivation of reforming catalysts by coking - a review. Appl. Catal. 1986;23(2):225–43.

[50] Cheekatamarla PK, Finnerty CM. Reforming catalysts for hydrogen generation in fuel cell applications. J. Power Sources 2006;160(1):490–99.

[51] Sopena D, Melgar a, Briceno Y, Navarro R, Alvarezgalvan M, Rosa F. Diesel fuel processor for hydrogen production for 5kW fuel cell application. Int. J. Hydrogen Energy 2007;32(10-11):1429–36.

[52] Ersoz A, Olgun H, Ozdogan S. Reforming options for hydrogen production from fossil fuels for PEM fuel cells. J. Power Sources 2006;154(1):67–73.

[53] Rawadieh S, Gomes V. Steam reforming for hydrogen generation with in situ adsorptive separation. Int. J. Hydrogen Energy 2009;34(1):343–55.

[54] Choi Y, Stenger HG. Water gas shift reaction kinetics and reactor modeling for fuel cell grade hydrogen. J. Power Sources 2003;124(2):432–39.

[55] Ilinich O, Ruettinger W, Liu X, Farrauto R. Cu–Al2O3–CuAl2O4 water–gas shift catalyst for hydrogen production in fuel cell applications: Mechanism of deactivation under start–stop operating conditions. J. Catal. 2007;247(1):112–18.

[56] Choudhury MBI, Ahmed S, Shalabi MA, Inui T. Preferential methanation of CO in a syngas involving CO2 at lower temperature range. Appl. Catal. A Gen. 2006;314(1):47–53.

[57] Bartholomew CH, Farrauto RJ. Fundamentals of Industrial Catalytic Processes. Wiley, 2005.

[58] Babita K, Sridhar S, Raghavan KV. Membrane reactors for fuel cell quality hydrogen through WGSR – Review of their status, challenges and opportunities. Int. J. Hydrogen Energy 2011;36(11):6671–88.

[59] Teixeira M, Madeira LM, Sousa JM, Mendes A. Modeling of a catalytic membrane reactor for CO removal from hydrogen streams – A theoretical study. Int. J. Hydrogen Energy 2010;35(20):11505–13.

[60] Rosso I, Galletti C, Saracco G, Garrone E, Specchia V. Development of A zeolites-supported noble-metal catalysts for CO preferential oxidation: H2 gas purification for fuel cell. Appl. Catal. B Environ. 2004;48(3):195–203.

[61] Marda JR, DiBenedetto J, McKibben S, Evans RJ, Czernik S, French RJ, et al. Non-catalytic partial oxidation of bio-oil to synthesis gas for distributed hydrogen production. Int. J. Hydrogen Energy 2009;34(20):8519–34.

[62] Lee WONJAE. ETHYLBENZENE DEHYDROGENATION INTO STYRENE : KINETIC MODELING AND REACTOR SIMULATION ETHYLBENZENE DEHYDROGENATION INTO STYRENE : KINETIC MODELING AND REACTOR SIMULATION 2005;(December).

[63] Gary JH, Handwerk GE, Kaiser MJ. Petroleum Refining. CRC Press Taylor & Francis Group, 2007.

[64] Corma A, Martinez A, Pergher S, Peratello S, Perego C, Bellusi G. Hydrocracking-hydroisomerization of n-decane on amorphous silica-alumina with uniform pore diameter. Appl. Catal. A Gen. 1997;152(1):107–25.

[65] Khademi MH, Setoodeh P, Rahimpour MR, Jahanmiri a. Optimization of methanol synthesis and cyclohexane dehydrogenation in a thermally coupled reactor using differential evolution (DE) method. Int. J. Hydrogen Energy 2009;34(16):6930–44.

[66] Bhasin MM, Mccain JH, Vora B V, Imai T, Pujad PR. Dehydrogenation and oxydehydrogenation of paraffins to olefins 2001;221:397–419.

[67] Donauer T. Nicht-oxidative katalytische Dehydrierung von Propan an platinhaltigen Trägerkatalysatoren. University of Stuttgart, 2006.

[68] Shah N, Wang Y, Panjala D, Huffman GP. Production of Hydrogen and Carbon Nanostructures by Non-oxidative Catalytic Dehydrogenation of Ethane and Propane 2004;76(9):727–35.

[69] Vincent R, Lindstedt R, Malik N, Reid I, Messenger B. The chemistry of ethane dehydrogenation over a supported platinum catalyst. J. Catal. 2008;260(1):37–64.

[70] Sebastian D. Hydrogen storage by decalin dehydrogenation/naphthalene hydrogenation pair over platinum catalysts supported on activated carbon. Int. J. Hydrogen Energy 2008;33(4):1329–34.

[71] Pande J V., Shukla A, Biniwale RB. Catalytic dehydrogenation of cyclohexane over Ag-M/ACC catalysts for hydrogen supply. Int. J. Hydrogen Energy 2012;37(8):6756–63.

[72] Hodoshima S, Shono A, Saito Y. Chemical Recuperation of Low-Quality Waste Heats by Catalytic Dehydrogenation of Organic Chemical Hydrides and Its Exergy Analysis. Energy & Fuels 2008;22(4):2559–69.

[73] Wang B. Applications of Hydrogenation and Dehydrogenation on Noble Metal Catalysts. Dalian University of Technology, 2007.

[74] Schildhauer T, Newson E, Mueller S. The Equilibrium Constant for the Methylcyclohexane–Toluene System. J. Catal. 2001;198(2):355–58.

[75] Wang B, Goodman D, Froment G. Kinetic modeling of pure hydrogen production from decalin. J. Catal. 2008;253(2):229–38.

[76] Usman MR. Kinetics of Methylcyclohexane Dehydrogenation and Reactor Simulation for “ On-board ” Hydrogen Storage. University of Manchester, 2010.

[77] Hodoshima S, Arai H, Saito Y. Liquid-film-type catalytic decalin dehydrogeno-aromatization for long-term storage and long-distance transportation of hydrogen 2003;28:197–204.

[78] Hodoshima S, Nagata H, Saito Y. Efficient hydrogen supply from tetralin with superheated liquid-film-type catalysis for operating fuel cells. Appl. Catal. A Gen. 2005;292:90–96.

[79] Saito Y, Aramaki K, Hodoshima S, Saito M, Shono A, Kuwano J, et al. Efficient hydrogen generation from organic chemical hydrides by using catalytic reactor on the basis of superheated liquid-film concept. Chem. Eng. Sci. 2008;63(20):4935–41.

[80] Kariya N, Fukuoka A, Utagawa T, Sakuramoto M, Goto Y, Ichikawa M. Efficient hydrogen production using cyclohexane and decalin by pulse-spray mode reactor with Pt catalysts. Appl. Catal. A Gen. 2003;247(2):247–59.

[81] Shukla A a., Gosavi P V., Pande J V., Kumar VP, Chary KVR, Biniwale RB. Efficient hydrogen supply through catalytic dehydrogenation of methylcyclohexane over Pt/metal oxide catalysts. Int. J. Hydrogen Energy 2010;35(9):4020–26.

[82] Jeong B-H, Sotowa K-I, Kusakabe K. Catalytic dehydrogenation of cyclohexane in an FAU-type zeolite membrane reactor. J. Memb. Sci. 2003;224(1-2):151–58.

[83] Ferreira-Aparicio P, Rodriguez-Ramos I, Guerrero-Ruiz a. On the Performance of Porous Vycor Membranes for Conversion Enhancement in the Dehydrogenation of Methylcyclohexane to Toluene. J. Catal. 2002;212(2):182–92.

[84] Quicker P, Höllein V, Dittmeyer R. Catalytic dehydrogenation of hydrocarbons in palladium composite membrane reactors. Catal. Today 2000;56(1-3):21–34.

[85] Casanave D, Ciavarella P, Fiaty K, Dalmon J. Zeolite membrane reactor for isobutane dehydrogenation : Experimental results and theoretical modelling 1999;54:2807–15.

[86] Lai Y, He S, Li X, Sun C, Seshan K. Dehydrogenation of n-dodecane over PtSn/MgAlO catalysts: Investigating the catalyst performance while monitoring the products. Appl. Catal. A Gen. 2014;469:74–80.

[87] Ahuja R, Punji B, Findlater M, Supplee C, Schinski W, Brookhart M, et al. Catalytic dehydroaromatization of n-alkanes by pincer-ligated iridium complexes. Nat. Chem. 2011;3:161–71.

[88] Lucarelli C, Albonetti S, Vaccari A, Resini C, Taillades G, Roziere J, et al. On-board H2 generation by catalytic dehydrogenation of hydrocarbon mixtures or fuels. Catal. Today 2011;175(1):504–8.

[89] Lucarelli C, Pavarelli G, Molinari C, Albonetti S, Mista W, Di Domenico D, et al. Catalyst deactivation in on-board H2 production by fuel dehydrogenation. Int. J. Hydrogen Energy 2013:1–14.

[90] Resini C, Lucarelli C, Taillades-Jacquin M, Liew K-E, Gabellini I, Albonetti S, et al. Pt–Sn γ-Al2O3 and Pt–Sn–Na γ-Al2O3 catalysts for hydrogen production by dehydrogenation of Jet A-1 fuel Characterisation and preliminary activity tests.pdf. Int. J. Hydrogen Energy 2011;36(10):5972–82.

[91] Reyes-Carmona Á, Gianotti E, Taillades-Jacquin M, Taillades G, Rozière J, Rodríguez-Castellón E, et al. High purity hydrogen from catalytic partial dehydrogenation of kerosene using saccharide-templated mesoporous alumina supported Pt–Sn. Catal. Today 2013;210:26–32.

[92] Warren KA. World Jet Fuel Specifications with Avgas Supplement Edition. Leatherhead, UK: 2008.

[93] Rachner M. Die Stoffeigenschaften von Kerosin Jet A-1. Köln: Deutsches Zentrum für Luft und Raumfahrt e.V Mitteilungen, 1998.

[94] Brune M, Reimert R. Desulfurization of Liquid Fuel via Fractional Evaporation and Subsequent Hydrodesulfurization Upstream a Fuel Cell System. Ind. Eng. Chem. Res. 2005;44(25):9691–94.

[95] Standard test method of boiling range distribution of petroleum fractions by gas chromatography ASTM D2887 - 13 2013.

[96] Brune M. Verfahren zur Entschwefelung flüssiger Brennstoffe. Karlsruhe Institute of Technology, n.d.

[97] Zahedi G, Yaghoobi H. Dynamic Modeling and Simulation of Heavy Paraffin Dehydrogenation Reactor for Selective Olefin Production in Linear Alkyl Benzene Production Plant 2008:114–19.

[98] Usman MR. Methylcyclohexane Dehydrogenation over Commercial 0 . 3 Wt % Pt / Al 2 O 3 Catalyst 2011;48(January):13–17.

[99] Sebastián D, Alegre C, Calvillo L, Pérez M, Moliner R, Lázaro MJ. Carbon supports for the catalytic dehydrogenation of liquid organic hydrides as hydrogen storage and delivery system. Int. J. Hydrogen Energy 2013:1–7.

[100] Yu J, Ge Q, Fang W, Xu H. Enhanced performance of Ca-doped Pt/γ-Al2O3 catalyst for cyclohexane dehydrogenation. Int. J. Hydrogen Energy 2011;36(18):11536–44.

[101] Kong C, Lu J, Yang J, Wang J. Catalytic dehydrogenation of ethylbenzene to styrene in a zeolite silicalite-1 membrane reactor. J. Memb. Sci. 2007;306(1-2):29–35.

[102] Dittmeyer R, Höllein V, Daub K. Membrane reactors for hydrogenation and dehydrogenation processes based on supported palladium. J. Mol. Catal. A Chem. 2001;173(1-2):135–84.

[103] Schildhauser TJ. Untersuchung zur Verbesserung des Wärmeübergangs in katalytischen Festbettreaktoren für Energiespeicheranwendungen. Eidgenössische Technische Hochschule Zürich, 2001.

[104] Gladrow ER, Krebs RW, Bimberlin CN. Reactions of Hydrocarbons over Cracking Catalysts. Indurstrial Eng. Chemestry 1953;45(1):142–47.

[105] Xing Y, Fang W, Xie W, Guo Y, Lin R. Thermal Cracking of JP-10 under Pressure. Ind. Eng. Chem. Res. 2008;47(24):10034–40.

[106] Sivasanker S, Padalkar SR. Mechanism of dehydrocyclization of n-alkanes over platinum—alumina Catalysts. Appl. Catal. 1988;39:123–26.

[107] Praserthdam P, Grisdanurak N, Yuangsawatdikul W. Coke formation over Pt–Sn–K / Al2O3 in C3 , C5 – C 8 alkane dehydrogenation 2000;77:215–19.

[108] Usman M, Cresswell D, Garforth A. Detailed Reaction Kinetics for the Dehydrogenation of Methylcyclohexane over Pt Catalyst. Ind. Eng. Chem. Res. 2012;51(1):158–70.

[109] Breitmaier E, Jung G. Organische Chemie. In:. Stuttgart: Thieme, 2013. p. 129–30.

[110] Camp CE Van, Damme PS Van, Froment GF. Thermal Cracking of Kerosene. Ind. Eng. Chem. Produktion Res. Develpment 1984;(23):155–62.

[111] Plank CJ, Sibbett D., Smith RB. Comparison of Catalysts in Cracking Pure Methylcyclhexane and n-Decane. Indurstrial Eng. Chemestry 1957;49(4):749–749.

[112] Xian X, Liu G, Zhang X, Wang L, Mi Z. Catalytic cracking of n-dodecane over HZSM-5 zeolite under supercritical conditions: Experiments and kinetics. Chem. Eng. Sci. 2010;65(20):5588–5604.

[113] World Jet Fuel Specifications with Avgas Supplement. Leatherhead, UK: 2005.

[114] Altin O, Eser S. CARBON DEPOSIT FORMATION FROM THERMAL STRESSING OF PETROLEUM FUELS. Ind. Eng. Chem. Res. 2004;49(5):764–66.

[115] Altin O, Eser S. Analysis of Solid Deposits from Thermal Stressing of a JP-8 Fuel on Different Tube Surfaces in a Flow Reactor. Indurstrial Eng. Chemestry 2001:596–603.

[116] Marteney P.J. SLJ. Thermal Decompositon of Aircraft Fuel. J. Eng. Gas Turbines Power 1986;108(4):648653.

[117] Taylor WF. Deposit Formation from Deoxygenated Hydrocarbons. II. Effect of Trace Sulfur Compounds. Ind. Eng. Chem. Produktion Res. Develpment 1976;15(1).

[118] Violi A. Cyclodehydrogenation reactions to cyclopentafused polycyclic aromatic hydrocarbons. J. Phys. Chem. A 2005;109(34):7781–87.

[119] Linnhoff B, Flower JR. Synthesis of Heat Exchanger Networks : 1. Systematic Genertation of Energy Optiomal Networks. AIChE J. 1978;24(4):633–42.

[120] Linnhoff B, Flower JR. Synthesis of heat exchanger networks: II Evolutionary generation of networks with various criteria of optimality. AIChE J. 1978;24(4):642–54.

[121] Haydary J. STEADY-STATE AND DYNAMIC SIMULATION OF CRUDE OIL DISTILLATION USING ASPEN PLUS AND ASPEN DYNAMICS 2009;51:100–109.

[122] Doust AM, Shahraki F, Sadeghi J. Simulation , control and sensitivity analysis of crude oil distillation unit 2012;3(November):99–113.

[123] Soave G. Equilibrium constans from a modified Redlich-Kwong equation of state 1972;27(6):1197–1203.

[124] Peng D-Y, Robinson DB. A New Two-Constant Equation of State. Ind. Eng. Chem. Fundam. 1976;15(1):59–64.

[125] Malek A, Farooq S. Study of a Six-Bed Pressure Process 1997;43(10).

[126] Malek a., Farooq S. Hydrogen purification from refinery fuel gas by pressure swing adsorption. AIChE J. 1998;44(9):1985–92.

[127] U.S. Depertment of Energy, Fuel Cell Handbook, 7th Edition. Morgantown, West Virginia: 2004.

[128] Benz W. Einfluss von Schwefelverbindungen in flüssigen Kohlenwasserstoffen auf ein Brennstoffzellen- Gesamtsystem am Beispiel eines Katalytischen Crackers mit nachgeschalteter PEMFC DOKTOR-INGENIEUR. University Duisburg-Essen, 2005.

[129] Kemp IC. Pinch Analysis and Process Integration. Elsevier Ltd, 2007.

[130] Linnhoff B, Hindmarsh E. THE PINCH DESIGN METHOD FOR NETWORKS. Chem. Eng. Sci. 1983;38(5):745–63.

[131] Rick H. Gasturbinen und Flugantriebe Grundlagen, Betreibsverhalten und Simulation. Springer Verlag, 2013.

[132] European Aviatio on Safety Agency Type-Certificate Data Sheet for Aibus A318 - A319 - A320 - A321. France: 2013.